POLITECNICO DI TORINO

Energy Department – DENERG

Master of Science program in Energy and Nuclear Engineering

MASTER THESIS

A case study of existing industrial trigeneration. Operating conditions analysis and revamping opportunities

Relatore:
Prof. Alberto Poggio

Correlatore:
Ing. Giulio Cerino Abdin
Ing. Chiara Monzani

Candidato:
Flavio Guida

Academic Year 2020/2021

Dedicata a mio nonno Augusto

Abstract

In Italy renewable energy sources (RES) covered the 18,2% of the gross final energy consumption in 2019, thus, exceeding the target of 17,0% renewables, assigned for the year 2020 by the Directive 2009/28/CE. While electricity and transport sector showed an increase of RES consumption, in absolute terms, a slight reduction of thermal energy production from RES has been observed. However, this last decrease was compensated by a greater decline of gross final energy consumption; consequently, all the three sectors were characterized by an increase of RES penetration, in percentage terms.

Industry is one of the main energy intensive sector in Italy, as it accounts for around 21% of final energy consumption; however, the reduction with respect to the previous year (-0,9 %) and the continuous decline of industrial sector energy intensity show that we are exploiting primary energy sources more and more efficiently.

Energy efficiency, indeed, will play a key role to achieve the target of net-zero emissions in the EU energy systems by 2050.

For this reason, it is fundamental to initiate energy efficiency processes in the residential sector and on cogeneration and trigeneration existing plants, in order to produce electricity and thermal energy from fossil fuels in a more sustainable and efficient way, supporting the industrial sector towards a decarbonization that does not compromise the productions.

This Thesis work has been carried out in collaboration with Edison Fenice S.p.A, in particular with the Energy and Environmental Service Division that focuses on the development and the operation of energy efficiency projects and environmental services for large industrial customers, small and medium companies, the service sector and the public administration.

This study analyzes a trigeneration plant owned by Fenice S.p.A and located in Melfi (PZ), at the service of the Plastic Components and Modules Automotive (PCMA) industrial site of the Stellantis Group.

Starting from the energy plant data obtained from the Online Data Collector, a data analysis has been performed in order to evaluate the Internal Combustion Engine (ICE) performance and the effectiveness of heat recovery and cold water production.

The analysis considers three years of operation (the year 2020 because of the Covid-19 pandemic that affected the industrial site productivity and, as a consequence, also the trigeneration plant operation was not included in the analysis) in order to examine more completely the evolution over time of the energy vectors provided to the PCMA industrial site

and, thus, to evaluate the dimensioning of the various energy plant components.

Starting from some criticalities highlighted by the analysis of plant operating data, some opportunities of energy efficiency optimization are investigated, particularly on the heat recovery from the ICE exhaust gases and on cold water production by means of water absorption refrigerator groups. The different optimization scenarios are completed with an economic analysis to evaluate the money savings with respect to the original plant configuration, due to the possibility to improve energy efficiency and to obtain a higher number of White Certificates intended for High Efficiency Cogeneration plants. In the last section of this study, there are presented some considerations on CO2 emissions and possible future negative implications on the analyzed trigeneration plant economic balance because of stricter Emission Trading System regulations.

Table of contents

List of figures

List of tables

Abbreviations and acronyms

ATU	Air Treatment Unit
BAT	Best Available Technology
BpST	Backpressure Steam Turbines
CAPEX	Capital Expenditure
CAR	Cogenerazione ad Alto Rendimento (High Efficiency Cogeneration)
CC	Combined Cycle
CCHP	Combined Cooling, Heating and Power
CdST	Condensation Steam Turbines
CERG	Compression Electric Refrigerator Group
CF	Capacity Factor
CHP	Combined Heat and Power
COP	Coefficient of Performance
ECC	Engine Control Console
ETS	Emission Trading System
EU	European Union
GME	Gestore dei Mercati Energetici
GSE	Gestore dei Servizi Energetici
GT	Gas Turbines
HRU	Heat Recovery Unit
HT	High Temperature
HW	Hot Water
ICE	Internal Combustion Engine
IEA	International Energy Agency
IPEX	Italian Power Exchange
LT	Low Temperature
MGT	Micro Gas Turbines
ORC	Organic Rankine Cycle
PES	Primary Energy Saving
PLC	Programmable Logic Controller

PSV	Punto di Scambio Virtuale
PUN	Prezzo Unico Nazionale
REMI	Reduction and Metering Station
SHW	Super-Heated Water
TEE	Titoli di Efficienza Energetica (White Certificates)
TOE	Tonnes of Oil Equivalent
WARG	Water Absorption Refrigerator Group

1 Introduction

Direct industrial CO_2 emissions accounts for 8,5 Gt in one year (2018). Although, they slightly declined (-0,6 %) with respect to the previous year, they represent 24 % of global CO_2 emissions [1]. Much is still to be done in order to meet the Paris Agreement (2015) target of "Holding the increase in the global average temperature to well below 2°C above pre-industrial levels and pursuing efforts to limit the temperature increase to 1.5°C above pre-industrial levels" [2].

The International Energy Agency (IEA) pointed out three main scenarios for future evolution of global emissions, according to policies that are being, or expected to be, implemented: STEPS (Stated Policies Scenario) is based on existing and announced policies; SDS (Sustainable Development Scenario) sets out the path to meet the energy-related SDGs (Sustainable Development Goals); NZE2050 (Net Zero Emissions by 2050) is a long-term strategy for energy sector to globally reach net zero emissions by 2050 [1]

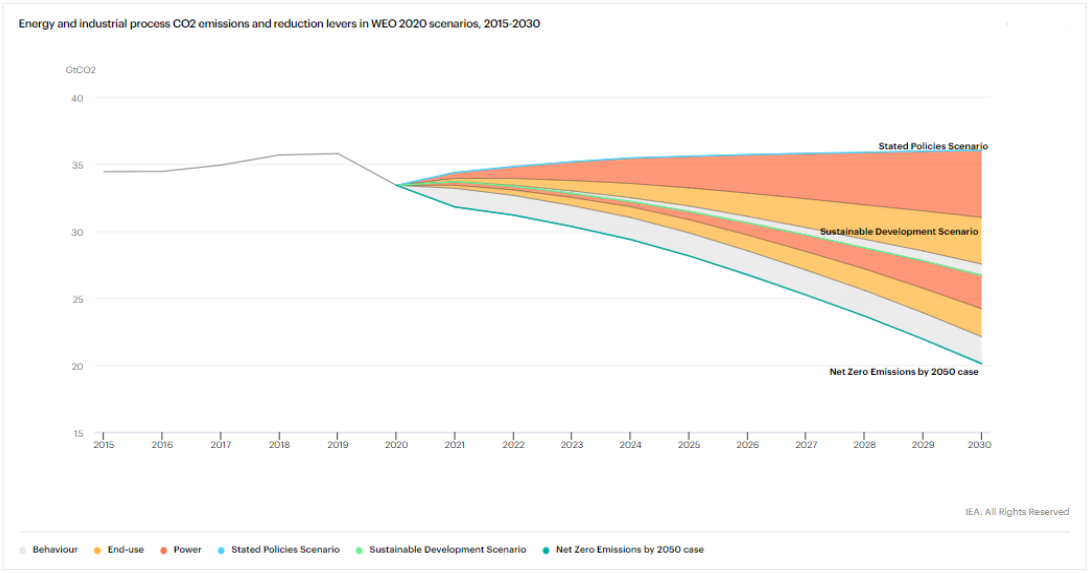

Figure 1.1: IEA scenarios for energy and industrial process CO2 emissions [1]

As it can be seen from *Figure 1.1*, strict measures must be taken in order to tackle climate change because a huge gap must be overwhelmed to align with the SDS. Governments must encourage energy efficiency and low carbon technologies in all sectors through price mechanisms.

The industry sector accounted for 37% (157 EJ) of total global final energy use in 2018: this represents a 0.9% annual increase in energy consumption since 2010 [1].

The industry sector's energy mix has remained relatively unchanged since 2010, but a slight decrease of fossil fuel consumption (from 73 % to 69 %) and a little increase of electricity (from

18 % to 21 %) have been observed [1].

Around 75% of the energy used in industry is for thermal end uses, which include industrial process steam as well as drying, refrigeration and other energy needs. The remaining share is for electrical end-uses, including the operation of machinery and lighting. Renewable energy covers around 14.5% of total industrial energy demand. Most of this renewable energy is in the form of low-temperature heat (below 100 °C) and is mainly supplied by bioenergy, while renewable electricity is consumed both for electrical end-uses as well as to meet thermal demands of some industrial process, for example through industrial heat pumps [3].

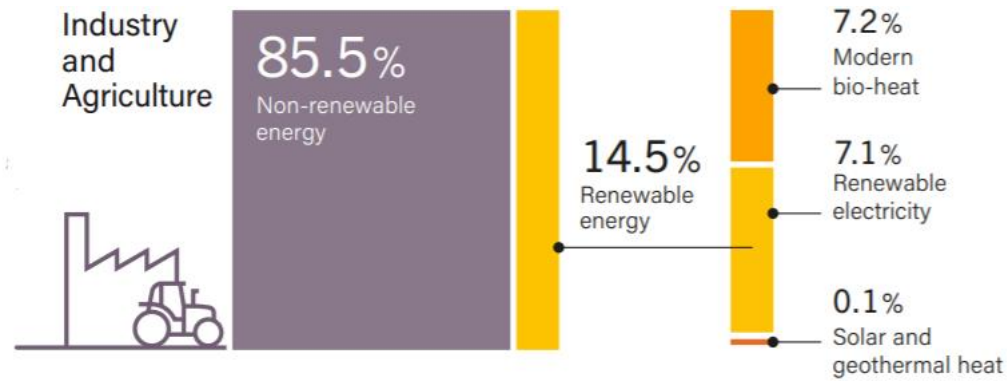

Figure 1.2: Detail of industry sector's energy mix [3]

Energy productivity of industrial sector is growing at global level, nevertheless not negligible differences can be noted in *Figure 1.3*, between productivity of more advanced regions, such as Europe and North America, and less developed or emerging countries like China, India and Africa.

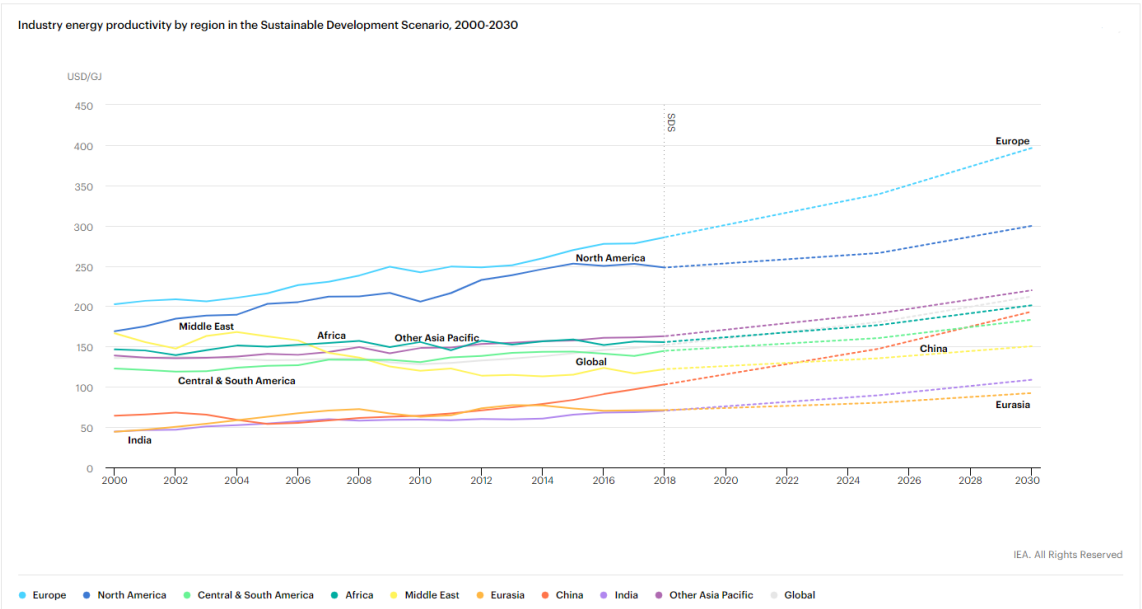

Figure 1.3: Energy productivity growth in industrial sector according to SDS [1]

The former regions benefit not only from the most advanced technologies that allow to achieve the highest efficiencies, but also from a structural industrial shift from energy-intensive industry (e.g. steel and cement) towards a larger share of added value from higher-value-added sectors that include the automotive industry, that is the user of the energy carriers produced by the energy plant that will be analyzed in this work.

Nevertheless, less developed countries could take advantage from the diffusion of existing technologies both to produce energy and for industrial applications, thus a path to "Green" and sustainable development should be followed, especially by means of renewable energy sources.

In order to achieve high CO_2 emission reduction, most advanced countries must implement energy efficiency policies, encouraging process optimization and technological shifts.

The adoption of energy management systems for system-level optimization of the productive industrial process and waste heat / gas recovery or cogeneration plants to provide the energy services and energy carriers to the industrial user can help to improve industry energy efficiency

Revamping of existing energy plants that serve industrial users, can be a good solution to increase the economic return of an investment, while improving the plant environmental sustainability due to the adoption of newer and higher-performance components.

Moreover, the modernization of an energy plant represents the possibility of increasing the efficiency of the system, subsequent to the analysis of the operating conditions during the years of energy production.

Indeed, criticalities that were not considered during the design phase can lead to a decrease in the expected productivity of the plant, thus providing a worst service to the user. At the end of life of the energy system, its revamping constitutes a money-saving alternative with respect to the installation of a new plant.

Energy plants revamping advantages can be resumed in:

- Improvement of the efficiency and productivity of the plant, thus resources optimization
- Less maintenance required with consequent cost reduction
- Longer lifetime of the plant
- Emissions reduction
- Possibility to access incentive mechanisms for energy-saving actions, e.g. White Certificates

A trigeneration plant revamping consists in the substitution of some electrical, mechanical or heat recovery components of the plant with the aim of improving the quality and the quantity of electricity, hot water or cold water energy carriers to the final user.

2 Cogeneration and trigeneration

2.1 Cogeneration general aspects

Cogeneration means the simultaneous production of electricity and thermal power, from the same primary energy source. It is also known with the acronym CHP, i.e. Combined Heat and Power. The aim of CHP is to produce the energy carriers, mostly needed for domestic uses (with a connection to a district heating network) or industrial purposes, achieving a higher plant efficiency, with a consequent more rational use of the energy source, with respect to the separate production.

In separate production configuration, the electricity is generally obtained in a thermoelectric plant while the hot water is produced in a boiler that can be located near to the point of utilization.

The most common users of cogeneration plants are characterized by an almost constant electric and thermal demand during time (e.g. hospitals, swimming pools, sports centers, shopping centers and so on). Domestic users have a higher thermal demand during winter (heating season) and they are fed with hot water at lower temperature and pressure with respect to some industrial users.

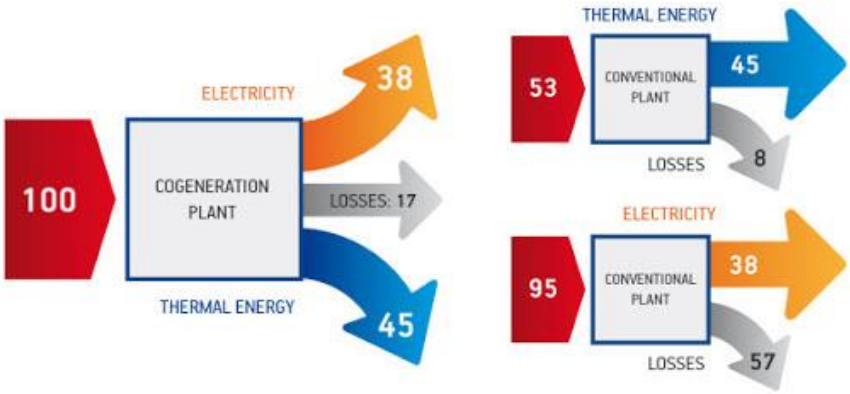

Figure 2.1: Comparison of separate production and CHP energy balance [4]

The advantages related to cogeneration are mainly linked to economic and environmental considerations: by burning a certain amount of fossil fuels, the waste thermal power can be recovered, thus the plant owner is able to sell it with a higher monetary return with respect to the production of the electricity. This economic advantage can be also reflected on the consumer side, with a reduced cost on the energy bill. From the environmental point of view, cogeneration, in comparison with separate production, allows to burn less fuels to obtain the

same amount of energy carriers. This implies that a lower amount of pollutants and greenhouse gases are emitted to the atmosphere, with a consequent advantage on the air quality.

Other advantages linked to energy production in cogeneration mode are the reduction of transmission losses due to the proximity of the plant to the user and the possibility to benefit from the economic incentives for high efficiency energy plants.

In Italy, the vast majority of cogeneration units are Internal Combustion Engines (ICE), even if the electric power that they produce corresponds to about 14 % of total electricity produced in national cogeneration plants. This means that they are mostly low or medium installed power units.

On the contrary, Combined Cycle plants (CC), that represents only the 3.3 % of installed cogeneration plants, cover around 75 % of cogeneration units electric power capacity.

Indeed, Combined Cycle plants' average size, in terms of electric nominal power, is around 165 MW, while Internal Combustion Engines average size is just 1 MW [5].

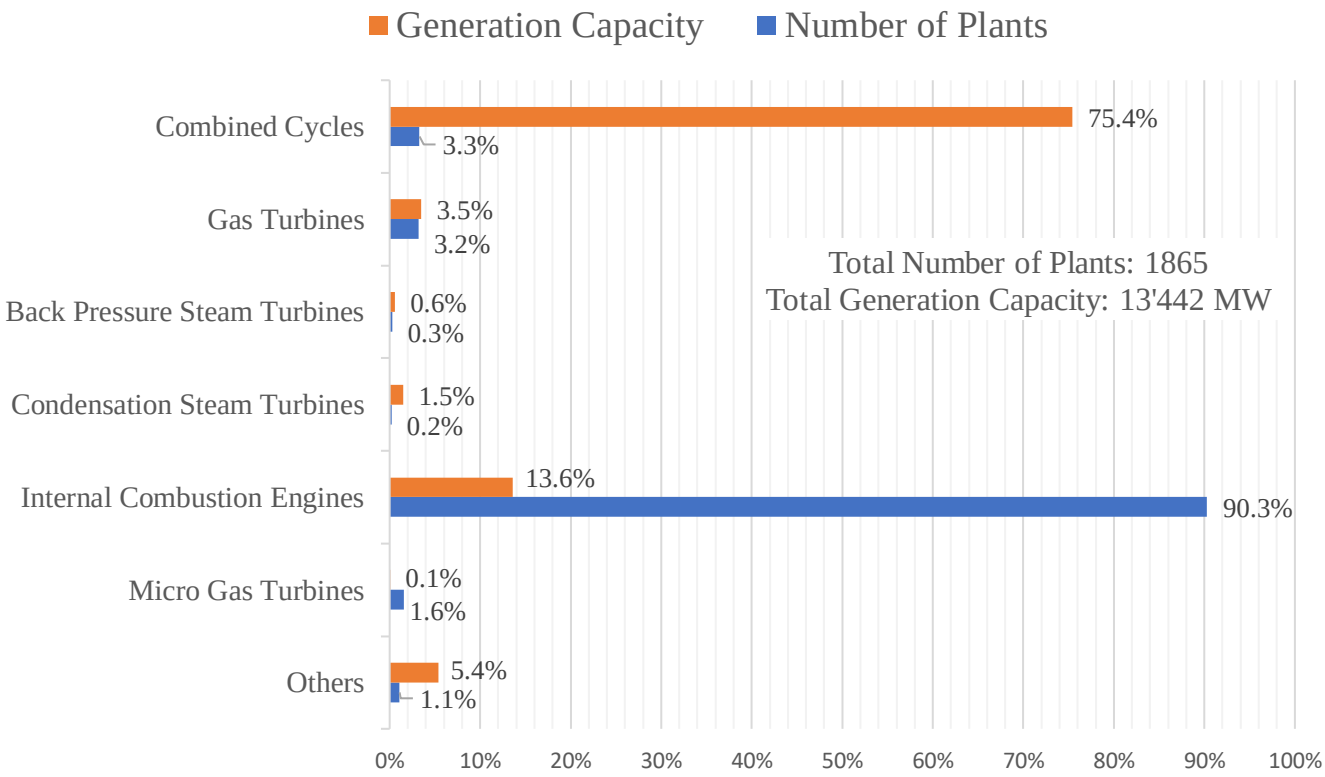

Figure 2.2: Nominal power and number of plants percentage for different plants typologies

The category represented in "Others" in *Figure 2.2* includes:

- Stirling engines
- Fuel cells
- Steam engines

- ORC (Organic Rankine Cycle) plants
- Other technologies not included in the other categories

Operative cogeneration plants average efficiency is dependent on the plant typology, as it is shown in *Table 2.1*. On a national level, the average First Law Efficiency is around 65 %.

First Law Efficiency is often used as a parameter to compare different energy conversion technologies; it implies that heat and electricity are considered with the same quality, thus the lower exergetic value of thermal power is not taken into account.

	Electrical efficiency	**Thermal Efficiency**	**First Law Efficiency**
Average	40,3 %	24,8 %	65,1 %
CC	42,7 %	19,2 %	61,9 %
GT	31,3 %	48,6 %	79,9 %
BpST	18,6 %	66,0 %	84,6 %
CdST	25,0 %	31,2 %	56,2 %
ICE	40,2 %	31,1 %	71,3 %
MGT	26,6 %	47,3 %	73,9 %
Others	31,2	45,5 %	76,7 %

Table 2.1: Average electrical and thermal efficiency of cogeneration units [5]

Internal Combustion Engines average efficiency is 71.3 % with a little higher electrical production with respect to the thermal one, even if those are quite balanced: the cogeneration ratio λ is near 1.

$$\lambda = \frac{\dot{H}_{chp}}{\dot{E}}$$

In the equation, $\dot{H}_{chp}$ is thermal power and $\dot{E}$ is electric power.

Combined Cycle plants show a quite low overall efficiency, due to the low contribution of thermal power provided to the users. Indeed, CC plants are mostly installed with the aim of producing electricity to be exported to the national electrical grid, or, alternatively, they are located nearby users with low thermal power demand [5].

Instead, all the other technologies, are characterized by high thermal efficiencies, in particular backpressure steam turbines: they are usually installed at industrial users that need steam at higher pressure, such as refineries, paper mills, desalination plants.

Plants with higher efficiency, thus allowing a larger primary energy savings can be classified as CAR (Cogenerazione ad Alto Rendimento), and, therefore, they can get access to incentive mechanisms.

2.2 High Efficiency Cogeneration

High Efficiency Cogeneration (CAR, Cogenerazione ad Alto Rendimento, in Italy), was firstly introduced by the European Parliament and the Council of the European Union by means of the Directive 2004/8 EC, with the aim of increasing energy efficiency and harmonizing, at European level, the definition of cogeneration products.

This Directive (High Efficiency Cogeneration), recognizes as electricity from cogeneration only the electricity which, together with useful heat, is produced by a portion of the cogeneration plant where the overall efficiency is 75 % (or 80 %, it depends on the typology of the cogeneration plant). For ICEs, overall efficiency must be higher than 75 %. Such electricity from cogeneration, together with useful heat, is then used as a parameter for the determination of the incentives (and/or reductions of charges) which the plant can receive.

Plant overall efficiency is defined by the following formula, that is equal to the First Law Efficiency:

$$\eta_{global} = \frac{E + H_{chp}}{F}$$

- E is electric energy produced.
- H_{chp} is cogenerated thermal power, effectively used, in a downstream process.
- F typically corresponds with the energy introduced by the fuel introduced in the plant, or, in some cases, it can be recovered thermal energy from an upstream process.

The guidelines for the application of calculation methodologies of the relevant quantities to get CAR recognition and, therefore, to have the possibility of gaining the White Certificates (TEE, Titoli di Efficienza Energetica), are reported in “Linee guida per l’applicazione del Decreto del Ministero dello Sviluppo Economico 5 settembre 2011 – Cogenerazione ad Alto Rendimento (CAR)” [6].

High Efficiency Cogeneration (CAR) plants are defined on the basis of an energy parameter: Primary Energy Saving (PES), that measures how much primary energy is saved due to cogeneration with respect to separate production.

In order to be classified as CAR, the following condition must be satisfied:

- PES must be higher or equal to 10 % for cogeneration plants with nominal electric power higher or equal to 1 MW_e.
- PES must be higher or equal to 0 for small size cogeneration unit (lower than 1 MW_e) and for micro-cogeneration units (lower than 50 kW_e).

PES index is calculated as follows:

$$PES = \left(1 - \frac{1}{\frac{CHP\ H_\eta}{Ref\ H_\eta} + \frac{CHP\ E_\eta}{Ref\ E_\eta}}\right) \cdot 100$$

- $CHP\ H_\eta$ is the thermal efficiency of the cogeneration production defined as useful heat output (H_{chp}) divided by the fuel input (F_{chp}) used to produce the sum of useful heat output and electricity from cogeneration.
- $Ref\ H_\eta$ is the efficiency reference value for separate heat production.
- $CHP\ E_\eta$ is the electrical efficiency of the cogeneration production defined as the electricity output (H_{chp}) divided by the fuel input (F_{chp}) used to produce the sum of useful heat output and electricity from cogeneration.
- $Ref\ E_\eta$ is the efficiency reference value for separate electricity production.

The efficiency reference values are defined in the Annex I of *Regolamento Delegato (UE) 2015/2402 [8]*. They are obtained by comparing the cogeneration unit with the best available and economically justifiable technology for separate production of heat and electricity on the market, in the year of construction of the cogeneration unit.

If the plant overall efficiency is below the threshold reference value, or if the minimum PES value is not reached, it is necessary to introduce the cogeneration virtual machine: in this case, all the useful thermal power is attributed to the CAR unit, thus valuing the produced heat H_{CHP}. It is the independent variable by which the amount of electricity produced by the CAR portion of the plant is calculated.

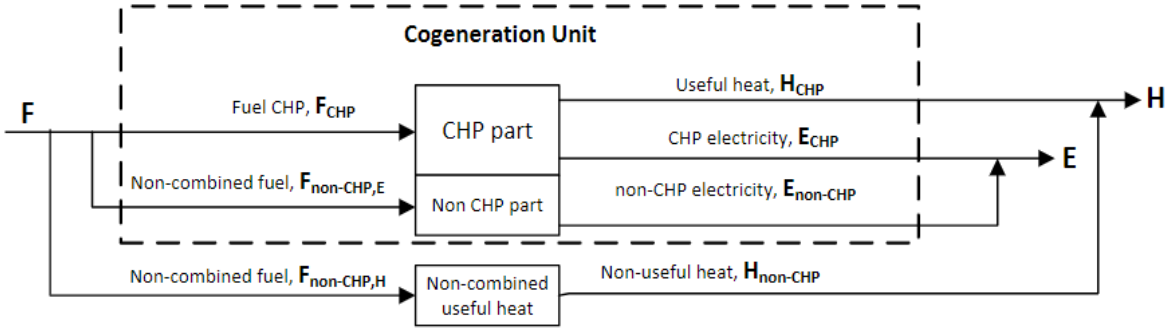

Figure 2.3: Cogeneration plant division in CHP and non-CHP part [7]

In *Figure 2.3,* the $H_{non-CHP}$ could be, for example, thermal power generated in separate boilers, thus by machines that do not operate in cogeneration mode.

In order to dimension the CHP virtual machine, it is necessary to calculate the parameter C_{eff} that is defined as follows:

$$C_{eff} = \frac{\eta_{non-CHP,e}}{\eta_{CHP} - \eta_{non-CHP,e}}$$

Where $\eta_{non-CHP,e}$ is the electrical efficiency of the non-CHP portion of the plant, while η_{CHP} is the reference efficiency value, i.e. 75 % for ICEs.

$$\eta_{non-CHP,e} = \frac{E}{F - F_{non-CHP,h}}$$

$F_{non-CHP,h}$ is the fuel needed for heat separate production.

It is important to consider that those reference values, published in [8] must be corrected, in order to take into account the different mean temperature in the area where the plant is located (climatic zone) and also to consider the avoided electric losses on the grid, as it is reported in *Table 2.2* and *Table 2.3.*

Climatic zone	**Average Temperature [°C]**	**Correction Factor expressed in %**
Zone A: Valle d'Aosta, Trentino Alto Adige, Piemonte, Friuli-Venezia Giulia, Lombardia, Veneto, Abruzzo, Emilia Romagna, Liguria, Umbria, Marche, Molise, Toscana	11,315	+ 0,369
Zone B: Lazio, Campania, Basilicata, Puglia, Calabria, Sardegna, Sicilia	16,043	- 0,104

Table 2.2: Correction factor for different climatic zones

Connection voltage to electric grid	**Correction factor for electricity exported to the grid**	**Correction factor for electricity self-consumption**
> 345 kV	1	0,976
200 – 345 kV	0,972	0,963
100 – 200 kV	0,963	0,951
50 – 100 kV	0,952	0,936
12 – 50 kV	0,935	0,914
0,45 – 12 kV	0,918	0,891
< 0,45 kV	0,888	0,851

Table 2.3: Correction factor for avoided electric losses on the grid

Then, it is possible to calculate the electricity produced by the cogeneration virtual machine as:

$$E_{CHP} = C_{eff} \cdot H_{CHP}$$

Therefore, the electricity produced by the non-CHP part is:

$$E_{non-CHP} = E - E_{CHP}$$

And the fuel needed for CHP and non-CHP parts can be obtained:

$$F_{non-CHP,e} = \frac{E_{non-CHP}}{\eta_{non-CHP,e}} \qquad \rightarrow \qquad F_{CHP} = F - F_{non-CHP,e}$$

This procedure is needed in order to calculate the useful parameters ($CHP\ H_\eta,\ CHP\ E_\eta$)to put into the PES formula:

$$CHP\ H_\eta = \frac{H_{CHP}}{F_{CHP}} \qquad CHP\ E_\eta = \frac{E_{CHP}}{F_{CHP}}$$

Cogeneration plants that obtain the CAR recognition have the possibility to take advantage of the following benefits:

- Possibility to obtain White Certificates due to a primary energy saving.
- Priority dispatching for the electricity produced from "mainly CAR" units (i.e. at least 50 % of total produced electricity has been produced in CAR regime).
- Advantages on techno-economic aspects for the connection to the grid.
- Net metering for cogeneration units with a nominal capacity lower than 200 kW.
- Possibility to be classified as SEU and SEESEU-B, with a consequent partial exemption of some tariff payments on the electricity self-consumed within the system, if the electricity produced in cogeneration mode E_{CHP} is higher than 50 % of total gross electricity production.
- Tax advantages for natural gas used for cogeneration

2.3 White Certificates

White certificates, also known as Energy Efficiency Certificates (TEE), are tradable assets that certify a reduction in primary energy consumption. They encourage a technological shift towards greater energy efficiency systems. Thus, producers, suppliers and distributors of electricity, gas and oil must undertake energy savings measures to cut their consumption, otherwise they must pay a penalty. Suppliers with more than 50'000 customers are classified as obliged entities ("Soggetto Obbligato") and they have a yearly energy saving target to achieve. They can fulfil their obligations by realizing energy efficiency projects or by acquiring

TEE on the market from other entities admitted to the market.

Indeed, volunteer entities can participate to TEE market and they are typically Energy Services Companies (ESCo) or those companies with a certified Energy Management Expert (EME, or EGE in Italy "Esperto Gestione Energia"). These entities voluntarily realize energy efficiency projects, thus they are allowed to get TEEs.

One White Certificate corresponds to 1 TOE (Tonnes of Oil Equivalent) of energy savings. White Certificates are released by GME (Gestore dei Mercati Energetici), on the advice of GSE (Gestore dei Servizi Energetici) and they can be traded on the market managed by GME.

TEE monetary value is defined during market exchange sessions. Their value on the market on May 2021 is around 270,00 €/TOE [9].

According to *DM 5 Settembre 2011*, cogeneration plants that have been classified as CAR, have the right to obtain TEEs, in proportion to the primary energy saving they have achieved. It is calculated as follows:

$$RISP = \frac{E_{CHP}}{\eta_{e,REF}} + \frac{H_{CHP}}{\eta_{h,REF}} - F_{CHP}$$

Where:

- $RISP$ corresponds to primary energy saving, expressed in MWh, realized by the cogeneration plant, during the year.
- E_{CHP} is the electricity produced by the CHP part of the cogeneration plant.
- H_{CHP} is the useful thermal power produced by the cogeneration plant.
- F_{CHP} is the primary energy consumption of the CHP part of the cogeneration plant,
- $\eta_{e,REF}$ is the conventional average efficiency of electricity generation facilities in Italy. It is assumed equal to 0,46, but it is corrected by considering the voltage level at the point of connection with the grid and the amount of energy locally consumed and exported to the grid.
- $\eta_{h,REF}$ is the conventional average efficiency of thermal power generation facilities in Italy. It is equal to 0,82 in the case of direct utilization of exhaust gases, or 0,90 in the case of steam/hot water production.

This primary energy saving is then converted in TEE by using the following equation:

$$TEE = RISP \cdot 0{,}086 \cdot K$$

Where 0,086 is the conversion factor from MWh to TOE, while K is a harmonization coefficient, that varies in accordance with the mean electric power of the cogeneration system in CAR regime, that is obtained on the basis of the produced energy and of the working hours.

$$Mean\ Power\ CHP = \frac{E_{CHP}}{working\ hours}$$

The value of K is obtained as a weighted average considering the following power classes.

Power Class	K
$E_{CHP} \leq 1$ MWe	1,4
1 MWe $\leq E_{CHP} \leq 10$ MWe	1,3
10 MWe $\leq E_{CHP} \leq 80$ MWe	1,2
80 MWe $\leq E_{CHP} \leq 100$ MWe	1,1
$E_{CHP} > 100$ MWe	1

Table 2.4: K coefficient factor for different power classes

2.4 Trigeneration: absorption refrigerating cycle

A cogeneration plant generates electricity and thermal power throughout the year, but, generally, a much lower amount of heat is requested during summer if the system is exploited for buildings heating only. Therefore, it is necessary to find a different application for the produced thermal energy in order to not waste it. In this way, the system can work at nominal power for a higher number of hours, thus increasing its efficiency and its economic return.

A possible solution is to install absorption chillers that generate cooling energy from thermal energy. Cooling power can be exploited for air conditioning of buildings or to provide cold water for industrial productive processes.

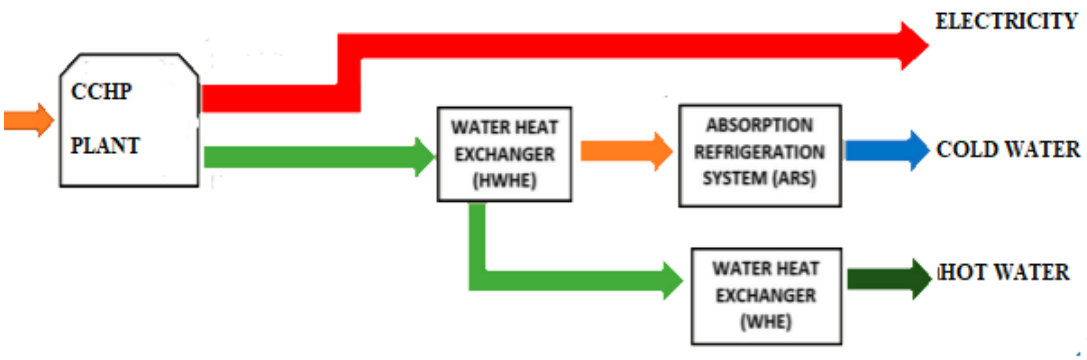

Figure 2.4: Example of energy balance of CCHP plant [10]

The cogeneration plant coupled with absorption chillers can provide electricity, hot water and cold water simultaneously to the served user. Therefore, these types of systems are called trigeneration plants, CCHP (Combined Cooling, Heating and Power).

Absorption chillers exploit hot water produced by the cogeneration system to generate cold water. Differently from the typical split units installed for air conditioning that use a compressor to increase the refrigerant pressure, absorption chillers need much less electrical energy because the compression is performed by a pump that consume less energy per unit of mass.

The working principle of an absorption chiller is based on a physical property of a two liquids solution: the condensation of the solution vapors even when the temperature of the liquid solution is higher.

The more volatile substance, thus with a lower boiling point with the same pressure, is the solute, while the less volatile one is the solvent. By heating the liquid solution, a vapor with a high concentration of solute is released. The solute concentration is always higher in the vapor phase than in the liquid phase with which the vapor is in equilibrium.

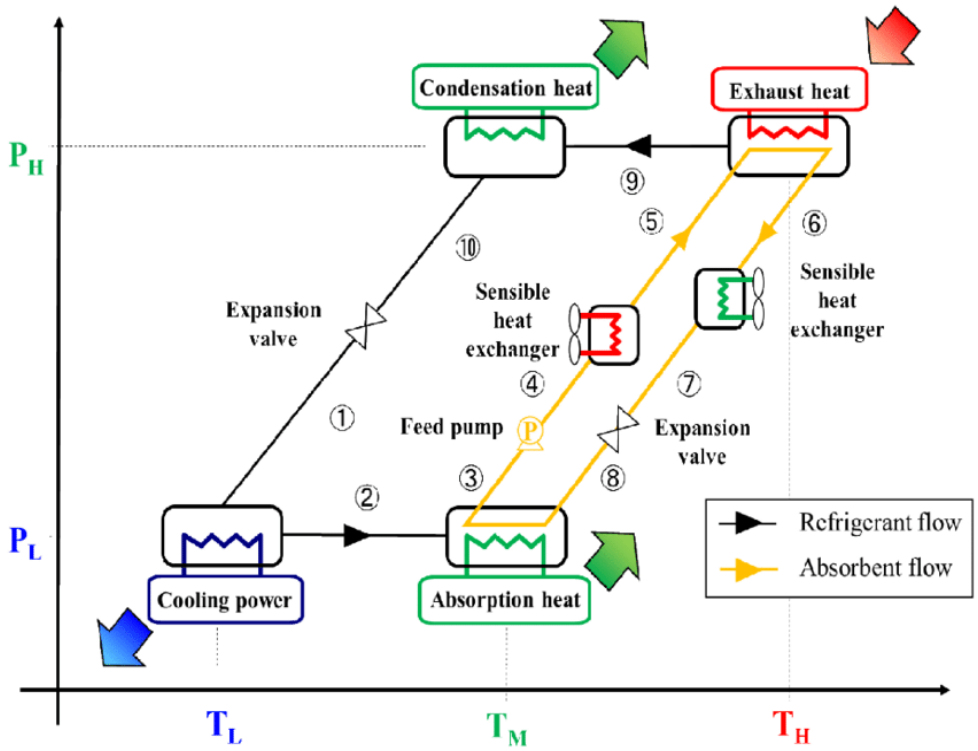

Figure 2.5: Functioning scheme of an absorption chiller in a T-p diagram [11]

The most used fluids in absorption chillers are water as solute and Lithium Bromide (LiBr) as solvent. Alternatively, water can be used as a solvent, with ammonia (NH_3) that serves as solute. The first solution is employed to produce cold water also for domestic purposes, in the

temperature range 7 – 12 °C, while the NH_3 – H_2O mixture is exploited for industrial processes that need cooling energy at lower temperatures (below 0 °C), because of the higher operating pressure. H_2O–LiBr mixture has the advantage of no toxicity and no flammability and low cost. From now on, the analysis will consider an absorption chiller with a solution H_2O – LiBr.

Chilled water is cooled down in the evaporator by exchanging heat with H_2O solute that evaporates. The evaporator is an airtight container under vacuum conditions (water saturation pressure at 4 °C is equal to 0,00813 bar), therefore water vapors would increase pressure in the vessel, but LiBr solvent absorbs water, restoring vacuum and diluting the liquid solution.

The absorption process is exothermic, thus, thermal power must be removed by a cooling water circuit that release heat by means of a cooling tower.

H_2O – LiBr liquid solution is sent to the generator by means of a pump. The driving heat source, that can be hot water from a cogeneration plant, allows the evaporation of the solute (H_2O) from the H_2O – LiBr solution.

Water vapor, at high temperature and high pressure, is sent to the condenser where it transfers heat to the cooling water circuit at lower temperature and then condenses. Liquid water is laminated through the expansion valve, therefore it undergoes a reduction in temperature and pressure and enters the evaporator to repeat the thermodynamic cycle.

LiBr cycle is highlighted in *Figure 2.5*, by the yellow arrows. After being separated from water in the generator, it is laminated through an expansion valve and sent back to the absorber.

A heat exchanger is usually located between the absorber and the generator, to transfer heat from the concentrated LiBr solution to the H_2O – LiBr mixture.

The efficiency of an absorption chiller is much lower than the COP (Coefficient Of Performance) of a traditional compression refrigerator, nevertheless they are being employed more and more thanks to some advantages:

- Possibility of using thermal energy instead of electricity as energy carrier.
- Less maintenance because of few moving parts that can be damaged after many hours of operation.
- High efficiency at partial load if modulation of thermal input is allowed.
- Low energy consumption domestic application
- Noiselessness
- Possibility of exploiting a low or null cost heat source, like hot water from solar energy or thermal wastes.

The COP of a compression refrigerator is defined as the ratio between the produced cooling

energy (Q_F) and the electricity needed as an input.

$$COP_{compression} = \frac{Q_F}{E_{el}}$$

Typical values of efficiency are around 3 and 4.

Absorption chillers' COP is calculated as the ratio between the produced cooling energy and the thermal energy made available by the driving heat source, like the hot water flow rate produced in the cogeneration system.

$$COP_{absorption} = \frac{Q_F}{H_{CHP}}$$

In this case, the electricity consumption can be neglected due to the substitution of the compressor with the pump.

Typical values of absorption chillers' COP are around 0,5 and 0,7 for water supply temperatures between 70 °C and 90 °C. By increasing the hot water temperature, the COP doesn't increase so much because the higher cooling energy produced is compensated by an increase of the thermal energy consumption.

The COP is much more dependent on the temperature at which heat is rejected towards the cooling tower. Absorption chillers are usually designed to perform condensation at around 29 °C; a slight increase in water condensation temperature could cause a not negligible reduction of the COP, as it can be noticed from *Figure 2.6*, where it is shown the variation in percent of the chiller COP as a function of the delivered cooling power and of the cooling water temperature.

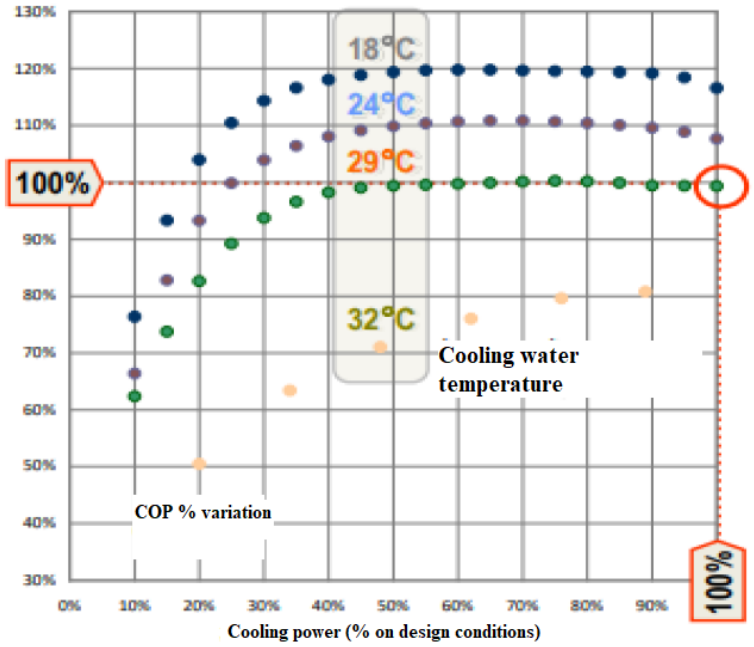

Figure 2.6: COP % variation as a function of cooling water temperature [12]

It is possible to achieve efficiencies higher than 1 only with double-effect absorption chillers. Differently from single-effect absorption chillers, they have two generators. In case of H_2O – LiBr solutions, water that evaporates in the first generator is then used as a heat source in the second generator that works at lower temperature and pressure. The intermediate LiBr solution that is produced in the first generator (HP generator in *Figure 2.7*) is then sent to the second generator (LP generator in *Figure 2.7*) where it is heated up by H_2O vapor, thus a more concentrated solution is obtained and a larger amount of water vapor is produced, without adding an external heating source.

In this way, the useful cooling power at the evaporator is almost doubled with respect to the single-effect configuration, while the thermal power consumption is the same. Then, COP can reach values around 1,2.

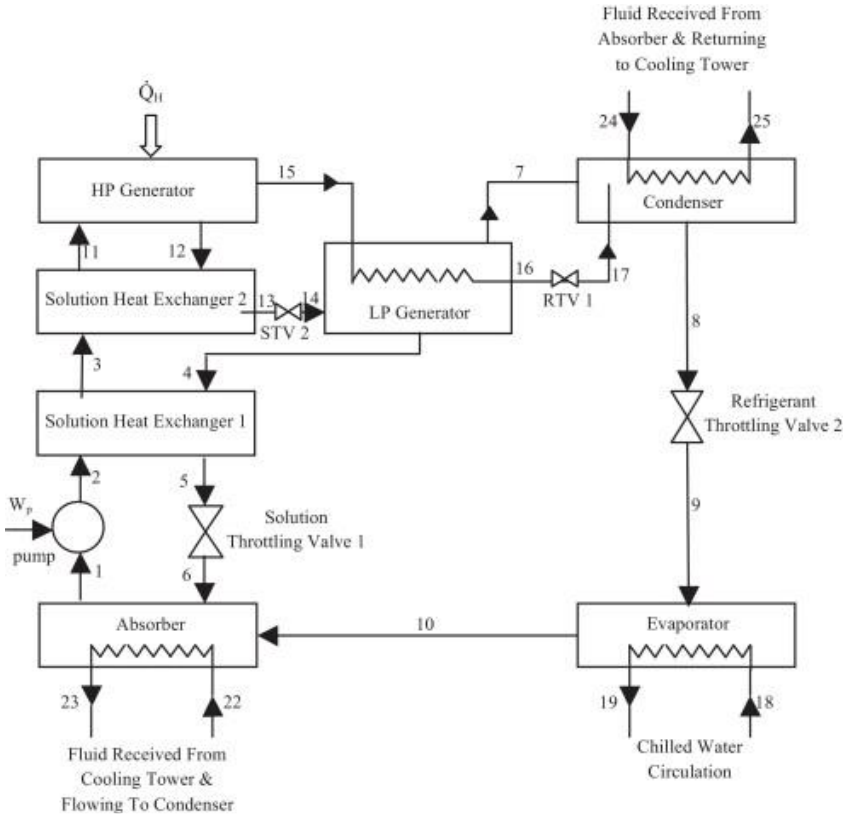

Figure 2.7: Simplified functioning scheme of double-effect absorption chillers [13]

Two heat exchangers (Solution Heat Exchanger 1 and Solution Heat Exchanger 2) are added to increase the energy efficiency of the system: the intermediate and concentrated LiBr solutions reject heat before being laminated through the expansion valve. In this way the diluted solution is partially heated up before entering the HP generator.

Nevertheless, the increase in efficiency achieved by a double-effect absorption chiller implies a higher economic and energy cost: the HP generator, indeed, must be supplied with a higher

temperature external hot source.
Typically, steam or super-heated water at around 150 – 165 °C are used.
As in single-effect absorption chillers, COP isn't much affected by the hot source temperature, while the cooling power increases with that parameter.
Cooling water temperature must be kept under control to guarantee high performances of the system, because it influences the absorption capability of the LiBr solution.

2.5 Cogeneration by Internal Combustion Engines (ICE)

Internal Combustion Engines are the most common typology of cogeneration plant (*Figure 2.2*) in Italy.
Differently from a car engine, these systems work in stationary conditions for many hours in a year, therefore they operate at nominal power as much as possible, in order to achieve the maximum efficiency.
The mechanical power produced by the system of cylinders and pistons, is then transferred, through the motor shaft, to the electric generator that must rotate at constant speed to produce electricity at constant frequency (50 Hz).
ICEs used for cogeneration purposes are not supplied by gasoline that is a too valuable fuel, therefore they are typically fueled by natural gas, provided by the gas network that is well distributed on the national territory. In this case, the adopted thermodynamic cycle is the Otto cycle: the air-fuel mixture is compressed, and a spark-ignition is performed.
In order to use renewable sources, it is also possible to supply the engine with biogas, that can be produced by agricultural and forestry residues, animal manure, organic fraction of wastes and energy crops, but the latter must be carefully analyzed in terms of energy sustainability and the interference with the food supply chain.
Biomasses can also be used to produce vegetable oils that can feed the engine. In this case the air-fuel mixture performs a Diesel cycle, in a compression-ignition engine. The oil must be pre-heated to reduce its viscosity, in order to create the suitable conditions for engine ignition. Even the use of vegetable oils must be carefully analyzed in terms of sustainability, particularly for what concerns the used primary energy sources in the cultivation.
Natural gas is the primary energy source for 99,3 % of CAR Internal Combustion Engines in Italy; they are small or medium size plants (typically between 100 kW_e and 10 MW_e), with an average size of 1 MW_e [5].

Thermal energy in ICE plants is typically recovered by means of 4 heat exchanges with the following circuits:

- Engine cooling water (also called HT, acronym for High Temperature), needed to keep temperature under control in the system, flowing through the jackets of the engine.
- Lubricating oil, needed to reduce friction between engine's moving parts.
- Intercooler, also called Charge Air Cooler, used to cool down the air that is compressed by the turbocharger. The aim of turbocharging is to increase the amount of air trapped within the cylinder in comparison with naturally aspirated engines, to achieve higher power with the same piston displacement. Compressed air must be cooled down, in order to obtain an effective density increase after the compression stage that heats up air. The compressor is driven by a turbine that receives the exhaust gases from the engine.
- Exhaust gases that come off the engine with a relatively large amount of thermal power that can be recovered.

These 4 circuits can transfer heat to a single water circuit, as it is shown in *Figure 2.8,* with the aim of producing hot water at 85 – 90 °C. Alternatively, different energy carriers could be produced by separating the heat exchangers circuits. As an example, super-heated water can be heated up by exhaust gases, thus reducing the difference in temperature between the two fluids and increasing the efficiency of the heat exchanger.

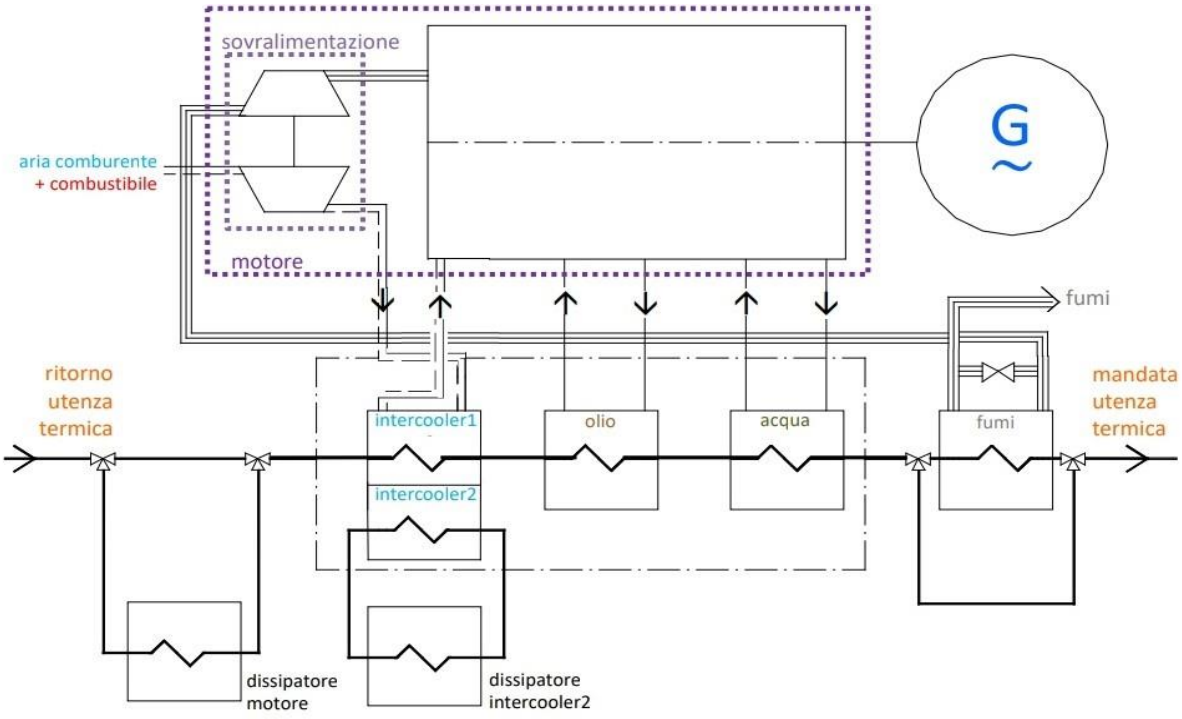

Figure 2.8: Scheme of a cogeneration ICE [12]

The heat exchangers are ordered on the basis of the heat sources temperature: the first one is the intercooler that produces hot water at the lowest temperature level. There are, typically, 2 levels of heat recovery:

- Low temperature (around 45 °C)
- High temperature (around 90 °C)

The high temperature level can be exploited for cogeneration purposes [14].

Lubricating oil and jacket water heat exchangers are located immediately after the intercooler, and they are used to produce hot water at around 85 – 90 °C.

The exhaust gases heat exchanger can heat up water to 90 °C, for example for district heating applications, or can be exploited to produce super-heated water or steam at 150 – 165 °C.

Typical advantages of adopting ICEs for cogeneration are:

- High reliability.
- Relatively low investment cost
- High availability on the market because it is a well-established technology
- High modularity
- High electrical and overall efficiency, also at partial load, therefore high flexibility. Differently from gas turbines that experience a dramatic decrease of the efficiency at partial load, ICEs can operate even at 50 % of nominal load, with an efficiency that is 85 – 90 % of the nominal one.

Disadvantages linked to the use of ICEs are:

- High noise levels
- Vibrations
- Necessity of quite frequent maintenance
- Relatively high pollutant emissions for Diesel engines

3 Fenice S.p.A trigeneration plant in Melfi

3.1 Plant description

The plant that will be analyzed in this work, is a trigeneration plant, owned by Fenice S.p.A (Edison), located in Melfi (PZ) and realized in 2009. It produces electricity, hot water and cold water for industrial purposes and cold water for air conditioning of the production site.
The user of those energy carriers is the division Plastic Components and Modules Automotive (PCMA) of Stellantis group, operating in the same location.

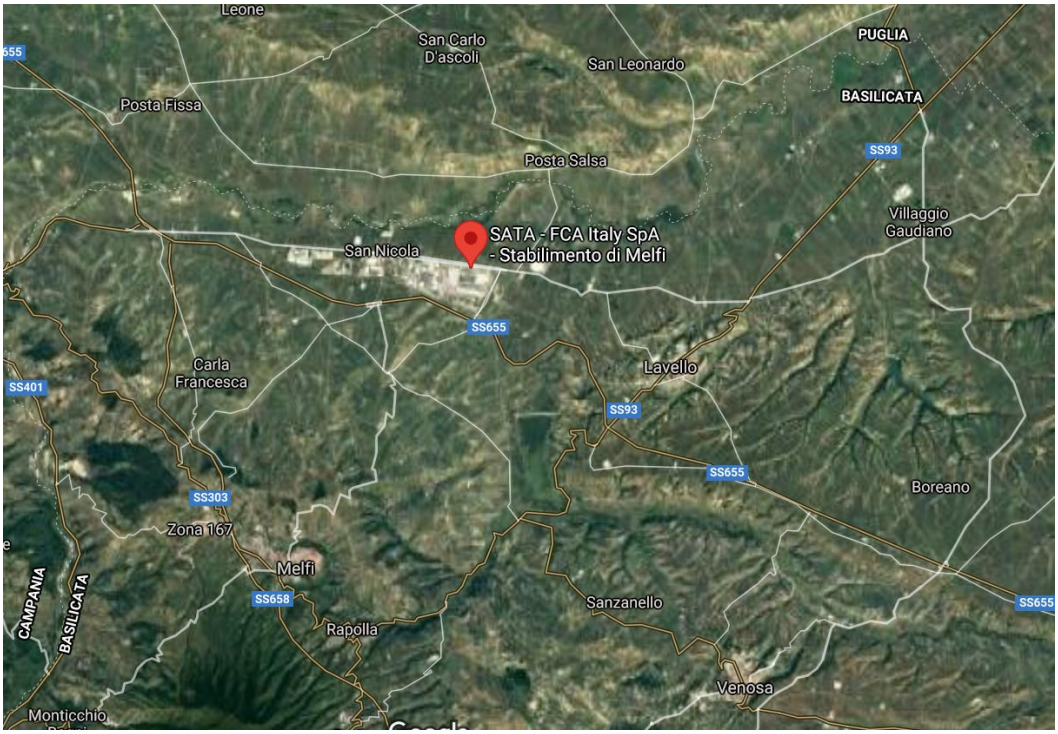

Figure 3.1: Satellite view of the trigeneration plant location

The PCMA productive process includes:

- Injection moulding for bumpers, car dashboards and tires repair;
- Paintings of dashboards and other components;
- Blowing of hollow bodies for fuel tanks;
- Components assembly.

Before 2009, the energy needs of the factory were covered by the national electricity grid that supplied also the electricity needed by the Compression Electric Refrigerator Groups (CERG). The aim of the trigeneration plant was to provide the energy services in order to limit the import of electricity and to make the industrial productive process self-sufficient as much as possible.

In this way, the whole system provides the energy carriers needed to satisfy the energy demand of the factory, at a lower cost with respect to the separate production, and with a reduced environmental impact: indeed, the trigeneration plant allows to exploit the primary energy source, i.e. the fossil fuel, in a highly efficient way, thus achieving a significant energy saving.
The trigeneration plant is composed by an internal combustion engine with an equivalent thermal potential of 11500 kW_{th}, based on the Lower Heating Value of the fuel, that is natural gas. The engine can provide 5120 kW_e, thus with a nominal electrical efficiency of 44,5%. The plant was originally expected to operate about 7000 hours in a year with a Capacity Factor of 0,8.
The internal combustion engine is coupled with a triphase synchronous machine to produce the electricity for the self-consumption. Electrical power is produced at 5 kV; a step-up transformer increases the voltage to 15 kV. The excess electricity is sold on the Medium Voltage electrical grid.
Thermal energy is produced by means of the engine cooling circuit and through a heat recovery generator that exploits the exhaust gases sensible heat to produce both hot water and super-heated water.
The hot water can be sent to the single-effect Water Absorption Refrigerator Group (WARG), with a nominal capacity of 1000 kW_f, or to a heat exchanger, during winter, to produce technological hot water on the secondary circuit. Hot water temperature is increased through a pre-heating in a heat exchanger with the engine cooling circuit (HT circuit) with nominal thermal power around 1000 kW_{th}. Then, water is heated up by exploiting the exhaust gases sensible heat in the temperature drop 180°C – 110°C, that cannot be used to heat up the super-heated water (recovered thermal power around 500 kW_{th}).
Super-heated water is sent to the two double-effect WARG, each of them can provide 1400 kW_f of refrigeration power. The recovered thermal power in the heat recovery section to produce super-heated water is around 2200 kW_{th}.
In addition to that, one CERG of 1322 kW_f and two others electric chiller with nominal power 750 kW_f can provide cold water during the periods of peak power demand.
The total cold water refrigeration power is, therefore 3800 kW_f,
The primary circuit cold water operates with a temperature range 7°C - 12°C.
The plant was programmed to operate 24 hours per day, with a stop of 1 day during the week, to perform the ordinary and preventive maintenance, during which the energy needs are covered by the national electrical grid for both electricity and cold power through electrical chillers.

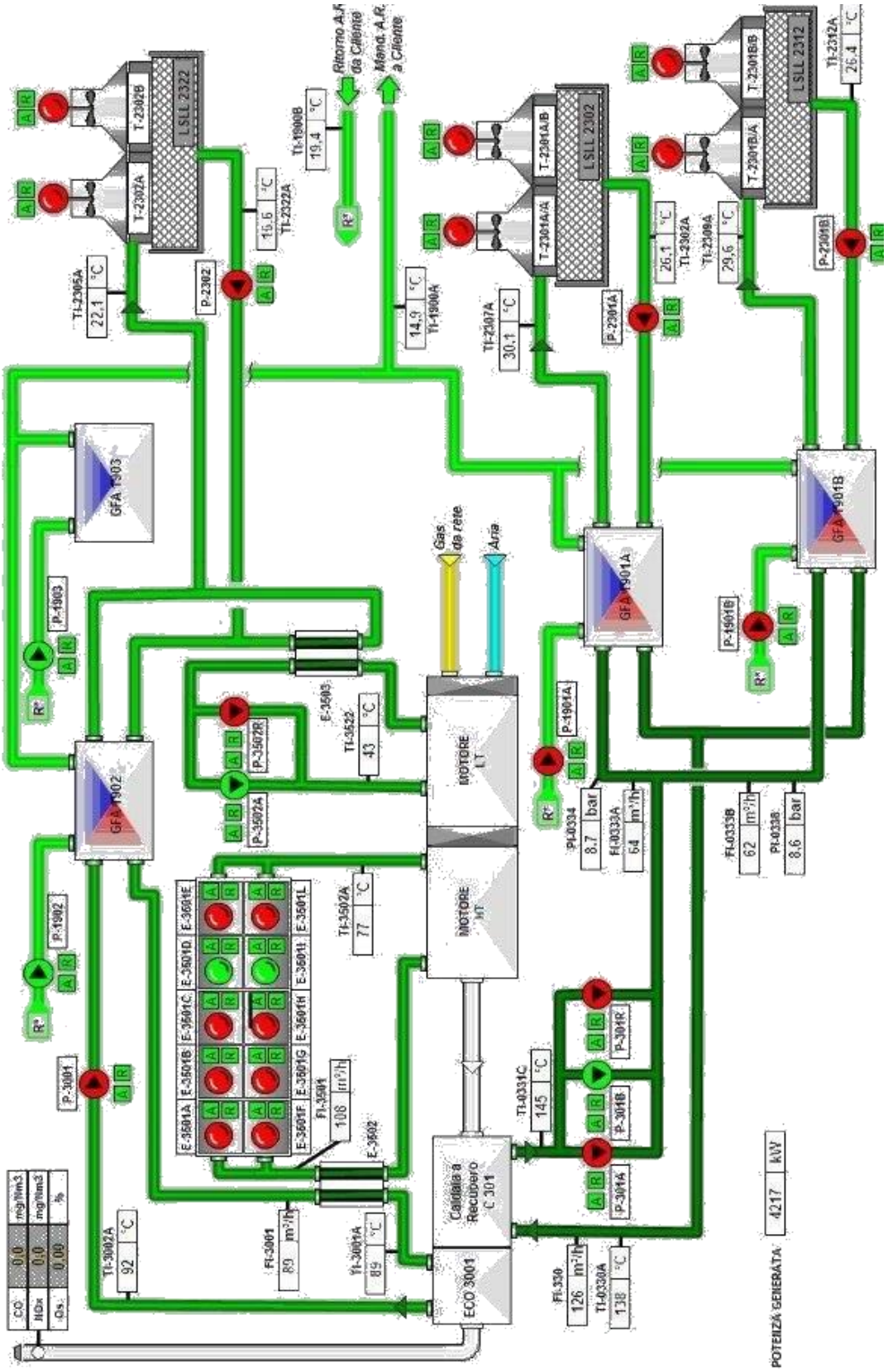

Figure 3.2: Simplified scheme of the energy plant process [16]

Figure 3.2 shows the simplified process scheme of the plant. Air is aspirated from the external environment (light-blue arrow) and enters the ICE together with natural gas.

The engine is virtually divided in two sections, according to the distinction of the two water cooling circuits:

- LT portion, where cooling water is needed to remove heat from the Charge Air Cooler and from the lubricating oil circuit
- HT portion, in which useful thermal power is produced by means of the engine jacket water that keeps under control the temperature of the engine's mechanical parts

On the left, by following the path of exhaust gases, there is the heat recovery section. The first portion is aimed at heating up super-heated water that supplies the two double-effects WARG located on the bottom of the scheme. Super-heated water circuit is the dark-green circuit in *Figure 3.2*. The downstream part of the heat recovery section is the economizer that heats up hot water from around 88 °C to 92 °C. Hot water is previously heated up from 80 °C to 88 °C (design condition) by the HT circuit through the heat exchanger E-3502.

Then, the exhaust gases that have been cooled down are released to the external environment.

On the right there are the three cooling tower that rejects heat to the external environment: two of them have a nominal power of 2600 kW and they remove thermal power from the cooling water circuits of double-effect WARG.

The third one releases to the external environment both the thermal power coming from the cooling water circuit of the single-effect WARG and the heat that is removed from the engine LT water circuit. This cooling tower is dimensioned to reject 3900 kW of thermal power.

The top-left absorption chiller in *Figure 3.2* is supplied by hot water, while the top-right refrigerator is the 1322 kW_f electric chiller (CERG).

The process scheme in *Figure 3.2* is aimed at showing the working principle of the plant and the supply circuits to the absorption chillers, nevertheless, the path of the produced cold water and hot water towards the final user are omitted.

3.2 Original design technical specifications

The Melfi trigeneration plant was originally dimensioned on the basis of the consumption data provided by the industrial user.

The expected annual energy consumption for the years beyond 2010 are resumed in *Table 3.1*.

Energy carrier	Unit of Measurement	Absolute value
Electricity	MWh	25’000
Cold Water	MWh	24’500
Natural gas	Sm^3	8’400’000

Table 3.1: PCMA expected energy consumption

In the original project, the production of hot water was aimed only at supplying the hot water WARG, thus no consumption of direct thermal power is reported in technical specifications.

The amount of electricity that the ICE was expected to produce can be easily calculated by multiplying the electric motor nominal power times the number of hours of operation:

$$E_{el} = P_{el} \cdot hours\ of\ operation = 5120\ kW\ \cdot 7000\ h\ \cong 35'000\ MWh$$

This amount of electrical energy is sufficient to cover the needs of the productive process and the excess electricity is exported to the Medium Voltage grid.

3.2.1 Natural gas

The installation of the plant made necessary a modification of the previous methane distribution circuit to the industrial user and also the installation of new components for the supply line of the ICE.

A new Reduction and Metering (REMI) Station was installed near to the already existing one that continued to supply natural gas to the user at a relative pressure of 2 barg. The new REMI station was dimensioned for reducing gas pressure to 5 barg and allowing a nominal volume flow rate of 1200 Sm^3/h, and a maximum flow rate of 1700 Sm^3/h.

A new filtering and metering station, a remote reading system and a new pipeline for the supply of natural gas to the ICE were installed. The technical parameters of the gas pipeline are:

- Length = 30 m
- Relative working pressure = 5 barg

- Nominal volume flow rate = 1200 Sm^3/h
- Pipeline diameter = DN80
- Maximum pressure drop = 0,2 bar

3.2.2 Internal Combustion Engine

The Internal Combustion Engine is manufactured by Rolls Royce. It is supplied by a standard volume flow rate of natural gas equal to 1200 Sm^3/h, which pressure is reduced in the REMI station from 12 barg to 5 barg. The engine is composed of 12 cylinders, arranged in a V configuration; the natural gas performs an Otto cycle. Air is not naturally aspirated; a turbocharger allows to maximize the ICE power.

The engine is equipped with several additional circuits:

- LT cooling water circuit
- HT cooling water circuit
- Lubricating oil circuit
- Natural gas supply line
- Compressed air line at 30 bar for engine start-up phases
- Compressed air line at 7 bar for the instrumentation
- Exhaust gases line

The ICE is provided with a control panel connected to PLC (Programmable Logic Controller) to keep under control the operating parameters.

The inlet air system is equipped with filters, mufflers and supply fans with inverters. The exhaust gases line is provided with a double mufflers system to reduce sound emissions.

Engine start-up time until stationary conditions is around 15 minutes.

Inlet and outlet engine flows design conditions are reported in the following tables:

- Natural gas

Flow Rate	Flow Rate	Pressure	Temperature
1200 Sm^3/h	28’800 Sm^3/day	6 bar	15 °C

Table 3.2: Natural gas inlet flow design conditions

- Inlet combustion air

Flow Rate	Flow Rate	Pressure	Temperature
30’271 kg/h	726’494 kg/day	1 bar	15 °C
23’429 Nm^3/h	562’302 Nm^3/day		

Table 3.3: Inlet combustion air design conditions

- Exhaust gases

Flow Rate	Flow Rate	Pressure	Temperature	% v/v O_2
31’185 kg/h	748’440 kg/day	1,1 bar	410 °C	10,7 %
24’802 Nm^3/h	595’246 Nm^3/day			

Table 3.4: Exhaust gases design parameters

The engine is equipped with a “Lean-Burn” combustion control system and with a catalytic converter, to reduce, respectively, the NO_x and the CO emissions.
In *Table 3.5*, the engine’s emissions in stationary conditions are reported.

Pollutant	ICE concentration
NO_x	300 mg/Nm^3
CO	300 mg/Nm^3

Table 3.5: Pollutant concentration in exhaust gases

Pollutants concentration in *Table 3.5* are referred to 5 % O_2 in exhaust gases. The values of emissions of the analyzed ICE are lower than the limits prescribed by regulations.
Low emissions are released to the external environment thanks to Lean Burn combustion technology and to a catalytic oxidant positioned upstream to the exhaust pipe.
The control of combustion parameters with Lean Burn technology allows to minimize mis-firing events, thus reducing the formation of Unburned Hydrocarbons, NO_x and CO.
Lean Burn Gas Engines operate with lean air-fuel mixture, therefore NO_x formation is inhibited due to a lower temperature in the combustion chamber.
These types of engines can extend the limit of mis-firing events to an air excess ratio around

1,8, instead of 1,3 of others spark ignition engines, allowing to obtain higher efficiencies, as it is shown in *Figure 3.3.*

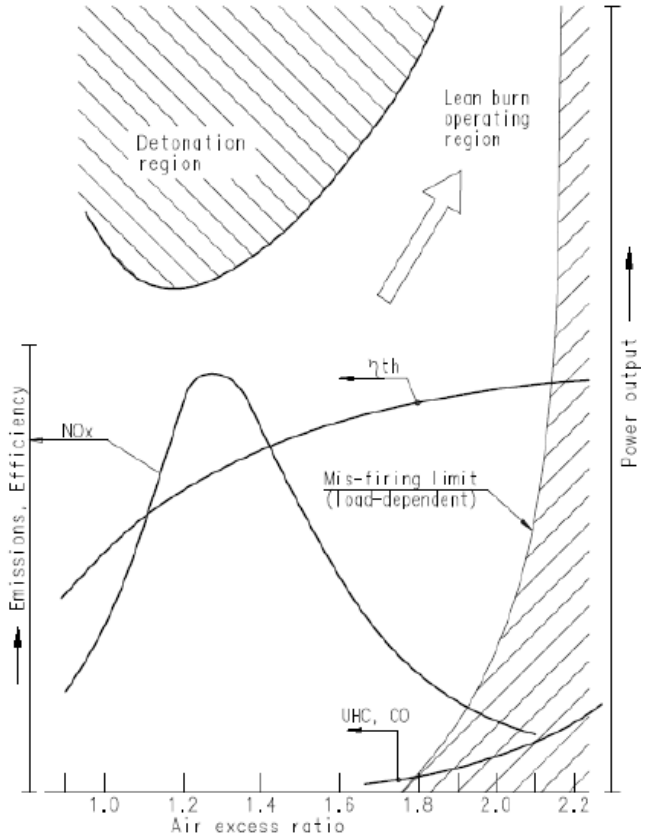

Figure 3.3: Engine performance curves as function of air-excess ratio [16]

By considering a Standard Density (15 °C and 1,013 bar) of natural gas equal to 0,68 kg/Sm^3

$$\dot{m}_{gas} = 0{,}68 \cdot 1200 = 816\ kg/h$$

The stoichiometric air-to-fuel mass ratio is around 17,2; the air-excess ratio of the 5120 kW_e can be calculated as follows:

$$Air\ to\ fuel\ Ratio = \frac{30'271\ kg/h}{816\ kg/h} \cong 37{,}1$$

$$Air\ excess\ Ratio = \frac{37{,}1}{17{,}2} \cong 2{,}2$$

Therefore, the amount of air forced into the engine is more than twice the stoichiometric quantity.

Air is aspirated by means of the turbocompressor, then it passes through the Charge Air Cooler heat exchangers and enters the engine. Air pressure is regulated by a Variable Geometry Turbine and the flow rate is controlled by a butterfly valve in order to optimize the amount of air inside the cylinders during the start-up and partial load phases.

A mechanical valve regulates the injection of gas to obtain a lean mixture with air. When the pressure in the cylinder is low, gas is injected inside a pre-chamber. The control is performed by the ECC (Engine Control Cabinet). During the compression phase, the lean mixture present in the cylinder is partially pushed into the pre-chamber where it is mixed with pure gas, thus creating a rich mixture that is easily ignited by the spark. In this way a complete combustion of the mixture in the cylinder is achieved.

The engine's operating parameters, like the gas pressure in the pre-chamber, the air-to fuel ratio, injection timing and the regulation of the valves position, are controlled and optimized by the ECC.

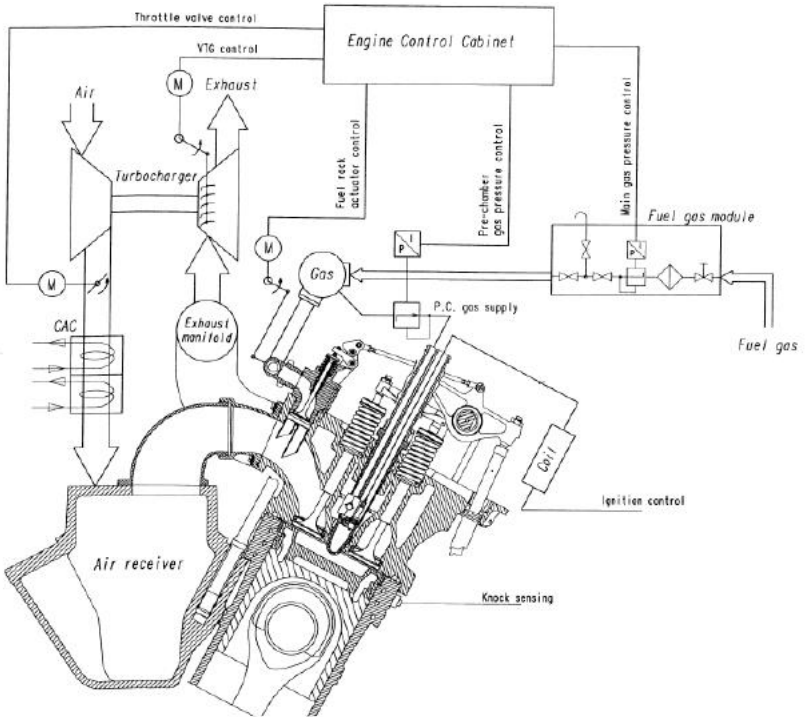

Figure 3.4: Lean Burn Gas Engine operating principle [16]

3.2.3 Heat Recovery Unit

The Heat Recovery Unit (HRU) receives exhaust gases from the ICE and transfers heat to super-heated water (SHW) and to hot water (HW).

The HRU is dimensioned for maximum recovery of thermal power from the exhausts, thus obtaining an outlet water temperature as high as possible.

A by-pass valve allows to send the exhausts directly to the chimney, in the case the HRU is not available.

HRU steady-state conditions are reached after around 1 hour of operation.

Three fluids are involved in HRU heat transfers; their parameters are reported in *Table 3.6*

Fluid	Flow Rate	Temperature IN	Temperature OUT
Exhaust gases	31’185 kg/h	410 °C	110 °C
Super-Heated Water	129’000 kg/h	150 °C	165 °C
Hot Water	109’000 kg/h	88 °C	92 °C

Table 3.6: HRU fluids design parameters

3.2.4 Cold Water Production Unit

As it was already pointed out, this trigeneration plant is equipped with three WARG: two of them are double-effect water absorber refrigerators and they are supplied with superheated water; their nominal power is 1400 kW_f. The third one is a single-effect WARG that exploits the hot water produced in the heat recovery unit to produce 1000 kW_f.
Nameplate data of the refrigerators are reported in *Table 3.7*

Parameter	U.M.	Single Effect WARG	Double Effect WARG
Chilled Water			
Volume Flow Rate	m^3/h	171	240
Inlet Temperature	°C	12	12
Outlet Temperature	°C	7	7
Pressure	bar	4	4
Power	kW_f	1000	1400
Refrigerating Water			
Volume Flow Rate	m^3/h	350	346
Inlet Temperature	°C	30	30
Outlet Temperature	°C	35,8	36,3
Pressure	bar	5	5
Power	kW_f	2322	2517

Hot Water			
Volume Flow Rate	m^3/h	98	68,7
Inlet Temperature	°C	92	165
Outlet Temperature	°C	80	150
Power	kW_f	1322	1117
COP	/	0,756	1,25
Partial Load	%	30	30

Table 3.7: WARG nameplate data

3.3 Current Plant Configuration

In this paragraph, the plant configuration will be analyzed, by considering the energy vector inputs to the trigeneration plant and the outputs delivered to the customer.
Particular attention will be given to the main hydraulic circuits, useful for heat recovery and to produce cold power.
Energy carriers provided to the Stellantis factory are:

- Electricity
- Technological Cold Water for the press unit
- Technological Cold Water for painting Air Treatment Unit (ATU), added in 2016
- Technological Hot Water for painting ATU, added in 2016
- Cold Water for the air conditioning of the production site, added in 2016

Technological Water for painting ATU is a seasonal energy carrier, thus hot water is provided in cold seasons while cold water is supplied to the industrial customer during summer.
Even the cold water for air conditioning, is a seasonal energy carrier that is supplied only during summer.
A simplified scheme of the energy production process with some useful temperatures and volume flow rate is showed in *Figure 3.5*.

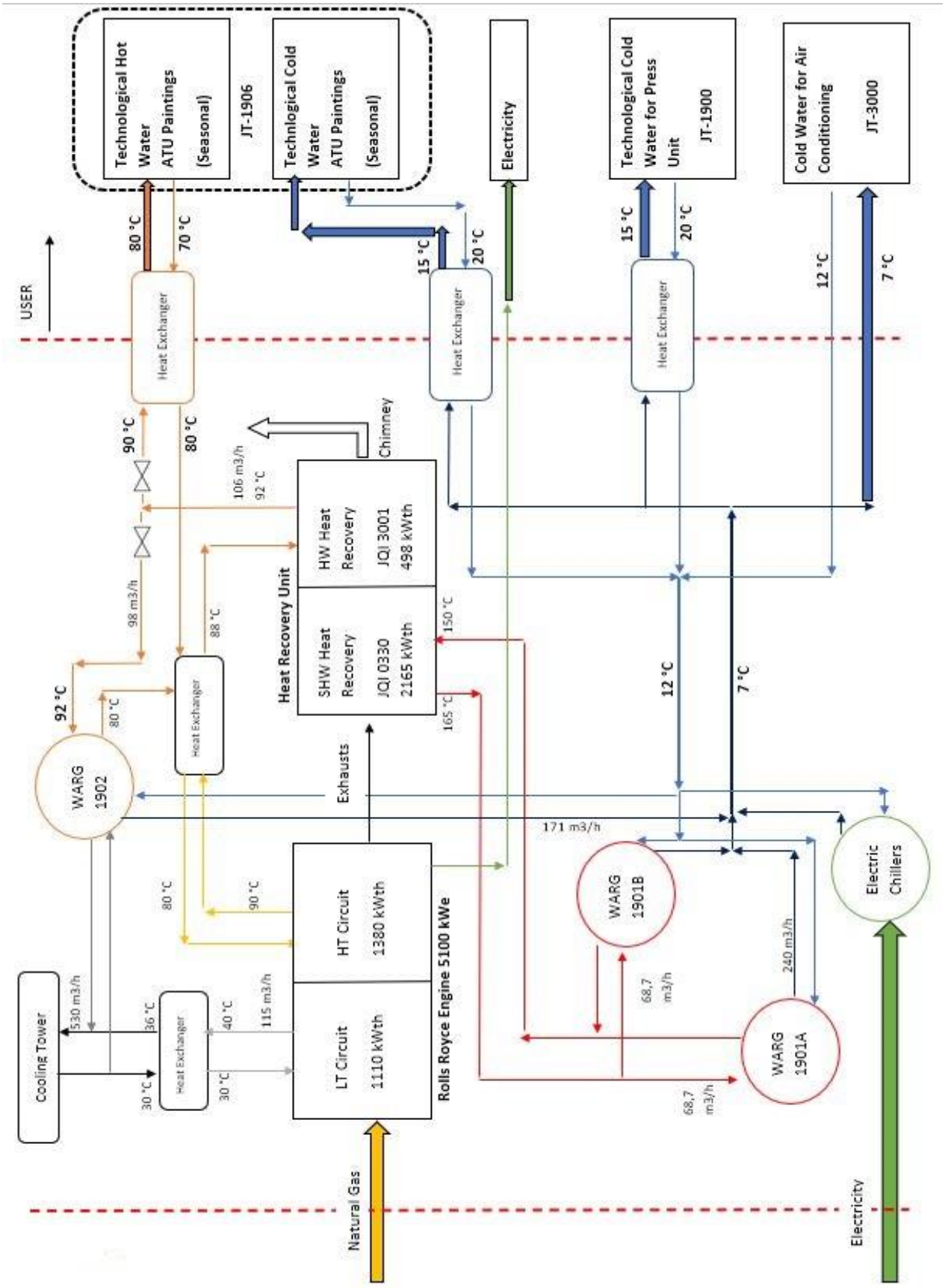

Figure 3.5: Simplified scheme of the energy production plant

The tags reported in *Figure 3.5* correspond to those that are used in the Online Data Collector. The red dashed line corresponds to the boundary of the energy plant, beyond which there is the industrial customer area of responsibility.

The LT water circuit recovers, respectively, 515 kW_{th} from the Intercooler 2nd stage and 595 kW_{th} from the lubricating oil circuit (Heat Exchanger E-3504). This thermal power is then rejected to the external environment by means of one cooling tower.

LT water circuit exchanges heat with the cooling water through the Heat Exchanger E-3503 (nominal power 1200 kW_{th}).

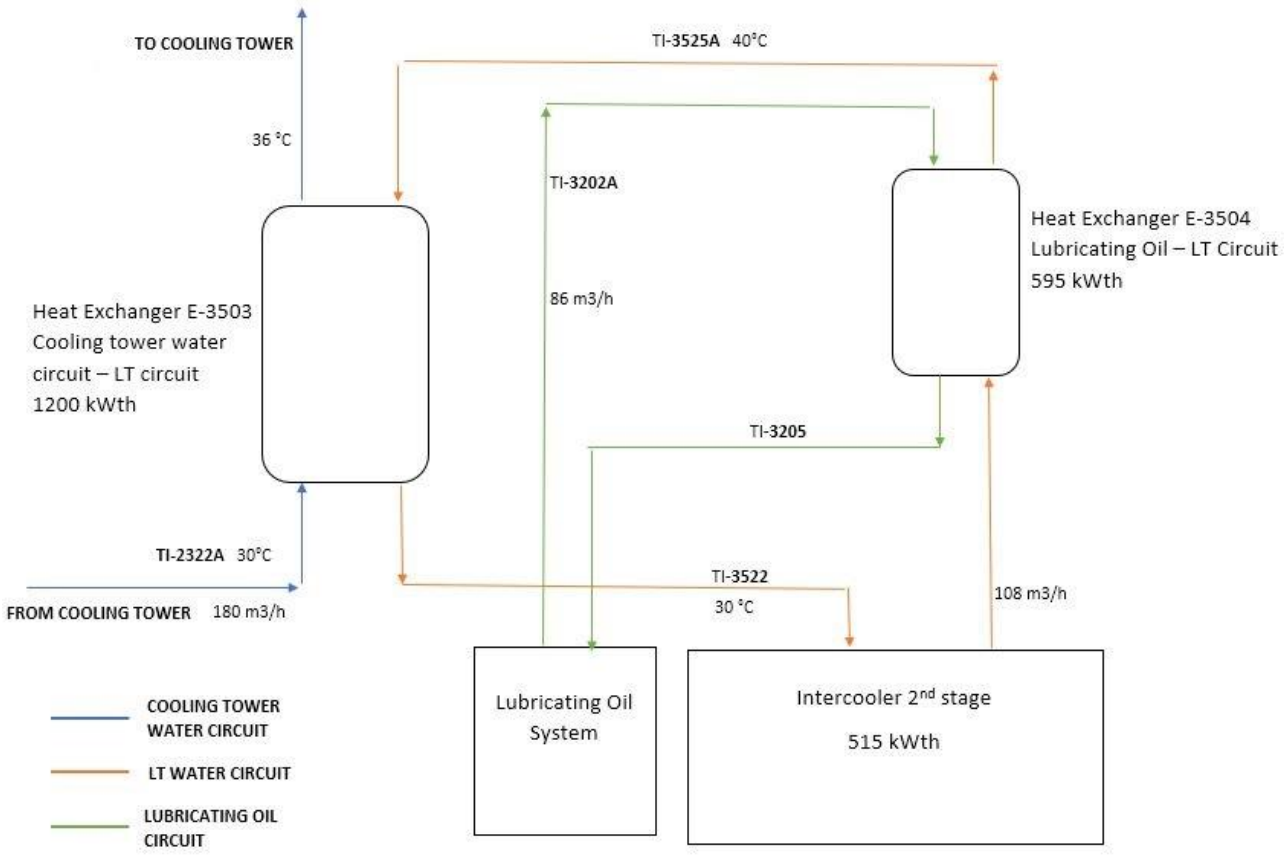

Figure 3.6: Schematic of LT water circuit heat exchanges

HT circuit water recovers 725 kW_{th} by recovering the heat of the engine (jacket water cooler) and 655 kW_{th} from the 1st stage of the Intercooler, with a total of 1380 kW_{th} heat recovery.

Then 1004 kW_{th} are delivered to the Hot Water circuit that is heated up to 88 °C (from 80 °C), while the remaining thermal power is dissipated to the external environment by means of the Heat Exchanger E-3501 (Air Cooler), with nominal power 1588 kW_{th}.

This allows to reject heat also during partial load conditions, when the Hot Water circuit is stopped.

Double-effect WARGs cooling towers are not shown in *Figure 3.5*.

Technological Cold Water for the press unit of the production site is supplied almost constantly during the year.

Cold water produced by WARGs is sent to a cold water collector, and then it is supplied to a Heat Exchanger that is useful to decouple the primary and the secondary water circuits.

Primary circuit cold water temperatures are 7 °C – 12 °C, while secondary circuit cold water temperatures are 20 °C – 15 °C.A detachment of the primary circuit cold water is sent to the production site for its air conditioning. However, the priority is given to the technological cold water supply. This means that water flow rate regulation is performed by means of a motorized valve that receives as an input the cold water temperature on the secondary circuit (water supplied to the press unit).

A setpoint value is imposed on that temperature and, if it is exceeded, the valve reduces the water flow rate to the air conditioning service.

Therefore, the cold water supply for technological purposes must be preserved.

Measurements of the energy delivered to the customer are performed on the secondary circuits in the case of:

- Technological Hot Water for painting ATU (JT-1906 Hot)
- Technological Cold Water for painting ATU (JT-1906 Cold)
- Technological Cold Water for the press unit (JT-1900)

In the case of Cold Water for air conditioning (JT-3000), the secondary circuit doesn't exist, so measurements are performed on the primary circuits.

The black dashed rectangle highlights the area of the painting ATU, with the two different energy vectors (hot water and cold water) that are never provided simultaneously. Indeed, the tag JT-1906 underlines that it is the same water circuit.

The hot water can alternatively be supplied to the single-effect WARG or to the painting ATU. In some cases, a partialization of the hot water flow rate can be set by means of the valves: in this condition, a portion of the flow rate is sent to the WARG and the remaining part is supplied to the painting ATU.

A simple representation of the various water circuits for the painting ATU service is visualized in *Figure 3.7*.

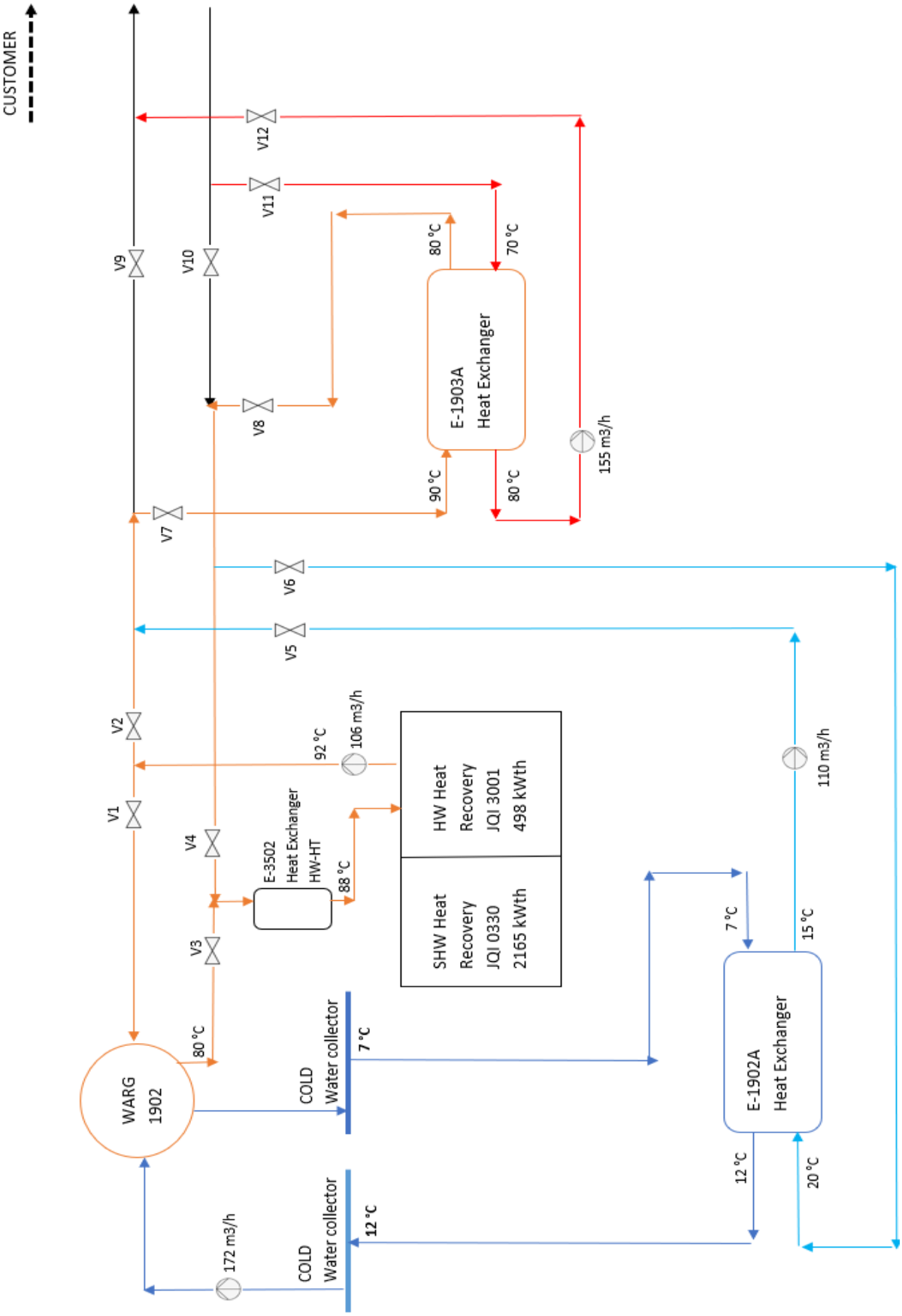

Figure 3.7: Scheme of painting ATU water supply

During the cold seasons, the hot water produced in the HRU is exploited to supply thermal power to the industrial customer.

Therefore, valve V1 and valve V3 are closed because no water flow rate is provided to the single-effect WARG (1902), while valves V2 and V4 are open. Then, hot water is sent to the decoupling heat exchanger E-1903A, so that thermal power is recovered by the hot water secondary circuit, that is supplied to the customer. In this case, valves V7 and V8 on the primary circuit and valves V11 and V12 on the secondary circuit are kept open. The remaining valves (V5, V6, V9, V10) are closed.

Temperature drop on the primary side, across Heat Exchanger E-1903A is 90 °C – 80 °C, while on the secondary circuit, hot water is heated up from 70 °C to 80 °C.

On the contrary, when cold water energy demand must be covered, hot water is supplied to the single-effect WARG. Cold water is produced at 7 °C and it is sent to the plant cold water collector. Then, it is supplied to the decoupling Heat Exchanger E-1902A, where primary circuit water is heated up (from 7 °C to 12 °C), while the secondary circuit cold water is cooled down from 20 °C to 15 °C, thus with a temperature drop of 5 °C.

Cold water is sent to the painting ATU by opening valves V5 and V9, and, on the return side, valves V6 and V10.

In *Figure 3.5*, the electric chillers (CERG) are indicated with a green circle; they produce cold water during peak periods or when one of the WARGs is under maintenance.

In conclusion, if this trigeneration plant was represented as a black box, the inputs would be:

- Natural Gas
- Electricity

While the outputs:

- Electricity
- 1 stream of Hot Water
- 3 streams of Cold Water

4. Data analysis

A data analysis is necessary to evaluate the operating conditions of the trigeneration plant.
All the data have been extracted from the online Data Collector for the specific production plant.
The analysis has been performed on different years of operation of the plant, in order to understand in a clearer way, the evolution of the energy demand from the Stellantis factory and the efficiency during time of the energy plant.
The trigeneration plant configuration has undergone some renovations during the years: for example, new energy services are provided to the customer since 2016. For this reason, the various data available for 2015 and previous years have not been considered in this work.
Nevertheless, also the data for the year 2016 are not complete and many fundamental information useful to evaluate the plant operation are missing, therefore only four years of operation (2017, 2018, 2019, 2020) can be considered for this analysis.
In addition to that, by analyzing the plant operation during 2020, it is important to consider that the Covid-19 global pandemic heavily affected the productivity of the industrial sector because of the lockdown. During that period (9 March 2020 – 3 May 2020), the plant was stopped, thus the energy consumption and production trends must be neglected for that year.

4.1 Rolls Royce Engine

All the available data from the Online Data Collector have been organized so to distinguish between the various components and the different water circuits in the plant.
As it was already mentioned, the nominal natural gas flow rate is around 1200 Sm^3/h. This input gas flow rate should correspond to a generated electric power equal to 5100 kW_e.
The following graphs, realized by means of data extracted from the Data Collector, show, as expected, a clear correspondence between the gas flow rate and the generated electric power during two different weeks of the year 2018. In particular, *Figure 4.1* is referred to a typical winter week (from 21st January to 28th January), while *Figure 4.2* shows the above-mentioned trend during a summer week (from 15th July to 22nd July).
In both cases, a sudden drop in generated electricity is clearly visible on 21st January and on 15th July. That's because during Sunday, the industrial user factory is stopped.

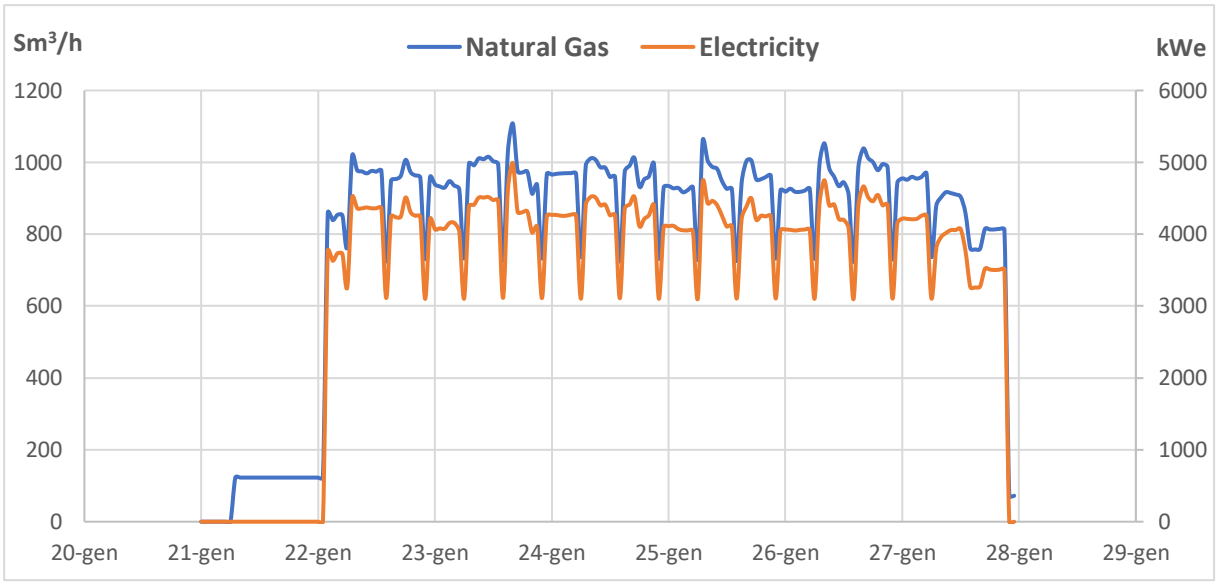

Figure 4.1: Trend correspondence between input natural gas and generated electricity during a winter week

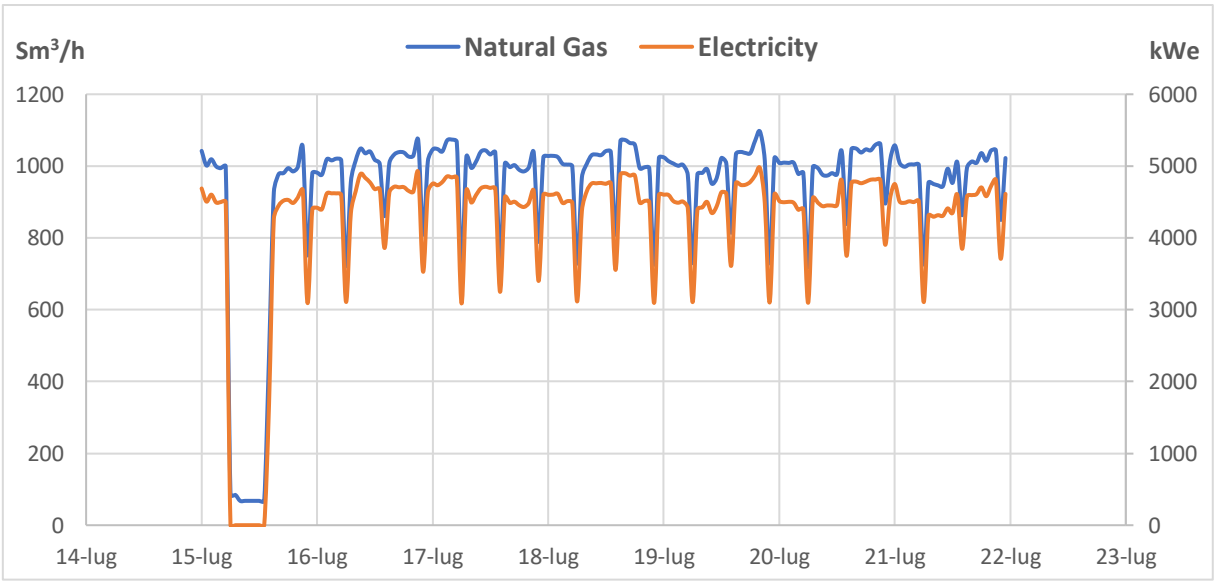

Figure 4.2: Trend correspondence between input natural gas and generated electricity during a summer week

Generated electricity is quite constant during a week, except for Sundays. This is highlighted in *Figure 4.3* that shows the mean active power for each day during a week.

The mean value has been calculated by neglecting the hourly values at 06:00, at 14:00 and at 22:00, because the shift change of the factory workers implies a reduction in productivity that could affect the truthfulness of the mean value of generated electricity in a day.

The generator active power oscillates between 4500 kW_e and 5000 kW_e from Monday to Saturday, thus between 90% and 100% of nominal power. These values are extracted from a random week in 2018, in particular, data are referred to days from 8th to 14th of July.

Weekdays are numbered from 1 (that corresponds to Monday) to 7 (corresponds to Sunday).

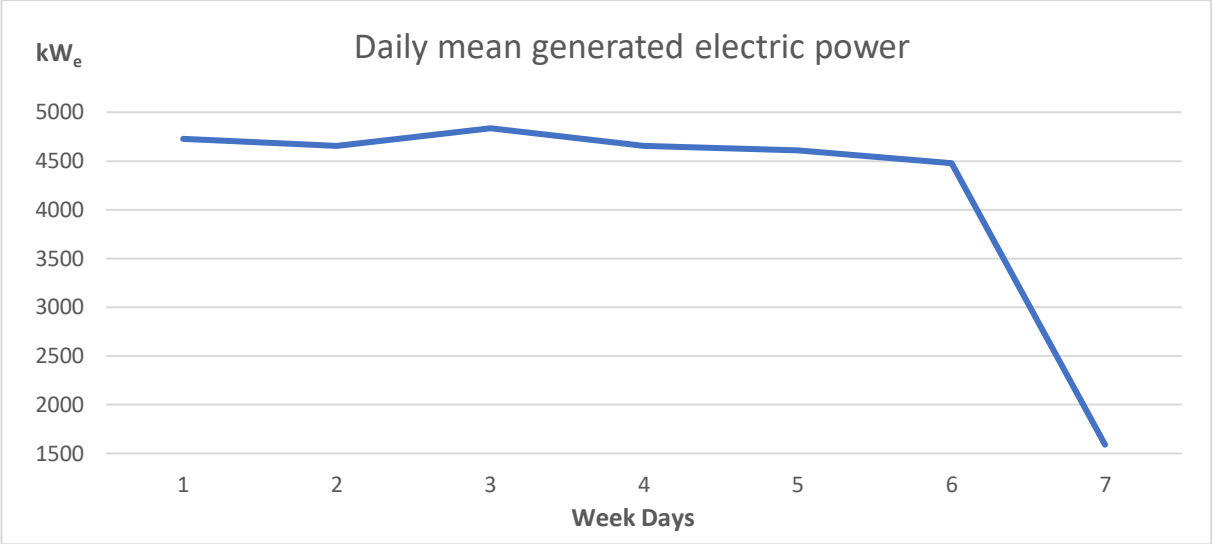

Figure 4.3: Daily mean value of engine electric power during a week (8th-14th July 2018)

In order to visualize in a clearer way the correspondence between the input power from natural gas and the generated active power, a $\dot{F}$ *vs* P_{el} graph has been plotted for each year (from 2017 to 2019).

$\dot{F}$ has been calculated by calculating the monthly mean value of natural gas Lower Heating Value, starting from the daily records provided by the gas distributor (SNAM) report.

Figure 4.4 and *Figure 4.5* show the $\dot{F}$ *vs* P_{el} graph for years 2018 and 2019, respectively.

On the x-axis it is represented the active power from the generator P_{el}, while on the y-axis the natural gas input power $\dot{F}$ has been set.

Each blue dot on the graph represents a mean daily operating condition of the engine. A denser point cloud is present in the top-right area of the graph, thus at almost nominal power (5100 kW_e generated electricity and 11'500 kW_{th} natural gas input power).

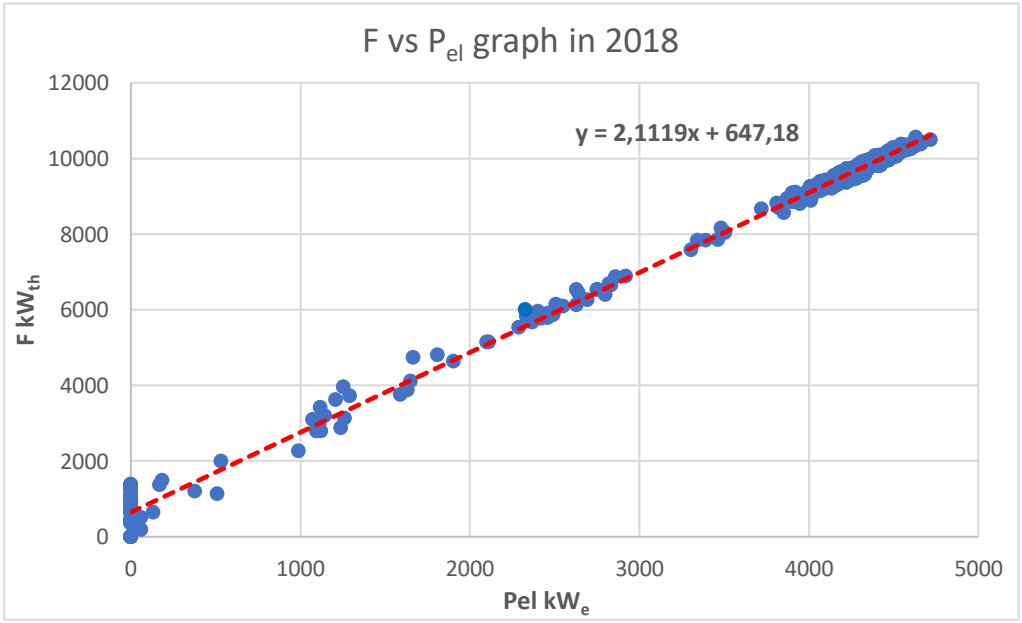

Figure 4.4: Natural gas input power vs Generated electricity on daily basis in 2018

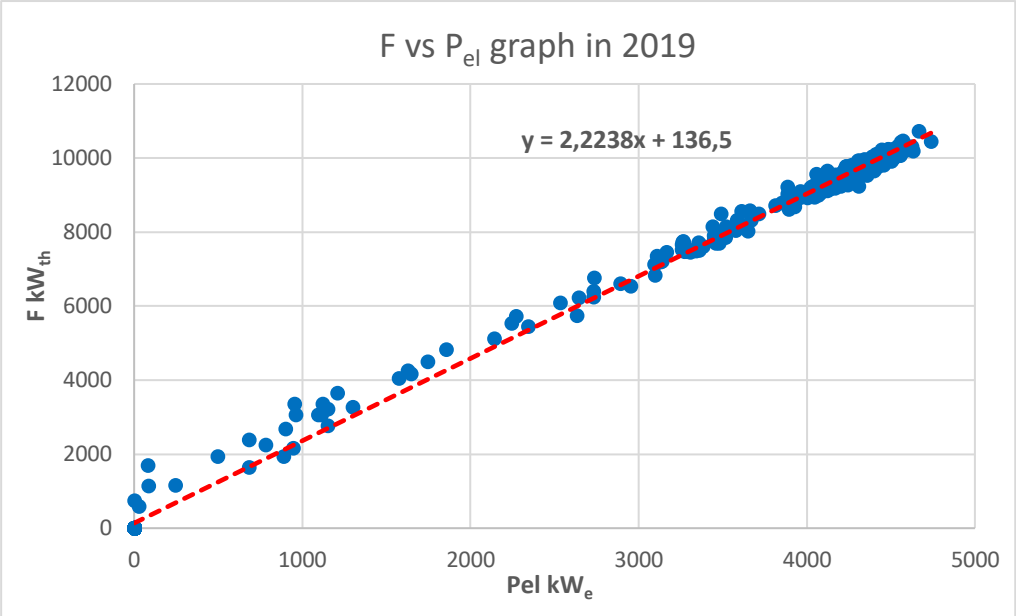

Figure 4.5: Natural gas input power vs Generated electricity on daily basis in 2019

A linear trend of the engine operating conditions is clearly visible in both representations, and it is underlined by the red dotted trend line. The equations of the two trend lines are shown in both graphs.

In 2018, the engine operating conditions can be resumed by the equation:

$$y = 2{,}1119x + 647{,}18$$

While, in 2019 the linear trend is:

$$y = 2{,}2238x + 136{,}5$$

In 2017, it was impossible to immediately plot a similar graph because of missing generated active power data in the period between 1st January and 30th June, thus, the electricity data are not available for the first half of the year.

Therefore, it was necessary to perform a data processing in order to analyze the engine operating conditions during the first six months of the year.

Starting from the natural gas mass flow rate data, the generated active power has been calculated. The 2018 and 2019 linear trend equations have been arithmetically averaged, obtaining the following equation:

$$y = 2{,}1678x + 391{,}84$$

Starting from this equation, an ideal generated electric power (the x variable) has been calculated for every operating hour of the six months with unavailable data.

Then, daily mean values were calculated to obtain 365 dots, each representing one day of operating conditions, so to plot a similar graph to those shown for years 2018 and 2019.

The processing results can be visualized in *Figure 4.6*.

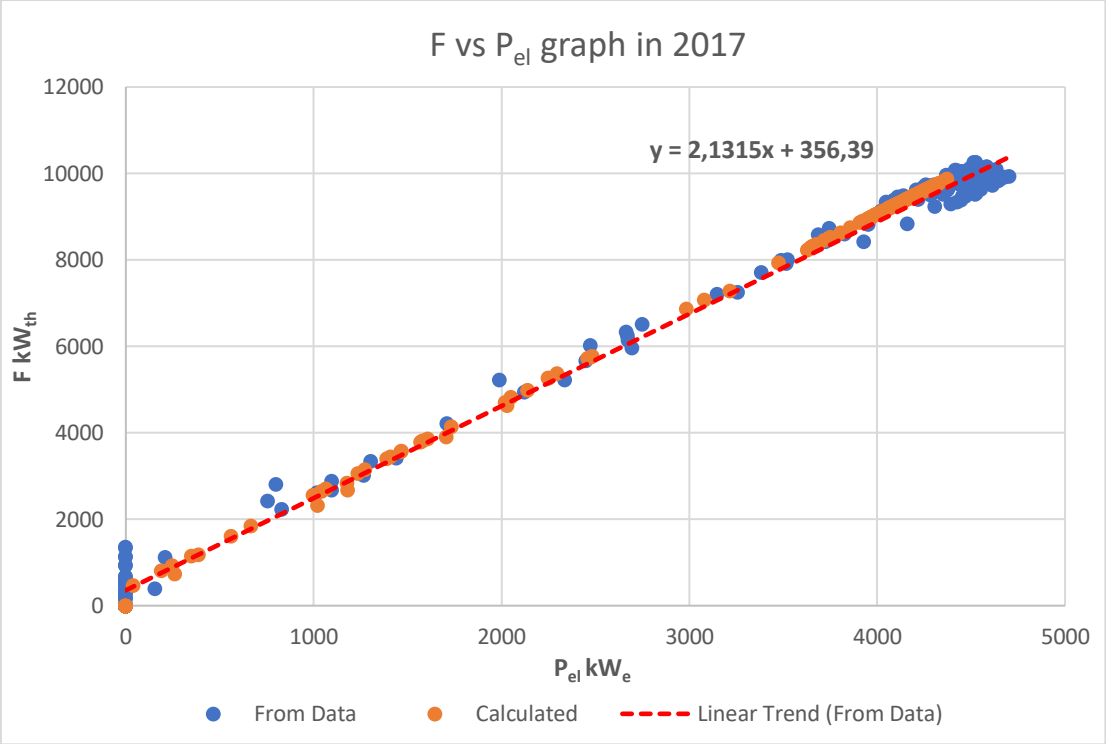

Figure 4.6: Natural gas input power vs Generated electricity on daily basis in 2017

Orange dots are referred to ideal conditions, following the aforementioned linear trend equation calculated by averaging the two equations obtained for the years 2018 and 2019.

Blue dots represent real engine working conditions, extracted from the Data Collector.

The linear equation shown in *Figure 4.6* is referred to the red dotted line, that has been calculated for blue points extracted from data.

It is possible to notice that engine working conditions follow almost the same trend in the three years of analysis. Indeed, the orange dots that have been obtained by averaging 2018 and 2019 engine operating conditions overlap the blue dots with a very similar trend.

Moreover, the linear equation obtained for the last six months of 2017 ($y = 2{,}1315x + 356{,}39$) is comparable to the 2018 and 2019 average.

It is interesting to notice that in all three years, the intercept on the y-axis is not at 0. This is due to a small gas consumption even when no electric power is produced, in order to run auxiliaries and to be immediately available to produce power when it is requested.

Another important parameter to evaluate the engine working conditions is the electrical efficiency evolution during time.

Engine datasheet provides a nominal electrical efficiency near 45 %.

In order to evaluate the proper functioning of the engine, the efficiency has been calculated for every year of analysis, on an hourly and daily basis. *Figure 4.7*, *4.8* and *4.9* represent the variation of electrical efficiency as a function of engine active power, on a daily basis.

For 2017, electrical efficiency has been calculated only for the last six months because of the unavailability of real data about the generated electrical power.

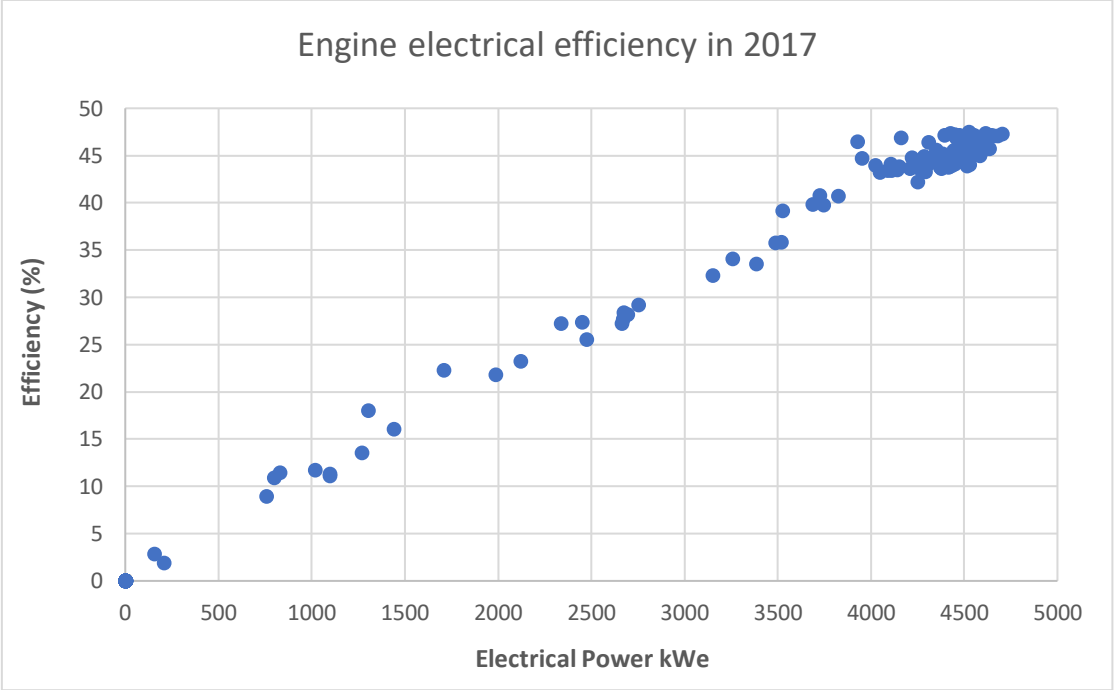

Figure 4.7: Engine electrical efficiency vs Generated electrical power in 2017 (daily)

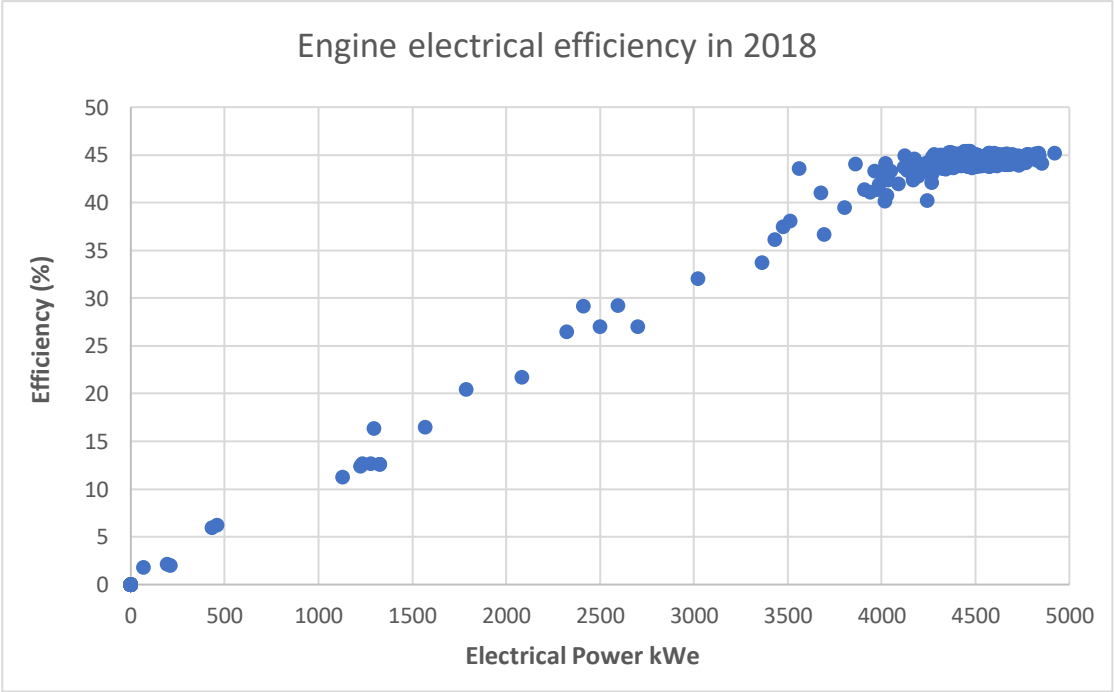

Figure 4.8: Engine electrical efficiency vs Generated electrical power in 2018 (daily)

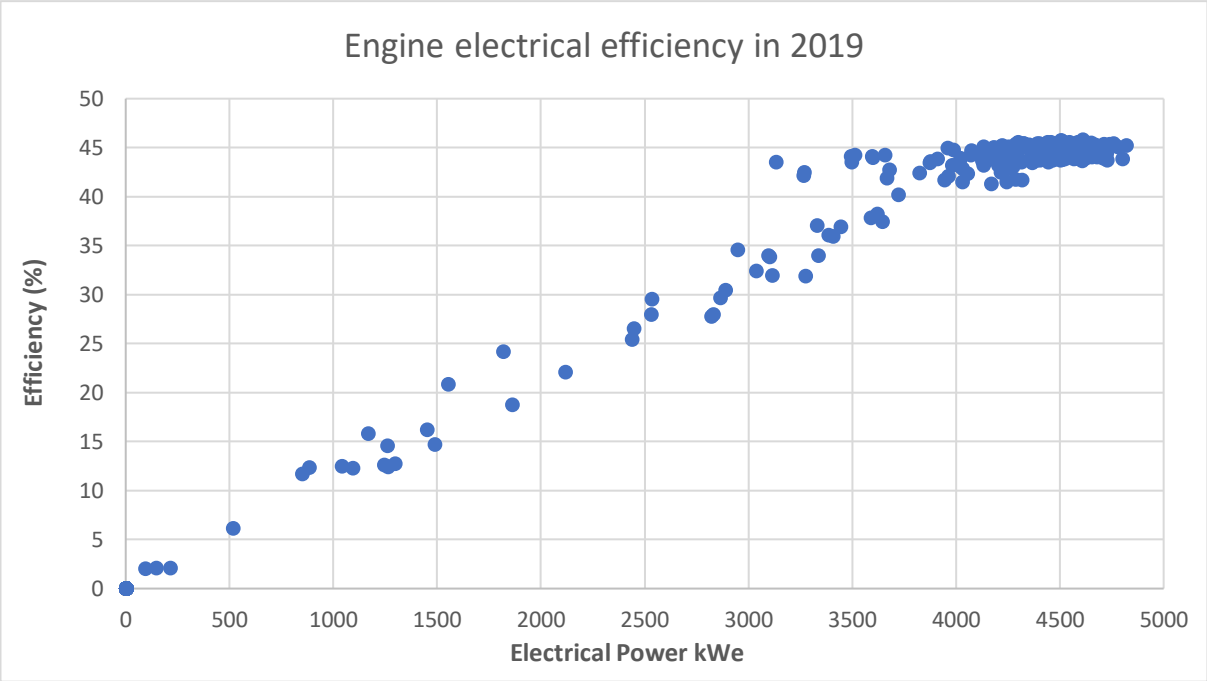

Figure 4.9: Engine electrical efficiency vs Generated electrical power in 2019 (daily)

Efficiency has been calculated on a daily basis by neglecting the shift change hours (06:00, 14:00, 22:00) that could have reduced the daily mean electrical efficiency because of the decrease of productivity in those periods of time.

Moreover, the blue dots in three graphs don't include Sundays that are not significant to evaluate the evolution of efficiency with the engine load.

In the three graphs a denser point cloud is located on the top-right position, at high load, thus, showing a correspondence with *Figure 4.4*, *4.5* and *4.6*. The engine has worked mostly at high load in the three years of analysis.

In accordance with the engine datasheet, it is noticeable that engine electrical efficiency is close to 45 % when it works at high load. Moreover, the efficiency remains quite constant and higher than 40 % until the generated electrical power is higher than 4000 kW_e, around 80 % of nominal power. Below this value, the efficiency decreases with a quite linear trend.

In order to understand in a better way the performance of this engine, a mean electrical efficiency has been calculated for each year of operation.

This value has been obtained by considering only the high load periods of time: starting from the hourly data, a yearly average has been calculated by neglecting the hours during which the natural gas volume flow rate was lower than 950 Sm^3/h, that corresponds to around 80 % of the full load natural gas flow rate (1200 Sm^3/h).

Results are presented in *Table 4.1*.

Year	Mean Electrical Efficiency at High Loads
2017	45,5 %
2018	44,5 %
2019	44,7 %

Table 4.1: Yearly mean electrical efficiency at high load

Electrical efficiency in the analyzed years is very close to the data declared by the manufacturer: at high loads the yearly mean electrical efficiency is around 45 % with just 1 % variation around this value.

This means that the engine has properly worked during the years of operation.

To graphically evaluate the number of hours of high load conditions, it is necessary to plot the cumulative curves of the generated electric power during the analyzed year.

This can be useful to understand the number of hours of full load conditions and how much the engine has worked in partial load condition for one year.

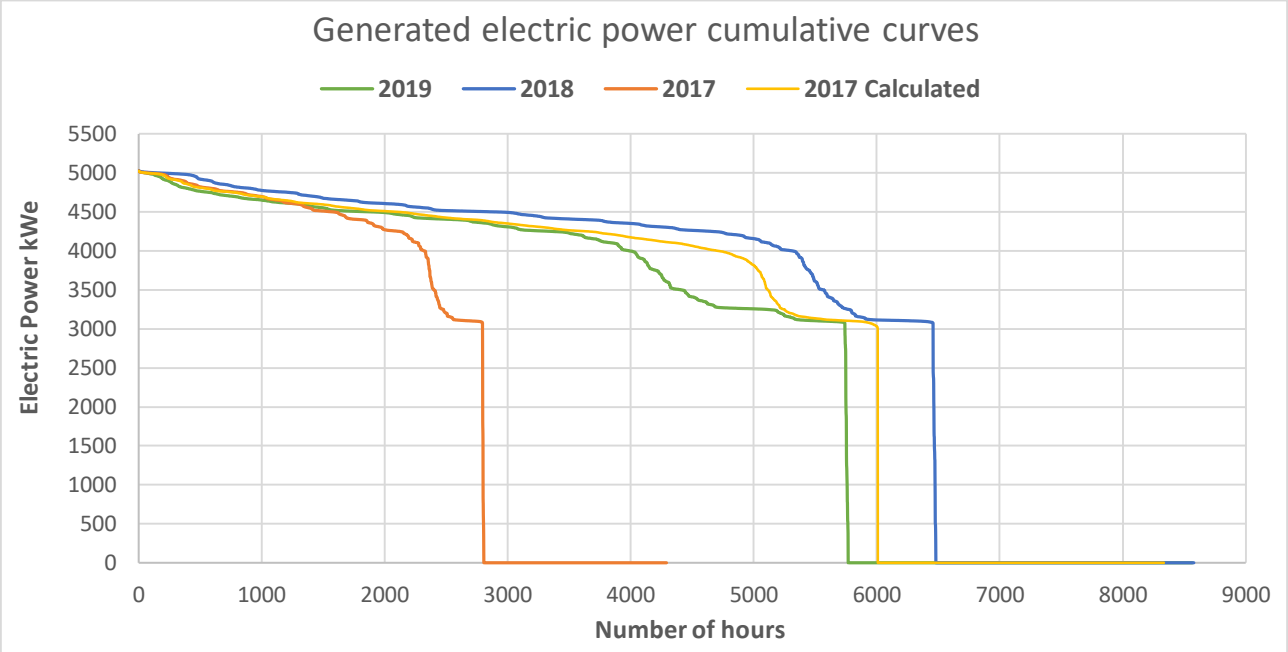

Figure 4.10: Cumulative curves of generated electric power in 2017, 2018 and 2019

From *Figure 4.10* it is possible to note that the engine works in full load conditions for few hours in a year, less than 1000 hours.

Nevertheless, it operates at high load (more than 4500 kW), for about 2000 hours.

The cumulative curve is quite linear and flat until 4000 hours, then a steeper decrease can be noticed, while at power lower than 3000 kW, that corresponds to around 60 % of nominal

power, the engine is stopped. Indeed, the cumulative curves show a step from 3000 kW to 0 kW, with no working hours.

The orange curve represented in *Figure 4.10* is referred to the available last six months data of 2017. In order to have a significant trend that could be compared to 2018 and 2019 cumulative curves, the yellow one has been obtained by calculating an ideal working condition starting from the available natural gas flow rate to the engine.

Therefore, the data processing is the same that made possible to obtain the orange dots in *Figure 4.6*.

Figure 4.10 shows that 2018 has been the year with higher electrical production, around 5000 hours at power higher than 4000 kW, while in 2019 the engine worked in the same conditions for 1000 hours less with respect to 2018.

It is interesting to analyze if the engine electrical productivity throughout one year is sufficient to cover the served industrial plant electricity demand or, if it could be increased so that the engine could work at nominal power for a higher number of hours. This could lead to money saving due to the unnecessary electricity import from the grid.

Figure 4.11 shows the energy plant electricity balance in 2018. It has been obtained by performing the difference between the engine generated electricity and the total electricity demand, that comprises the user electricity demand and the energy plant electricity consumption for auxiliaries and electric chillers cold water production.

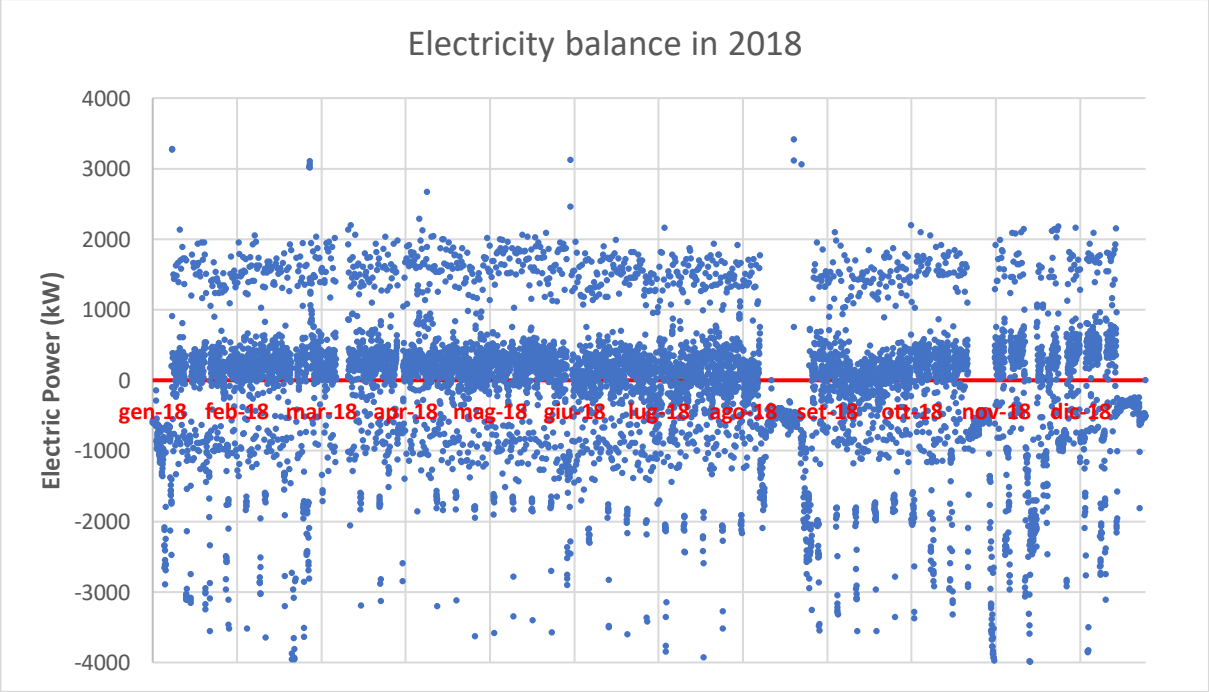

Figure 4.11: Electricity balance in 2018

From *Figure 4.11* it is possible to notice that the electricity balance is positive for most of the year, but with low absolute values: this means that in those periods, electricity is exported towards the national grid because the production is larger than the total electricity consumption. There are some negative peaks, mostly during the periods when the plant is stopped, therefore, electricity must be imported from the electricity network.

4.2 Heat Recovery Unit

The HRU of this plant is dimensioned to recover 2663 kW_{th} from the exhaust gases sensible heat. It is divided in two sections:

- 2165 kW_{th} recovered by heating up super-heated water from 150 °C to 165 °C
- 498 kW_{th} recovered by heating up hot water from 88 °C to 92 °C in the economizer

Nevertheless, such a high thermal recovery was never achieved during the three years of analysis.

In the next paragraphs, the two different portions of the HRU will be analyzed separately, in order to understand the criticalities of the two circuits.

4.2.1 Super-Heated Water

The thermal recovery in the high-temperature section of the HRU has been much lower than expected. An important issue of this section is about the super-heated water temperature that should undergo an increase of 15 °C.

By analyzing the temperature evolution, it is possible to notice that the maximum temperature reached in the HRU is around 150 °C, instead of 165 °C.

Moreover, by analyzing the maximum monthly super-heated water temperature, it never reached 160 °C in all three years of analysis, as it is shown in *Figure 4.12*, *4.13* and *4.14*.

For the year 2017, only the last six months data are available.

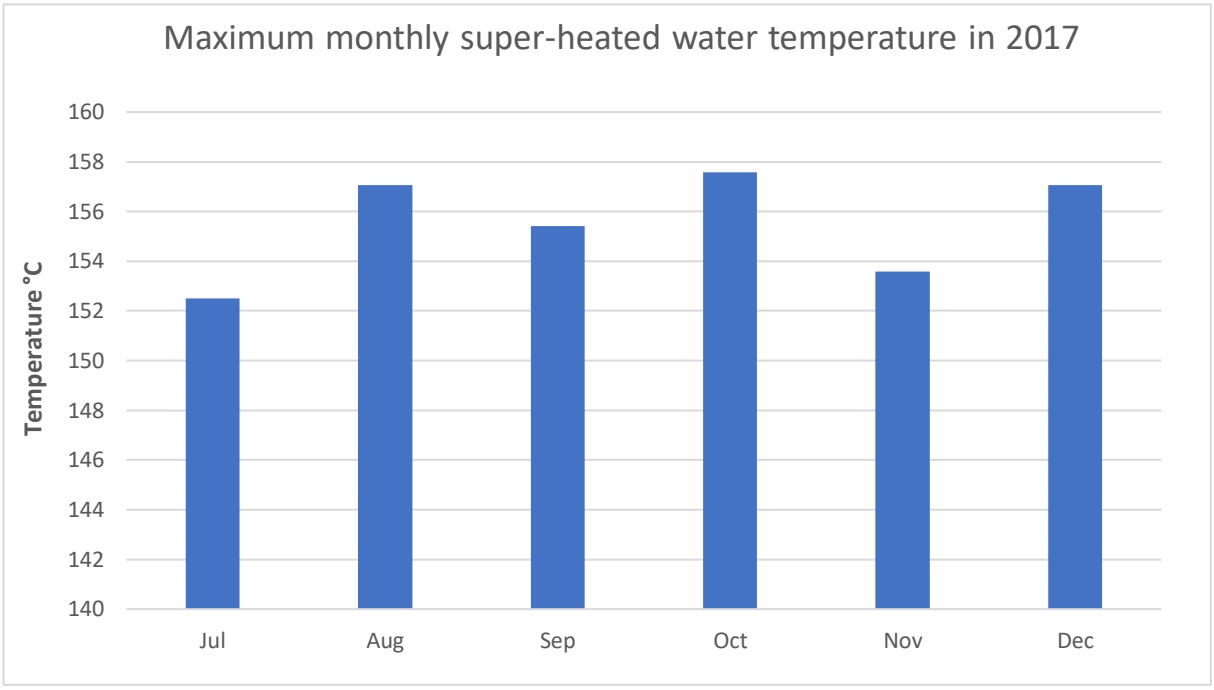

Figure 4.12: Maximum super-heated water temperature for every month in 2017

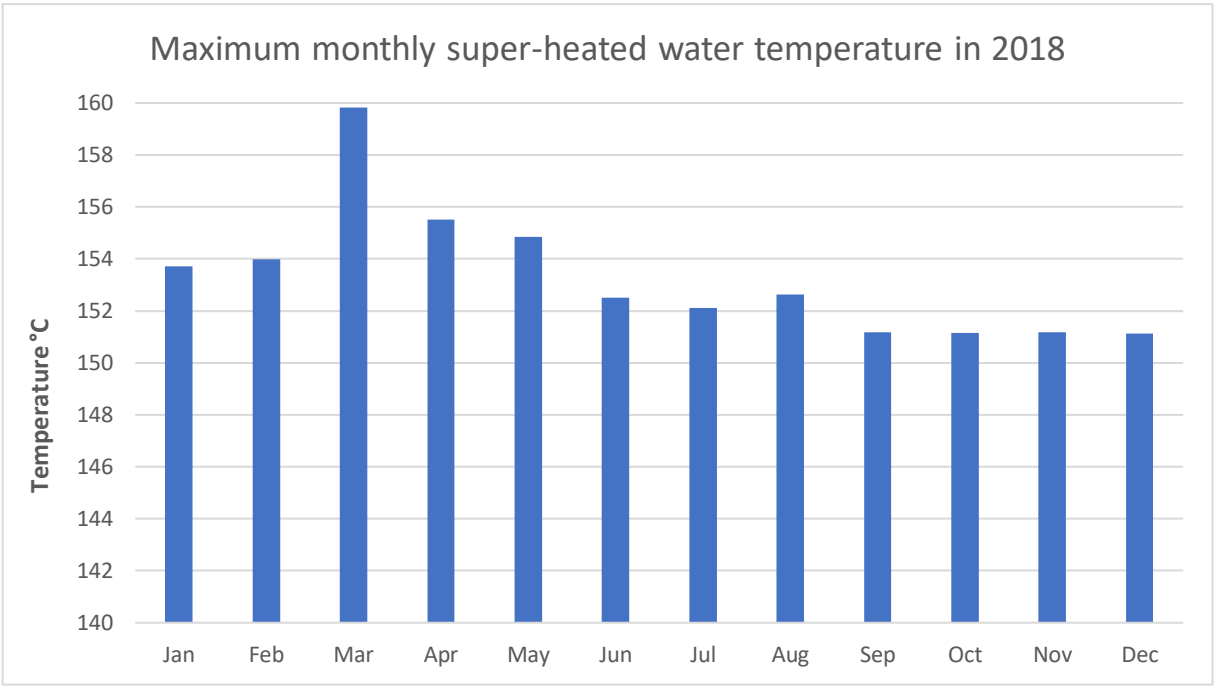

Figure 4.13: Maximum super-heated water temperature for every month in 2018

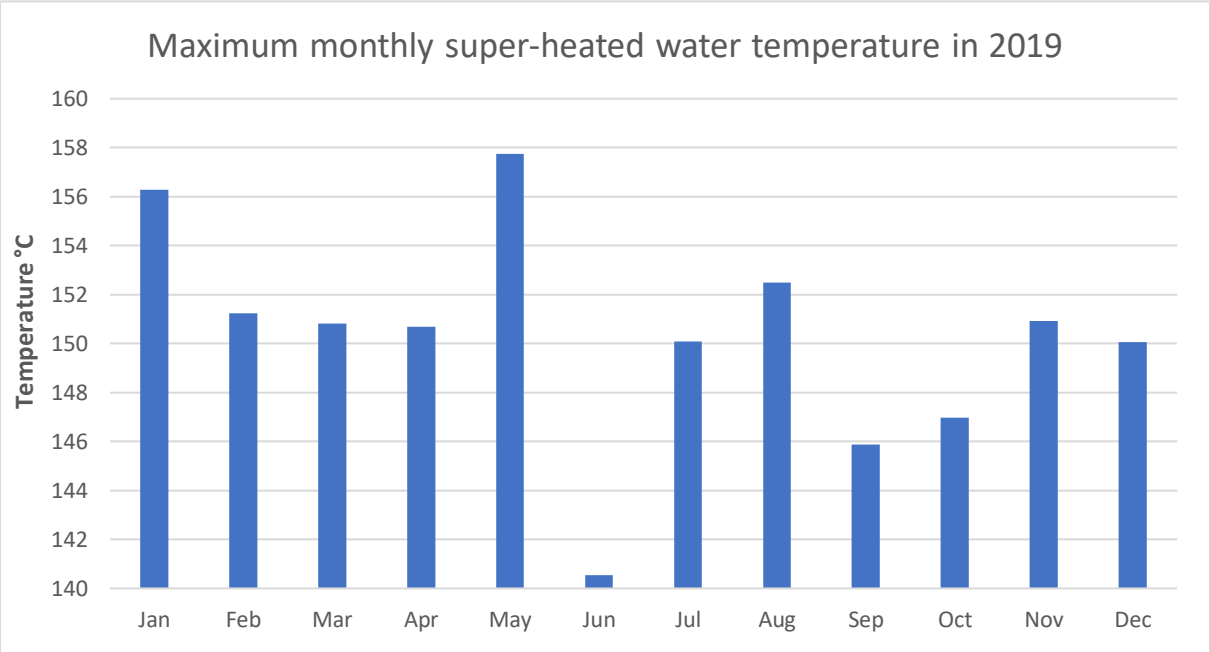

Figure 4.14: Maximum super-heated water temperature for every month in 2019

Only in March 2018, the super-heated maximum water temperature reached a value close to 160 °C.

Nevertheless, that is the maximum temperature, therefore, in order to understand the HRU performance throughout the year, it is interesting to plot the super-heated water temperature at the outlet of the thermal recovery section.

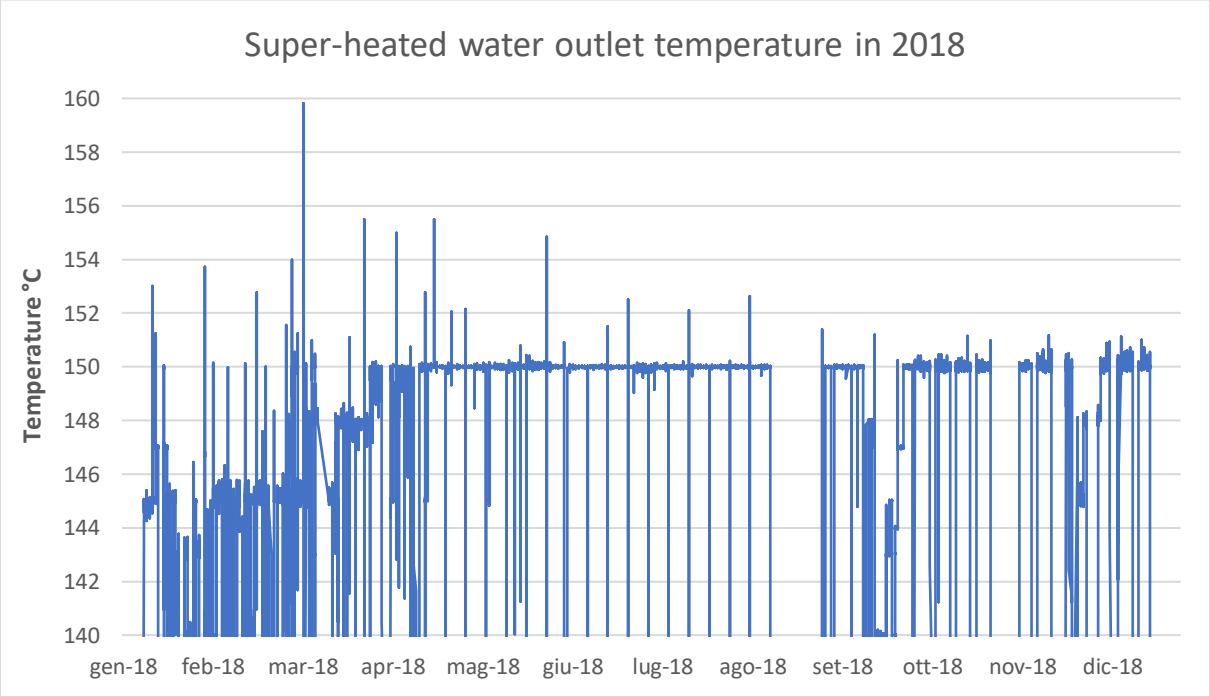

Figure 4.15: Super-heated water temperature at HRU outlet in 2018

From *Figure 4.15*, it is possible to notice that, except for some spikes, the outlet temperature is quite constant at 150 °C during the considered year.

This has a negative impact on thermal recovery and on double-effects WARGs, which nominal hot water inlet temperature is 165 °C.

Super-heated water temperature drop, in all three years is not 15 °C, as expected to recover 2165 kW_{th}, but as it can be seen from *Figure 4.16*, it is around 5 °C.

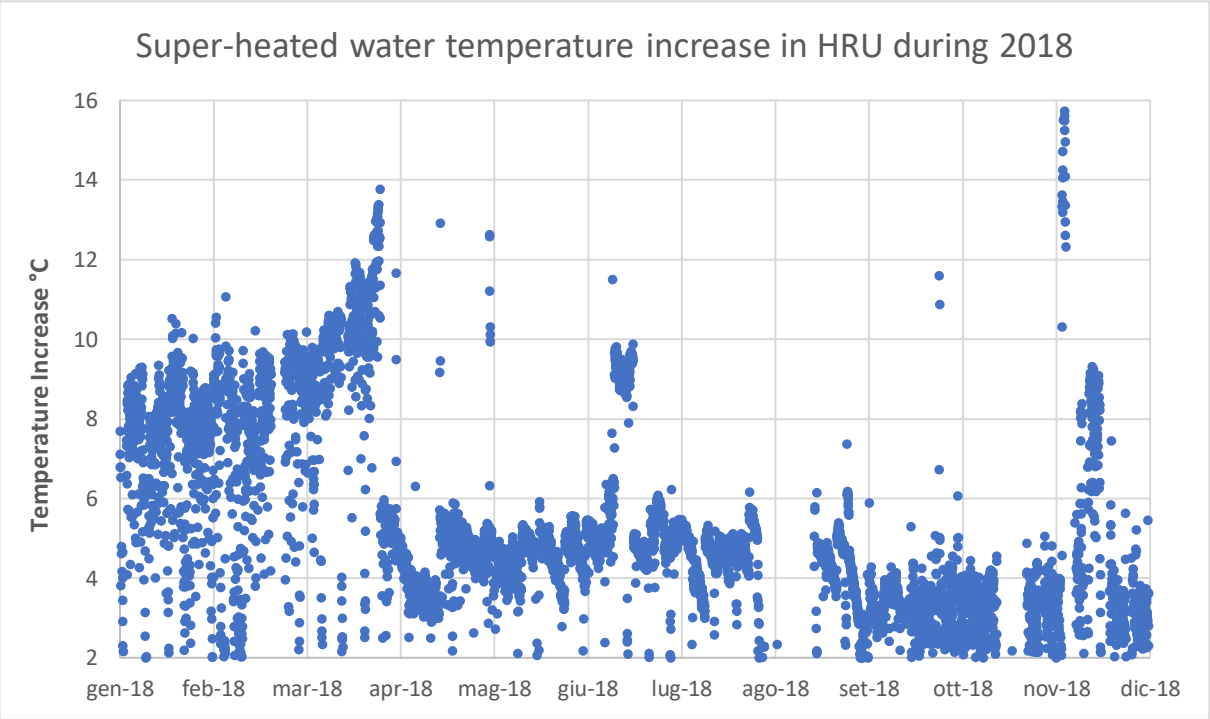

Figure 4.16: Super-heated water temperature increase across HRU in 2018

Only during the first three months of 2018, super-heated water temperature drop is between 8 and 10 °C, but from April 2018 to December 2018, the average temperature drop is between 4 and 6 °C, thus one third of the expected 15 °C.

Every point on the graph in *Figure 4.16* represents an hourly value of the difference between HRU inlet and outlet super-heated water temperature.

Because of this reduced temperature drop, the thermal recovery is lower than half of the nominal one. Indeed, by keeping constant the super-heated water flow rate, if the temperature drop is two or three times lower than expected, then the thermal power recovered will be, consequently, two or three times lower than 2165 kW_{th}.

This aspect is confirmed by analyzing the evolution of thermal power recovered in the super-heated section, during 2018.

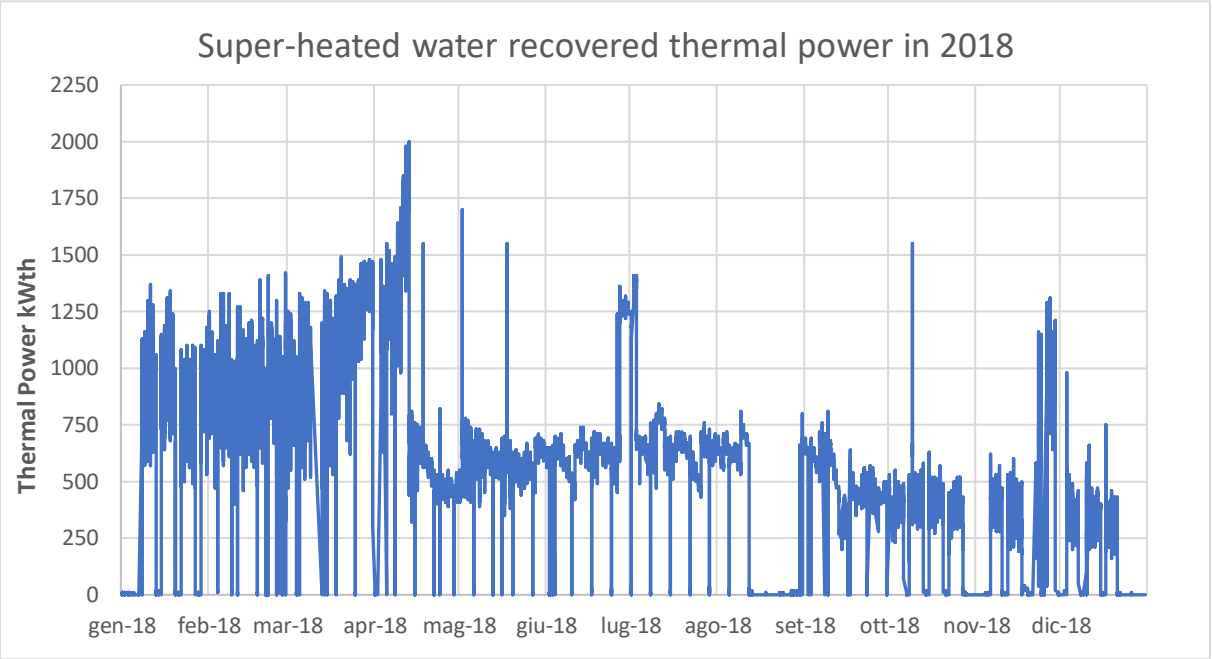

Figure 4.17: Thermal power recovered in super-heated HRU section during 2018

Figure 4.17 shows a clear correspondence with temperature drop data in *Figure 4.14*.
Recovered thermal power has been extracted from the Online Data Collector under the tag JQI 0330, relative to super-heated thermal recovery totalizer.
During the first three months, 1000 – 1250 kW_{th}, but from April to the end of the year, only around 700 kW_{th} are recovered, that corresponds to around one third of the nominal 2165 kW_{th}.
Almost the same thermal recovery trend can be seen during the year 2019, in *Figure 4.18*.

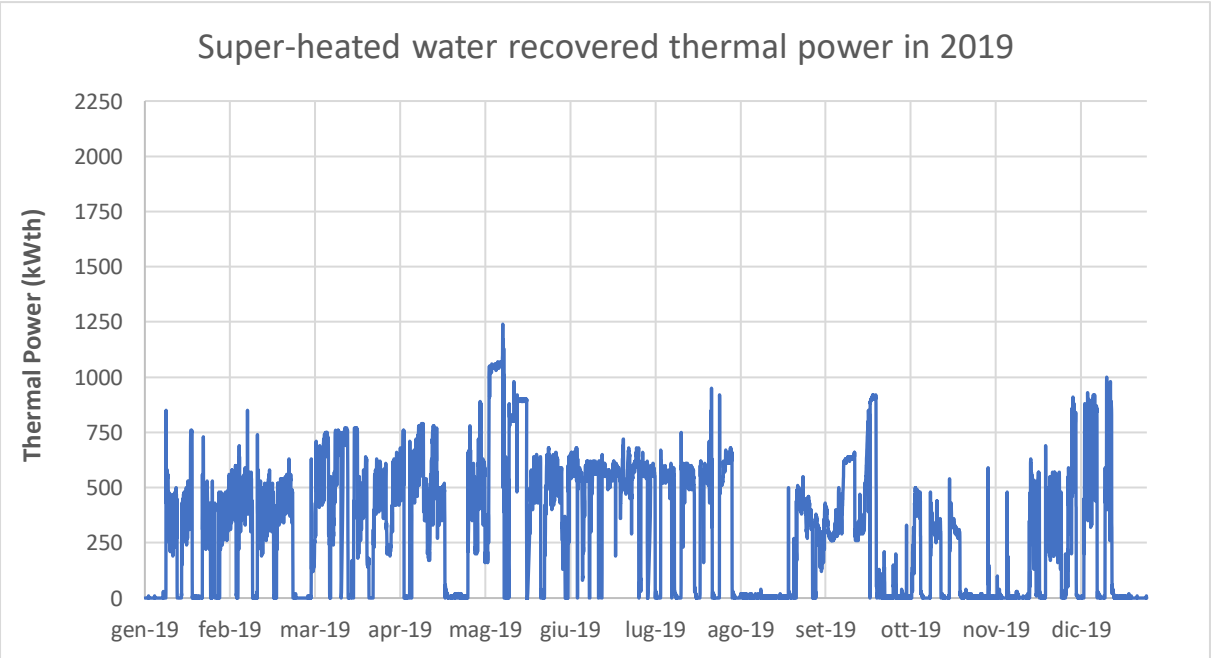

Figure 4.18: Thermal power recovered in super-heated HRU section during 2019

Also in this graph, it is possible to notice that super-heated recovered thermal power is below 750 kW_{th} for most of the year.

The year 2017 has been omitted in this analysis because of the unavailable data about the first six months.

4.2.2 Hot Water (HT section and Economizer)

As already mentioned, hot water at 92 °C, can be supplied both to the single-effect WARG and to the paintings ATU.

Hot water is pre-heated by the HT circuit water in a heat exchanger, which nominal power is 1004 kW_{th}.

A scheme of the HT and Hot Water circuits is represented in *Figure 4.19*.

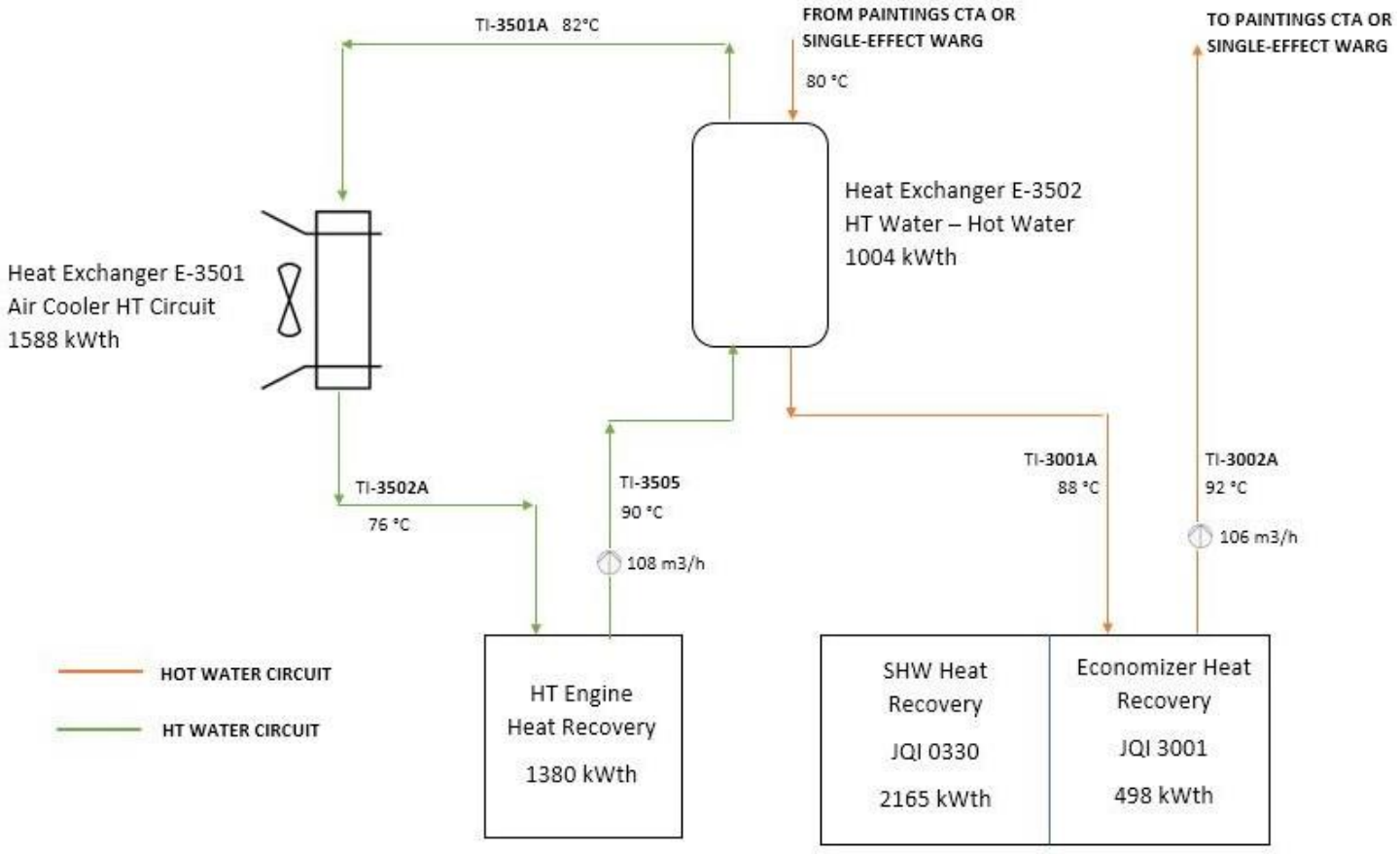

Figure 4.19: Simplified scheme of the HT and Hot Water circuits

In *Figure 4.20* and *4.21*, it is shown the evolution of the three main temperatures of the HT Water circuit (temperatures with tags TI-3505, TI-3501A and TI-3502A on *Figure 4.17*), respectively during the years 2018 and 2019.

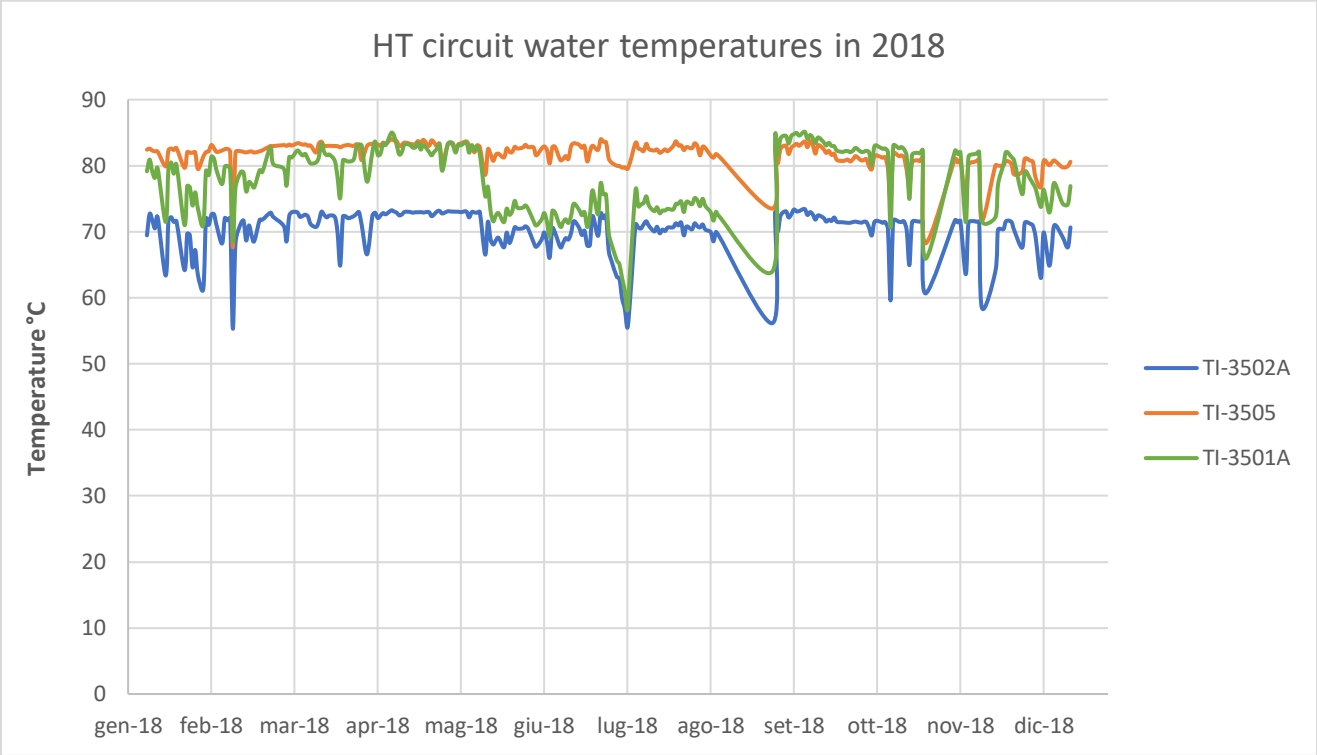

Figure 4.20: HT circuit daily mean temperatures during 2018

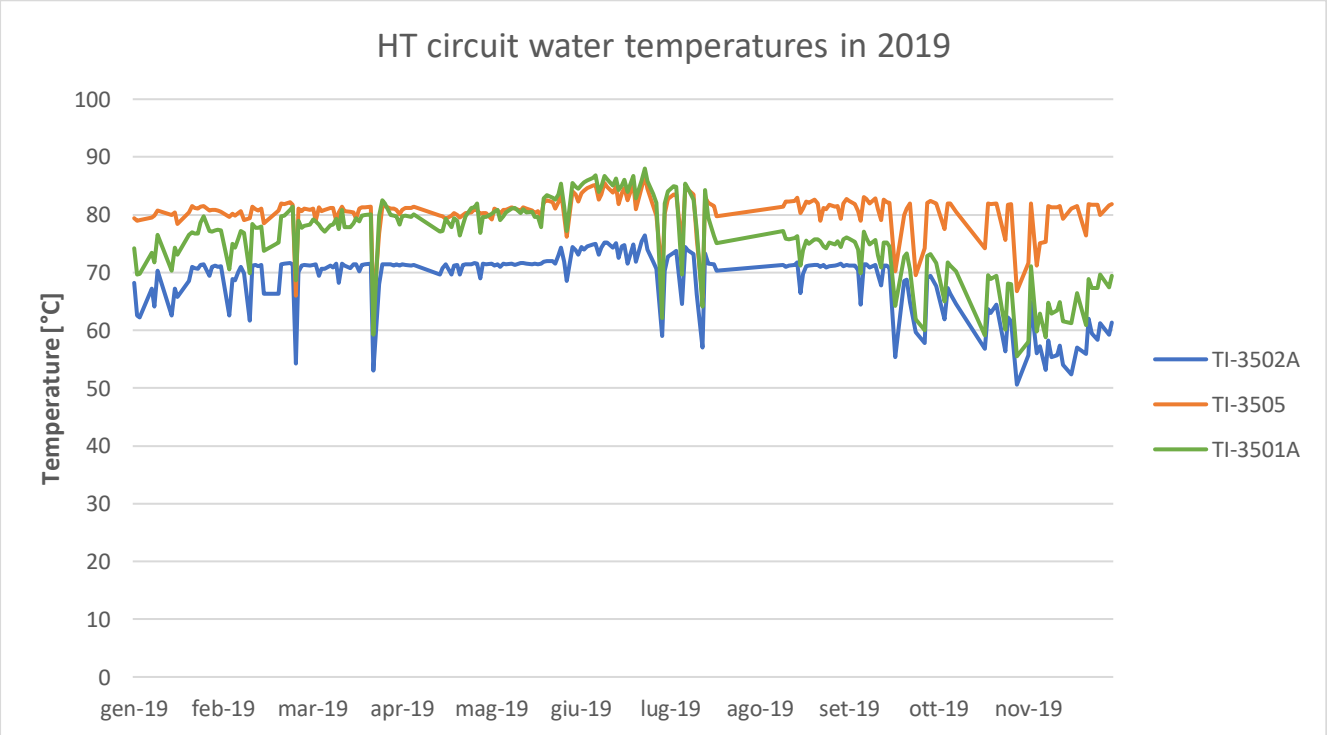

Figure 4.21: HT circuit daily mean temperatures during 2019

Temperatures reported in the previous two graphs are mean daily temperatures, obtained by neglecting Sundays and shift change hours.

A first observation regards the temperature drop across the engine, thus the temperatures with tags TI-3502A (blue curve) and TI-3505 (orange curve). Their daily mean value is quite constant during the two years to a value of 70 °C for the inlet water to the engine and between 80 °C and 85 °C for the outlet water.

Engine jacket water is necessary to keep under control the engine's temperature, thus it is fundamental to dissipate the heat that jacket water absorbs during the operation.

In this plant, part of that absorbed heat should be rejected to the Hot Water circuit in the Heat Exchanger E-3502.

HT Water circuit nominal flow rate and the Hot Water circuit nominal flow rate are very similar, respectively 108 m^3/h and 106 m^3/h, thus the delta of temperature across the heat exchanger should be almost the same, and, in full load conditions this means that Hot Water should be heated up from 80 °C to 88 °C, thus with 8 °C of temperature increase.

Nevertheless, by observing the HT circuit temperatures across the heat exchanger E-3502, thus temperatures TI-3505 and TI-3501A, it is possible to note that during the two analyzed years, for most of the time, the orange and the green curves are almost overlapped, therefore less useful heat is recovered by the Hot Water circuit.

This reduced temperature drop across the heat exchanger can be caused by a lower heat rejection from the Hot Water circuit, during periods in which there is less demand of heat.

In this case, the Hot Water on the primary circuit flows back to the heat exchanger E-3502 at higher temperatures, or, alternatively, if there is not Hot Water demand, it doesn't flow in the pipes.

This causes a complete heat rejection from the HT Water circuit to the external environment, by means of the air cooler E-3501, which nominal power is 1588 kW_{th}, so it can remove the 1380 kW_{th} recovered from the engine jacket water and the 1st stage of the Intercooler.

At full load conditions, after being heated up in the E-3502, Hot water flows across the Economizer section in the HRU, and it should be heated up from 88 °C to 92 °C, thus absorbing 498 kW_{th} from the exhaust gases.

In *Figure 4.22*, *4.23* and *4.24*, the hourly values of temperature increase across the economizer during the years 2017, 2018 and 2019 respectively.

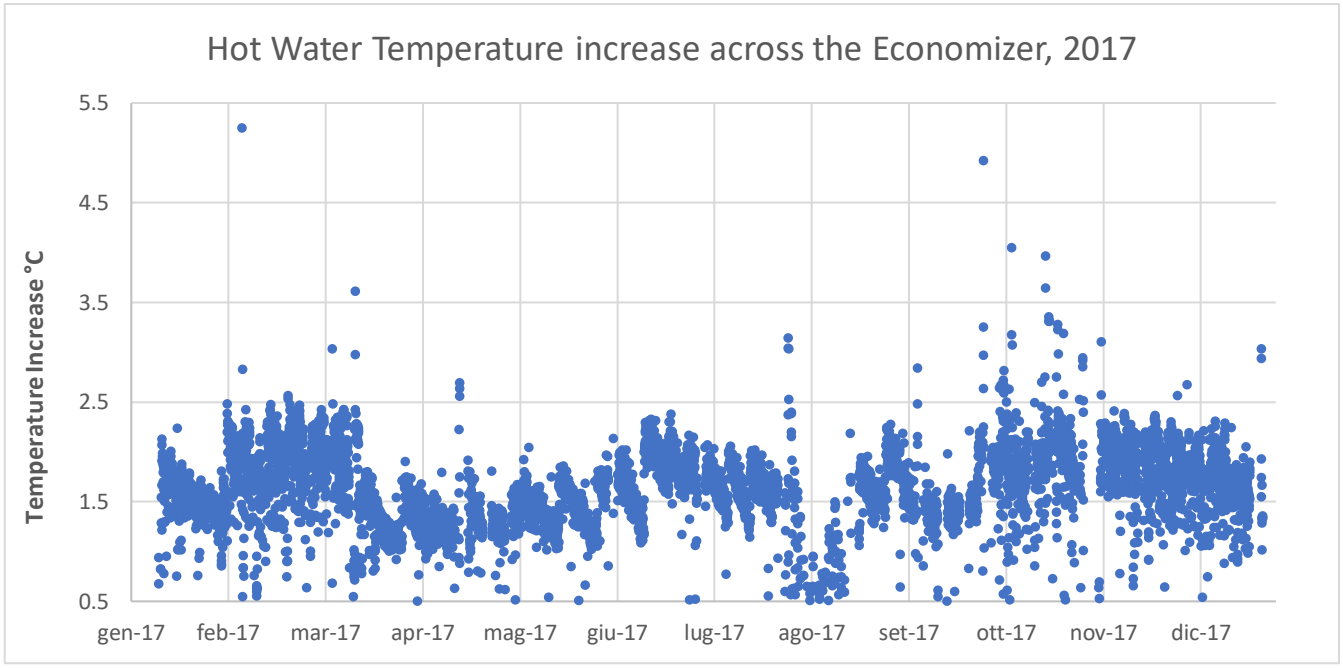

Figure 4.22: Hot Water hourly temperature increase across the Economizer in 2017

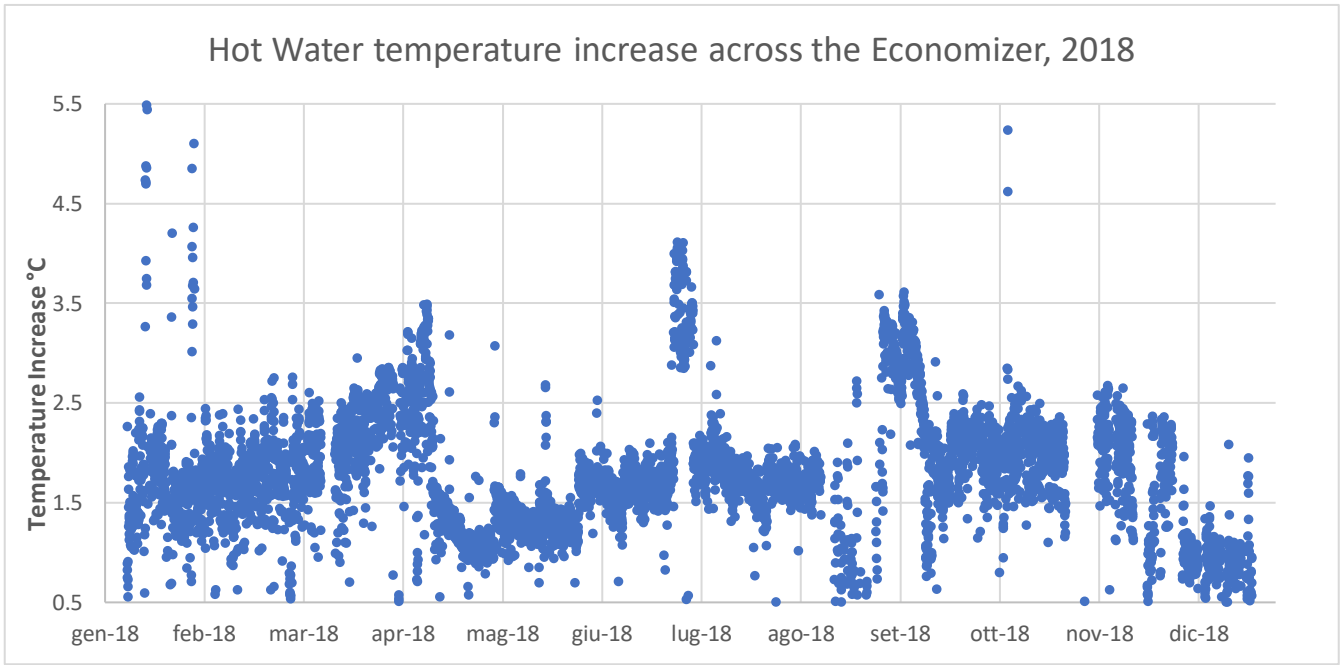

Figure 4.23: Hot Water hourly temperature increase across the Economizer in 2018

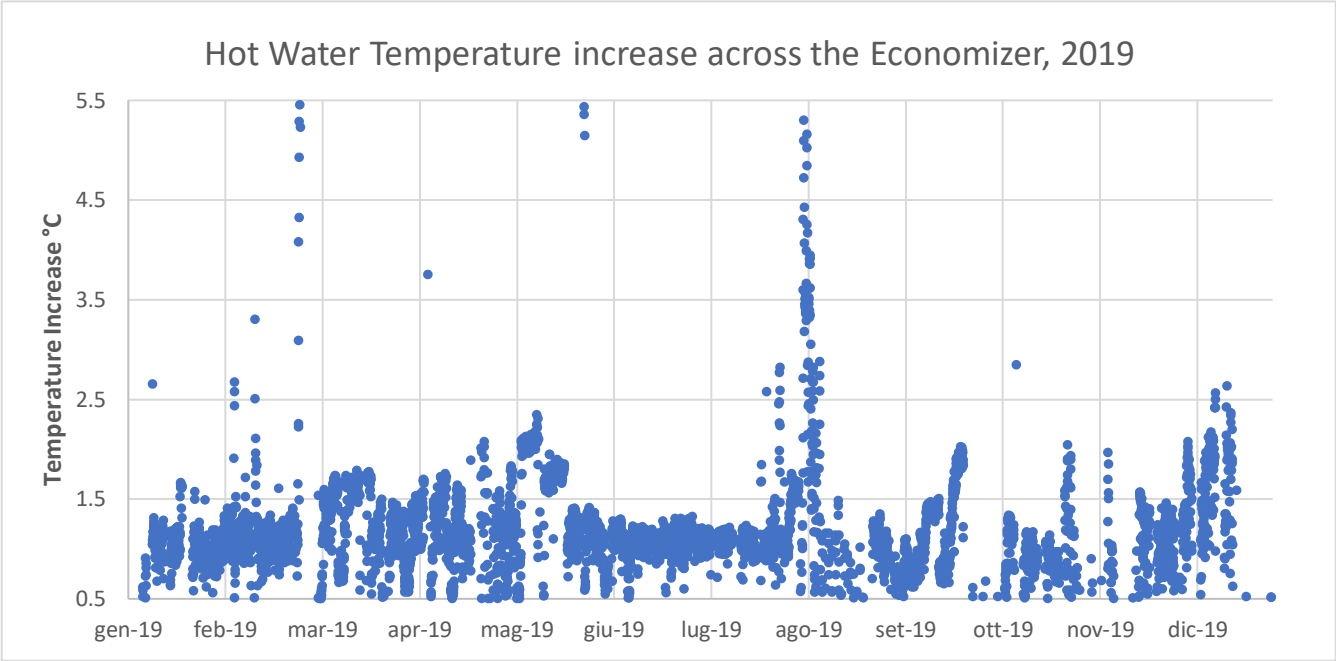

Figure 4.24: Hot Water hourly temperature increase across the Economizer in 2019

Except for some peaks in temperature increase that cannot be considered as significant values, for example in August 2019, it can be noted that Hot Water is rarely heated up by 4 °C, as expected in nominal conditions. On the contrary, the water temperature increase across the economizer is closer to a mean value of 2 °C, with a slight increase during 2018, during which the temperature difference touched 3 °C, and a little decrease during 2019.

The smaller temperature difference in the economizer is related to a particular operating condition, characterized by a reduction of the Hot Water demand or Cold Water demand. In this case, the HRU diverter is partially open, and a portion of the exhaust gases bypass the thermal recovery section.

This can be also due to a malfunctioning or maintenance of the single-effect or double-effect WARGs: for example, if one of the two double-effect WARGs is under maintenance, consequently there is less need for super-heated water heating up; the exhausts gases partially bypass the HRU, thus, also the Hot Water in the economizer absorbs less heat.

This operating condition represents an important issue for the correct plant functioning and it is the main reason why Fenice SpA has planned the Revamping of Melfi energy plant.

In *Figure 4.25* and *4.26* it is shown the evolution of the recovered thermal power by Hot Water: it is the sum of the heat absorbed across the heat exchanger E-3502 and the thermal power gained in the economizer.

By considering the two contributions, the total nominal power absorbed by Hot Water should be equal to around 1500 kW_{th}.

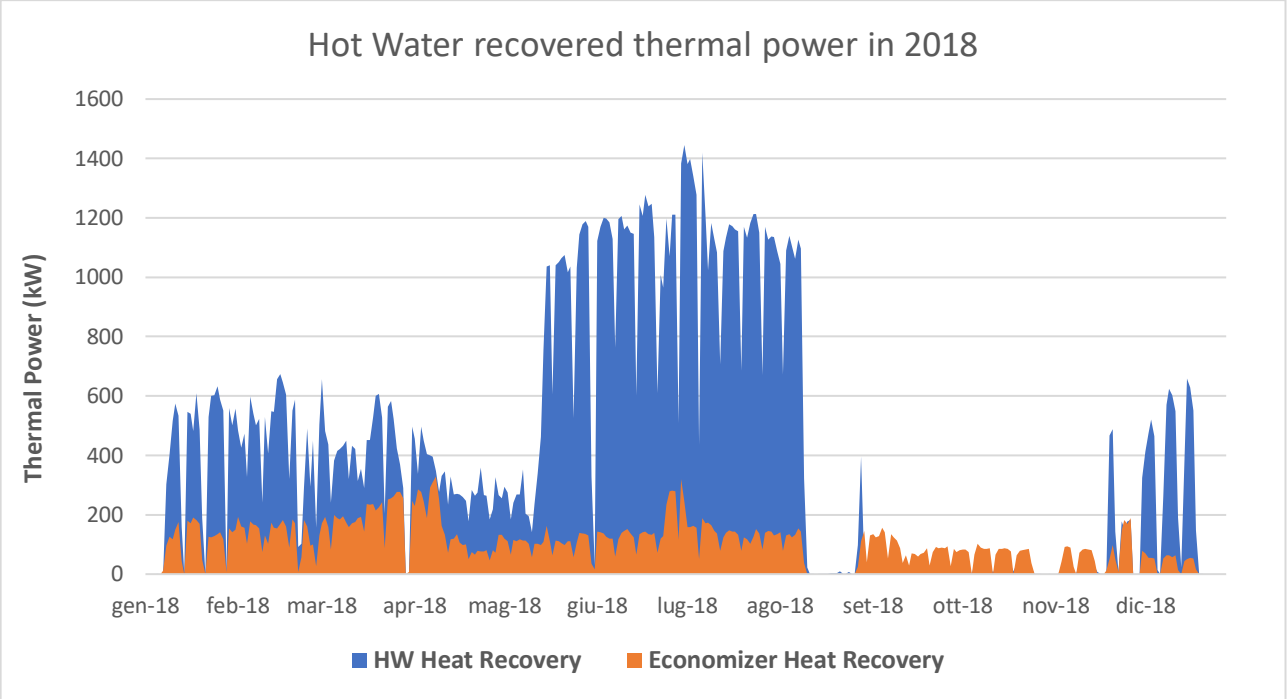

Figure 4.25: Hot Water recovered thermal power during 2018

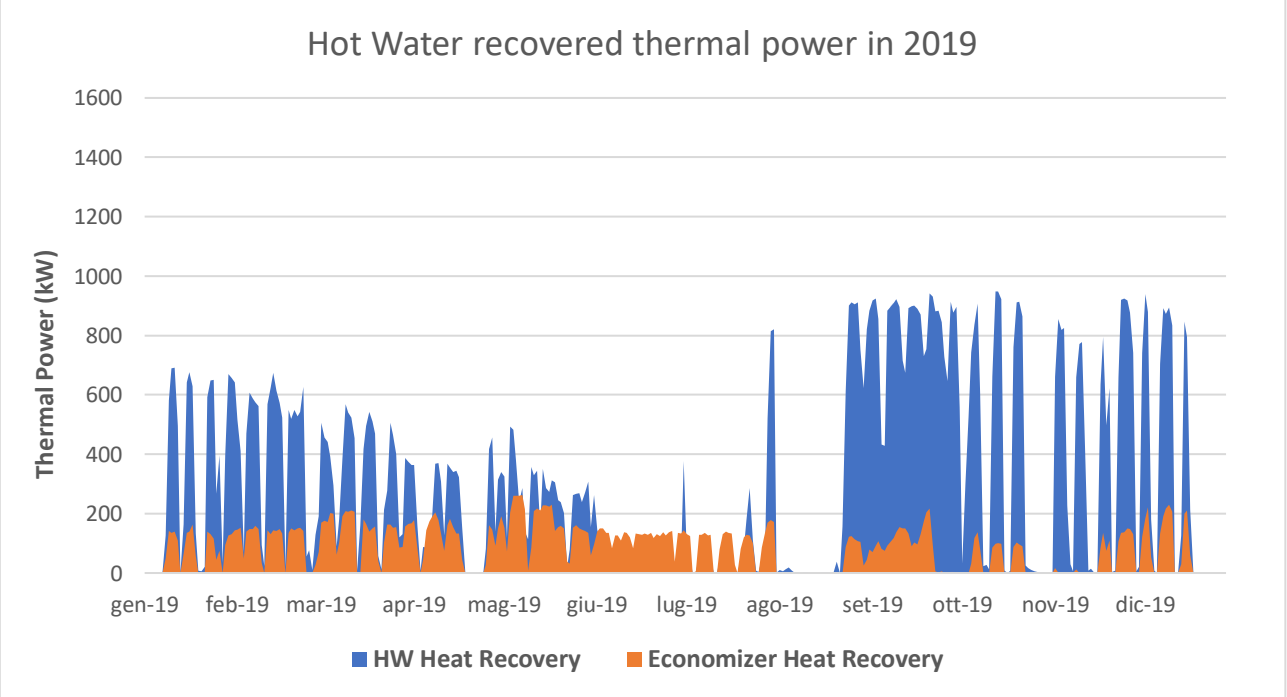

Figure 4.26: Hot Water recovered thermal power during 2019

By analyzing the two previous graphs, it is immediately noticeable that less thermal power has been recovered by the Hot Water circuit during 2019. This shows a correlation with super-heated recovered thermal power in 2019, *Figure 4.18*: indeed, by comparing *Figure 4.17* and *4.18*, it is clear that thermal recovery has been higher in 2018 with respect to 2019.

Even by looking to electrical cumulative curves in *Figure 4.10*, it can be noticed that in 2019 the engine worked for less hours with respect to2018: as a consequence of a reduced electrical generation, also the thermal energy recovered during the year 2019 has been affected.
Moreover, in *Figure 4.26*, the period between June and August 2019 cannot be taken into account because of the malfunctioning of some sensors for thermal energy measurement.
In *Figure 4.25*, it is clear that the most of thermal energy recovered by Hot Water was absorbed across the heat exchanger E-3502, by exchanging heat with the HT Water circuit. Indeed, the orange area shows the economizer contribution on the total heat recovery.
The economizer is dimensioned to allow almost 500 kW_{th} of heat exchange between exhaust gases and Hot Water, nevertheless, by looking to the daily mean values of absorbed heat in *Figure 4.25* and *4.26*, it is possible to see that, on average, the recovered thermal power was around 200 kW_{th} or less.
In *Figure 4.25*, it is shown that between May and August 2018, a great contribution to heat recovery was provided by the heat exchanger E-3502, that corresponds to the difference between the blue and the orange area. This can be confirmed by looking at *Figure 4.20*: during those months it is possible to notice that temperature of the HT circuit water TI-3501A was closer to the temperature of the same circuit at the outlet of the air cooler E-3501, while a greater temperature difference existed between TI-3501A and TI-3505 (the latter represents the HT circuit water temperature at the outlet of the engine). This means that the HT circuit water transferred more thermal energy to pre-heat the Hot Water before the economizer, while less heat was rejected to the external environment by means of the air cooler.
The same consideration can be done for the year 2019: by analyzing *Figure 4.26*, it can be seen that more thermal energy was recovered across the heat exchanger E-3502 between September and December 2019. By looking at *Figure 4.21*, it is clear that during the same period of time, the green curve was closer to the blue one, while a greater temperature difference existed between temperature TI-3501A and TI-3505.
A clear graphic correlation can be noticed between the evolution of the Hot Water temperature increase across the economizer during 2018 in *Figure 4.23*, the economizer heat recovery that corresponds to the orange area in *Figure 4.25* and the super-heated water thermal recovery during 2018 in *Figure 4.17*.
For simplicity, in *Figure 4.27*, it is shown the correlation between the recovered thermal power across the economizer and across the super-heated HRU section.

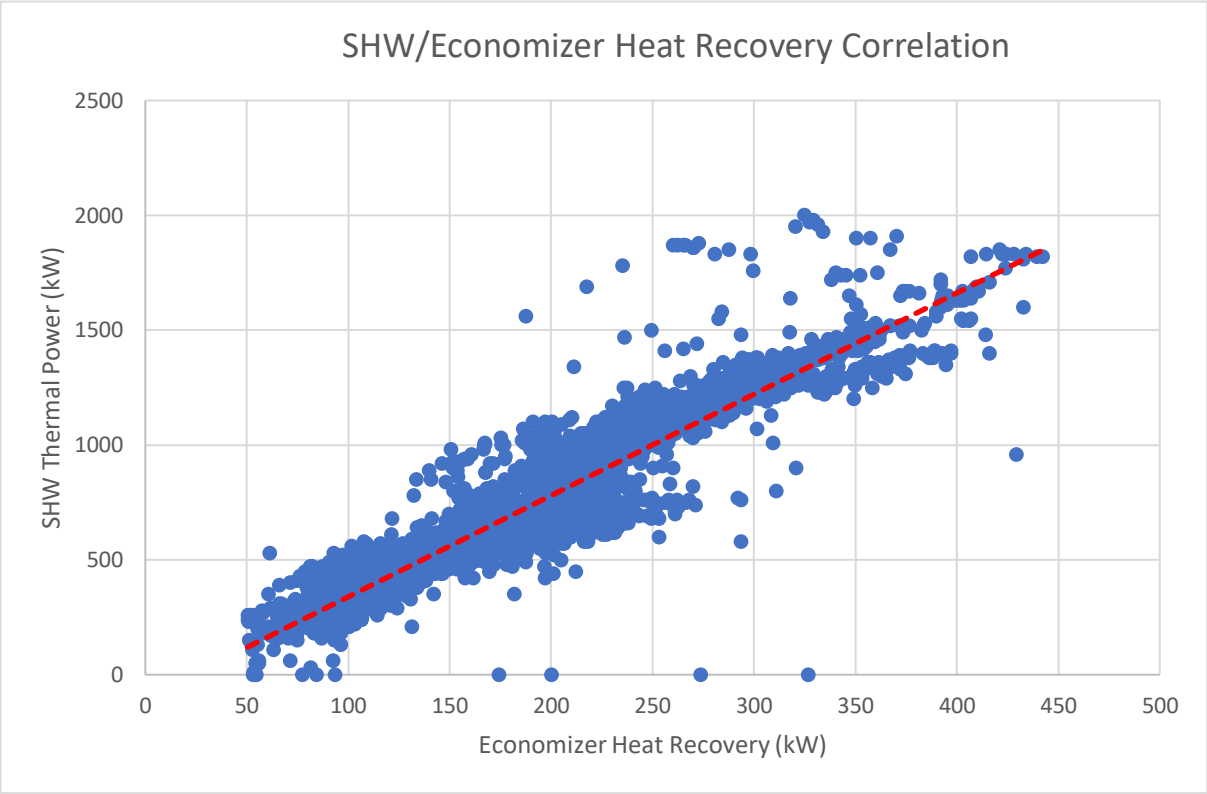

Figure 4.27: Correlation of super-heated water and Economizer heat recovery in 2018

The increase and the reduction of thermal recovery in both sections of the HRU is correlated with the user's energy demand, thus, the diverter is partially closed or opened, directing a larger or smaller exhaust gases flow rate to the bypass and then to the chimney.

4.2.3 Heat Recovery cumulative curves

In order to analyze the efficiency of heat recovery during the different years, it is interesting to plot the cumulative curves of heat recovery.

In *Figure 4.28* the 2018 and 2019 cumulative curves are plotted.

As already mentioned, it is clear that, during 2018, more energy has been absorbed from the exhaust gases. The curves have been obtained by summing up the hourly values of super-heated water heat recovery in the HRU and the hot water thermal recovery, which includes both the economizer and the heat exchanger E-3502 contributions.

The two cumulative curves peaks are very different: around 3000 kW_{th} in 2018, while throughout 2019 the maximum recovered heat corresponds to around 2000 kW_{th}.

At full load conditions, the maximum possible thermal recovery is 3667 kW_{th}: it is the sum of

2663 kW_{th} of the HRU and the 1004 kW_{th} of heat exchanger E-3502.

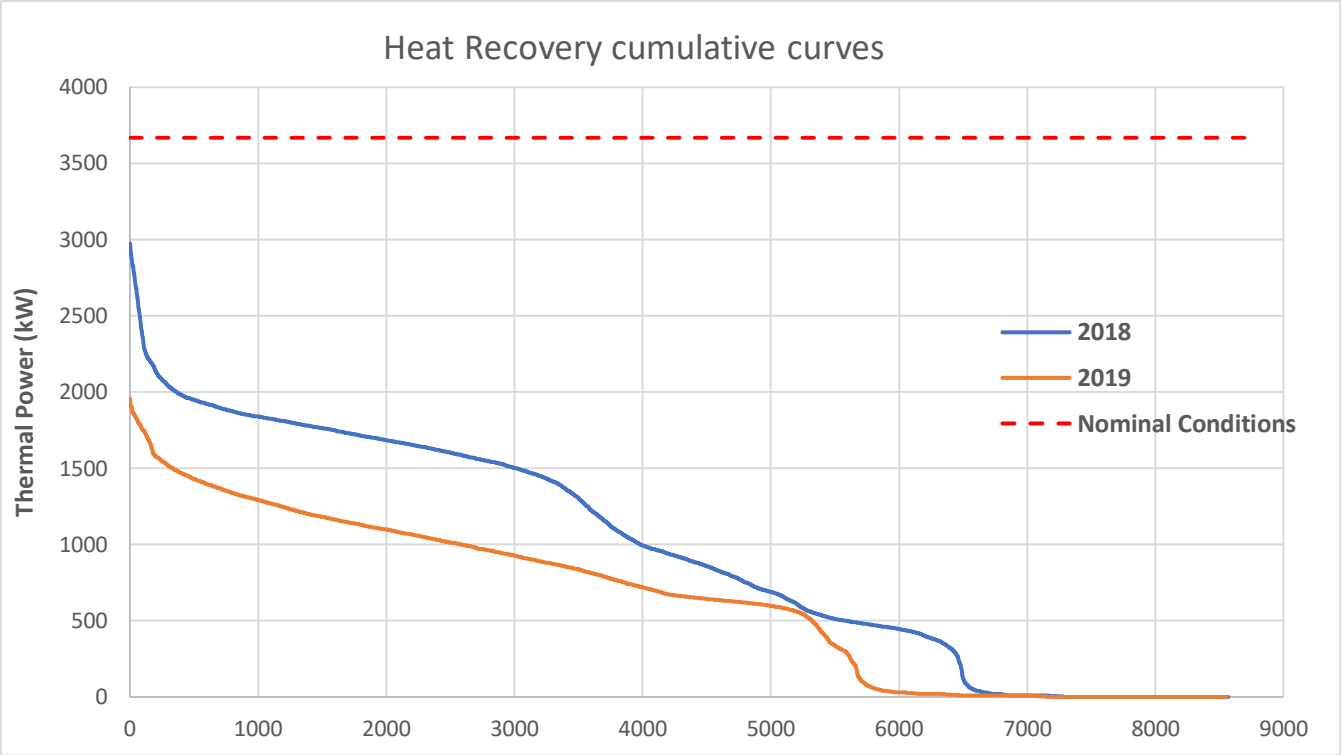

Figure 4.28: Heat recovery cumulative curves in 2018 and 2019

The red dashed line in *Figure 4.28* corresponds to 3667 kW_{th}, thus it represents the maximum thermal recovery that would be possible in nominal conditions.

During the two analyzed years, heat recovery never overcame 3000 kW_{th} that corresponds to around 80 % of nominal conditions. Nevertheless, except for about 500 hours in 2018, during the rest of the time, heat recovery was lower than 2000 kW_{th}, that is around 55 % of nominal conditions.

In the graph of *Figure 4.28* it was not possible to reconstruct a plausible cumulative curve for the year 2017 because of unavailable data about super-heated water thermal recovery and about the heat exchanger E-3502.

Moreover, it was not possible to deduce thermal recovery starting from generated electricity data, because the Rolls Royce engine operation is based on the tracking of the user's electric load, thus it is not possible to build a correlation between electricity and thermal recovery.

The independence of those two variables is shown in *Figure 4.29* and *Figure 4.30*, both referred to year 2018: in the former the hourly engine operating conditions in terms of generated electricity and thermal recovery are shown, while in the latter the same engine operating conditions are represented but on a daily mean basis.

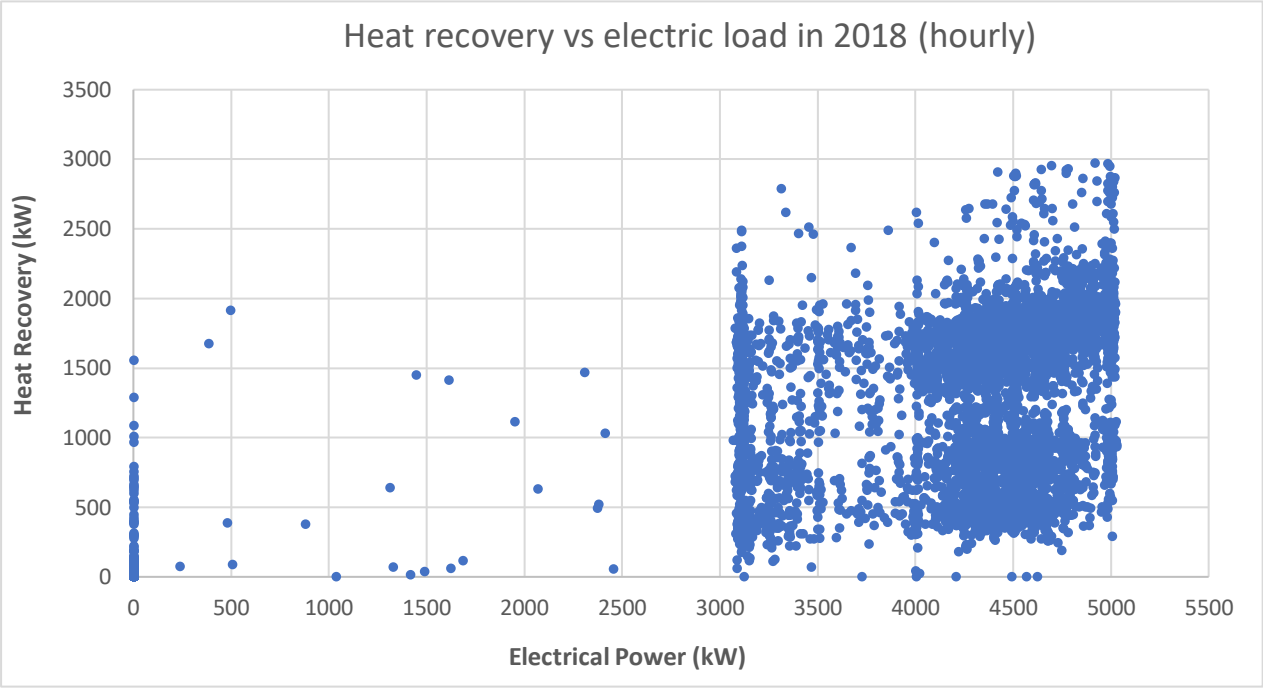

Figure 4.29: Heat recovery and Electricity generated in 2018, hourly basis

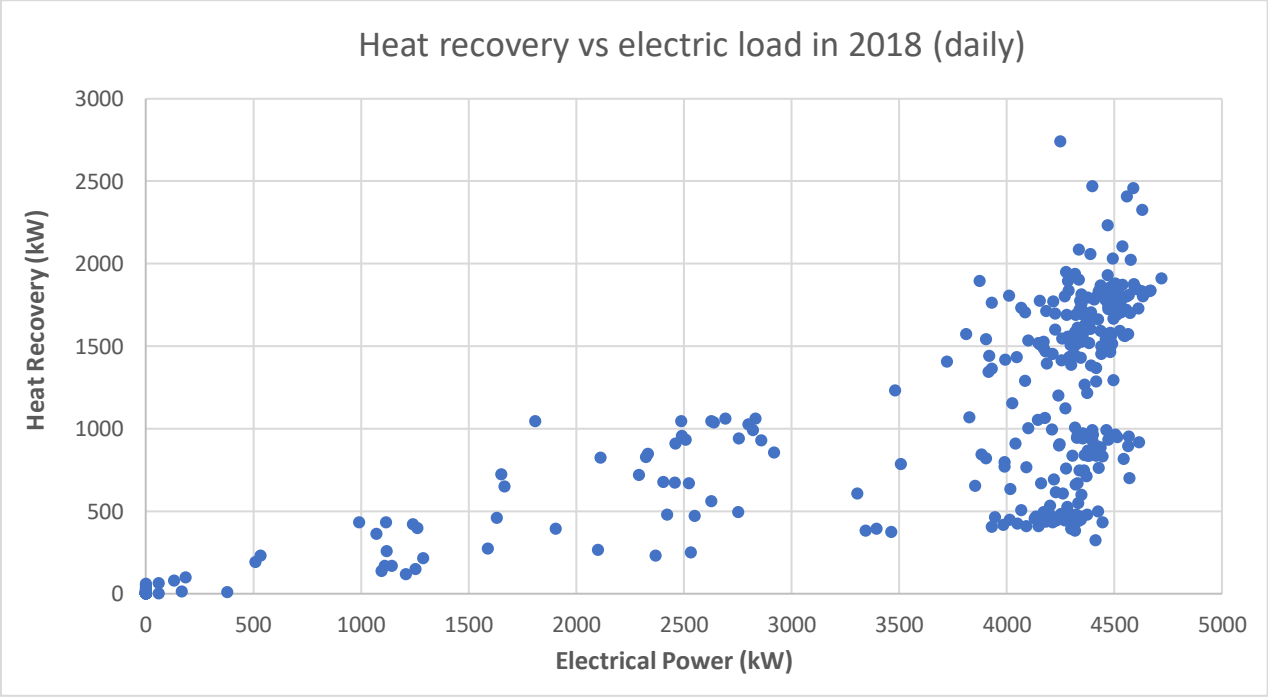

Figure 4.30: Heat recovery and Electricity generated in 2018, daily basis

From both the previous graphs it is clear that it's not possible to extract a trend line that can express the correlation between thermal recovery and engine electric load.

By looking at *Figure 4.29*, a cloud of points is present between the values 3000 kW_e and 5000 kW_e on the abscissa axis.

Even by analyzing the daily mean engine operating conditions, although it can be noticed that by increasing the generated electricity, also the thermal recovery increases, it is not possible to obtain a clear correlation between the two variables. Indeed, also in *Figure 4.30* the points are randomly positioned on the graph without showing a linear trend, in particular, close to full load conditions.

4.2.4 First Law Efficiency

In order to obtain a plant overall efficiency, the First Law Efficiency has been calculated by summing up the generated electric power and the thermal recovery, thus considering that they have the same exergy value.

In *Figure 4.31*, *4.32* and *4.33* it is shown the values of First Law Efficiency, calculated on a daily basis by obtaining a mean value for each day of operation, for the years 2017, 2018 and 2019 respectively.

Every point in the graphs represent one day; Sundays are not reported in those graphical representations.

Daily mean values are calculated by neglecting the shift change hours.

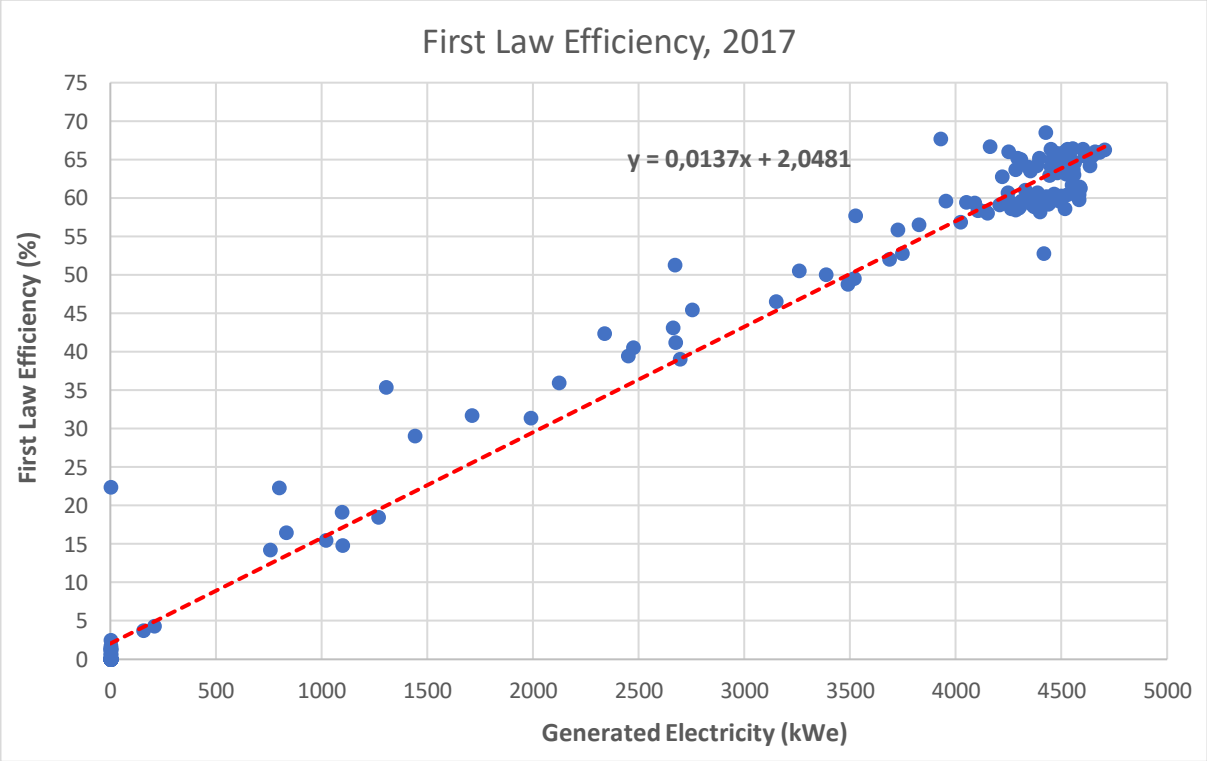

Figure 4.31: First Law Efficiency as a function of generated electricity in 2017

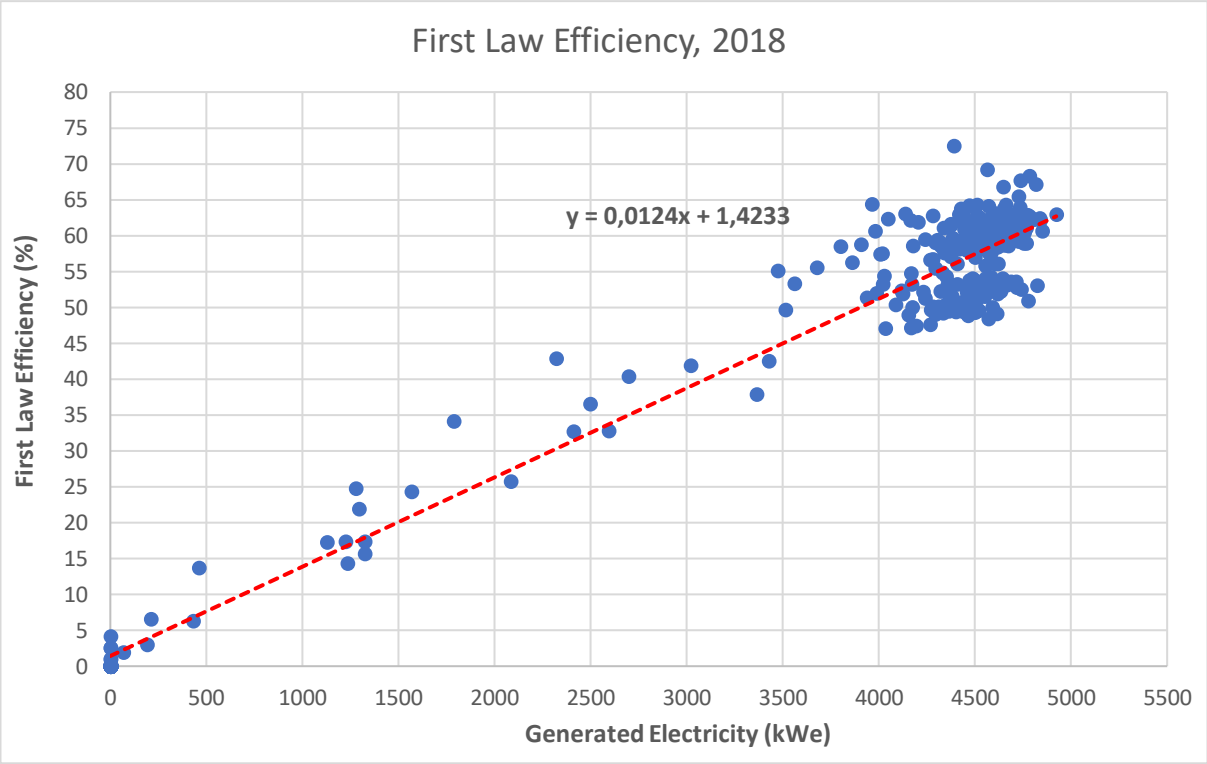

Figure 4.32: First Law Efficiency as a function of generated electricity in 2018

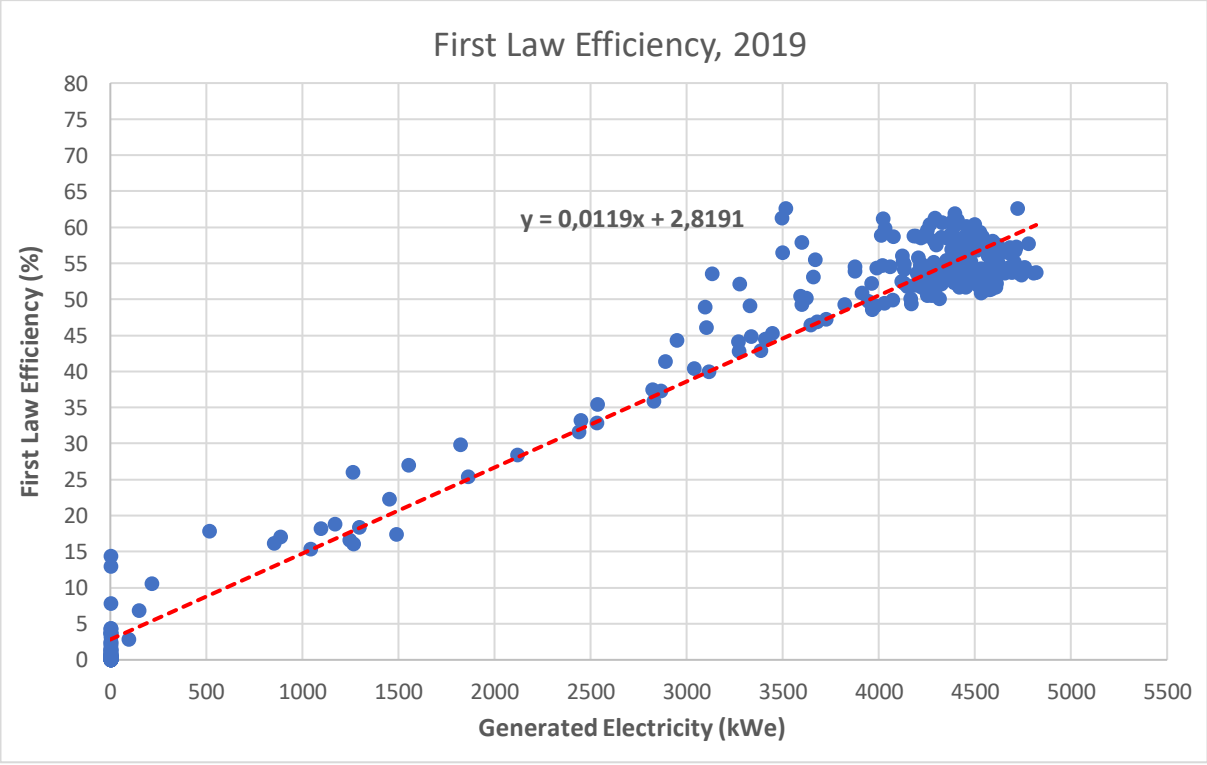

Figure 4.33: First Law Efficiency as a function of generated electricity in 2019

In *Figure 4.31*, First Law Efficiency points are calculated only for the second half of the year because of the unavailable data from January to June 2017.

In the three graphs it is possible to notice almost a linear trend of First Law Efficiency as a function of the generated electricity, but this is mainly due to the linear dependence of the engine electrical efficiency to the generated electricity. Indeed, as previously mentioned, it's not possible to establish a linear correlation between heat recovery and generated electricity.

However, it is clear that, by increasing engine electrical load, also the First Law Efficiency increases.

Near full load conditions, thus, at electric power higher than 4000 kW_e, it is possible to notice a dense cloud of points that do not follow the red dashed trend line, and this is due to the variation of thermal recovery.

During 2017 and 2018, First Law Efficiency reached a maximum of 70 %, and for many days it has been close to a value of 65 %. On the contrary, during 2019 First Law Efficiency calculated as a daily mean value, never reached 65 %. This is coherent with the observed lower thermal recovery during that year with respect, for example, to 2018.

To resume with just one value the plant efficiency during each of the three analyzed years, a yearly efficiency has been calculated: it has been obtained by summing up the electricity and thermal recovery in kWh for each operating hour, and then by dividing by the inlet natural gas energy throughout the year.

Year	First Law Efficiency
2017	60,7 %
2018	56,4 %
2019	52,6 %

Table 4.2: Yearly First Law Efficiency

Differently from the engine electrical efficiency, in this case the First Law Efficiency Values are quite different one year from another. As expected, First Law Efficiency in 2019 is the lowest value between the three analyzed years, but this is also a consequence of sensors malfunctioning in the measurement of Hot Water thermal recovery during June and July 2019.

Also, a yearly mean value at high load conditions has been calculated but it is not reported because the values are quite similar to those presented in *Table 4.2*.

This plant efficiency values can still be increased by improving the thermal recovery from the exhaust gases, in order to reach an efficiency value of around 70 or 75 %, in line with the

average First Law Efficiency at national level for Internal Combustion Engine that corresponds to 71,3 %, as reported in *Table 2.1*.
Revamping of this energy plant is therefore necessary to optimize its performance, increase the economic returns and improve the environmental sustainability.

4.3 Cold Water production

WARGs operation is necessary in order to provide cold water to the user and to exploit the useful heat produced in the HRU.
In this paragraph the WARGs functioning, and their efficiency will be analyzed.

4.3.1 Double-effect WARGs

Double-effect WARGs are indicated in *Figure 3.5* with their tags, thus, respectively GFA 1901A and GFA 1901B. Their nameplate data are reported in *Table 3.7*.
WARGs operation is quite complex because three main different water circuits are involved:

- Hot Water/ Super-heated Water circuit
- Cold Water
- Cooling Water

Then, a problem in one of these circuits can lead to a malfunctioning of the entire system and then to a prolonged maintenance.
WARGs maintenance, therefore, is quite frequent and this represent an issue for this energy plant because it means that electricity must be used to produce cold water, by means of CERGs.
It has been quite difficult to analyze WARGs operation because data were not completely available: for example, in order to obtain the produced refrigerating power, cold water mass flow rate reported in the datasheet has been used due to lack of information about this parameter. Moreover, for some periods of the analyzed years, temperatures data were not registered by sensors, therefore, it is not possible to know if some cold power was produced or if the WARG was under maintenance.
In order to evaluate WARG efficiency, the COP parameter has been calculated, starting from the thermal energy provided to the absorber and then by utilizing the calculated hourly value of

produced cold power. In the following graphs, COP hourly value are shown for the three analyzed years.

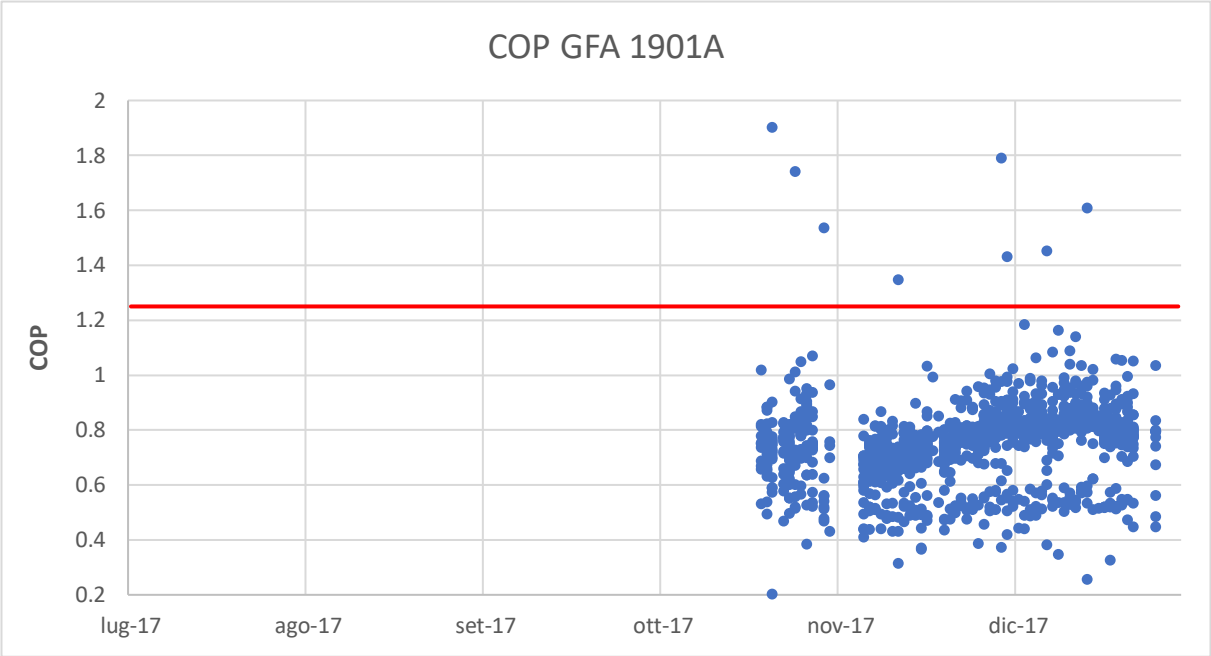

Figure 4.34: Calculated COP for double-effect GFA 1901A in 2017

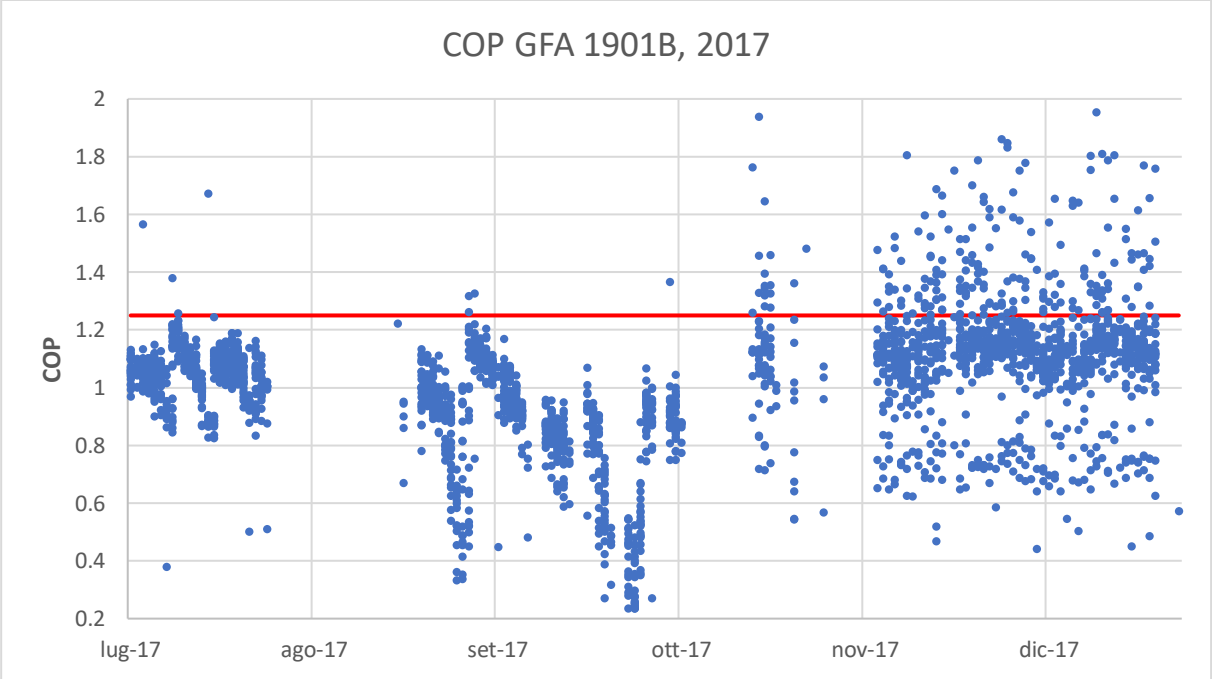

Figure 4.35: Calculated COP for double-effect GFA 1901B in 2017

For both WARGs, data were available only for the last six months of 2017. Moreover for the absorber GFA 1901A, temperature measurements were freezed until October 2017, then the

COP was equal to zero until that month but it is not possible to know from data if temperature sensors were not correctly working or if the WARG was under maintenance.

In both graphs a red line has been plotted and it represents the COP equal to 1,25 that corresponds to the nameplate efficiency of the two double-effect WARGs.

In *Figure 4.34*, it can be noticed that GFA 1901A COP is quite stable between the values of 0,6 and 1, thus quite far from the expected COP of 1,25.

On the contrary, the absorber GFA 1901B worked for much more hours in the last six months of 2017 and, moreover, the COP calculated values are positioned mostly between 1 and 1,25, therefore it worked more efficiently with respect to the other absorber.

In the case of GFA 1901B, there are also some values over the 1,25 COP line; this shows that it is not trivial to obtain a significant trend when some data are missing or if they are not correct.

The following *Figure 4.36* and *4.37* show the same COP analysis for the year 2018.

It is possible to notice that the COP of the absorber GFA 1901A is similar to the values shown in *Figure 4.34* for the year 2017. Indeed, also in this case the maximum COP was around 1 for many hours of the year.

From May to the end of the year, the absorber didn't work or was under maintenance. During August and September 2018, data about temperatures and mass flows were not available.

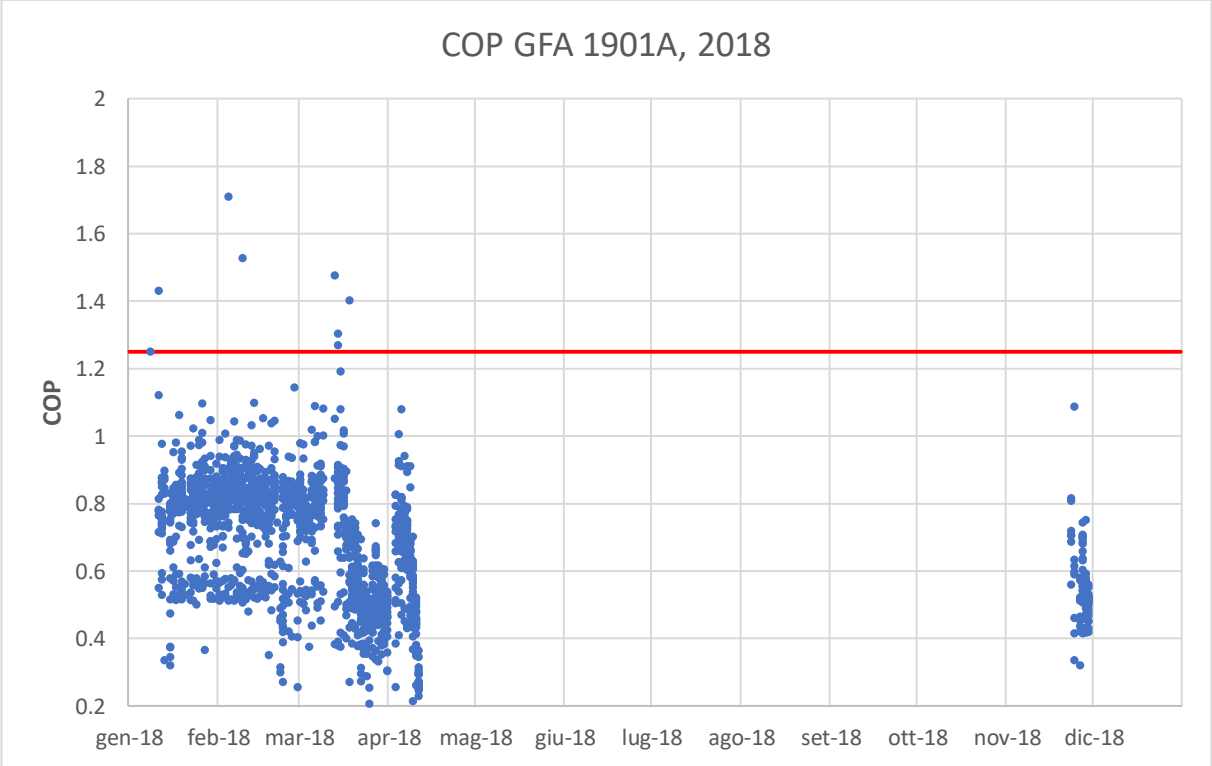

Figure 4.36: Calculated COP for double-effect GFA 1901A in 2018

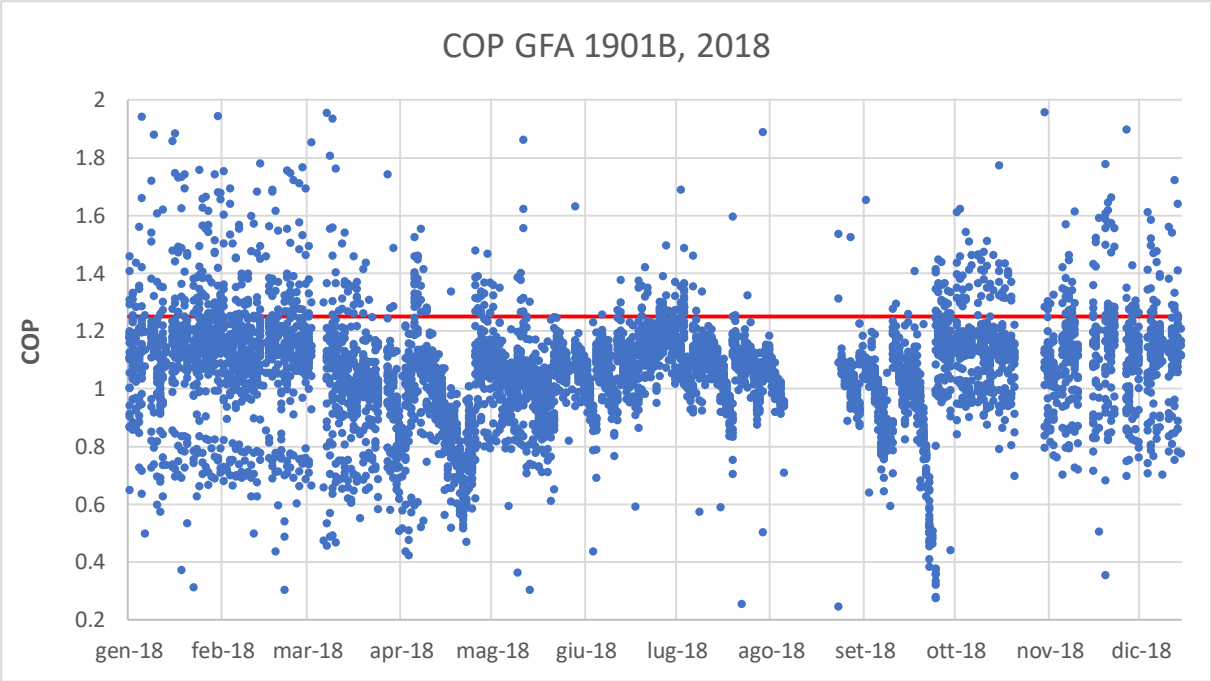

Figure 4.37: Calculated COP for double-effect GFA 1901B in 2018

The same considerations can be done about the operation of the absorber GFA 1901B and the similarity of the COP trend throughout the year 2018 with respect to 2017.

Also in 2018, the WARG GFA 1901B worked for much more hours than GFA 1901B and the efficiency (COP), is higher with respect to that of the other double-effect absorber. In this case, indeed, it is possible to say that the absorber worked correctly and with a very high efficiency, near to the nameplate value of 1,25.

For what regards the year 2019, the COP graphical evaluation for both absorbers is not reported: indeed, the GFA 1901A didn't operate for most of the year, while GFA 1901B efficiency is very similar to the COP value during the years 2018 and 2019.

In order to calculate the COP, every hour during which the produced cold power was lower than 150 kW_f (around 10 % of nominal cold power of 1400 kW_f) have been neglected because those small values of cold power may be due to small temperature differences between the inlet and outlet cold water temperatures, that do not correspond to an actual refrigerating power produced by the absorber and provided to the user.

It can be interesting to analyze if the absorber COP varies according to the super-heated water temperature provided to the absorbers. It has been graphically evaluated in *Figure 4.38*.

In the following graph the temperature of super-heated water supplied to the WARG GFA 1901B during the year 2018 has been positioned on the x-axis, while on the y-axis there is the absorber COP.

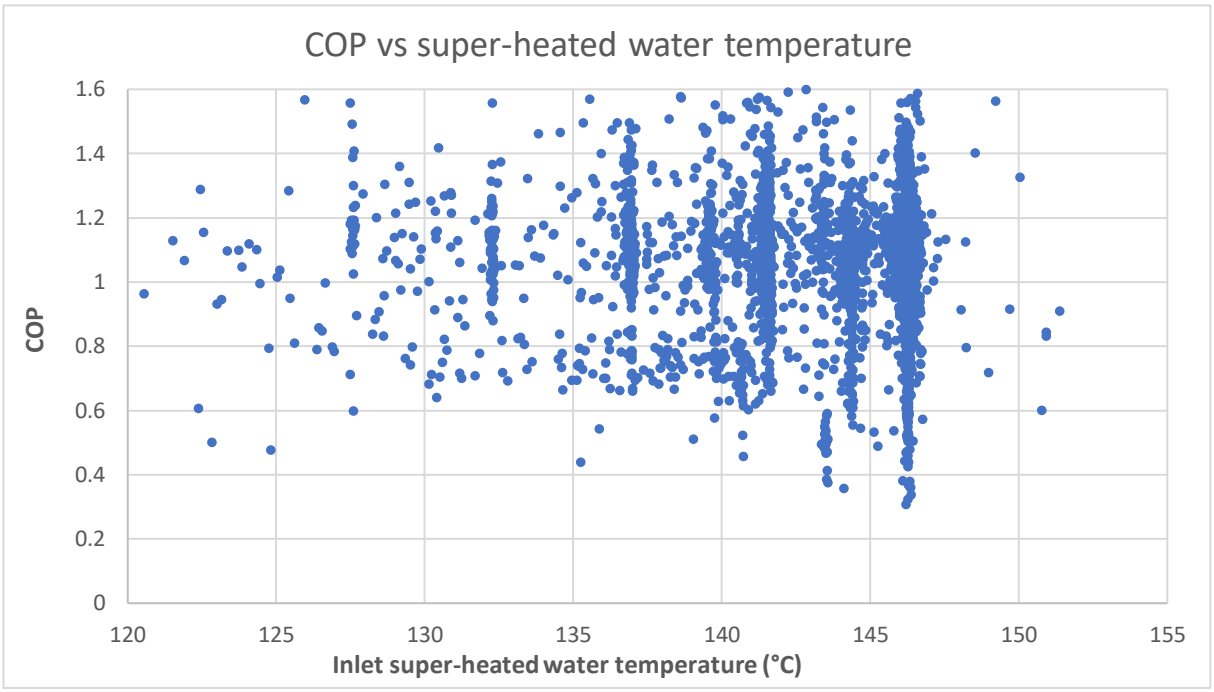

Figure 4.38: COP as a function of inlet super-heated water temperature for GFA 1901B in 2018

According to what has been said in the **Paragraph 2.4**, by increasing the water temperature, the COP doesn't increase maintaining floating values.

Indeed, in *Figure 4.38* it is not possible to extrapolate a clear trend that expresses the COP as a function of inlet super-heated water temperatures. On the contrary it is possible to see a cloud of points randomly positioned on the graph.

In *Figure 4.39*, it is shown the variation of the COP with the cooling water temperature.

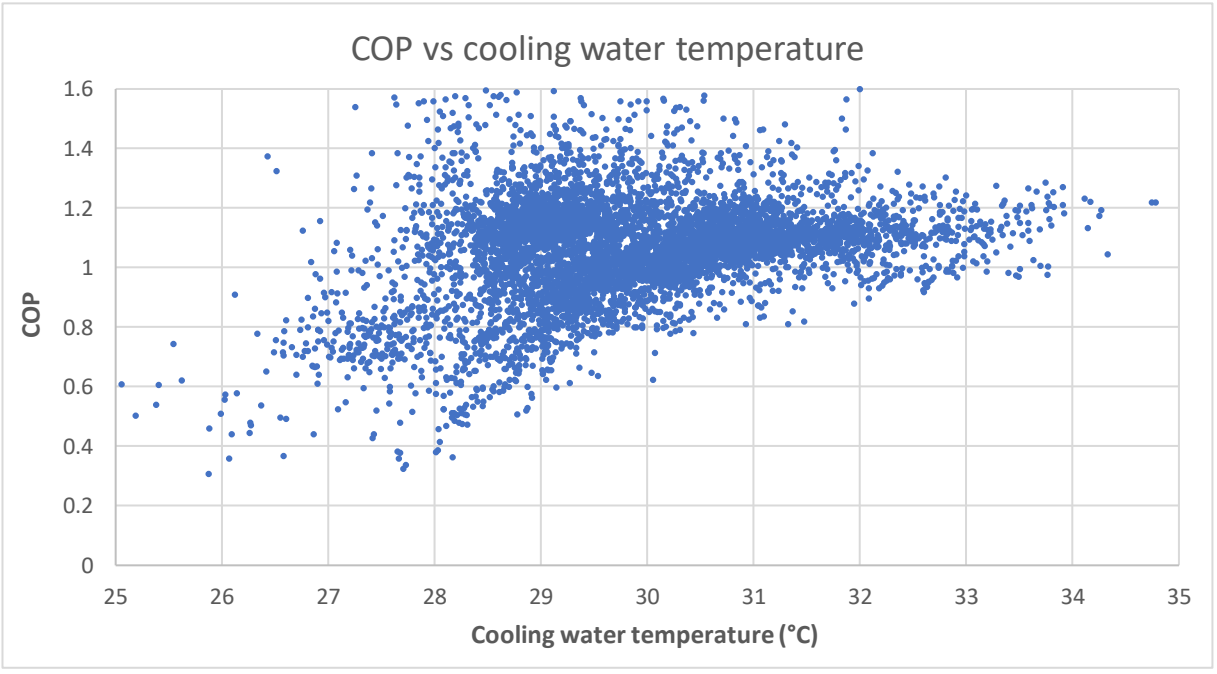

Figure 4.39: COP as a function of cooling water temperature for GFA 1901B in 2018

Contrary to what has been said in **Paragraph 2.4**, even in *Figure 4.39*, it is not possible to see a sharp decrease of the COP as the cooling water temperature increases.

In *Figure 4.*39, the COP is quite stable between 0,8 and 1,2 for cooling water temperatures that vary between 27 and 33 °C.

In *Table 4.3* a yearly mean COP value for both double-effect absorbers is reported. The mean value has been calculated by performing an arithmetic average of the COP during the hours of absorber operation.

Year	GFA 1901A COP	GFA 1901B COP
2017	0,76	1,02
2018	0,70	1,07
2019	0,78	1,00

Table 4.3: Double-effect absorbers COP mean value

In addition to a COP analysis, it is also important to investigate the cold power produced by the WARGs during the years, in order to establish if they have worked near full load conditions or at partial load for most of the time.

In both absorbers datasheet it is indicated that WARGs can modulate their production down to 30 % of full load conditions.

In the following graphs in *Figure 4.40* and *4.41*, it is shown the average hourly cold power produced by GFA 1901A and GFA 1901B during the last six months of 2017.

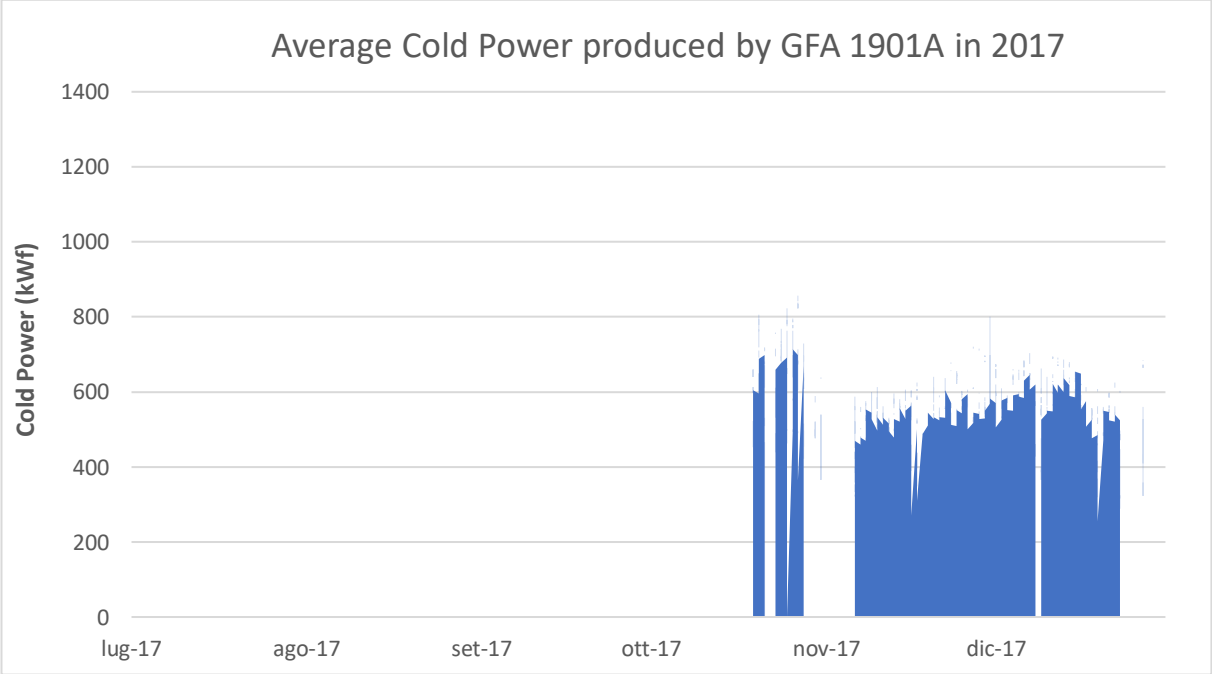

Figure 4.40: Average Cold power produced by GFA 1901A during 2017

By scaling the y-axis so that the maximum value on the vertical axis corresponds to the nominal power of the absorber (1400 kW_f), it is possible to notice that the WARG GFA 1901A worked at less than 50 % of full load conditions.

Since the nominal chilled water mass flow rate has been employed to calculate the produced cold power, this means that the temperature difference between inlet and outlet chilled water is around 2 °C, rather than 5 °C, in the temperature range 12 – 7 °C.

The assumption of using the nominal cold water mass flow rate can be considered realistic, because it is realistic to assume that the cold water pump works at fixed flow rate.

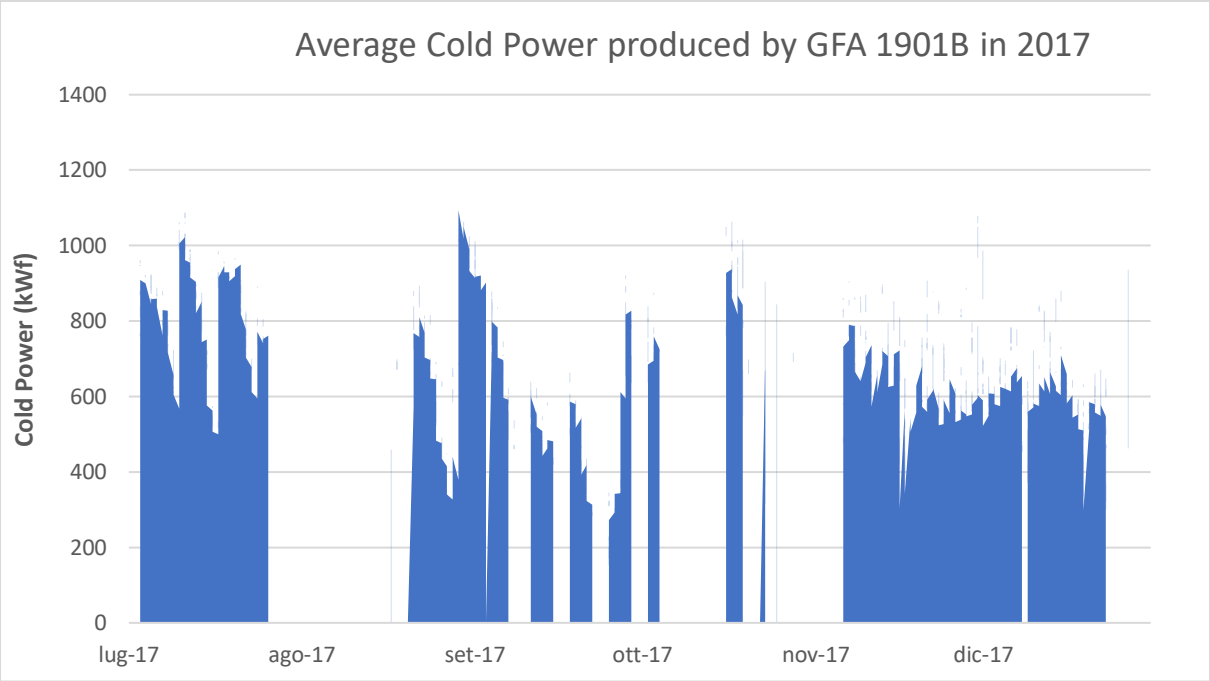

Figure 4.41: Average Cold power produced by GFA 1901B during 2017

In the case of GFA 1901B, the maximum produced cold power reached even 1000 kW_f, but it is still only the 70 % of nominal power. In addition to that, the absorber worked at a power lower than 1000 kW_f for most of the time.

Therefore, the absorbers worked at low power for many hours, and this led to the utilization of CERGs in order to cover the user cold water demand.

Even in 2018, the absorber operated at low power, as it is shown in *Figure 4.42* and *4.43*.

It is noticeable from *Figure 4.40* and *Figure 4.42* that the absorber GFA 1901A was stopped for most of the time during 2017 and 2018.

Problems in one absorber functioning or frequent maintenance cause serious issue to the efficient performance of the energy plant. Indeed, if one absorber is offline, then the super-heated water demand is reduced, therefore a larger exhaust gases mass flow rate bypass the

HRU and less thermal energy is recovered. This represents a dramatic problem because even the hot water is not heated up adequately in the economizer by the exhausts, thus, the hot water demand from the paintings ATU cannot be covered, or, alternatively, hot water cannot be supplied at the correct temperature level to the single-effect absorber. In this case, therefore, it is not possible to provide the energy carriers to the user, thus the CERGs must be switched on to produce cold water.

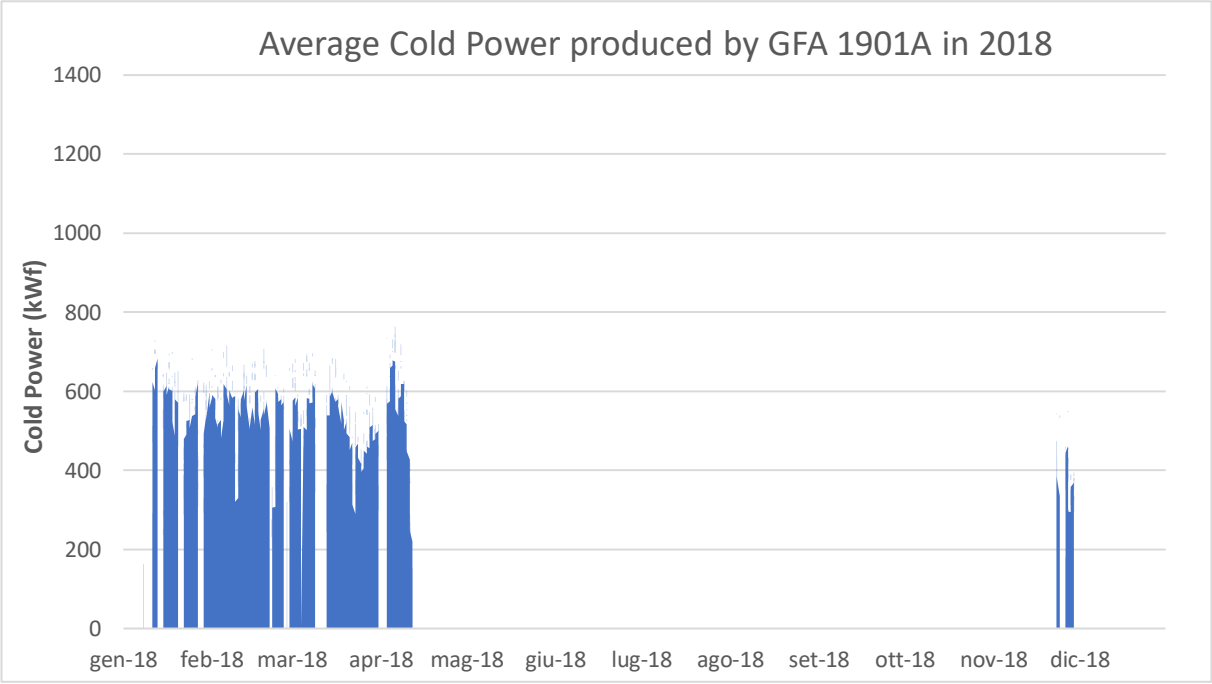

Figure 4.42: Average Cold power produced by GFA 1901A during 2018

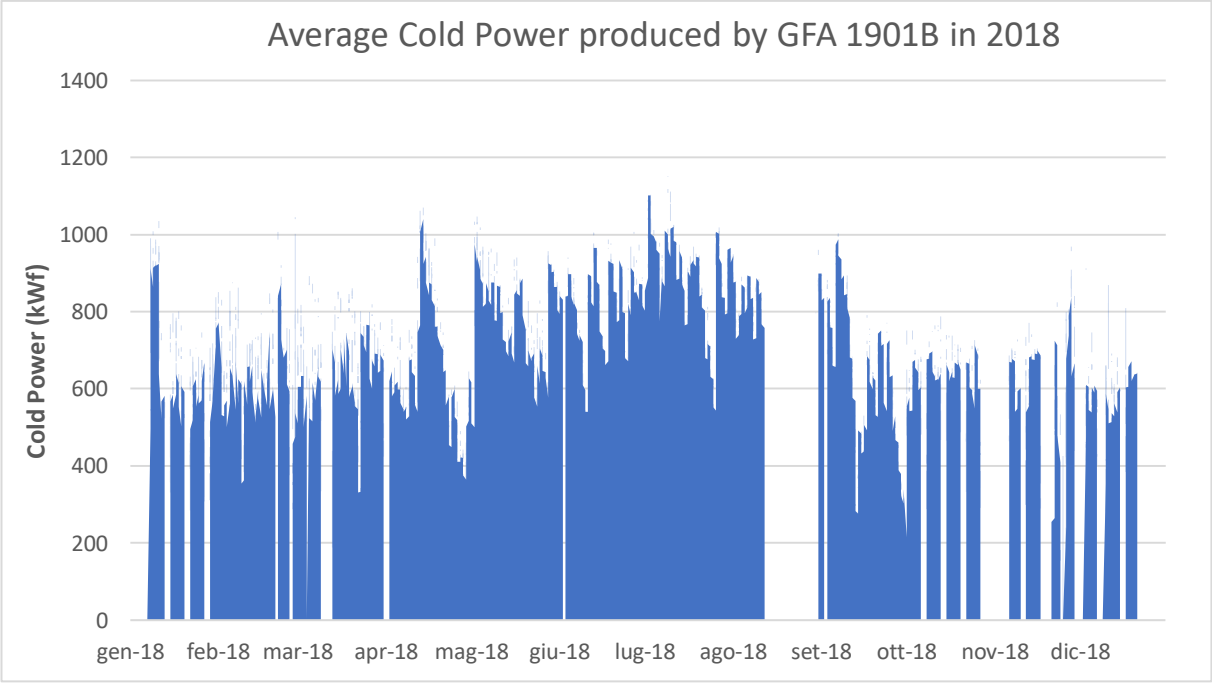

Figure 4.43: Average Cold power produced by GFA 1901B during 2018

Graphical representations of cold power produced during 2019 is not reported because, as already mentioned, GFA 1901A didn't work for most of the year, while GFA 1901B produced power trend throughout the year is similar to that of years 2017 and 2018.
It can be interesting to evaluate a sort of absorber yearly equivalent hours, calculated by dividing the total refrigerating energy produced in one year by the WARGs nominal capacity.
Then a Capacity Factor is obtained by dividing the equivalent hours by 8760 hours in a year (or by 4380 in 2017 because only the last six months have been analyzed).
Results are reported in *Table 4.4*.

Year	GFA 1901A Capacity Factor	GFA 1901B Capacity Factor
2017	11,0 %	25,6 %
2018	7,5 %	35,6 %
2019	0,7 %	24,1 %

Table 4.4: Double-effect absorbers Capacity Factor

It is immediately noticeable that GFA 1901 didn't operate as expected during the three analyzed years; in particular, 2019 cannot be considered in this analysis because temperature sensors were not registering data for a long period.
On the contrary, GFA 1901B produced the same energy that he could have produced if it operated at nominal power for approximately one fourth of the year in 2017 and 2019, and around one third of the year during 2018.

4.3.2 Single-effect WARG

In this paragraph the operation of the single-effect WARG GFA 1902 during the years will be analyzed.
Even for this hot water absorber, nameplate data are reported in *Table 3.7*.
Also in this case, the chilled water mass flow rate data were not available, therefore the value of produced cold power has been calculated with the assumption that the water pump operates at fixed flow rate, equal to the nominal one.
In this case, differently from the double-effect absorbers, a totalizer meter that measures the supplied thermal energy to the WARG is not available.

Indeed, as it is shown in *Figure 3.7*, hot water can be directed towards the absorber and/or to the decoupling heat exchanger E-1903, in order to provide heat to the paintings ATU.
Therefore, to calculate the thermal energy provided to the single-effect absorber, the thermal energy supplied to the paintings ATU has been subtracted from the Hot Water total thermal recovery.
Nevertheless, it almost never happened that hot water was supplied to both the paintings ATU and the absorber: generally, hot water was directed to the paintings ATU during cold seasons and towards the absorber during summer. This can be clearly seen in *Figure 4.44*, where it is graphically represented the thermal power supplied to the single-effect absorber GFA 1902 and the heat provided to the paintings ATU during 2018.

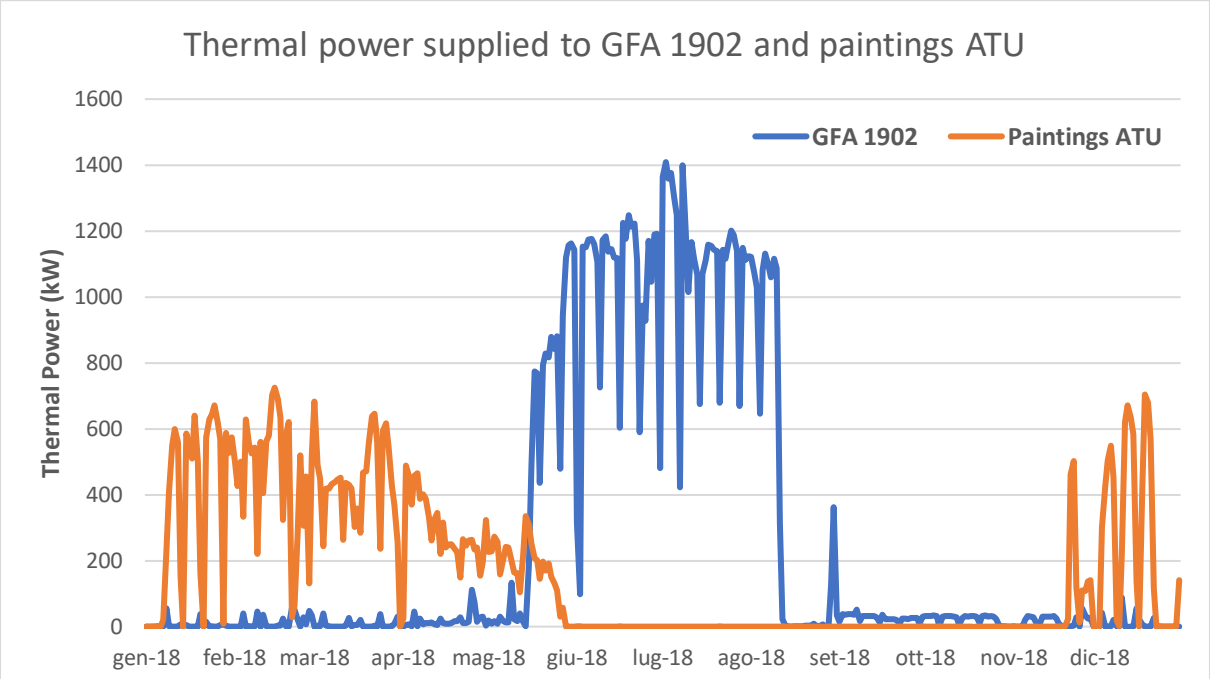

Figure 4.44: Thermal power supplied to GFA 1902 or to Paintings ATU

The previous graph has been obtained by calculating a daily mean value of thermal power provided to the two different circuits.
It is possible to notice that the two energy demands didn't overlap, except for some days during May 2018, nevertheless that superimposition can be due to some small errors in energy measurements. Issues about hot water recovered thermal energy also occurred between September and December 2018: from *Figure 4.25*, it was possible to notice that thermal energy was not recovered in that period, consequently, in *Figure 4.44*, thermal power wasn't supplied neither towards paintings ATU nor to the single-effect WARG.
In the following graphs, the COP evolution, during the three analyzed years, is reported.

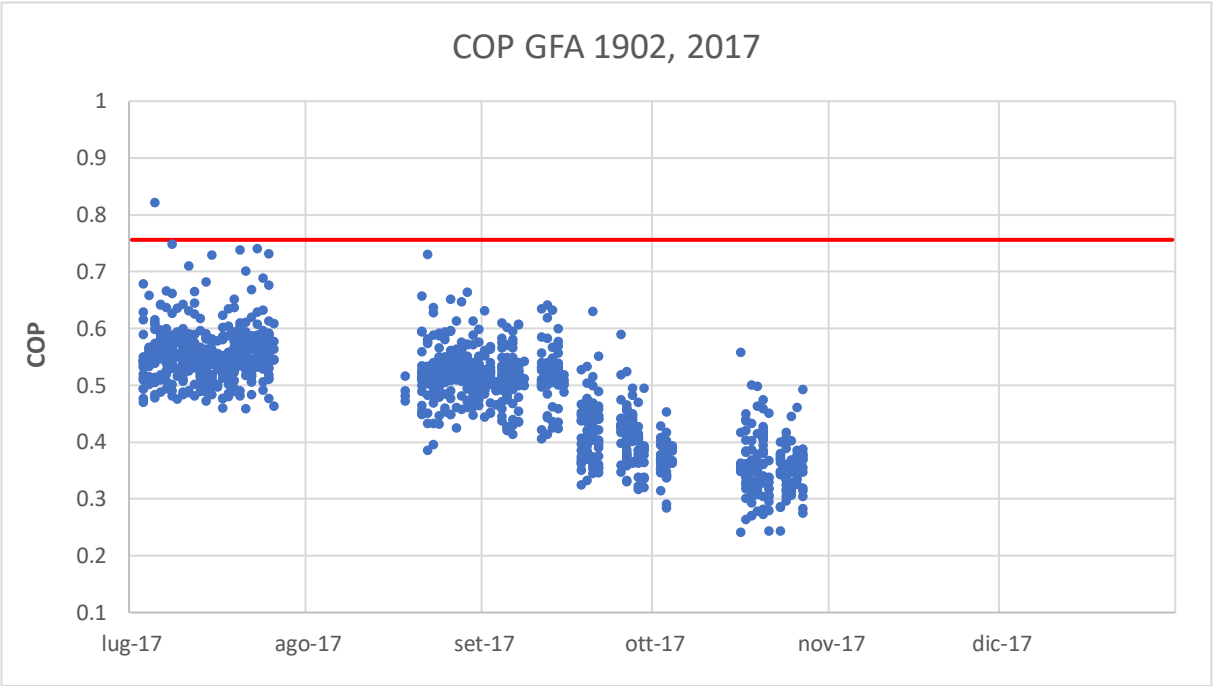

Figure 4.45: Calculated COP for single-effect GFA 1902 in 2017

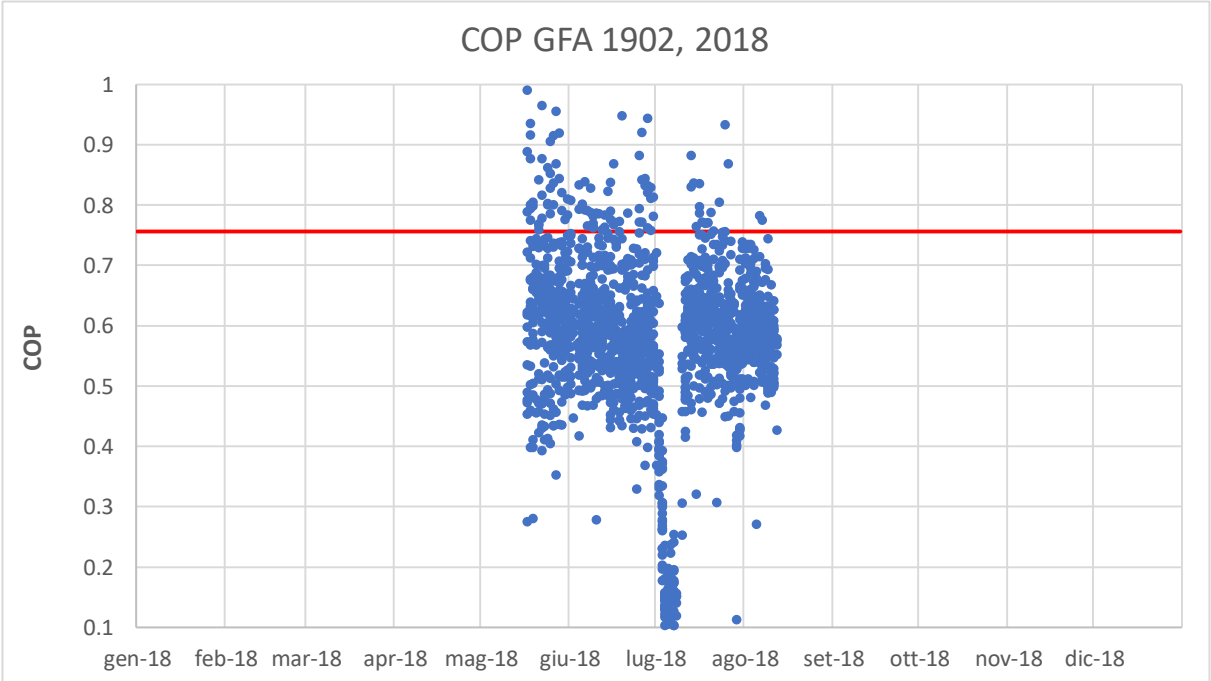

Figure 4.46: Calculated COP for single-effect GFA 1902 in 2018

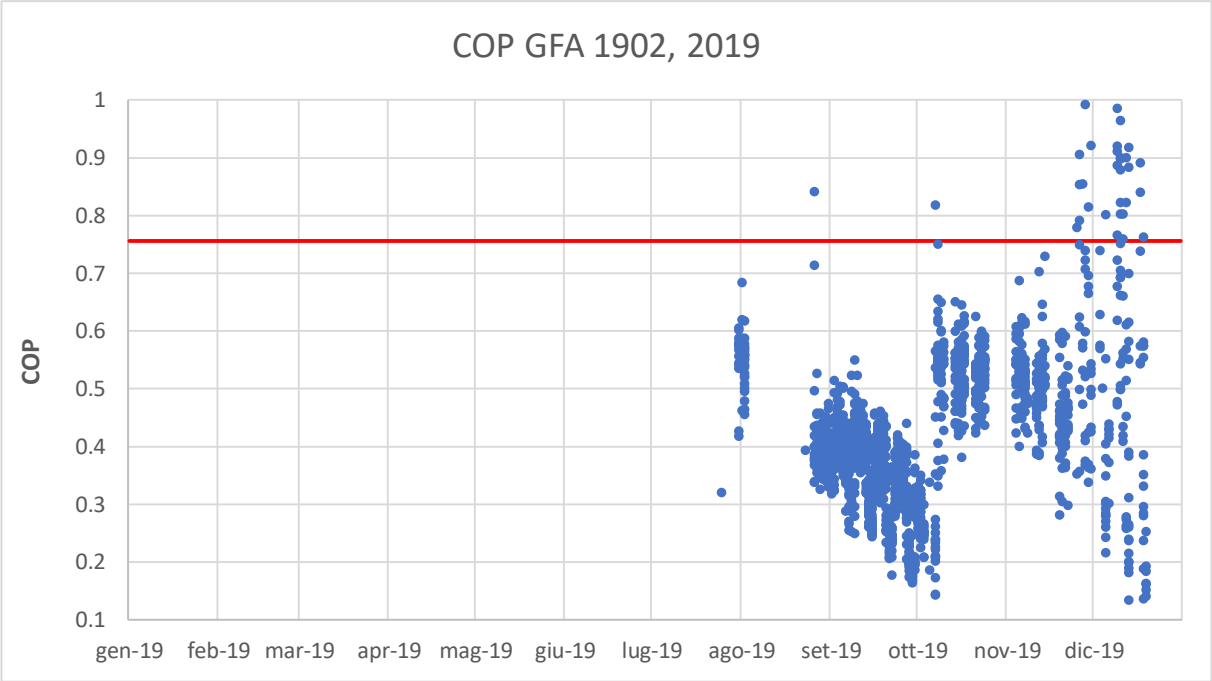

Figure 4.47: Calculated COP for single-effect GFA 1902 in 2019

It is possible to see, from *Figure 4.44* and *4.45* that, during 2017 and 2018, the single-effect absorber operated only during summer, while in 2019 the absorber worked in the last three months of the year.

For what regards the single-effect absorber in 2019, data about cold water temperature were not available until the end of July 2017, therefore, it is not possible to know if it worked correctly or if it was under maintenance.

In 2017, the COP value is mostly located between 0,4 and 0,6, then it decreases at the end of October.

In *Figure 4.46*, instead, the hourly COP values are closer to the nameplate efficiency of 0,756: indeed, during summer 2018, the WARG efficiency is mostly located between 0,45 and 0,75, thus with a very high efficiency for a single-effect absorber.

In 2019 (*Figure 4.47*) it is more difficult to extrapolate an average value because the calculated COP values are located quite randomly on the graph; some small deviations on measurements can lead to less significant values: for example, it is not probable that, during December 2019, the absorber worked with an efficiency higher than 0,75 and really close to 1.

Values between August and October 2019 are more realistic; in that period, the hourly calculated COP was mostly between 0,2 and 0,5.

Also for the single-effect absorber, a yearly average COP has been calculated as the mean value of the WARG COP during the hours of operation.

Results are shown in *Table 4.5*.

Year	GFA 1902 COP
2017	0,49
2018	0,58
2019	0,43

Table 4.5: Single-effect absorber COP mean value

In the three analyzed years, the COP mean value was between 0,4 and 0,6, and they can be considered realistic values for a single-effect absorber.

The highest COP mean value has been reached in 2018, while the lowest COP is the mean value of 2019, probably because of a long period (September 2019) at low efficiency, between 0,2 and 0,4.

In order to analyze the operation of the single-effect absorber, it is necessary to evaluate the average hourly cold power that has been produced in the three years.

Even in the hot water WARG datasheet it is written that it can modulate the production down to 30 % of nominal conditions (that corresponds to 300 kW_f).

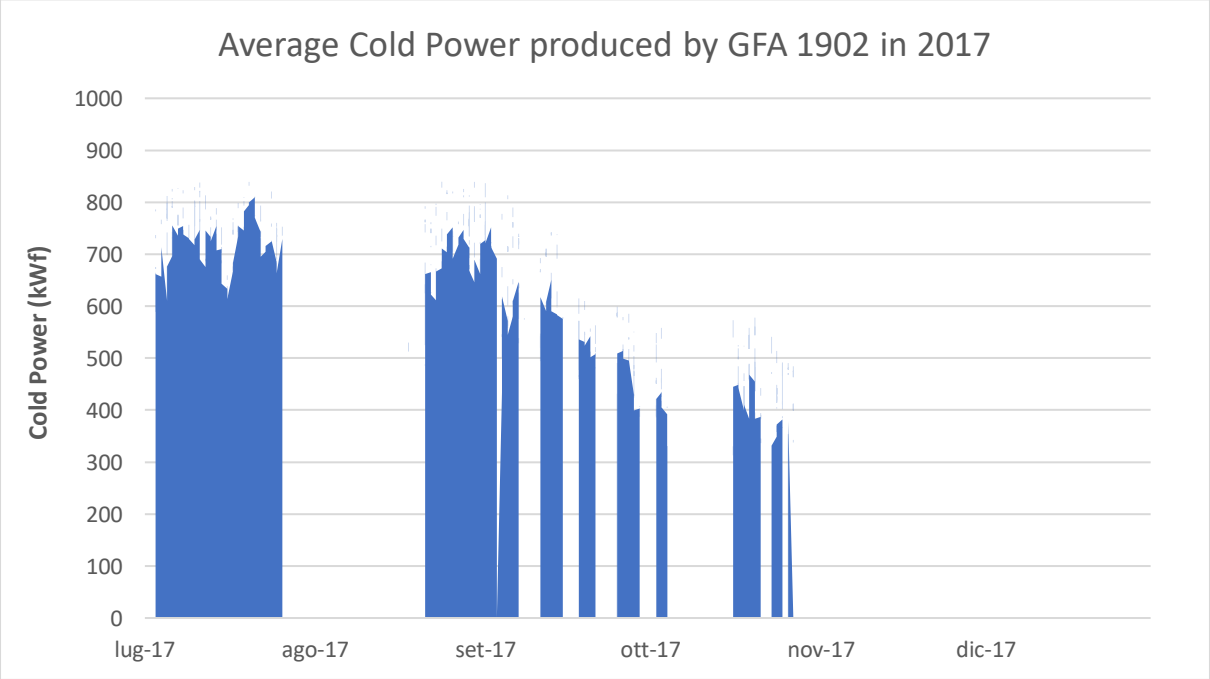

Figure 4.48: Average Cold power produced by GFA 1902 during 2017

Even in this case, the y-axis has been scaled so that the absorber nominal power corresponds to the maximum value on the vertical axis, thus 1000 kW_f.

In *Figure 4.48* it is shown that in July and September 2018, the absorber operated at around 70

% of full load conditions, then the produced cold power decreased.

This is coherent with the graph in *Figure 4.45*, where it is shown that the COP decreased in the last months of 2017: indeed, by reducing the produced cold power, and operating farther from nominal conditions, then the efficiency decreases.

In *Figure 4.49* and *4.50* the average produced cold power during 2018 and 2019.is represented.

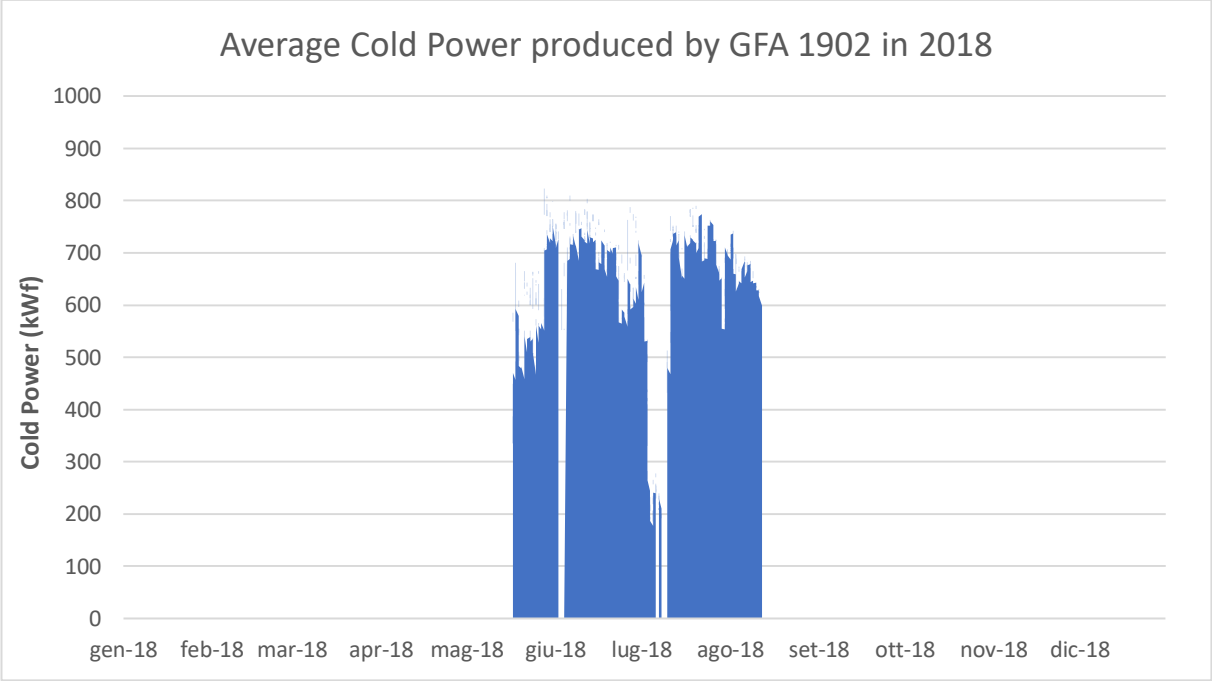

Figure 4.49: Average Cold power produced by GFA 1902 during 2018

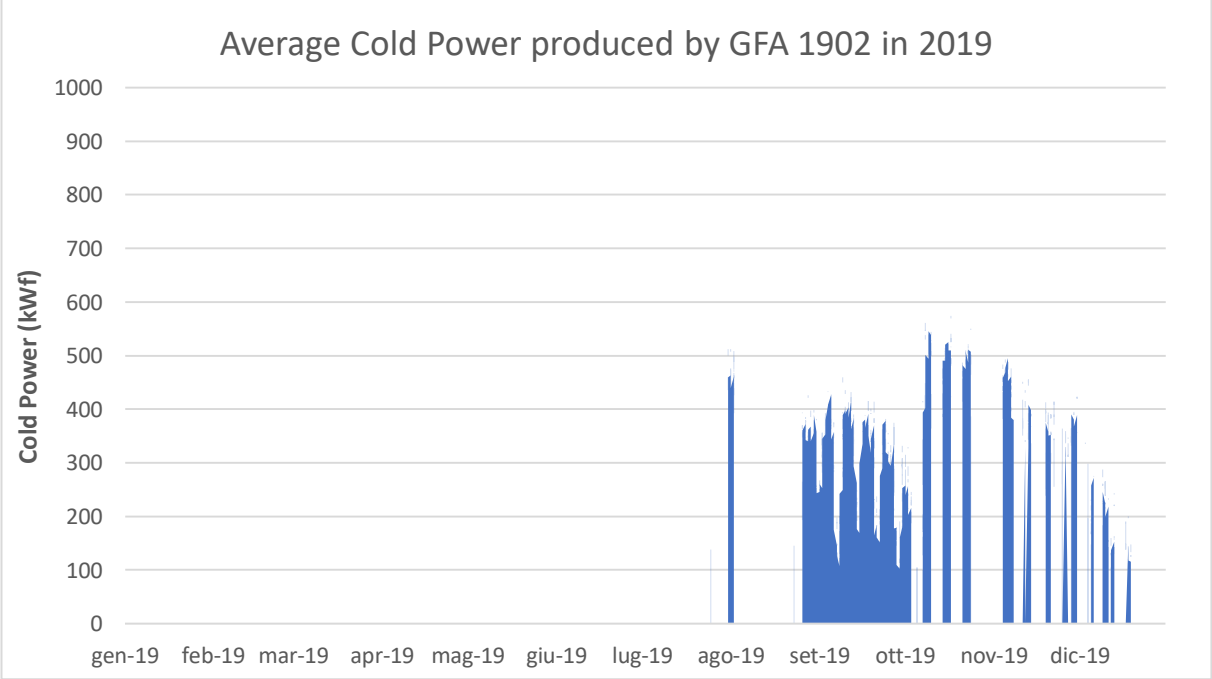

Figure 4.50: Average Cold power produced by GFA 1902 during 2019

During summer 2018, the GFA 1902 worked almost constantly between 60 and 70 % of nominal conditions and this explains why, in *Table 4.5*, the highest yearly average COP was reached in 2018.

On the contrary, in the last months of 2019, the absorber operated at low power: in particular, during September it produced a maximum of 400 kW_f, that corresponds to 40 % of full load conditions. This shows that September 2019 COP values are realistic because partial load conditions lead to low efficiency.

On the contrary, the blue dots above the 0,756 red line in *Figure 4.47* cannot be considered as significant values: in the same period, the produced cold power shown in *Figure 4.50* is low.

It is important to underline that temperatures data were not available from 17/10/2018 until 22/07/2019, therefore it is not possible to establish if the WARG operated in that period of time and which power has been produced, or, if it was not available because of maintenance.

A Capacity Factor has been evaluated also for the single-effect absorber GFA 1902, even if, differently from the two double-effect absorbers, the hot-water-supplied WARG is not programmed to operate for the whole year, because hot water is also supplied to the paintings ATU.

Year	**GFA 1902 Capacity Factor**
2017	19,9 %
2018	13,0 %
2019	6,2 %

Table 4.6: Single-effect absorber Capacity Factor

Results reported in *Table 4.6* show that the hot water absorber worked for more equivalent hours during 2017 (in order to obtain the Capacity Factor in 2017, the equivalent hours have been divided by 4380 because data are only available starting from July 2017).

On the contrary, during 2019, the Capacity Factor was around 6 %, and this is coherent with the produced power graphical evaluation in *Figure 4.50*.

4.3.3 Compression Electric Refrigerator Groups

As already mentioned, the energy plant is equipped with three electric chillers with a total electric nominal power equal to around 2800 kW_e, that are useful to cover the cold water demand peaks and the periods of time during which the WARGs are under maintenance.

It is not possible to correctly evaluate the contribution of CERGs in the production of cold power: indeed, the only available data about electric chillers is the absorbed electricity.

Data about cold water temperatures and mass flow rate are not available.

Moreover, by performing some graphical evaluation, it is immediately clear that there is a mismatch between the cold power demand and the production.

In the following *Figure 4.51* the cold water demand curve is plotted against the WARGs and CERGs production. The analyzed year is 2018.

In the graph, the CERGs production is plotted in terms of absorbed electricity, thus in order to obtain the actual production of cold power, it would be necessary to multiply the value of absorbed electricity by the CERGs COP.

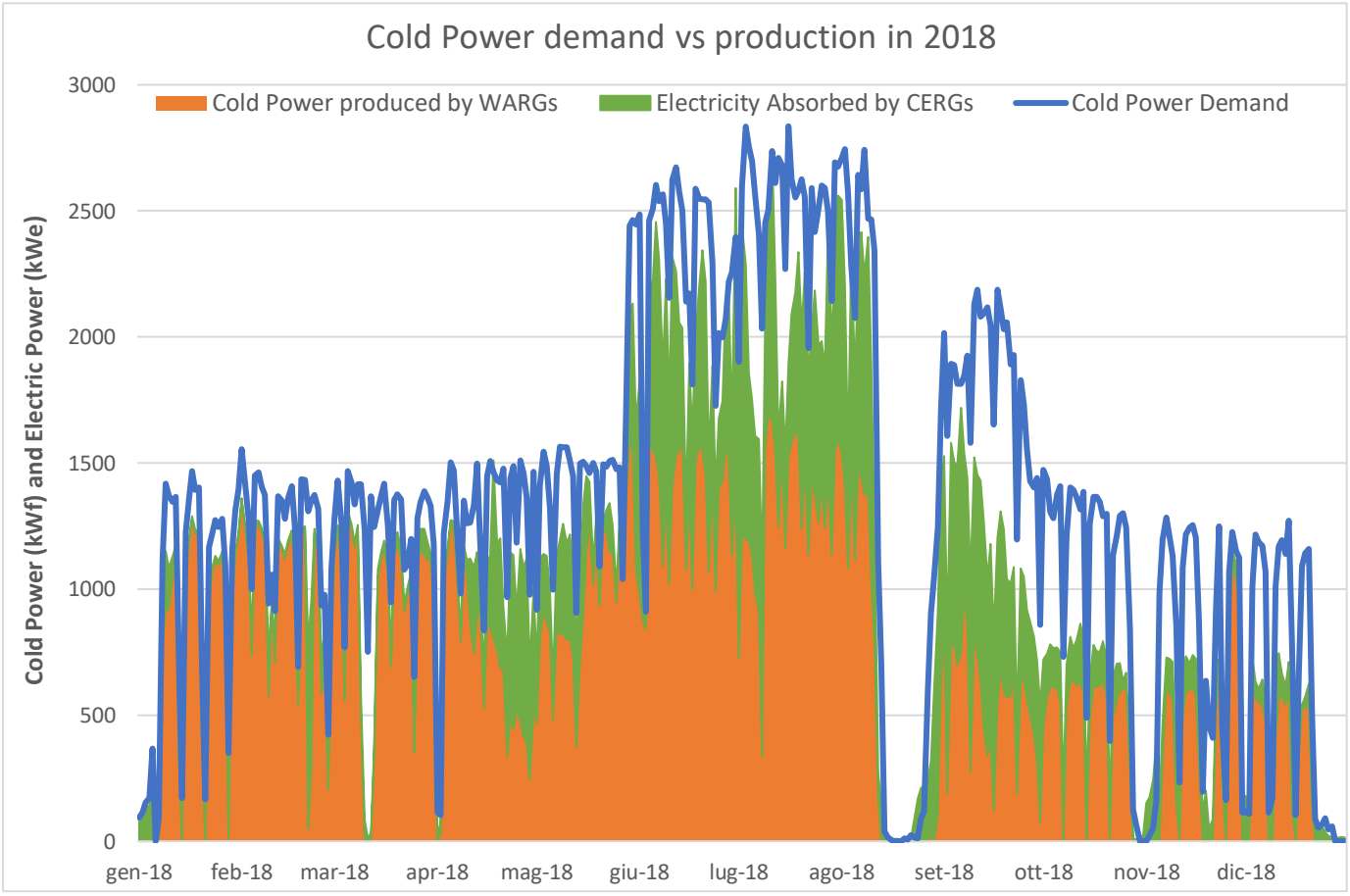

Figure 4.51: Cold power demand against demand in 2018

The blue line represents the total cold power supplied to the user, while the orange area is the sum of WARGs cold power production.
The green area represents the sum of the electricity absorbed by three electric chillers: it is clear that by multiplying the green area by the COP (it is reasonable to assume a COP value between 3 and 4 in the case of compression electric chillers), then the sum of the orange and the green area will largely overcome the blue line, but this is not coherent with reality.
Thus, by assuming that the user cold water demand data and that the calculated WARGs cold power production can be considered realistic values, then it is not possible to establish the actual cold power production from the electric chillers.

4.4 Energy Services

In this paragraph, the three main energy services provided to the user, except for electricity, will be analyzed in order to understand the evolution of energy demand from the three different circuits, during time.
The three water circuits are:

- Cold water circuit for the press unit
- Cold water circuit for air conditioning of the production site
- Hot/Cold water circuit for paintings ATU

Each section is analyzed in terms of energy demand time evolution, cumulative curves and energy signature.

4.4.1 Press unit

The press unit requires technological cold water with a temperature jump between 15 °C and 20 °C.
In the original plant configuration, this was the only circuit to be supplied from the Fenice SpA energy plant.
In this case, the cold water energy vector must be supplied to the user almost constantly throughout the year, independently from the outdoor temperature.

The press unit section is indicated in *Figure 3.5* with the tag JQ-1900, that is referred to the totalizer meter that records the energy provided to the user, on the secondary circuit.

In the following graphical representations, the cold water energy delivered to the user is represented with its time evolution during 2017 and 2018; the 2019 analysis is here omitted for simplicity because the curve trend throughout the year is similar to the 2017 and 2018 trends.

The totalizer meter also recorded the energy data in the first six months of 2017.

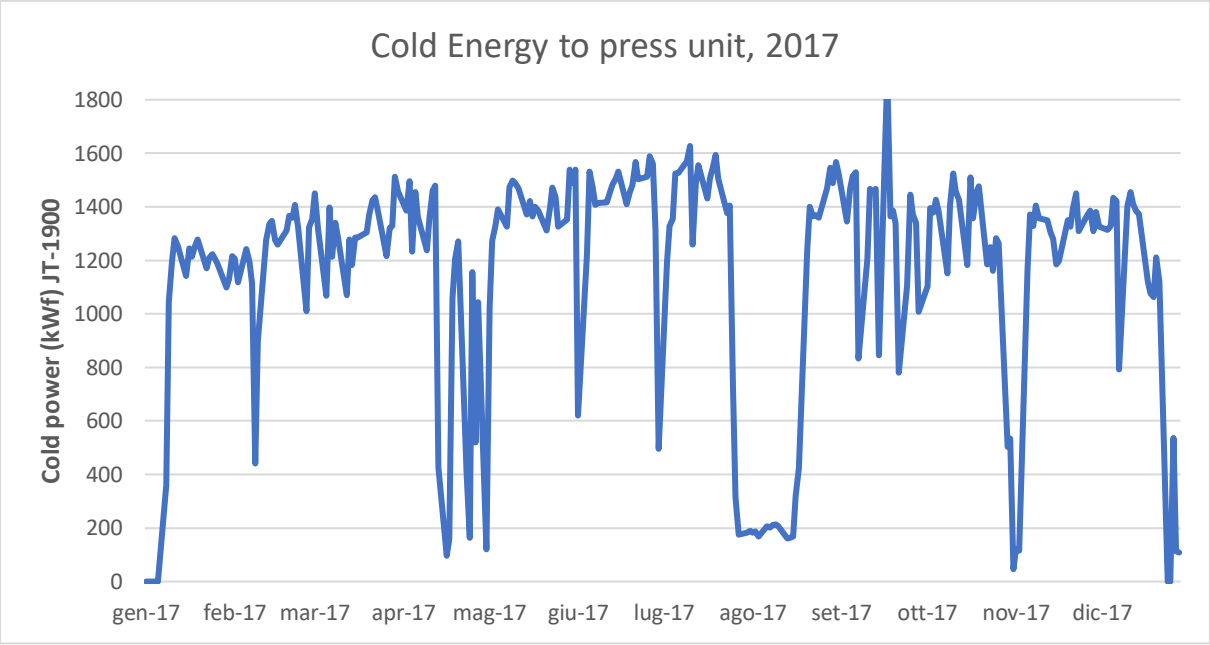

Figure 4.52: Cold energy delivered to the press unit in 2017

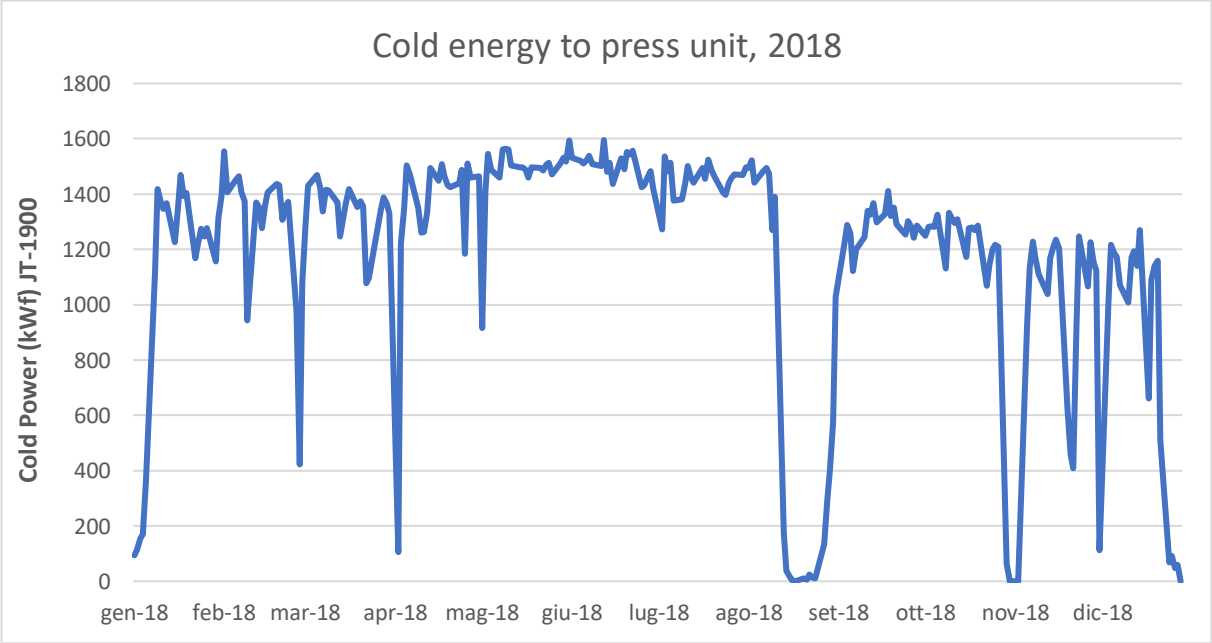

Figure 4.53: Cold energy delivered to the press unit in 2018

The curves have been obtained by calculating the daily mean values of cold power supplied to the user, thanks to the totalizer meter JQ-1900.

Moreover, the shift changes hours have been neglected in the calculation of the daily average cold power and, also Saturdays and Sundays' cold energy demand are not present in *Figure 4.52* and *4.53*, in order to have flatter curves.

Nevertheless, the 2017 cold energy curve is much less constant than the 2018 curve.

It is immediately noticeable the decrease of energy demand during the two middle weeks of August due to the shutdown of the plant, in both 2017 and 2018 curves.

During high energy demand periods, the daily mean cold power supplied to the press unit, in 2017 and 2018, lies mainly between 1200 kW_f and 1600 kW_f.

From the two previous graphs, it is clear that cold energy is delivered throughout the year, with no dependence from the season: this is much more evident by means of an energy signature graphical representation.

The energy signature method allows to express and visualize a relationship between the outdoor temperature and the hot/cold energy delivered to a final user.

The energy signature graphical representation is realized with points graph where, on the x-axis there is the outdoor temperature, while the energy delivered to the user is positioned on the y-axis.

If the energy vector demand is dependent on the outdoor temperature, then a non-flat curve will be originated: for example, if the user requires energy for air conditioning, in order to keep the indoor temperature constant, then the energy signature will be characterized by a U-shape curve, with high energy demand both at very low and very high temperatures

Since the press unit requires cold water almost constantly throughout the year, a flat energy signature curve is expected, because demand is not dependent on outdoor temperature.

The energy signature curves for the press unit have been realized by using the daily mean data, neglecting the shift change hours; in addition to that, also Sundays are not considered in the graphical evaluation.

Moreover, some weeks, for example the first and the last weeks of the year, and the middle august weeks have been neglected, in order not to affect the energy signature curves and, therefore, to obtain clearer trends.

Graphical results for the three analyzed years are shown in *Figure 4.54*, *4.55* and *4.56*.

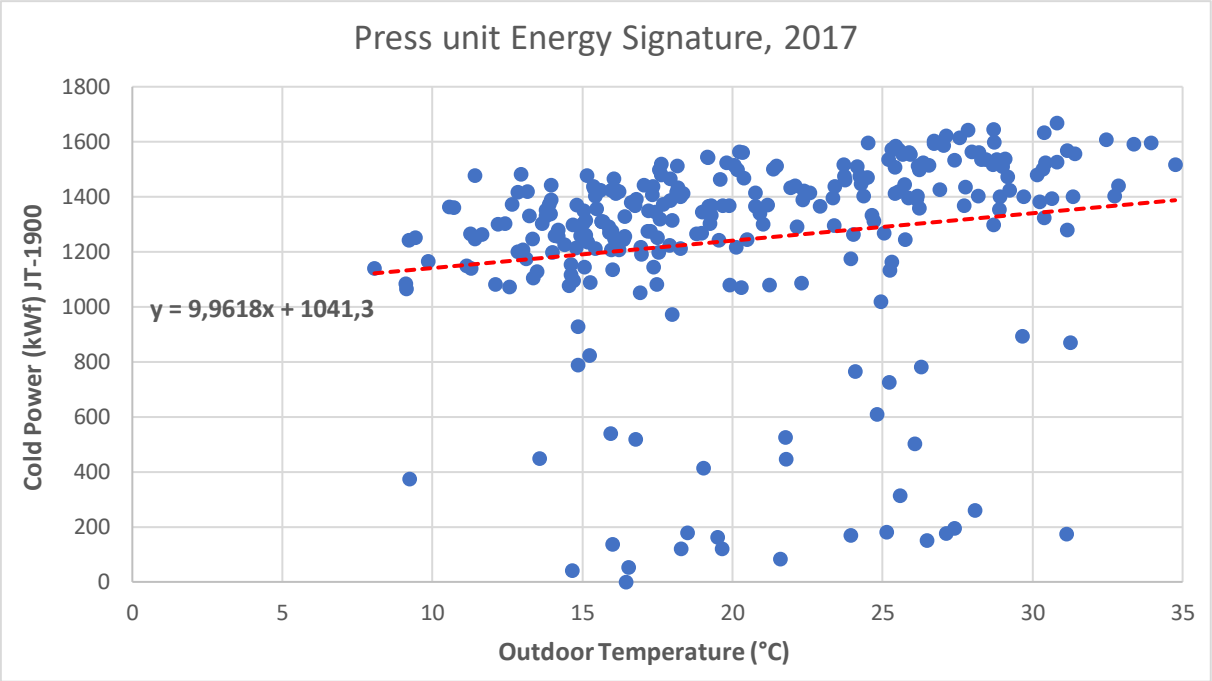

Figure 4.54: Energy Signature for the press unit in 2017

In *Figure 4.54*, it is noticeable that, despite a small cold energy increase at higher outdoor temperatures, the majority of the blue points, representing a daily mean cold power demand, are located between 1200 and 1600 kW_f, with little dependence on the outdoor temperature.

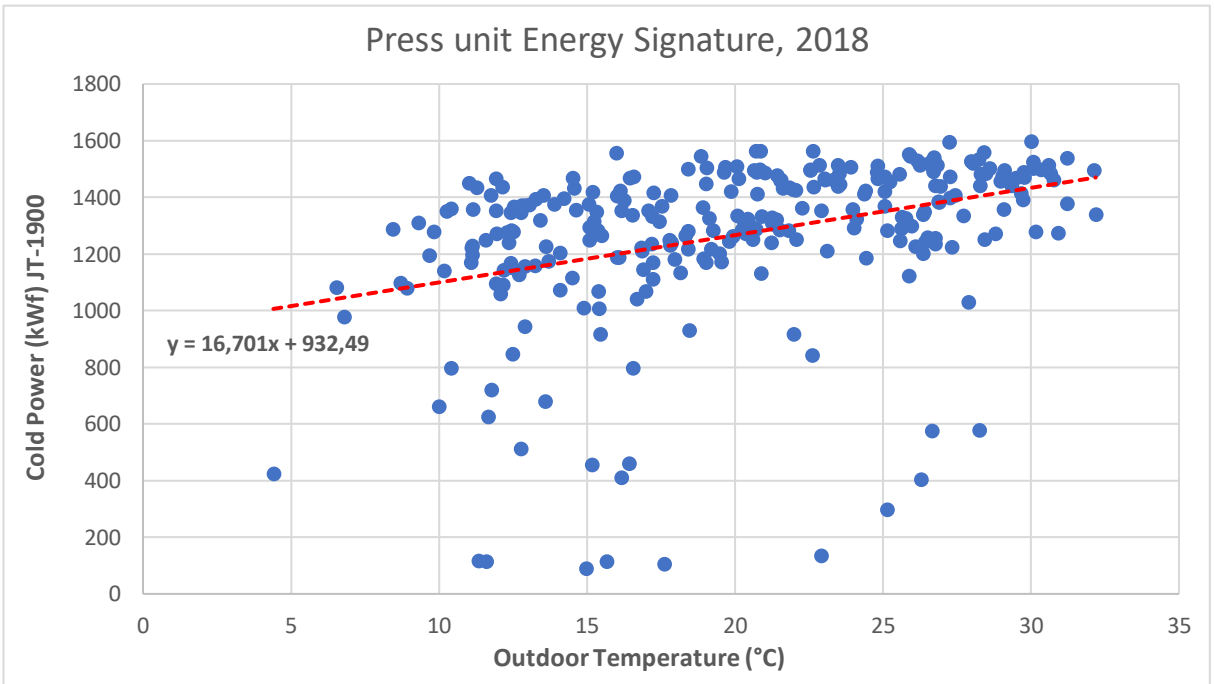

Figure 4.55: Energy Signature for the press unit in 2018

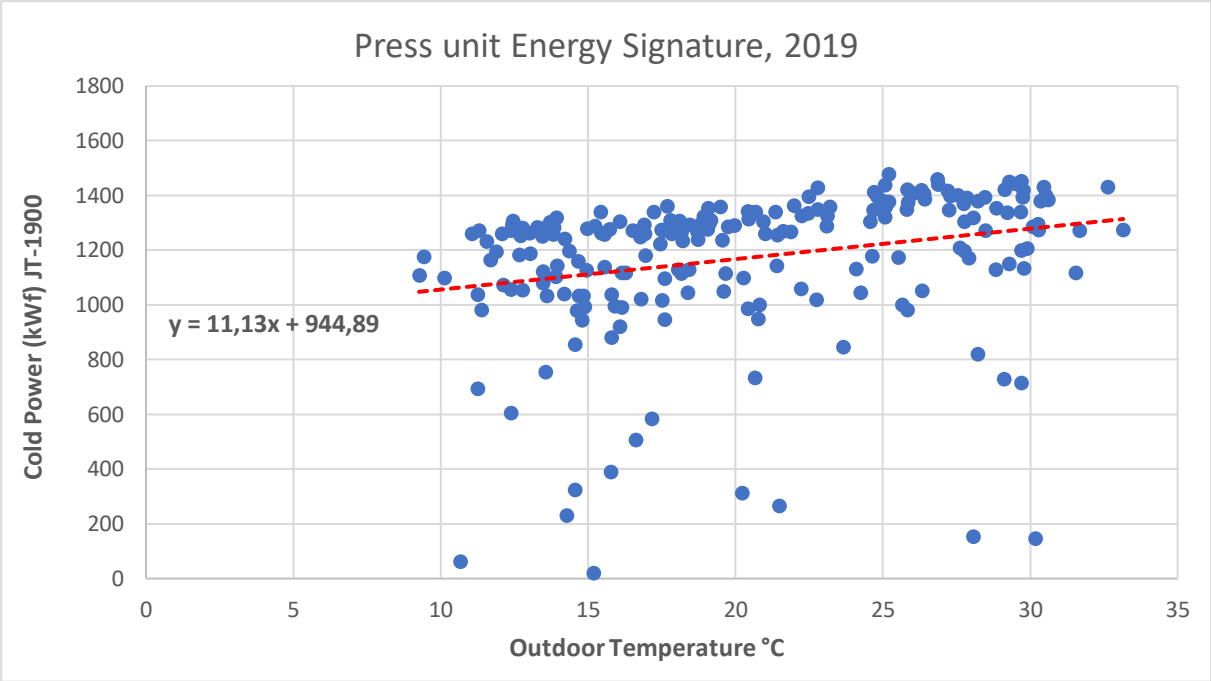

Figure 4.56: Energy Signature for the press unit in 2019

In the three graphical representations, the trend lines have been traced in order to underline the evolution of cold energy demand as a function of outdoor temperature.

It is noticeable that cold energy demand slightly increases with outdoor temperature, nevertheless the slope of the trend line is low and in all three cases, the intercept with the y-axis is between 930 kW_f and 1040 kW_f.

It is also clear that, during 2019, as expected from the previous analysis on heat recovery and cold water production, the maximum daily mean cold power delivered to the user were lower with respect to 2017 and 2018: indeed, in the 2019 Energy signature evaluation, almost no points are located between 1400 and 1600 kW_f, differently from the 2017 and 2018 curves.

Moreover, Saturdays have been neglected in 2019, because those days were characterized by very low cold power production, therefore those days can be considered as not significant in order to evaluate the press unit energy signature.

To analyze the press unit cold water demand during the year, it is interesting to plot the cumulative curves for the three analyzed years. This allows to understand the energy demand peak and for how many hours in a year, a certain cold energy has been delivered to the user.

It could also help in components dimensioning, so that the peaks of the demand can be covered by a lower Capital expenditure technology, while the larger area should be covered by a higher capital expenditure technology, in order to allow the latter to operate for a high number of hours in a year at full load conditions.

The press unit cumulative curves of years 2017, 2018 and 2019 are represented in *Figure 4.57*.

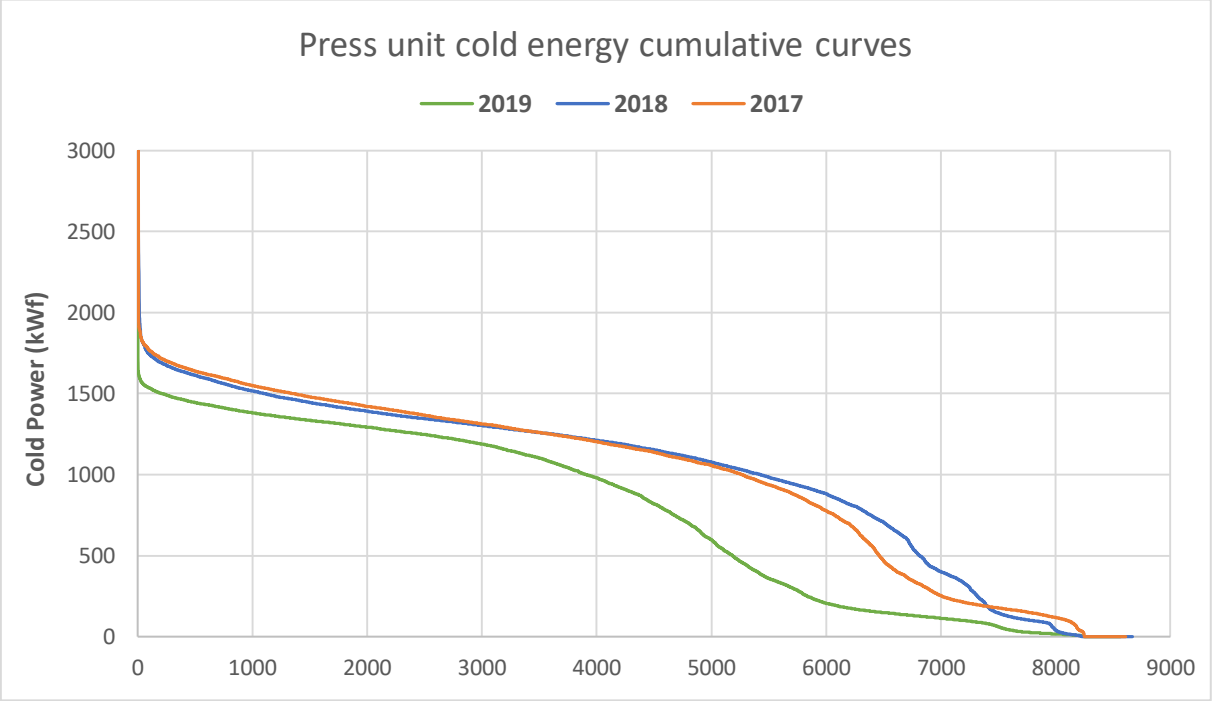

Figure 4.57: Cumulative curves of cold energy delivered to the press unit

The cumulative curves peak is around 3000 kW_f, but then a steep decrease can be observed. 2017 and 2018 curves are quite similar and they are almost superimposed until 5000 hours; during both years the press unit required a cold power higher than 1500 kW_f for about 1000 hours. After 1500 kW_f, the cumulative curves are quite flat until 5000 hours in a year then they decrease in a steeper way.

The 2019 cumulative curve, as expected, is positioned below the other two curves because less energy was demanded, indeed a mean cold power higher than 1000 kW_f was produced only for around 4000 hours of the year.

In *Table 4.7* the total amount of cold energy supplied to the user's press unit is reported.

Year	Press unit cold energy
2017	8541 MWh
2018	8699 MWh
2019	6536 MWh

Table 4.7: Total amount of cold energy supplied to the press unit

4.4.2 Air Conditioning

The air conditioning water circuit has been added from 2016; in this case, the air conditioning is needed to cool down the industrial site, so to increase the workers' thermohygrometric comfort. Indeed, during summer, external temperature in Melfi can easily reach more than 30 °C.

The air conditioning water circuit constitutes a detachment of the cold water primary circuit: in this case, the required temperature range of cold water is 7 – 12 °C, differently from the press unit and paintings ATU requirements.

Then the air conditioning totalizer meter records the energy supplied to the user on the only available water circuit: the power supplied to the user from that circuit is indicated in *Figure 3.5* with the tag JT-3000.

Obviously, it is expected that this energy vector is supplied to the user only during summer, since this is a seasonal energy service to be delivered.

In the following *Figure 4.58*, the daily evolution of cold power delivered for air conditioning is graphically represented. Year 2018 has been taken into account for this evaluation, while 2017 and 2019 trends are not reported for simplicity; indeed, the air conditioning energy evolution is quite similar in the three different years.

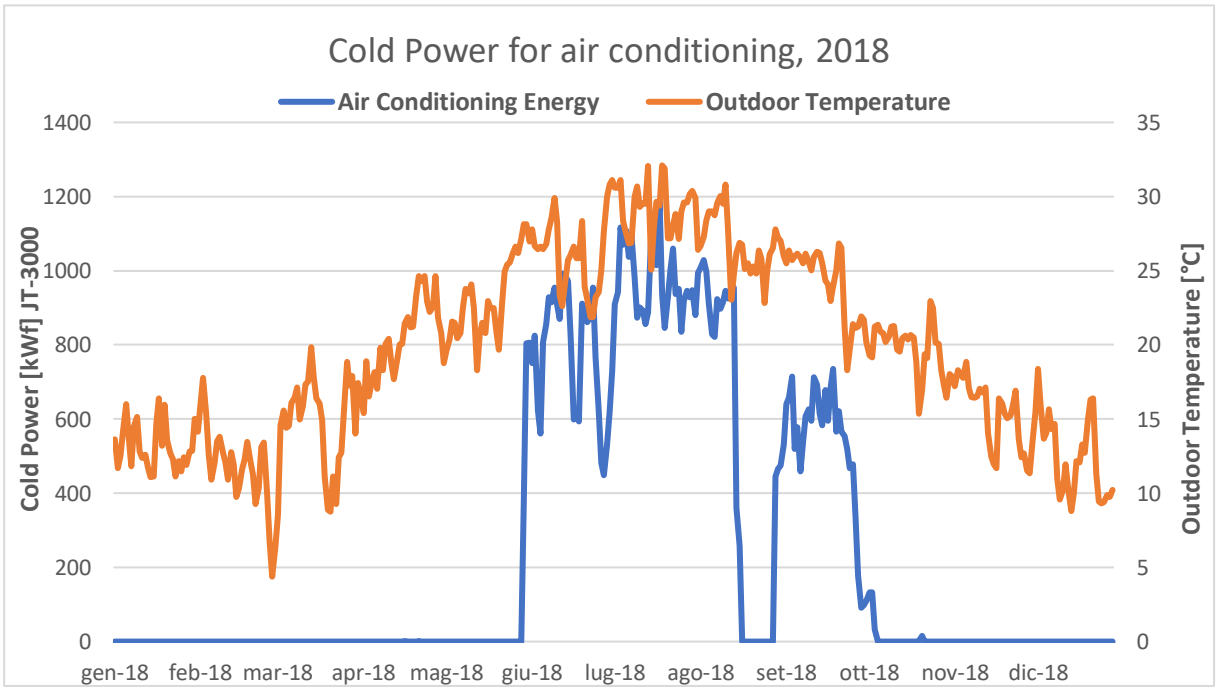

Figure 4.58: Cold energy delivered for air conditioning in 2018

The previous graph has been obtained by calculating the daily mean cold power supplied to the

air conditioning circuit. In this case, the shift change hours have not been neglected because the production site air conditioning is dependent on temperature, thus it is not correlated to the productivity of the site.

As expected, the energy demand is concentrated during Summer, from the end of May to the beginning of October 2018; the reduction of supplied energy during the two middle weeks of August are linked to the stop of the industrial site production for holidays.

Cold power peaks are between 1000 kW_f and 1200 kW_f, and they happened on the hottest days in July and August, when even the daily average temperature overcame 30 °C, as it is shown on the orange line in *Figure 4.58*.

It is noticeable that the air conditioning system has been switched on when daily average temperature reached 25 °C (between May and June 2018), and then it was switched off in October when average external temperature was around 20 °C.

It is interesting also to evaluate the cold power time evolution on an hourly basis, in order to analyze the peaks in energy demand. Air conditioning is dependent on external temperature, therefore it is expected that some demand peaks may occur during some very hot days.

Moreover, by calculating a daily mean value, this is also affected by the reduction of air conditioning energy demand during cooler nights.

A graphical evaluation of air conditioning power demand is shown in *Figure 4.59*.

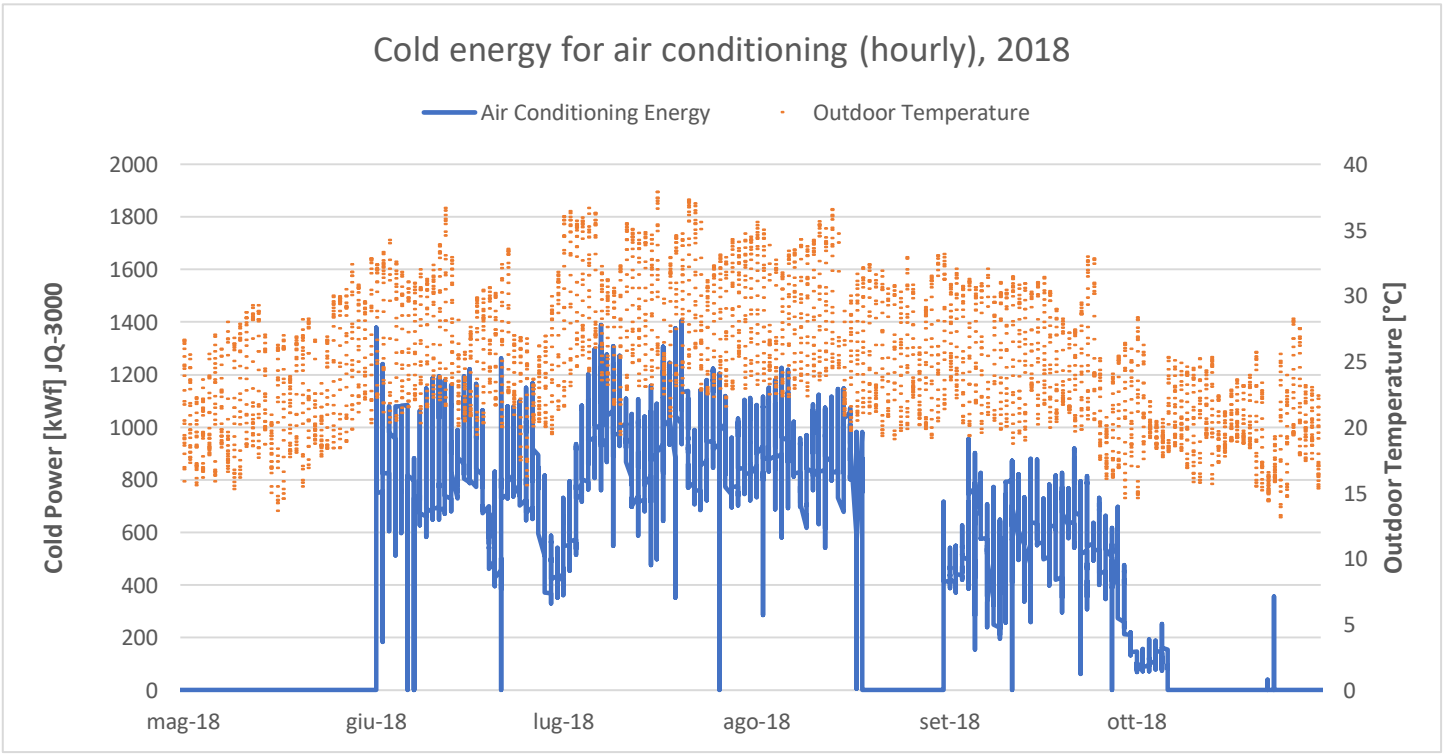

Figure 4.59: Cold energy delivered for air conditioning in 2018, hourly basis

In order to guarantee a clearer visualization of the graph in *Figure 4.59*, the x-axis has been set in order to analyze only the summer period.

From the hourly based graph, it is clear that for many hours, the hourly mean cold power overcame 1200 kW_f, thus, to characterize the air conditioning load, it might be more suitable to consider the hourly data in order to visualize the demand peaks that may occur during the hottest time of the day.

To visualize in a more immediate way the dependance of the cold energy demand on the external temperature the energy signature method can be employed.

In this case, it is expected to obtain a flat line coincident with the x-axis (null power demand) until a temperature equal to 20 °C is reached; after that, a steep increase of energy demand as a function of external temperature should occur.

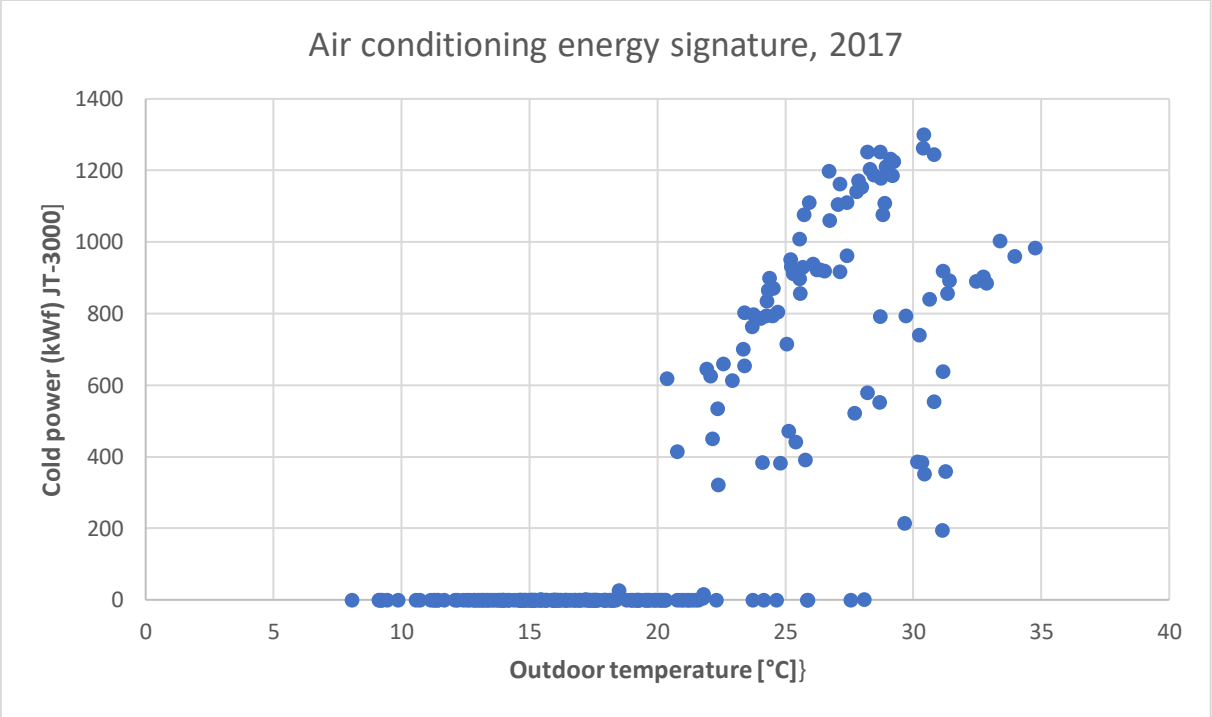

Figure 4.60: Energy Signature for air conditioning in 2017

Even if a clear linear trend is not visible in *Figure 4.60* about the air conditioning energy signature in 2017, it is noticeable that the energy demand is equal to zero until a temperature near 20 °C is reached.

This energy signature graph has been obtained by considering hourly data, so to be coherent with the previous analysis about energy demand peaks.

The cause of such a scattered graph for air conditioning energy signature in 2017 might be the priority given to satisfy the press unit cold energy demand, as already said.

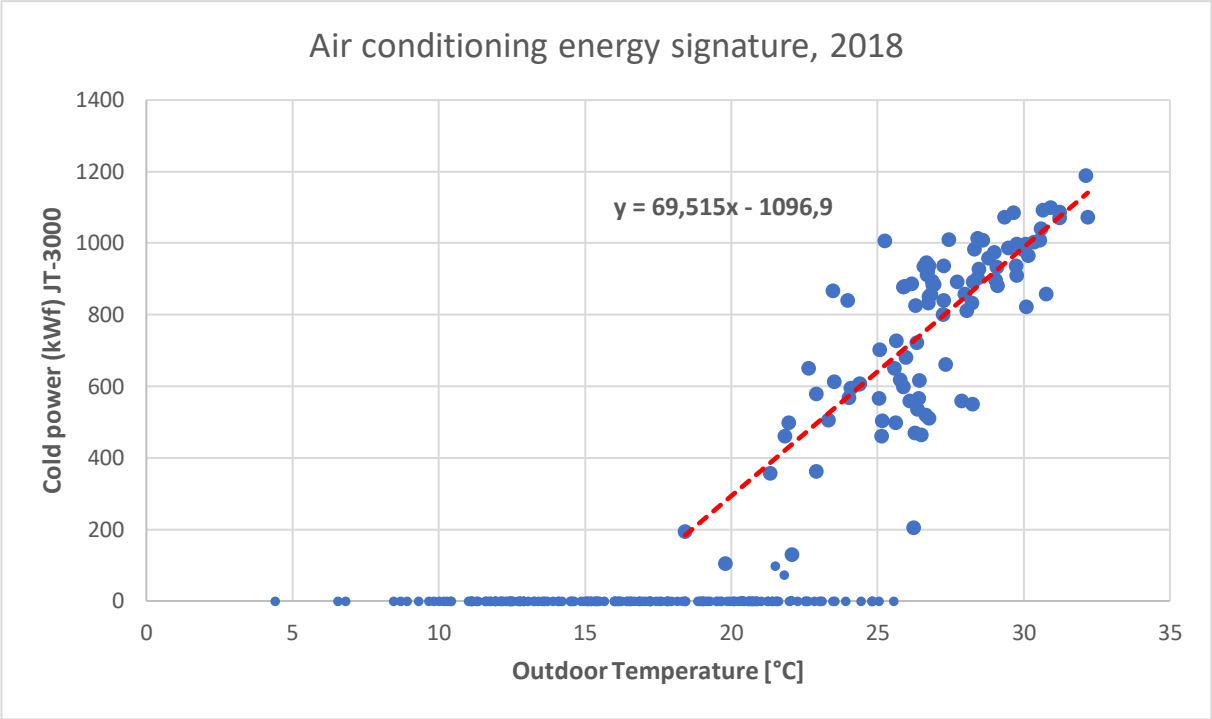

Figure 4.61: Energy Signature for air conditioning in 2018

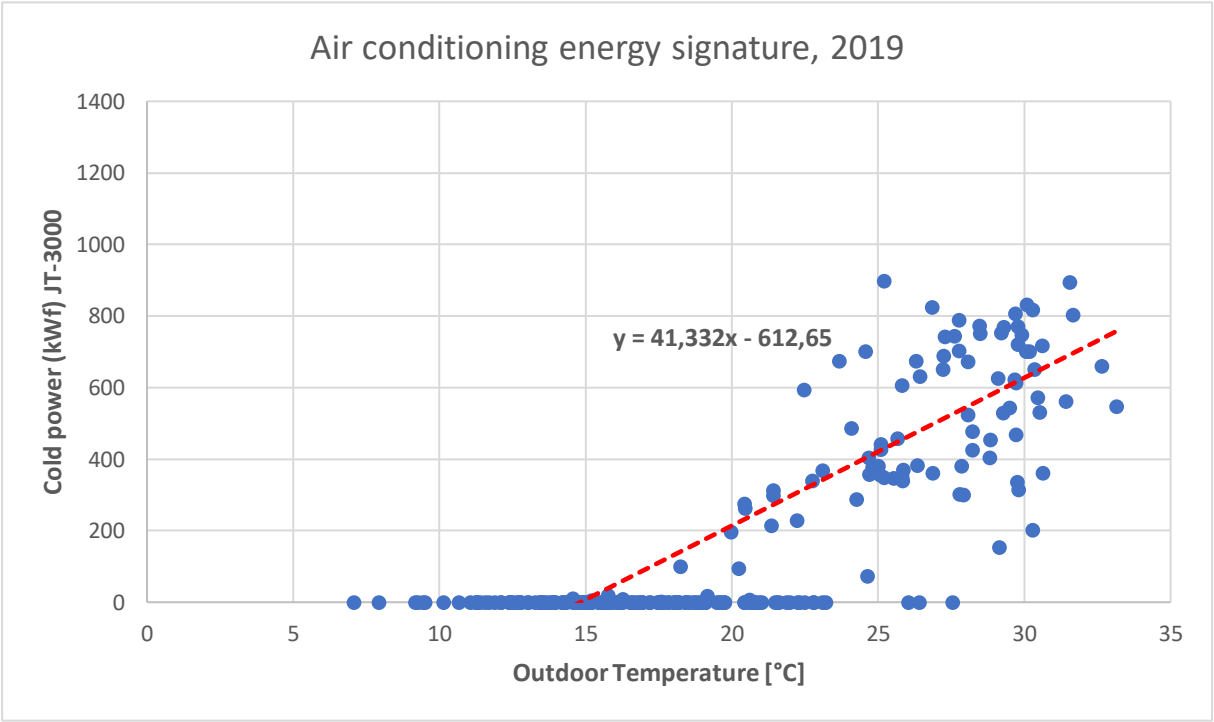

Figure 4.62: Energy Signature for air conditioning in 2019

2017 trend line has not been plotted because it was not meaningful, since it is possible to notice that almost two different trends can be recognized. Indeed, during the last two weeks of August, the energy demand for air conditioning was lower with respect to the demand during the rest of summer season, despite mean daily temperatures were higher.

In the three previous graphs it can be noted that, below an external temperature of 15 °C, there are no points with an y-value higher than 0.

2018 and 2019 trend lines show a very negative intercept.

In all cases, it is not possible to identify a clear trend that follows the trend line, on the contrary it is possible to notice a cloud of points that begins from the 15 °C value on the abscissa axis and develops towards the top-right corner of the quadrant.

2019 trend line equation is less steep than the 2018 curve: this is due to the lower cold energy demand; while in *Figure 4.60* and *4.61* the denser portion of the cloud is located at high mean power values, in *Figure 4.62*, on the contrary the denser part of the cloud is visible at low power, between 200 kW_f and 800 kW_f. This affects the trend line equation, that show a lower slope and a less negative intercept with the y-axis.

Even for the air conditioning unit, the cumulative curves have been plotted, so to understand the number of hours during which a certain cold power has been supplied to cool down the production site.

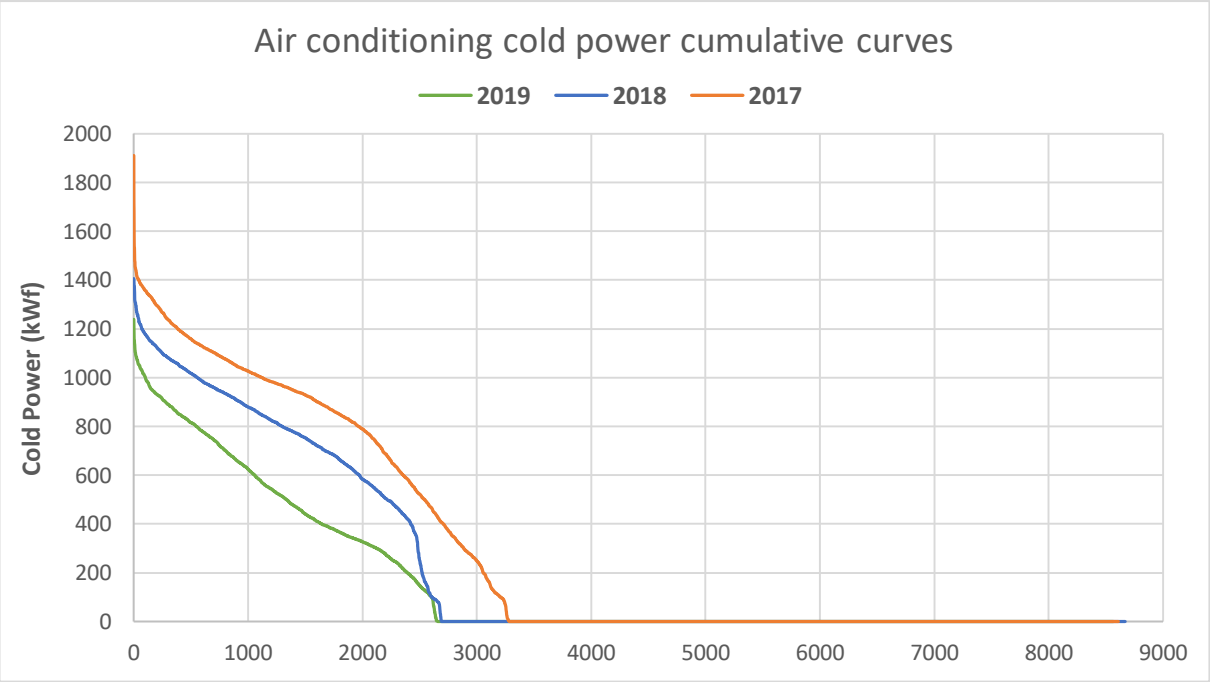

Figure 4.63: Cumulative curves of cold power supplied for production site air conditioning

As expected, the three curves decrease steeply because cold power for air conditioning is demanded only during Summer, therefore, energy is supplied only for 2000 or 3000 hours in a year.

The highest cumulative curve is the 2017 one, while less power has been delivered in 2019.

In all three curves, except for the peak power, that has been demanded for very few hours, the

curves develop across the quadrant, starting from around 1200 or 1400 kW_f.
In this case, differently from other cumulative curves, a reduced slope portion of the curves is less recognizable, in particular for the 2019 cumulative curve which decreases very steeply and intersects the x-axis at about 2500 hours.
Even in 2018, cold power for air conditioning was supplied for little more than 2500 hours, while, during 2017, the air conditioning circuit operated for more than 3000 hours.
In *Table 4.8*, the amount of cold energy supplied for air conditioning is presented for the three different years.

Year	Air conditioning cold energy
2017	2661 MWh
2018	2040 MWh
2019	1419 MWh

Table 4.8: Total amount of cold energy supplied for air conditioning

4.4.3 Paintings ATU

Even the paintings ATU circuit has been added in 2016. Cold or hot water, depending on external temperature, is supplied to the user towards the ATU that serves the paintings section of the industrial site. The aim is to keep the internal temperature constant, and this explains why it is a seasonal energy vector.
As it is shown in *Figure 3.7*, two decoupling heat exchangers are needed:

- E-1902A heat exchanger to supply cold water with a temperature range 15 – 20 °C on the secondary circuit, even if, from real time data, the temperature range lies more between 10 – 15 °C;
- E-1903A heat exchanger to supply hot water at a temperature range, between supply and return that is 70 – 80 °C on the secondary circuit.

The paintings ATU totalizer meter is positioned on the secondary circuit, and it is indicated in *Figure 3.5* with the tag JT-1906, as it is the same meter that records hot and cold water data.

In the following *Figure 4.64* and *4.65* the evolution of hot and cold energy demand throughout the years 2018 and 2019 is represented.

In this case, the 2017 energy demand trend cannot be analyzed because no data regarding water temperatures and mass flow rates are available for the first six months of year.

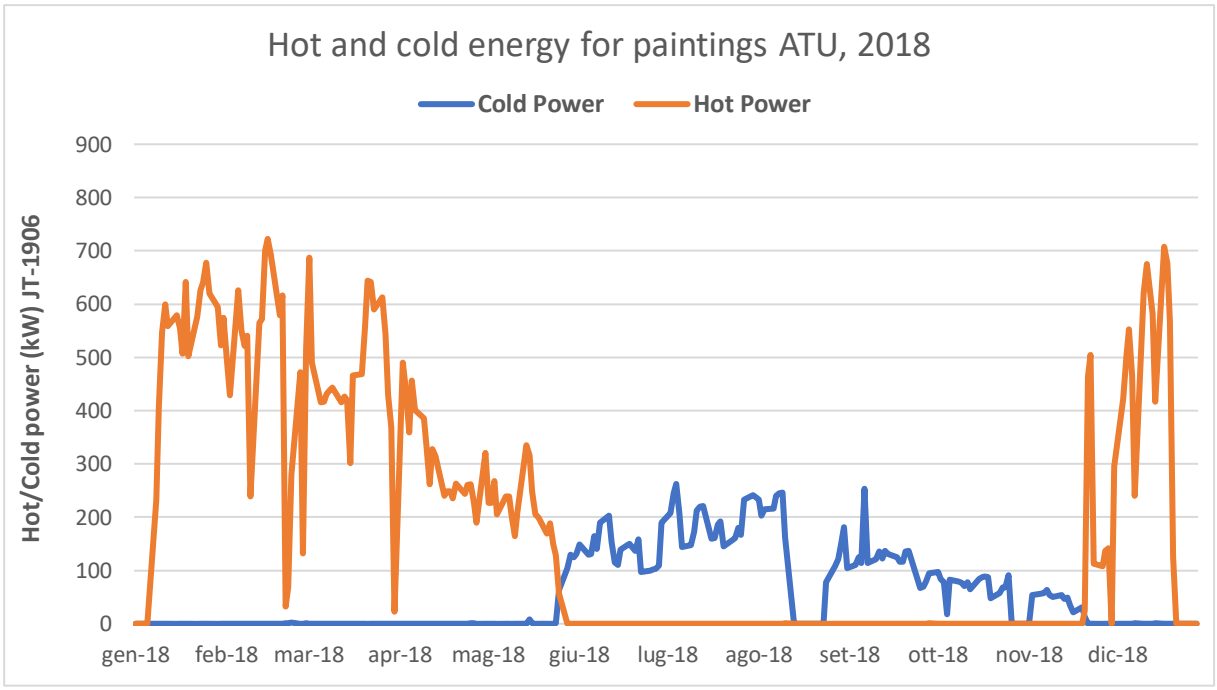

Figure 4.64: Average daily Hot and cold power supplied to paintings ATU in 2018

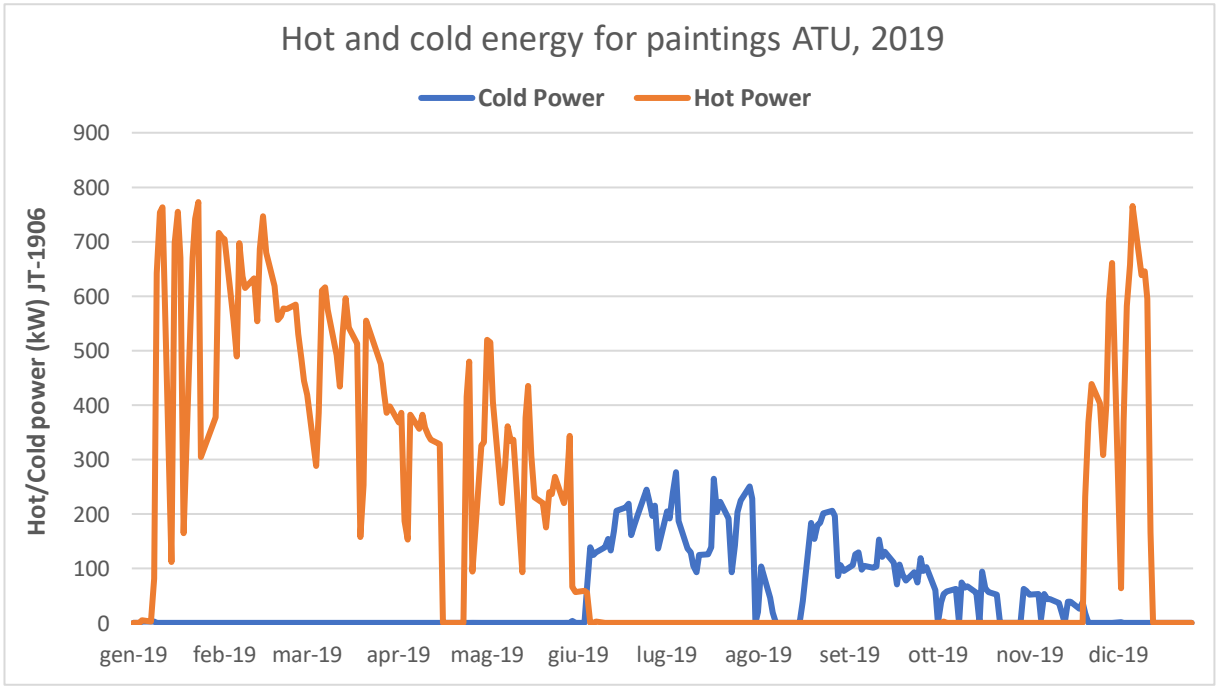

Figure 4.65: Average daily Hot and cold power supplied to paintings ATU in 2019

The previous graphs have been obtained by calculating the daily mean hot/cold power supplied to the paintings ATU; shift change hours have been neglected because energy demand, in this case, may depend on the industrial site productivity.

Moreover, Sundays and even Saturdays are not present in the graphs because energy supplied in those days was lower, so it could affect a clear visualization of demand evolution throughout the year.

It is immediately clear that the energy service provided to the user, in this case, is seasonal: cold water is supplied from the beginning of June until November, while hot water is provided during the first six months of the year and during the end of November in addition to December.

Both graphs are characterized by many spikes, therefore it can be deduced that paintings ATU didn't demand an almost constant power during the year. Nevertheless, it is possible to notice that the maximum absolute value of supplied thermal power is almost three times higher than the demanded cold power. This could be expected as the temperature difference between supply and return is doubled for what regards hot water with respect to cold water; moreover, the hot water volume flow rate (155 m^3/h) is larger than the supplied nominal cold water flow rate (110 m^3/h).

The energy signature for paintings ATU during the years 2018 and 2019 are shown in *Figure 4.66* and *4.67*.

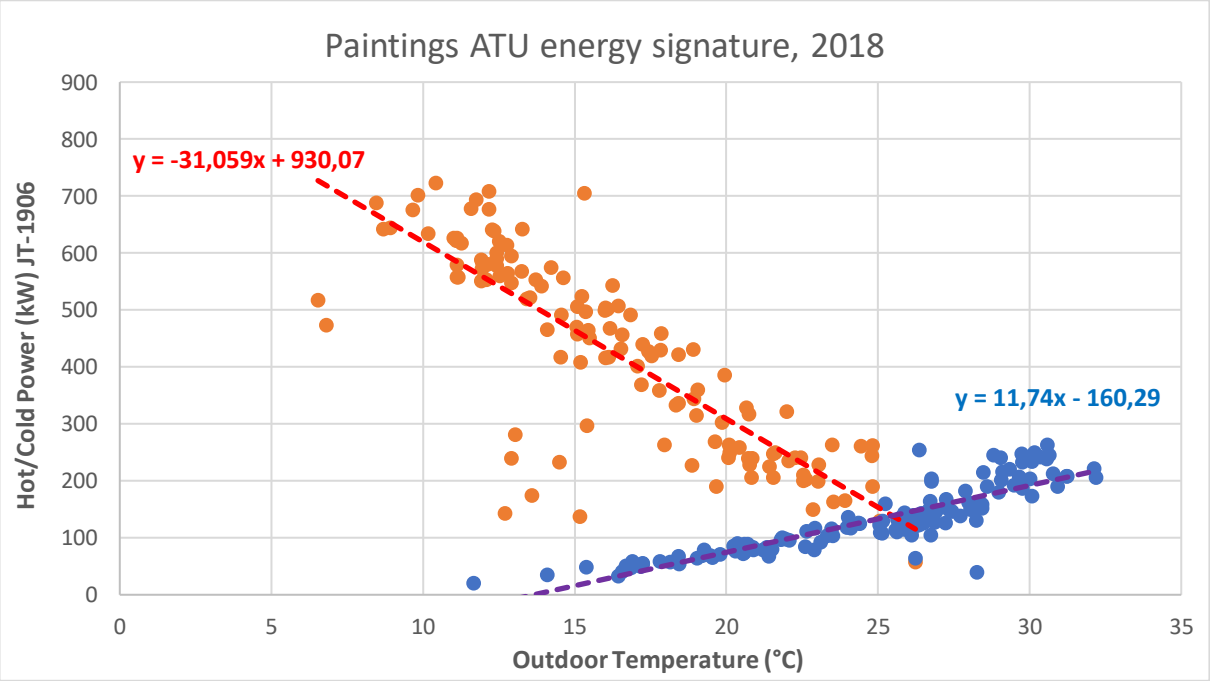

Figure 4.66: Energy Signature for paintings ATU in 2018

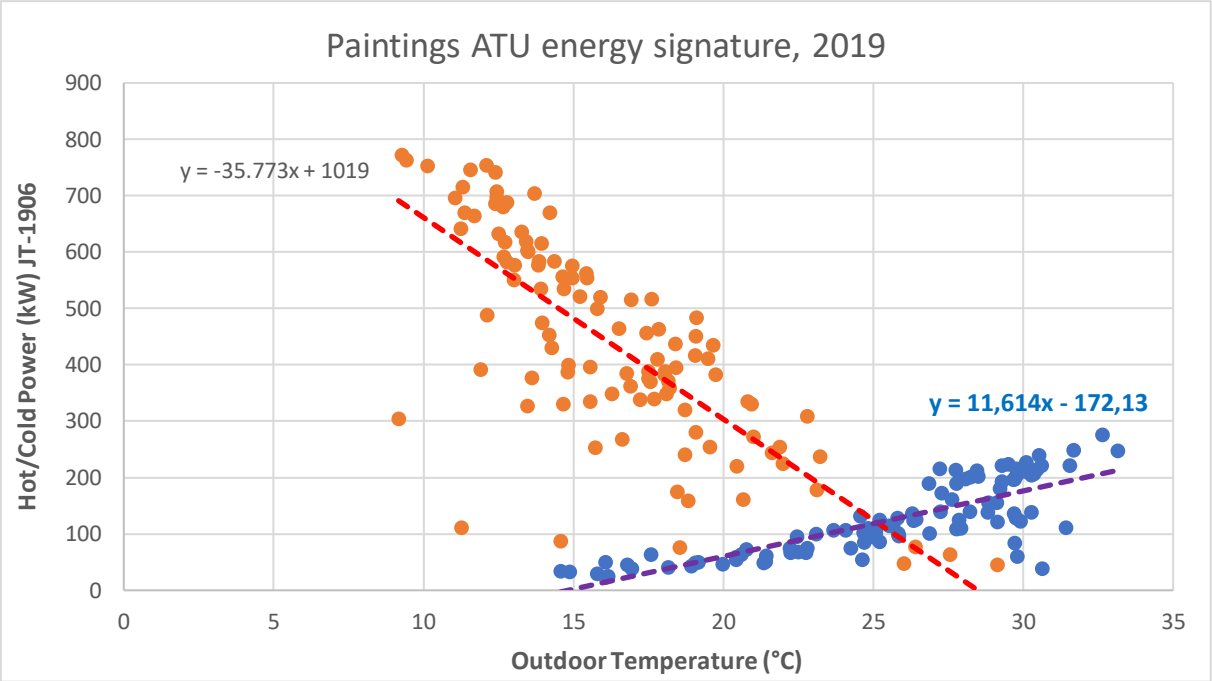

Figure 4.67: Energy Signature for paintings ATU in 2019

Energy signature graphs have been plotted by using the daily mean values of hot (orange points) and cold (blue points) power delivered to the paintings ATU.

The trend lines of thermal and cold power intersect at around 25 °C; before that value and down to around 15 °C, both hot and cold energy are supplied because cold power is delivered until November, when external temperatures are lower.

Thermal power trend lines slope is much steeper, this means that it is much more dependent on the external temperature than cold power.

In order to obtain the energy signature graphical evaluations, shift change hours and Sundays have been neglected, and also the first and the last weeks of the year and the two middle weeks of August have not been considered.

Even the days characterized by very low supplied energy have been neglected because they could have affected the energy signature significance; this assumption is based on the hypothesis that low power values are correlated to low industrial site productivity, so those days are not meaningful to obtain a correlation between delivered power and external temperature.

The 2017 energy signature has been obtained by considering an arithmetic average trend line calculated from the 2018 and 2019 trend lines equations.

The trend lines equations used to calculate hot and cold power are the following:

- Hot Power, $y = -33{,}416\,x + 974{,}54$;
- Cold Power, $y = 11{,}677\,x - 166{,}21$.

This procedure is similar to the one that has been used to obtain the data shown in *Figure 4.6*. In this energy signature derivation, to calculate the daily mean hot or cold power, it was not sufficient to consider only the external temperature: indeed, during some periods of the year, thermal energy is supplied at temperatures near 25 °C, while cold energy is delivered at 15 °C; since, from *Figure 4.64* and *4.65* it is clear that thermal energy is supplied from January to May, while cold energy is delivered on June, then this logic has been applied in order to calculate daily average power for the first six months of 2017.

Moreover, Sundays and the first week of the year have been neglected, independently from outdoor temperature.

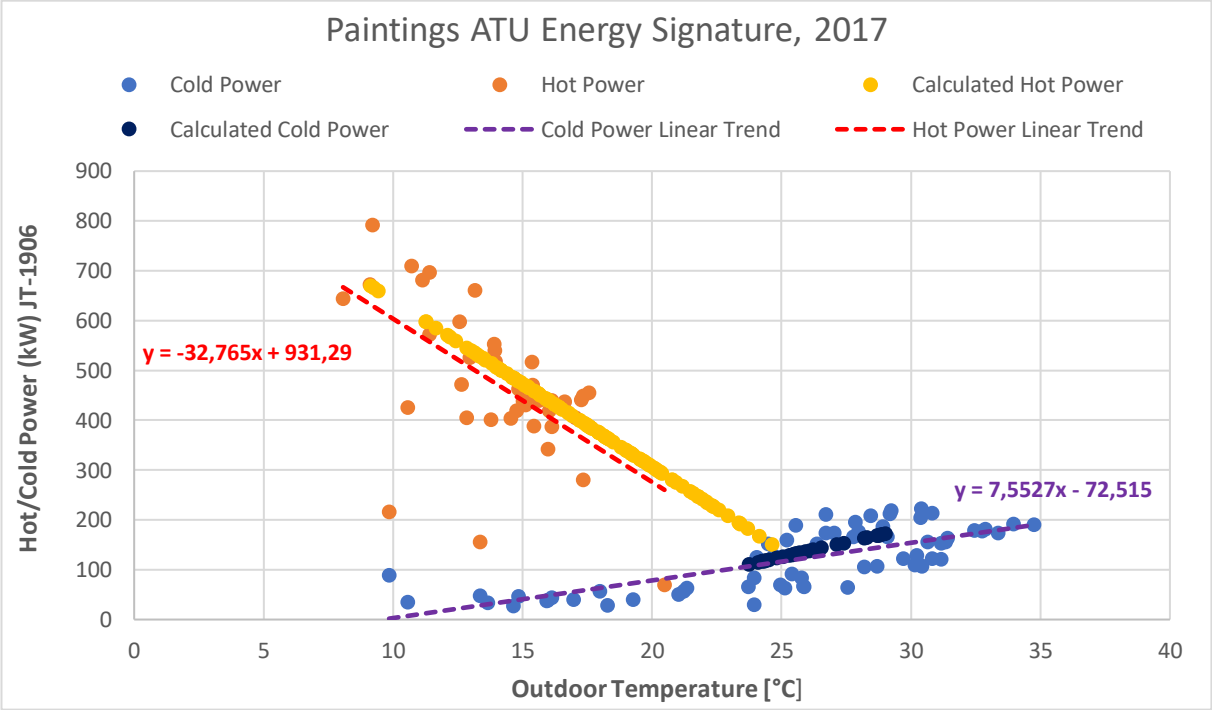

Figure 4.68: Energy Signature for paintings ATU in 2017

Yellow and dark blue points on the graph in *Figure 4.68* represent the calculated daily mean power values obtained by means of the previously mentioned equations.

The red and the purple trend lines are referred to the set of points without considering those obtained from calculations; of course, this doesn't correspond to the plant real behavior and, therefore, to the actual power that has been supplied to the paintings ATU but this constitutes a method that allow to deduce the plant operation and then to build the cumulative curves, starting from the other analyzed years data.

Cumulative curves for paintings ATU thermal energy and cold energy are represented in *Figure 4.69* and *4.70* respectively.

For thermal energy delivered to paintings ATU, the 2017 calculated cumulative curve has been

plotted in yellow. Nevertheless, its trend may be far from reality because all data between January and May were not available, therefore the 2017 calculated curve represents an estimate, obtained on the basis of next two years.

On the contrary, the 2017 calculated cold power cumulative curve represented in *Figure 4.70* might be more realistic, because only the daily mean power supplied in June has been obtained from calculations, while data from July to November were available, so a more significant curve could be plotted.

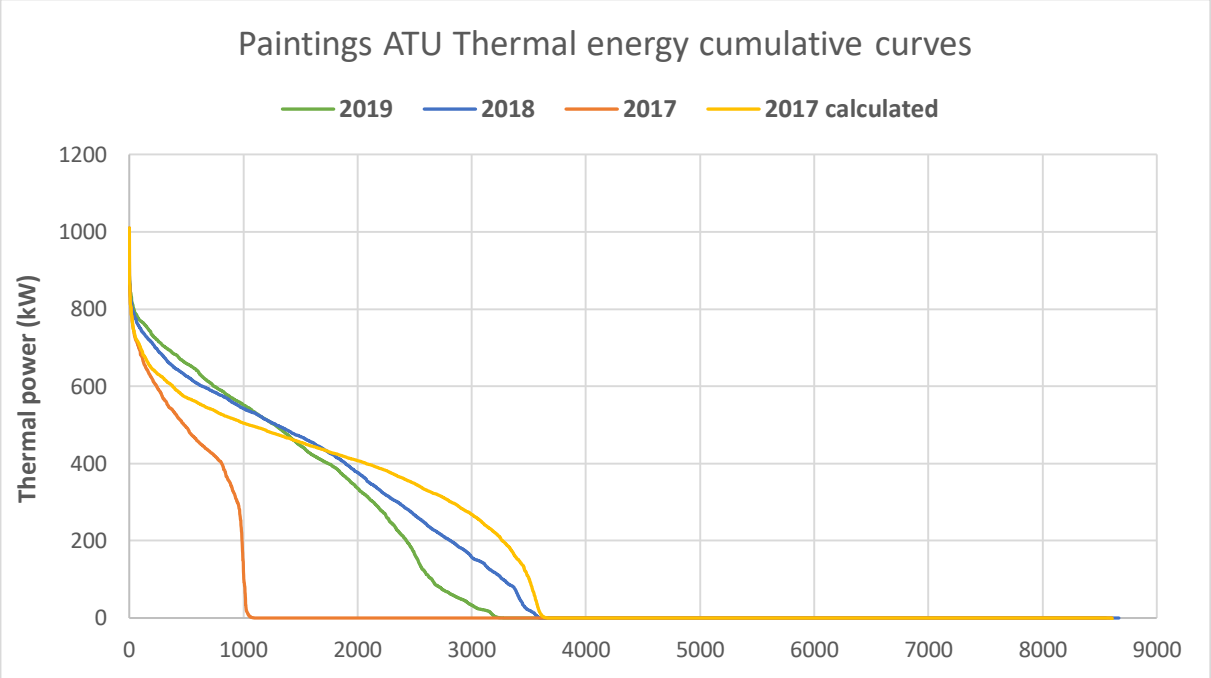

Figure 4.69: Cumulative curves of thermal power supplied to paintings ATU

The 2017 curve indicated in *Figure 4.69* refers to the cumulative curve based on data available only for the last six months of the year, thus the thermal energy supplied to the paintings ATU during the end of November and in December is considered. As a consequence, the 2017 cumulative curve intersects the x-axis at 1000 hours, while the 2018 and 2019 curves show that thermal power has been supplied for around 3000 or 3500 hours in one year.

2018 and 2019 cumulative curves are quite similar: their slope decreases at a value lower than 800 kW_{th} and, after that, they are almost superimposed for around 2000 hours.

Then the 2019 curve drops more steeply to a zero value, while, during 2018, low thermal power has been delivered for a larger number of hours.

By analyzing the cold power cumulative curves in *Figure 4.70*, it is immediately noticeable that the cold power values are much lower than those of cold power supplied to the press unit and for the production site air conditioning.

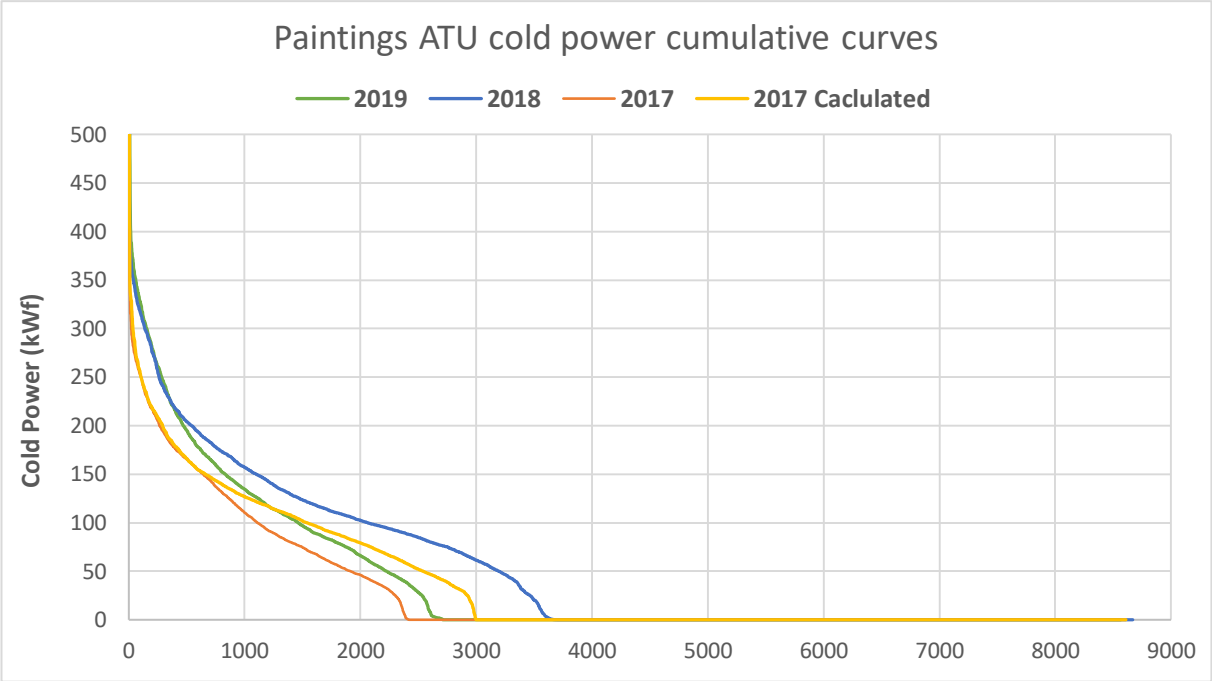

Figure 4.70: Cumulative curves of cold power supplied to paintings ATU

The orange 2017 curve is based on data from July to December. In order to obtain the "2017 calculated" cumulative curve, it was necessary to estimate the cold power supplied in June; therefore, the 2019 cold power trend line equation reported in *Figure 4.70* has been used to obtain the hourly values of supplied cold power, starting from the hourly data about outdoor temperature.

In this way, the "2017 calculated" curve intersects the x-axis at 3000 hours, thus, it added around 700 hours of operation to the 2017 cumulative curve.

During 2018, cold power has been delivered to paintings ATU for around 3500 hours, while in 2019 and, according to estimates, also in 2017, cold power has been supplied for no more than 3000 hours.

In *Table 4.9* the thermal and cold energy supplied to the paintings ATU during the analyzed years are presented. 2017 values are referred to the period from July to December 2017, but also the estimate from calculation is reported in brackets.

Year	Thermal Energy Paintings ATU	Cold Energy Paintings ATU
2017	505 MWh (1498 MWh)	266 MWh (337 MWh)
2018	1427 MWh	460 MWh
2019	1288 MWh	345 MWh

Table 4.9: Total amount of thermal/cold energy supplied to paintings ATU

5. Optimization proposals

5.1 Total cold water demand

In order to improve the energy efficiency of this trigeneration plant without changing the core component, i.e. the engine, two fundamental circuits must be considered:

- Super-heated/ Hot Water circuits in the HRU
- Cold Water production by means of WARGS.

In a trigeneration plant, those two circuits are not independent since hot water is necessary to produce cold water. Moreover, by looking at *Figure 5.1*, that shows the percentage of each water energy vector on the total amount of hot/cold energy provided to the user to cover the energy services, it is clear that it is necessary to produce cold water efficiently.

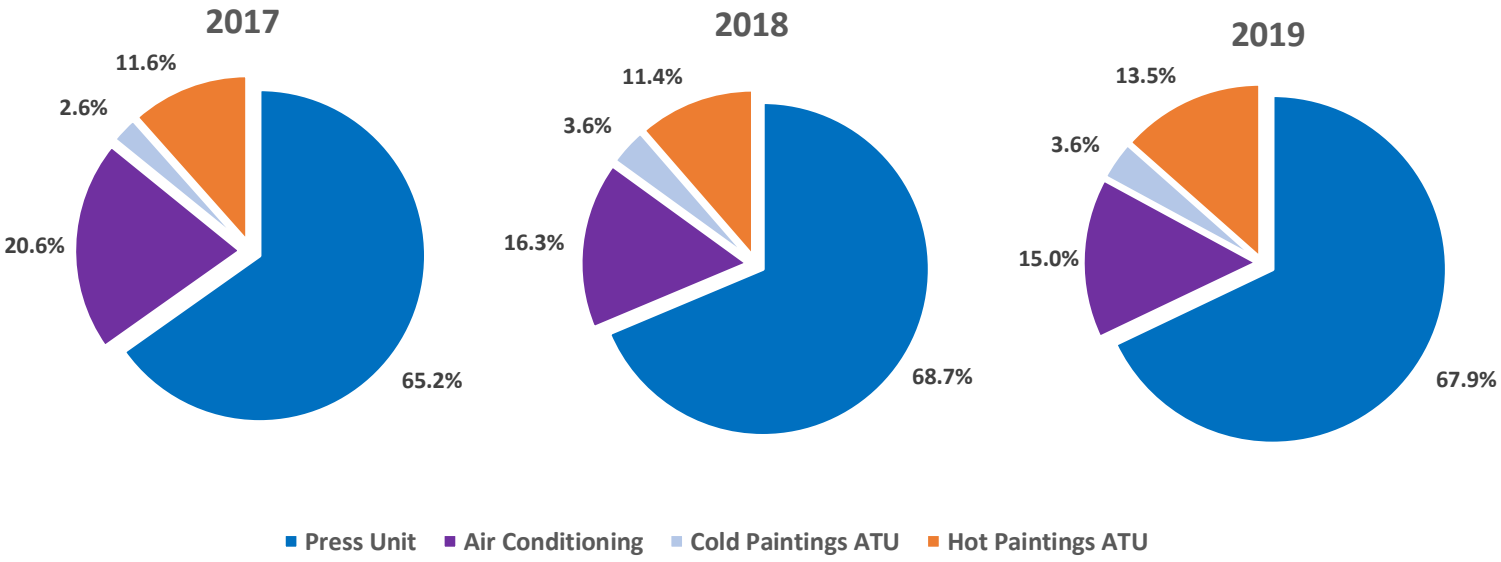

Figure 5.1: Energy vectors percentage during 2017, 2018 and 2019

The pie chart showed for the year 2017 has been obtained by considering also the first six months of the year, thus by taking into account the calculated delivered power to paintings ATU by means of the equations reported in *Figure 4.68*.

By looking at all three pie charts, it is noticeable that cold water covers between 85 and 90 % of the user hot/cold energy demand.

To evaluate the correct dimensioning of the WARGs it is necessary to graphically evaluate the evolution of the chronological overall cold water supply during the analyzed years; in this way, it would be possible to notice if there is a roughly constant cold water demand basis.

The following graphs show the aforementioned evolution over time, on an hourly basis.

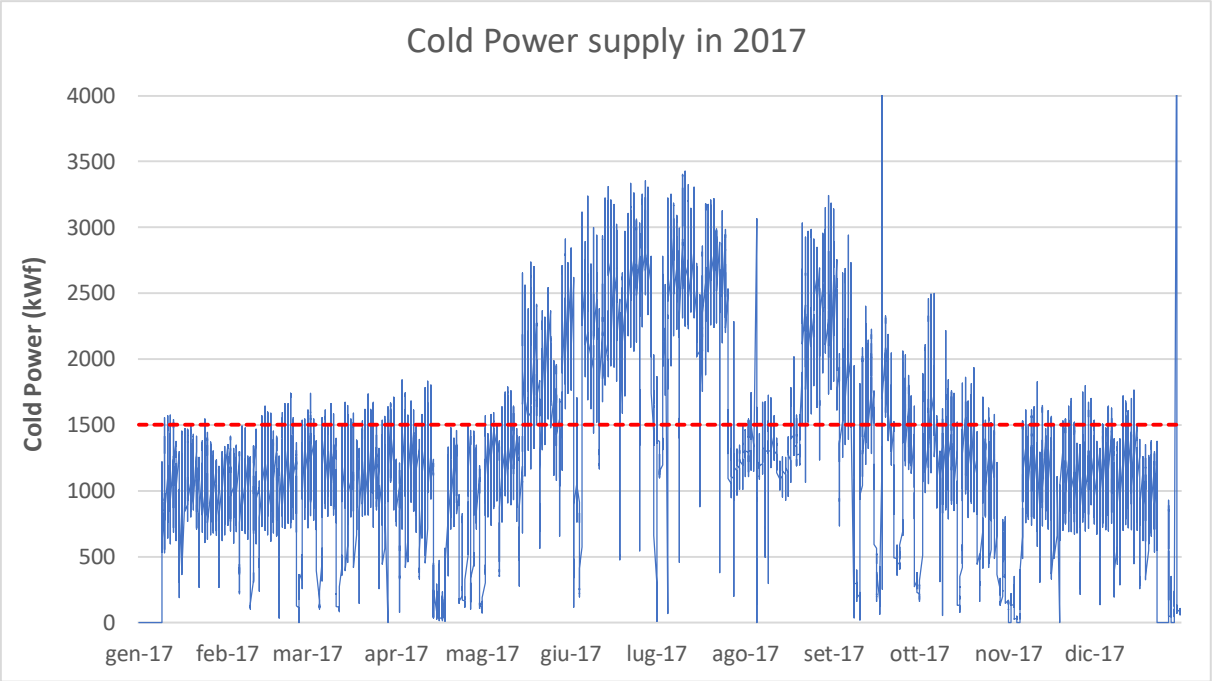

Figure 5.2: Evolution over time of cold water supply in 2017 (hourly)

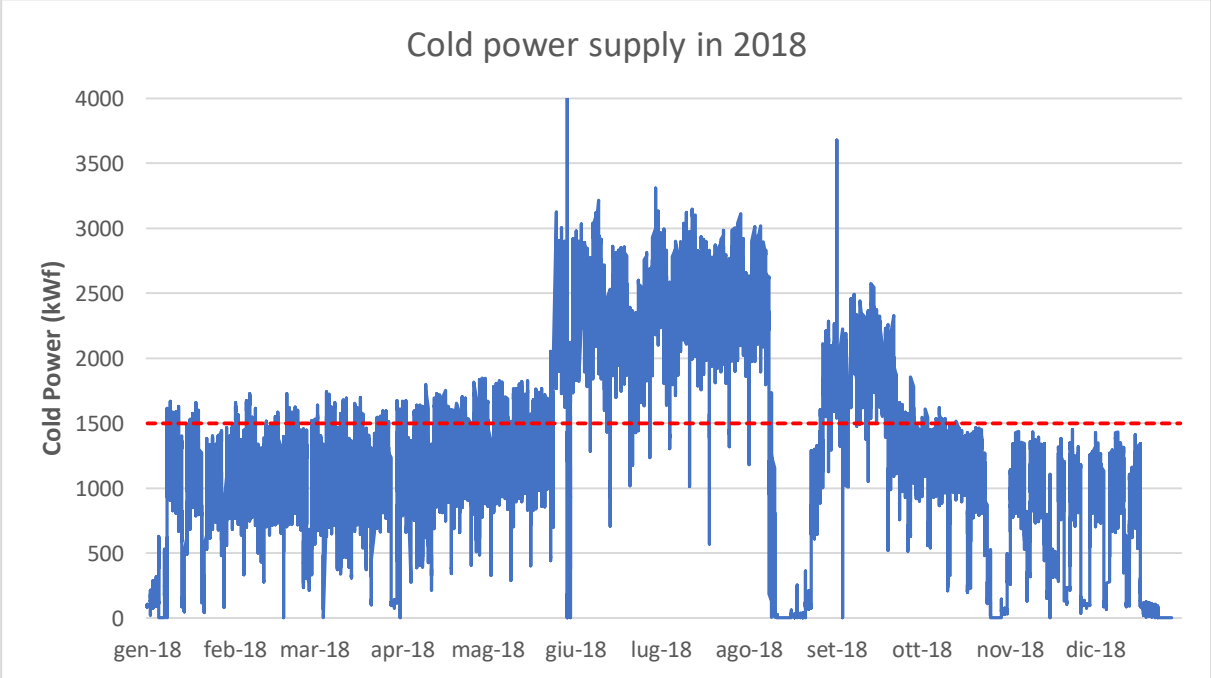

Figure 5.3: Evolution over time of cold water supply in 2018 (hourly)

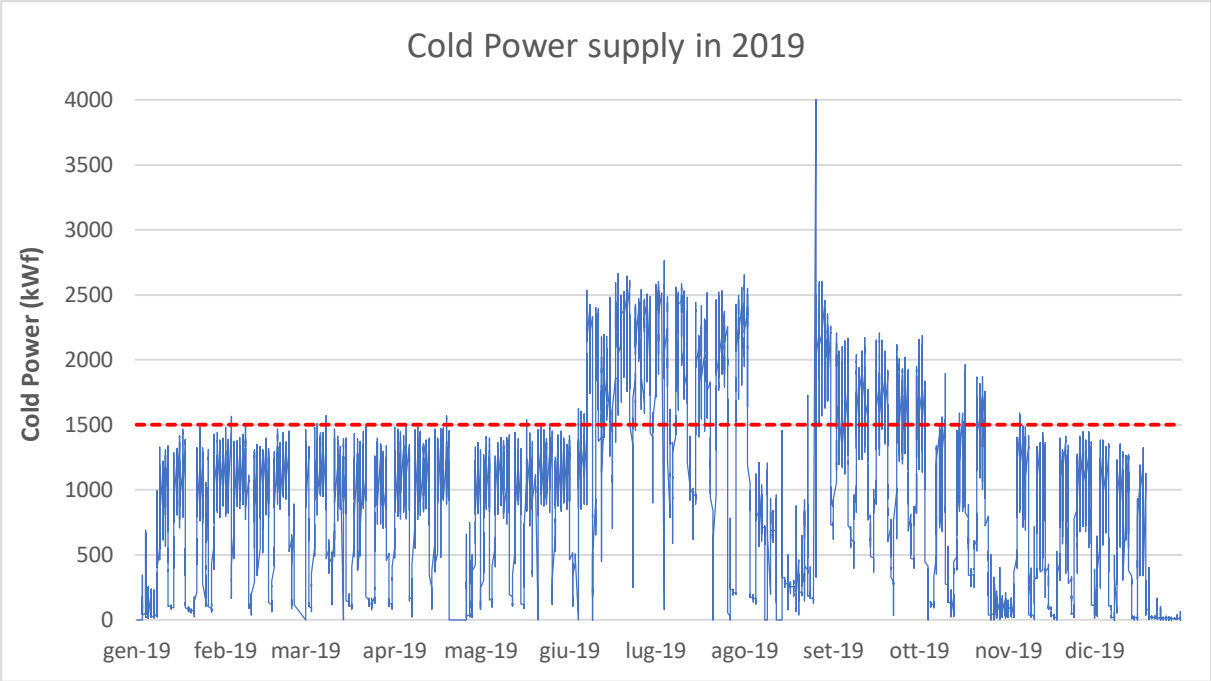

Figure 5.4: Evolution over time of cold water supply in 2019 (hourly)

It can be noticed that, except for the summer months during which the cold water demand increased, especially because of the industrial site air conditioning, for the rest of the year the cold power demand was almost constant, near 1500 kW_f.

In the three graphs, the red dashed line indicates the 1500 kW_f y-value, so that it is clear that the cold power demand basis is quite similar during the three analyzed years, even if, in 2019 the demand was a little lower with respect to 2017 and 2018.

It can be deduced that some WARGs with an overall nominal power of around 1500 kW_f, operating at full load conditions for most of the year, would be sufficient to cover the cold power demand for about 8 months in a year.

In order to analyze the cold power demand trend and to propose a cold water production optimization, it is interesting to plot the cold power cumulative curves for all the three considered years.

To evaluate the current WARGs dimensioning, a flat line has been traced in correspondence to the trigeneration plant WARGs nominal power, equal to 3800 kW_f.

It is clear that, in the present situation, the WARGs are oversized with respect to the user cold power needs: this leads to absorbers operating at partial load, thus working less efficiently.

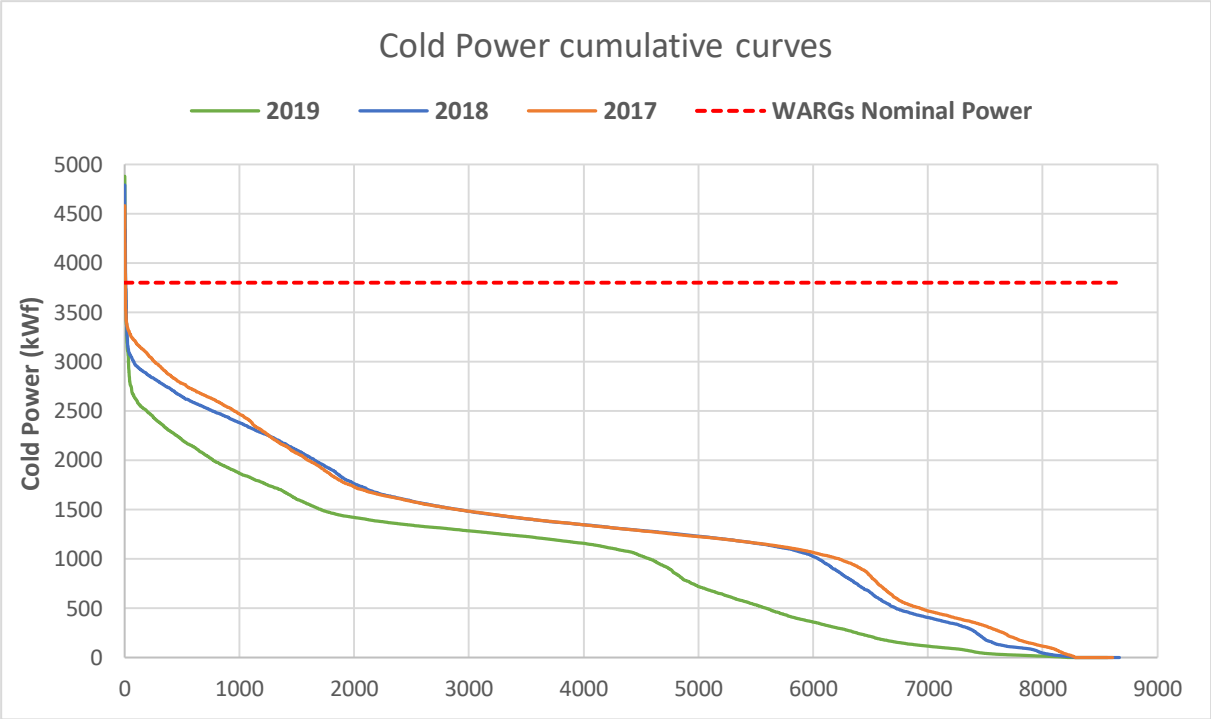

Figure 5.5: Total cold power supply cumulative curves

2017 and 2018 cumulative curves are very similar, while 2019 was characterized by a lower cold energy demand, therefore it will not be considered for further analyses.

During 2017 and 2018, a cold power higher than 2500 kW_f has been supplied for only 1000 hours. If WARGs nominal power was 1500 kW_f and they would have been able to operate throughout the year, the entire area from 3000 hours to 8760 hours would have been covered, while the high power area above 1500 kW_f would have been supplied by means of electric chillers.

Nevertheless, these are only estimates, indeed, although the current absorbers nominal power would be enough to cover the whole cold energy needs, they were not able to satisfy the demand, therefore it was necessary to utilize the electric chillers.

In *Table 5.1* it is reported the share of the total cold energy supplied by means of WARGs.

Year	Share of Cold energy by WARGs
2017	52 %
2018	58 %
2019	43 %

Table 5.1: Share of total cold energy supplied by means of WARGs

Absorbers never covered more than 60 % of total cold energy needs; those reported in *Table*

5.1 are estimates because the cold power provided by means of WARGs has been calculated since no totalizer meters are available to account for the real cold energy supplied to the user; moreover, in some periods, temperature and flow rate data were not available from the Online Data Collector, therefore those percentages might be susceptible to errors.
Nevertheless, those estimates are useful to conclude that, due to frequent maintenance or malfunctioning, the absorbers didn't operate as efficiently as expected in the design phase, so it is necessary to optimize the cold power production, in order to improve the trigeneration plant efficiency.

5.2 Heat Recovery Unit substitution

In order to optimize the cold power production it is fundamental to provide the necessary thermal energy to the absorbers. In the current plant configuration, super-heated water is useful to supply the double-effect absorbers; nevertheless, these WARGs undergo frequent maintenance because of their complexity.
This leads to some issues in the normal plant operating conditions because, as already mentioned, when a double-effect WARGs is not available, there is a reduction of super-heated water demand, therefore a portion of ICE exhaust gases bypass the HRU. In this case, hot water might not be heated up sufficiently to provide thermal energy to the paintings ATU or to the single-effect 1000 kW_f WARG.
Moreover, double-effect WARGs need an inlet super-heated water temperature equal to 165 °C, but, as it can be noticed from *Figure 4.15*, SHW outlet temperature from the HRU rarely exceeded 150 °C. thus leading the WARGs to operate in different conditions with respect to the nameplate ones.
To simplify the plant configuration, avoid complex maintenance and optimize the cold water production, one solution may be to substitute the existing HRU with a simple hot water heat recovery unit. In this case the super-heated water circuit and the double-effect WARGs would be dismantled.
Hot water would be supplied to the paintings ATU and/or to single-effect WARGs to produce cold water. A simple schematic of this renovated plant configuration is shown in *Figure 5.6*.

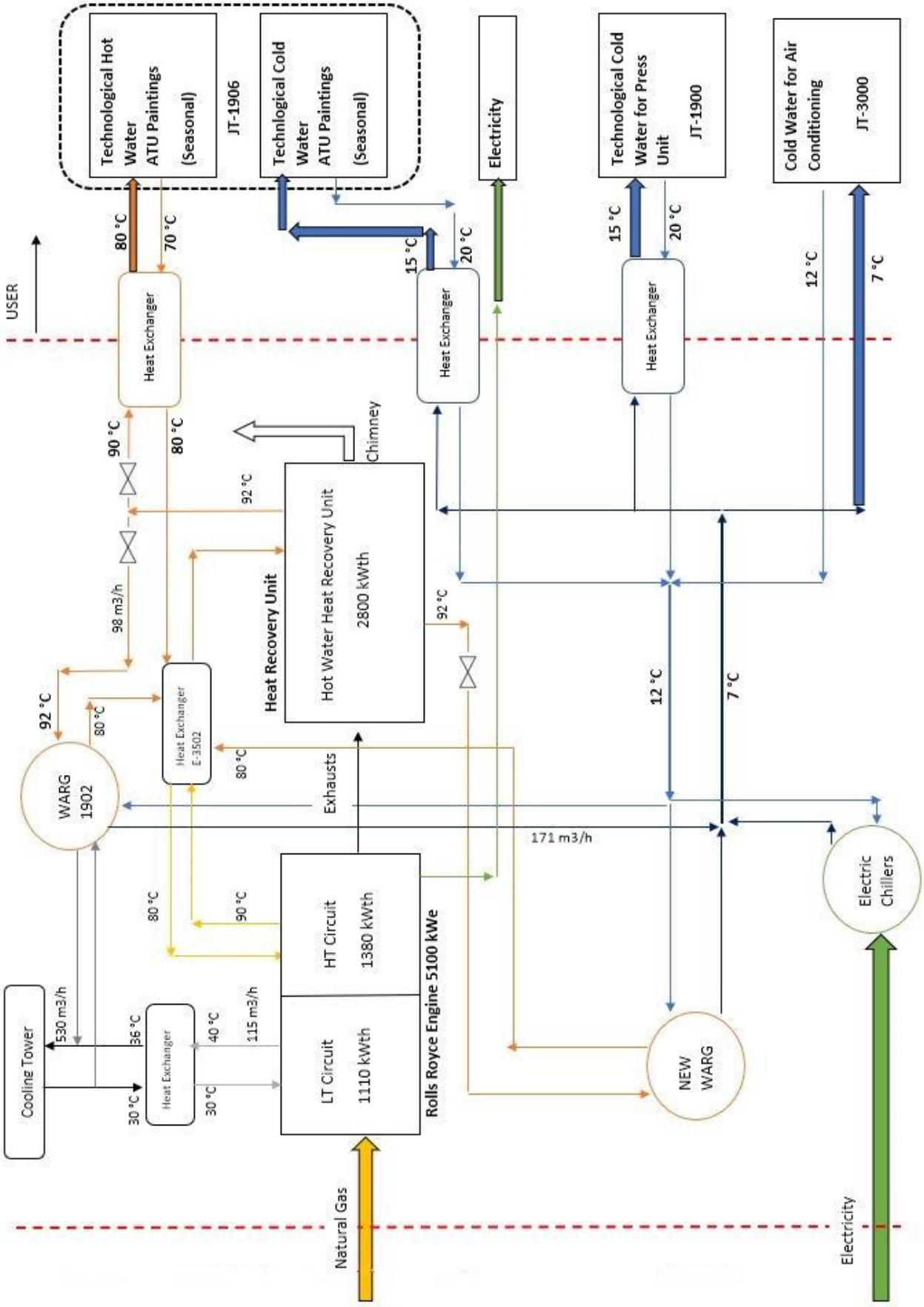

Figure 5.6: Simplified scheme of the renovated energy plant

To dimension the new HRU, the exhaust gases nameplate data reported in *Table 3.6* have been employed. The exhausts mass flow rate has been multiplied by a specific heat approximated to 1,1 kJ/(kg*K) and by a temperature difference equal to 300 °C (temperature drop between 400 °C and 100 °C). The resulting obtainable thermal power has been rounded down to 2800 kW_{th} in order to take into account the thermal losses by radiation.

It is necessary to calculate the hot water flow rate that could be heated up from 80 °C to 92 °C by means of the heat exchanger E-3502, and then by the 2800 kW_{th} HRU.

The total thermal recovery corresponds to 3800 kW_{th}.

Hot water flow rate is obtained by considering a specific heat capacity equal to 4,186 kJ/(kg*K) and the temperature difference of 12 °C.

$$\dot{Q} = \dot{m} \cdot c_p \cdot \Delta T$$

The resulting hot water mass flow rate is around 75 kg/s, that corresponds to a volume flow rate of about 270 m^3/h.

Thus, the hot water flow rate is almost three times higher with respect to the original plant configuration (106 m^3/h), therefore it is necessary also to substitute the heat exchanger E-3502. Hot water outlet temperature from that exchanger would be equal to around 83 °C; then the temperature would be increased to 92 °C by the exhausts in the HRU.

The hot water circuit in the HRU would be equipped with a three-way valve that partializes the flow rate according to the energy needs: this would allow to reduce or increase the mass flow rate in order to always reach 92 °C at the outlet of the thermal recovery section, thus guaranteeing an optimal WARGs operation by supplying hot water at the nominal temperature level.

To estimate the potential thermal energy that could be produced with this new plant configuration, some other cogeneration ICEs have been used as a reference [12]: their real operating conditions data have been averaged in order to obtain a mean possible working condition of the Rolls Royce 5,1 MW_e engine.

Table 5.2 shows the real working condition data about load variation that have been used to obtain the load curve for the trigeneration plant engine.

By varying the load conditions from 100 % to 75 % and 50 %, it is possible to see the correspondent variation, with respect to full load conditions, of the natural gas inlet power, the generated electric power, the thermal power that can be recovered and the electric and cogeneration efficiencies

ICE Manufacturer	ICE model	Load Variation	Inlet Gas Power	Electric Power	Thermal Power	η_e	η_t
1	1	100%	*100,00%*	*100,00%*	*100,00%*	*41,94%*	*47,35%*
		75%	*76,62%*	*75,00%*	*78,31%*	*41,06%*	*48,39%*
		50%	*53,24%*	*50,00%*	*57,28%*	*39,39%*	*50,94%*
2	2	100%	*100,00%*	*100,00%*	*100,00%*	*35,28%*	*53,26%*
		75%	*77,73%*	*75,00%*	*79,45%*	*34,04%*	*54,45%*
		50%	*55,45%*	*50,00%*	*59,18%*	*31,81%*	*56,84%*
3	3	100%	*100,00%*	*100,00%*	*100,00%*	*41,30%*	*51,05%*
		75%	*77,46%*	*75,00%*	*78,90%*	*39,99%*	*52,01%*
		50%	*54,92%*	*50,00%*	*58,18%*	*37,60%*	*54,09%*
4	4	100%	*100,00%*	*100,00%*	*100,00%*	*39,21%*	*52,06%*
		75%	*76,77%*	*74,74%*	*79,43%*	*38,17%*	*53,86%*
		50%	*53,44%*	*49,35%*	*59,22%*	*36,21%*	*57,68%*
5	5	100%	*100,00%*	*100,00%*	*100,00%*	*42,32%*	*49,07%*
		75%	*77,46%*	*75,00%*	*79,58%*	*40,97%*	*50,41%*
		50%	*54,92%*	*50,00%*	*61,48%*	*38,53%*	*54,93%*
6	6	100%	*100,00%*	*100,00%*	*100,00%*	*43,38%*	*49,01%*
		75%	*77,46%*	*75,00%*	*79,87%*	*42,00%*	*50,54%*
		50%	*54,92%*	*50,00%*	*61,51%*	*39,49%*	*54,89%*

Table 5.2: ICEs operating conditions with load variation

From data reported in *Table 5.2* a mean ICE working condition have been extracted and it has been used to characterize the Rolls Royce engine, in order to extrapolate a load curve.
Load variation data for the trigeneration engine are shown in *Table 5.3*.

	Load Variation	Inlet Gas Power	Electric Power	Thermal Power
Rolls Royce ICE	100%	*100,00%*	*100,00%*	*100,00%*
	75%	*77,25%*	*74,96%*	*79,26%*
	50%	*54,48%*	*49,89%*	*59,47%*

Table 5.3: Load variation assumption for the Rolls Royce engine

From these assumptions, two useful load curves have been plotted: indeed, these load variation

data are useful to obtain the producible thermal energy in different operating conditions, in order to estimate the maximum thermal power that could be recovered if this energy plant configuration was adopted.

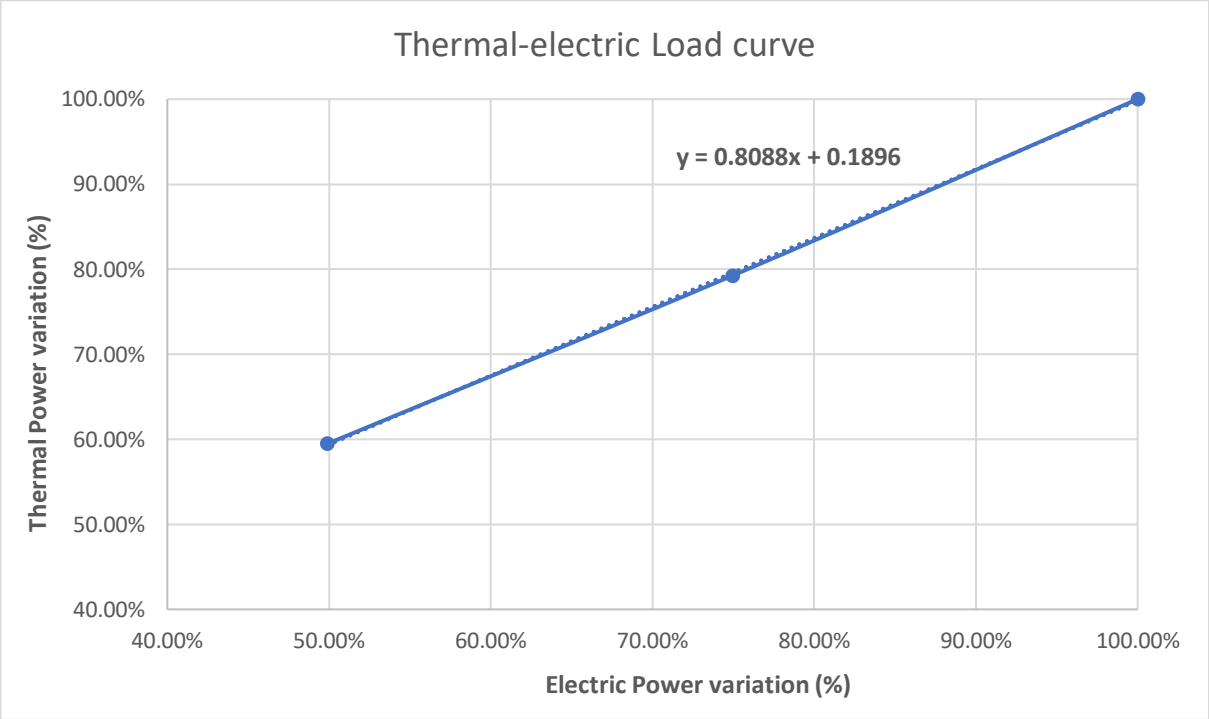

Figure 5.7: Load curve with thermal and electric power variation

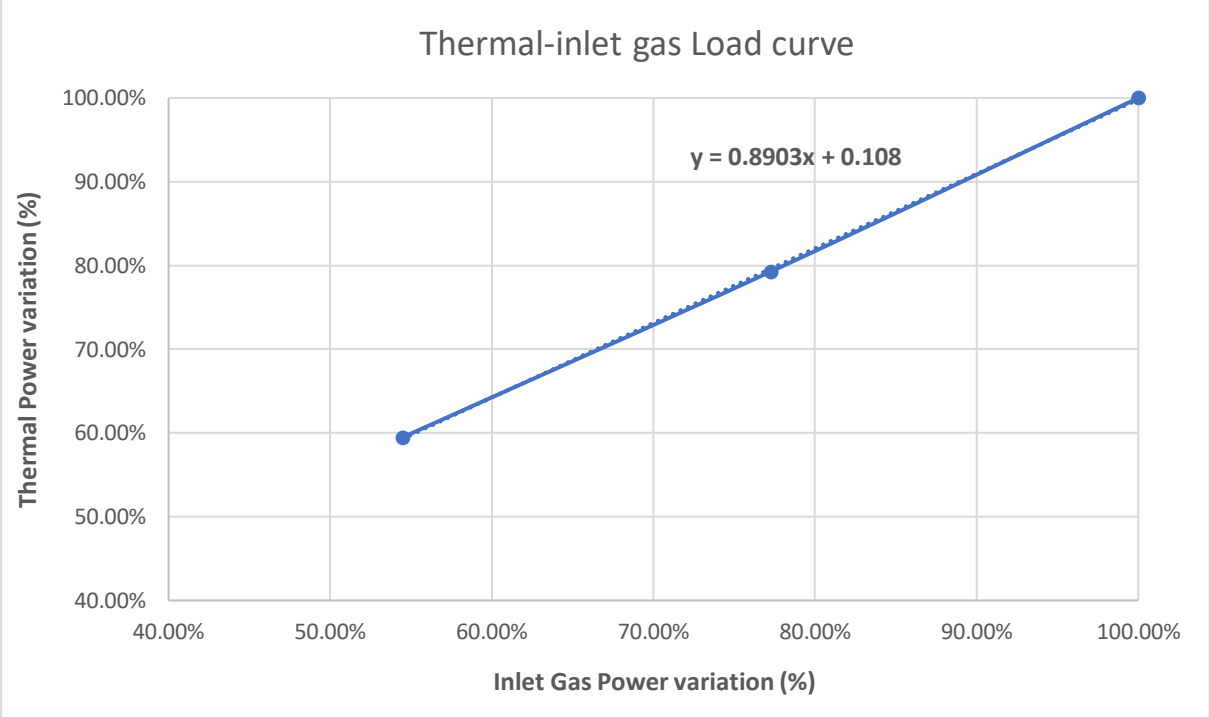

Figure 5.8: Load curve with thermal and inlet gas power variation

The graph in *Figure 5.7* shows the thermal power variation as a function of the generated electricity, while, in *Figure 5.8*, thermal power is related to the inlet natural gas power variation The two load curves can be resumed with the two following equations.

Thermal-electric load curve, correlation 1: $y = 0{,}8088\,x + 0{,}1896$

Thermal-gas load curve, correlation 2: $y = 0{,}8903x + 0{,}108$

In order to estimate the thermal power that could be produced in real operating conditions, the year 2018 has been considered as a reference: indeed, 2017 could not be taken into account for this analysis because of the lack of data, while 2019 was characterized by a reduced energy carriers demand.

Both correlations have been employed to calculate the maximum recoverable thermal energy by means of hourly engine working conditions data about produced electric power and inlet natural gas power.

The full load conditions are reported in *Table 5.4*.

100 % Load conditions		
Inlet Gas Power	**Electric Power**	**Thermal Power**
11’500 kW	5100 kW	3800 kW

Table 5.4: Rolls Royce ICE full load conditions

From the calculations, two slightly different results have been obtained about the maximum recoverable thermal energy during 2018.

Maximum thermal energy, correlation 1	**Maximum thermal energy, correlation 2**	**Percentage Variation**
21’416 MWh	21’219 MWh	0,93 %

Table 5.5: 2018 maximum recoverable thermal energy

The results in *Table 5.5* show a percentage variation that is lower than 1 %. In order to be conservative, the result from correlation 2 will be used from now on to perform further calculations about cold water production.

It must be noticed that results in *Table 5.5* correspond to a thermal recovery more than twice the actual 2018 recovered thermal energy (around 8500 MWh).

5.3 Optimized cold water production

The HRU substitution allows to optimize the hot water production; in order to produce cold energy it is necessary to supply thermal energy to single-effect absorbers that operate with hot water.

To optimize the cold water production, three different scenarios have been considered for this analysis:

- Scenario 1: no additional WARG capacity installed. Total absorber nominal power, 1 MWf (only GFA 1902).
- Scenario 2: additional WARG capacity installed equal to 500 kWf. Total absorbers nominal power, 1,5 MWf.
- Scenario 3: additional WARG capacity installed equal to 1000 kWf. Total absorbers nominal power, 2 MWf.

In order to estimate the money savings obtained by means of an efficient cold energy production, it is necessary to consider a reference condition against which it is possible to determine if the benefits outweigh the costs. The year 2018 has been considered as a reference. The electricity balance shown in Figure 4.11 was necessary to determine the costs incurred for the electricity imports and the gains obtained by exporting electricity to the grid. To give value to this electricity input-output, it was fundamental to assess the unitary cost of electric energy purchase and sale.

To estimate the electricity sale price, the PUN (Prezzo Unico Nazionale) has been considered; its value has been extracted from GME database [17]. PUN is defined as the electricity reference price detected on the electricity stock market (IPEX, Italian Power Exchange).

On the other hand, to determine the electricity purchase price, the Politecnico di Torino electric energy bills for the year 2018 have been used to evaluate the electricity unitary cost, since the university constitutes a medium-sized consumer that can be treated as such a medium energy plant.

Of course, these documents are reserved but their consultation was made possible for this Master Thesis work, thanks to the Professor Alberto Poggio,

PUN values and electricity costs are different because of taxes, fees and system charges.

Monthly PUN values and electricity unitary costs are reported in Table 5.6.

Month (2018)	PUN (c€/kWh)	Unitary cost (c€/kWh)
January	4,90	17,23
February	5,70	17,37
March	5,69	17,44
April	4,94	17,41
May	5,35	17,43
June	5,73	17,78
July	6,27	17,97
August	6,77	16,98
September	7,63	17,06
October	7,39	17,07
November	6,66	17,12
December	6,52	17,00

Table 5.6: 2018 monthly PUN values and electricity unitary cost

Estimates of electricity inputs and outputs, calculated as the difference between the generated electricity and the total electricity consumption (user's demand and internal consumption), are shown in *Table 5.7*, together with the correspondent monetary values. Electricity purchases are reported with the negative sign.

	MWh	€	Mean €/MWh
Electricity Import from the grid	-3618,17	-624'647	172,64
Electricity Export to the grid	2435,50	147'062	60,39
Balance	-1182,67	-477'585	/

Table 5.7: 2018 electricity input-output balance with monetary values

Optimization scenarios are realized by considering the same conditions occurred during 2018: this means, same electric power generation, same thermal demand (from Paintings ATU), same total cold energy demand and same auxiliaries' consumption.

The optimized energy plant configuration will lead to a different internal total consumption because of the different needs for the electric chillers.

Therefore, it was necessary to separate the two different electricity consumption in:

- Energy plant auxiliaries
- Electricity needed by the CERGs

Data about electricity demand from chillers during 2018 are present in the Online Data Collector but they are not considered in this analysis since they didn't fit with data about total internal electricity consumption: indeed, electricity consumption by chillers, reported in the Online Data Collector are extremely high, therefore they can be considered inaccurate.

In order to estimate the chillers consumption, the cold water hourly demand, and the cold water hourly production by WARGs have been employed.

Chillers' electricity has been obtained by using the following equation, for each hour of 2018:

$$Chillers\ electricity = \frac{Cold\ energy\ demand - Cold\ energy\ production\ by\ WARGs}{Reference\ Chillers\ COP}$$

Where the reference COP has been considered equal to 3,5.

Energy plants auxiliaries' consumption has been assumed to be constant since it was not possible to build a significative correlation neither with the engine electricity load nor with the cold energy production by means of WARGs.

Moreover, it is reasonable to assume that the auxiliaries' consumption could depend on the total cold energy demand because it implies a higher electricity consumption for water pumping. Since this optimization analysis is performed by considering always the same total cold energy demand, it is not unrealistic to assume that the auxiliaries' consumption might be almost constant.

It must not be neglected that Scenario 2 and Scenario 3 requires the availability of cooling towers, to reject the absorption and condensation heat (*Figure 2.5*). This thermal energy that must be rejected is almost equal to the sum of the generated cold energy and the supplied heat. Scenario 3 would require a cooling tower nominal power equal to 2700 kW (sum of 1000 kW_f cold power and 1700 kW_{th} of thermal power supplied to the absorber).

Nevertheless, no additional cooling tower should be installed since the dismantled double-effect absorbers rejected heat to two cooling towers, each of 2600 kW of nominal power. These components could be adapted and reused for these optimization Scenarios.

5.3.1 Scenario 1

Scenario 1 is characterized by a total absorber installed nominal capacity equal to 1 MW_f. This means that no additional WARGs are installed in the energy plant.

Consequently, it is not possible to cover the entire cold energy demand for most of the year,

since it was clear from *Figure 5.3* that the cold power demand basis corresponds to around 1,5 MW_f. Electric chillers are necessary to cover the demand, particularly during summer, when the cold energy requirements can exceed 3 MW_f.

Scenario 1 objective is to analyze if it can be economically convenient to avoid the CAPEX (Capital Expenditure) costs related to additional WARGs installation at the cost of a higher electricity consumption by chillers.

To estimate the potential cold energy that can be produced by means of GFA 1902 with this new thermal recovery system, it is necessary to consider the hourly maximum recoverable thermal energy (obtained by Correlation 2 in **Paragraph 5.2**).

Then, in order to account for the heat that could be supplied to the absorber, the thermal energy demand from the Paintings ATU must be subtracted by the maximum heat recovery.

The difference between those two quantities represents the maximum thermal energy that could be provided to GFA 1902. By multiplying that quantity by a reference WARG COP, it is possible to obtain the maximum cold energy that could be produced with the new plant configuration. Obviously, the maximum cold energy that can be produced in one hour depends on the absorber nominal capacity; in this scenario, it corresponds to 1000 kWh.

$$Max\ cold\ energy = (Max\ recovered\ heat - Paintings\ ATU\ hot\ demand) \cdot COP$$

The reference absorber COP has been set equal to 0,6, that is a reasonable value for a single-effect absorber [12].

Nevertheless, since the cold energy demand assumed for this analysis is the same occurred during the year 2018, the effective cold energy production must correspond to the hourly minimum between the demand and the maximum production.

Therefore, if the maximum possible cold energy production is higher than the demand, then the effective production corresponds to the demand itself, on the contrary, if the maximum cold energy production is lower than the demand, then the effective production corresponds to the maximum production.

In the latter case, the cold energy demand that is not satisfied by WARG production, will be covered by the electric chillers.

Then, it is necessary to divide the hourly effective cold power by the absorber COP in order to obtain the useful thermal energy supplied to the WARG. By adding the thermal energy provided to the paintings ATU to the heat provided to the absorber, it will be possible to obtain the total useful thermal energy that can be considered for the White Certificates procedure.

Figure 5.9 illustrates a flux diagram useful to resume the steps to be followed to calculate the effective cold energy production.

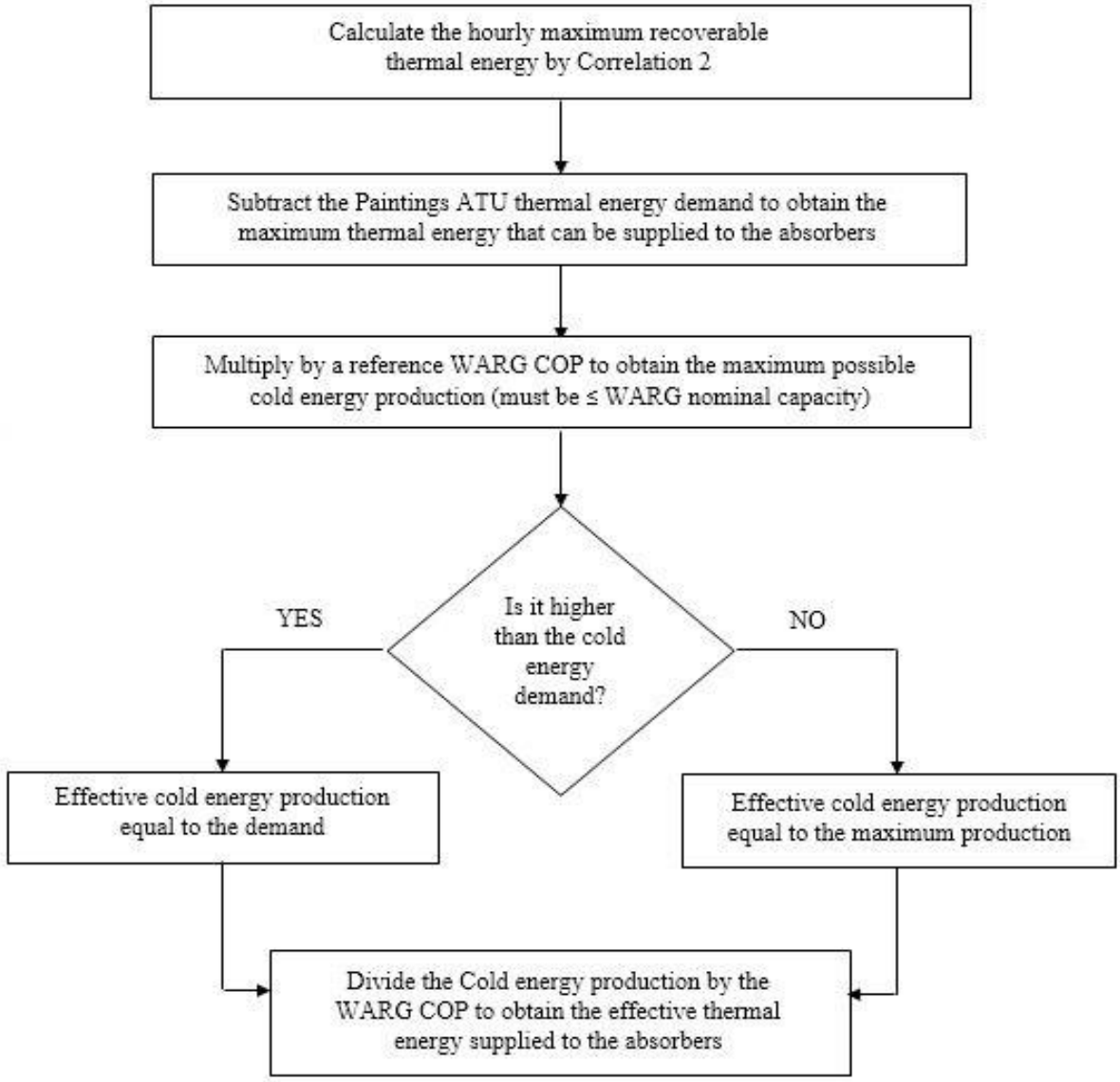

Figure 5.9: Flux diagram for optimized cold energy production

To assess the electricity savings, the electricity needed by the CERGs must be estimated; the reference equation, that has been already explained in **Paragraph 5.3**, is the following:

$$Chillers\ electricity = \frac{Cold\ energy\ demand - Cold\ energy\ production\ by\ WARGs}{Reference\ Chillers\ COP}$$

Figure 5.10 shows the evolution of total cold energy demand (blue area); the orange area corresponds to the cold energy produced by the absorber GFA 1902 in these ideal conditions of constant COP and no maintenance or malfunctioning periods.

The total cold energy that could be produced in these optimal conditions is around 6288 MWh, that corresponds to 57 % of total cold energy demand.

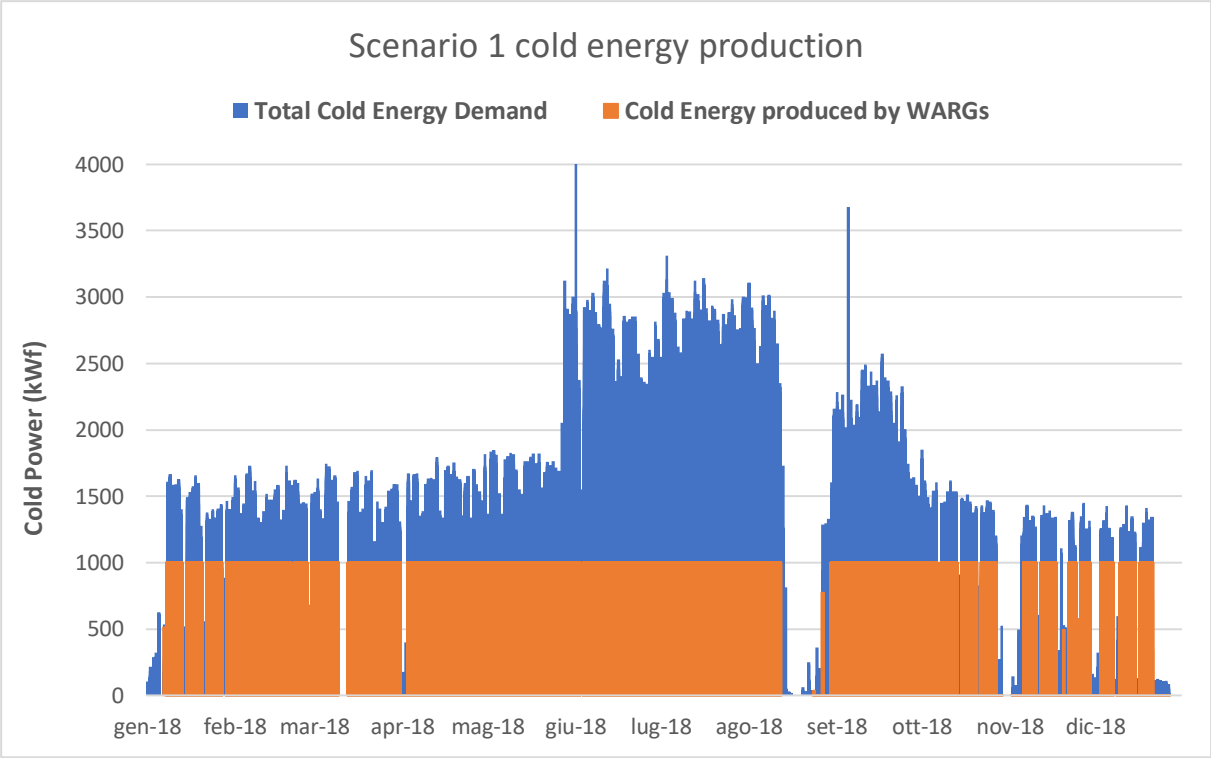

Figure 5.10: Cold energy demand and production, optimization Scenario 1

It is possible to notice that the WARG should operate at full load conditions for most of the time, since the cold energy demand is almost always greater than 1000 kW_f. This implies that the absorber could actually produce cold water with a COP near 0,6 if the supply hot water temperature and the refrigerating water temperature fulfill the nameplate requirements.
The electricity balance for this Scenario is shown in *Table 5.8*.

	MWh	**€**
Electricity Import from the grid	-3701,82	-639’675
Electricity Export to the grid	2490,32	151’997
Balance	-1211,50	-487’678

Table 5.8: Scenario 1 electricity input-output balance with monetary values

In this case, the electricity expenditure is higher than the one occurred during 2018, reported in *Table 5.7*. This is due to the electricity needed by CERGs to cover the cold energy demand. Total useful thermal energy is around 11’900 MWh, while during 2018 thermal recovery accounted for less than 8500 MWh.

In *Table 5.9* some useful information about interesting physical quantities or monetary balance are reported and compared to 2018 real operating conditions.

	Scenario 1	**2018**	**% Variation**
Useful Thermal Energy	11'896 MWh	8465 MWh	+40,5 %
Cold Energy by WARG	6288 MWh	6386 MWh	-1,5 %
Plant's electricity consumption	3838 MWh	3809 MWh	+0,8 %
Electricity total expenditure	487'678 €	477'585 €	+2,1 %

Table 5.9: Comparison between Scenario 1 and 2018 plant's performance

Cold energy produced by GFA 1902 is around 6288 MWh. Since the absorber nominal power is 1000 kW_f, the equivalent hours of operation are 6288 hours in a year, thus the Capacity Factor is around 72 %.

It can be interesting to assign a monetary value to the thermal energy that could be recovered but it has not been exploited; indeed, as it is reported in *Table 5.5*, with the same engine working conditions it would be possible to recover around 21'200 MWh, but, in Scenario 1, only the 56 % of this energy is effectively used.

In order to perform this estimate, it is necessary to know the natural gas price. PSV (Punto di Scambio Virtuale) represents the intersection between natural gas supply and demand in Italy; on this basis, the natural gas wholesale price is defined.

To evaluate more accurately the gas price for a cogeneration plant, it is necessary to also consider the excise duties, distribution costs and then the value-added tax.

Since this energy plant produces both electricity and thermal energy, it can benefit from a reduced excise duty on the natural gas. In particular, as it is described by D.L n.119 [18], for each kWh of produced electricity, 0,22 Sm^3 of natural gas are subjected to the electricity production excise duty, equal to 0,04493 c€/Sm^3.

Fenice trigeneration plant, during 2018, consumed around 6'369'470 Sm^3 of natural gas; 6'139'279 Sm^3 of that gas, that correspond to more than 96 % of total gas consumption, can benefit from the privileged tariff, while the remaining part is subjected to the reduced excise duty for industrial consumers.

Since almost the total gas consumption (96 %) can be accounted for as gas used for cogeneration purposes, it can be simplified so that all of the gas is used to produce electricity and thermal energy.

Moreover, the natural gas used for cogeneration purposes can benefit from a value-added tax equal to 10 %, rather than 22 %.

Distribution costs are unknown, therefore, in this analysis, they are assumed to correspond to 10 % of PSV quotation.

PSV monthly quotations, extracted from [17], are reported in *Table 5.10*.

Month (2018)	**PSV (€/MWh)**
January	19,91
February	23,49
March	24,45
April	21,84
May	23,38
June	23,99
July	24,50
August	25,24
September	29,59
October	27,38
November	24,86
December	23,12

Table 5.10: 2018 monthly PSV quotation

The total monthly gas cost can be obtained by summing up the PSV gas quotation, distribution costs, and the cogeneration excise duty (properly transformed to €/MWh).

Then, it is necessary to calculate the value-added tax, as the 10 % of the previously obtained subtotal.

In order to get a recovered thermal energy economic value, natural gas final unitary cost is divided by an ideal boiler efficiency, that is assumed to be equal to 0,9.

Recovered thermal energy monetary values are shown in *Table 5.11*.

Month (2018)	**Thermal energy value (€/MWh)**
January	26,82
February	31,64
March	32,93
April	29,42

May	31,49
June	32,31
July	32,99
August	33,99
September	38,84
October	36,87
November	33,48
December	31,14

Table 5.11: Thermal energy monetary value

By obtaining the monthly difference between the maximum recoverable thermal energy (from Correlation 2) and the effective useful heat, and then by multiplying those quantities by the monetary values reported in *Table 5.11,* it is possible to quantify the amount of money that constitutes a loss of potential profit.
Indeed, if it was possible to exploit that thermal energy by supplying it to another division of the Stellantis industrial site, that recovered heat could represent another source of income.
Table 5.12 shows this loss of profit comparison between Scenario 1 and 2018 real operating conditions.

	Scenario 1	**2018**	**% Variation**
Loss of profit from recovered thermal energy	307’840 €	431’462 €	-28,7 %

Table 5.12: Loss of potential profit derived from the non-complete utilization of recovered heat

Loss of potential profit in Scenario 1 accounts for around 310’000 €; nevertheless, it is 30 % lower than the lost earnings occurred during 2018. This is due to a more efficient utilization of thermal energy with the new energy plant configuration.
First Law Efficiency for Scenario 1 is around 62 %, thus showing a slight increase with respect to 56 % efficiency obtained during 2018.

5.3.2 Scenario 2

Scenario 2 involves the installation of an additional WARG, so that total absorbers installed nominal capacity is equal to 1,5 MW_f. Therefore, it is necessary to install an absorber, which nominal cold power is equal to 500 kW_f. This absorber would support the already working GFA 1902.

This cold power capacity should allow to cover the cold energy demand for most of the year, except for summer months, during which it will be necessary to switch on the electric chillers. It is then necessary to perform a cash flow analysis in order to evaluate if money savings derived from the additional absorber installation could compensate this CAPEX expenditure and, therefore, if Scenario 2 could be more economically convenient than Scenario 1.

The procedure followed to estimate the new cold energy productivity is the same that has been explained in **Paragraph 5.3.1** and graphically illustrated by means of *Figure 5.9*.

Figure 5.11 shows the total cold energy demand (blue) and the cold energy production by means of 1,5 MW_f absorbers.

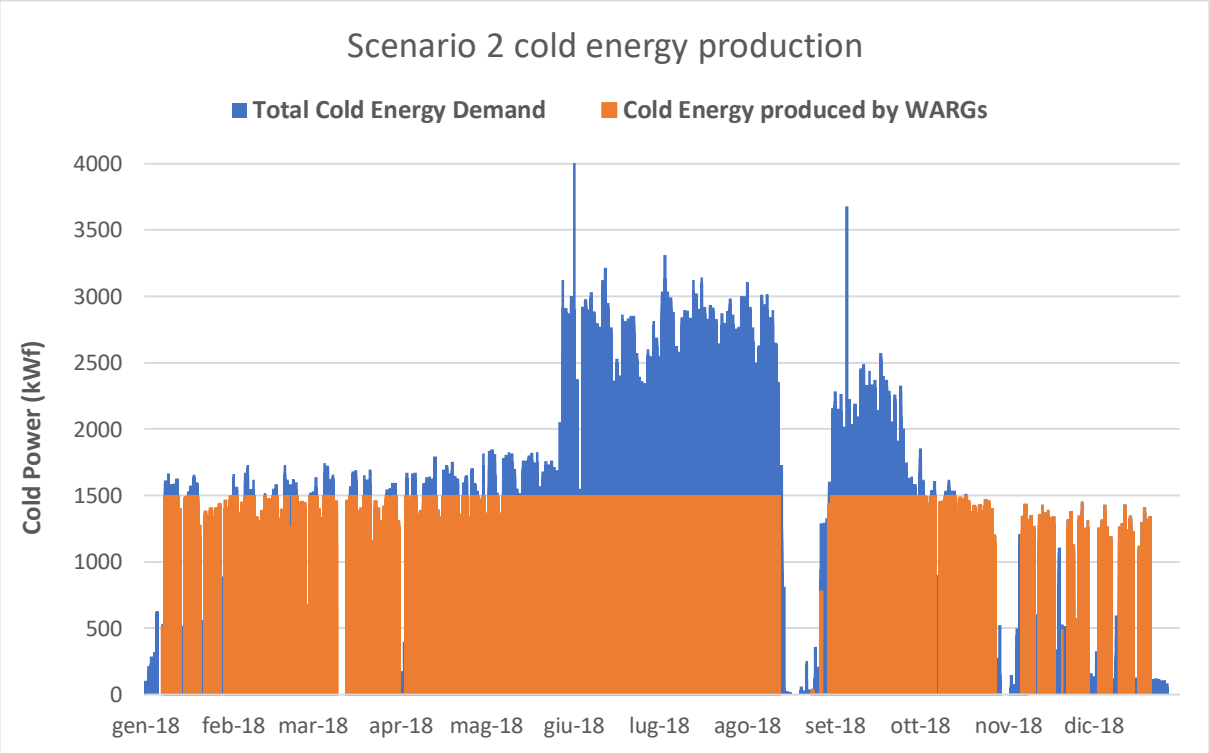

Figure 5.11: Cold energy demand and production, optimization Scenario 2

Also in this Scenario, WARGs operate at full load conditions for most of the year. Moreover, absorbers are able to almost completely satisfy the cold energy demand, except during Summer

months. This could allow to not witch on electric chillers for most of the year, thus saving electricity and, therefore, also money.

Electricity balance is reported in *Table 5.13*

	MWh	**€**
Electricity Import from the grid	-3541,32	-611’506
Electricity Export to the grid	2944,20	179’852
Balance	-597,12	-431’655

Table 5.13: Scenario 2 electricity input-output balance with monetary values

Even in this Scenario, the amount of electricity that must be imported from the national grid is higher than that exported to the network.

Nevertheless, due to the higher cold energy production by WARGs, it is possible to use less electricity produced by the engine to supply the chillers; the electricity exported to the grid shows an increase of around 18 % with respect to Scenario 1.

The comparison between Scenario 2 and 2018 energy plant’s performance is reported in *Table 5.14*. In this Table it is also shown the loss of profit due to the non-complete utilization of recovered thermal energy.

The procedure followed to quantify this loss of earnings is the same that has been used in **Paragraph 5.3.1**.

	Scenario 2	**2018**	**% Variation**
Useful Thermal Energy	15’480 MWh	8465 MWh	+82,9 %
Cold Energy by WARG	8438 MWh	6386 MWh	+32,1 %
Plant’s electricity consumption	3223 MWh	3809 MWh	-15,4 %
Electricity total expenditure	431’655 €	477’585 €	-9,6 %
Loss of profit from recovered thermal energy	188’702 €	431’462 €	-56,3 %

Table 5.14: Comparison between Scenario 2 and 2018 plant’s performance

Useful thermal energy accounts for almost 15’500 MWh, thus an 83 % increase can be realized with respect to 2018 original plant configuration.

WARGs could ideally produce around 8440 MWh of cold energy if no maintenance and malfunctioning occurs. This corresponds to 76 % of total cold energy demand and, moreover, to 5627 equivalent hours of operation at nominal conditions. Therefore the WARGs Capacity Factor is around 64 %, slightly lower than the absorbers CF in Scenario 1.

Also in this Scenario, the absorber could work with a high COP because of the full load operating conditions, as it is possible to notice from *Figure 5.11*.

Moreover, it is interesting to notice that, since much more recovered thermal energy can be effectively exploited, then the loss of profit related to the waste of heat decreases of around 56%.

It is possible to say that Scenario 2 could allow to achieve much greater performances with respect to the original trigeneration plant configuration, at the cost of a 500 kW_f additional absorber installation.

Scenario 2 First Law Efficiency is equal to 67,3 %.

5.3.3. Scenario 3

Scenario 3 implies the installation of an additional absorber with nominal capacity equal to 1 MW_f, so that the total installed cold power capacity corresponds to 2 MW_f.

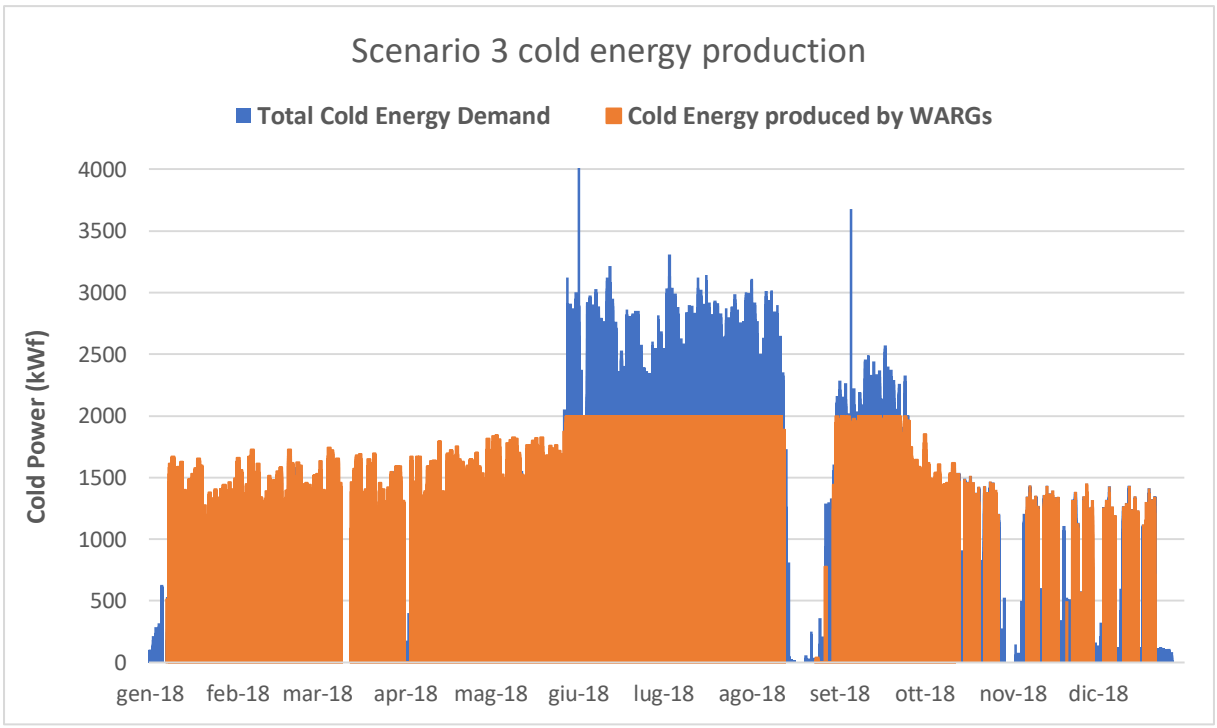

Figure 5.12: Cold energy demand and production, optimization Scenario 3

As it can be noticed from *Figure 5.12*, the absorbers are able to satisfy the cold energy demand for most of the year if they operate correctly. Moreover, around 2/3 of summer months demand could be covered, thus implying less electricity import from the national grid.
Nevertheless it should be considered that the installation of a 1 MW_f absorber would imply that it would work at around 50 % of full load conditions during winter and mid-seasons. This could lead to a reduction of cold water production efficiency, therefore it might operate with a COP lower than the expected COP equal to 0,6.

	MWh	**€**
Electricity Import from the grid	-3488,85	-602’238
Electricity Export to the grid	3165,44	193’916
Balance	-323,41	-408’322

Table 5.15: Scenario 3 electricity input-output balance with monetary values

Electricity import from the grid is higher than the export, but the balance approaches to zero, i.e. those two quantities are more similar than in the other Scenarios.
The comparison between Scenario 3 and the original trigeneration plant configuration is shown in *Table 5.16*.

	Scenario 3	**2018**	**% Variation**
Useful Thermal Energy	17’077 MWh	8465 MWh	+101,7 %
Cold Energy by WARG	9396 MWh	6386 MWh	+47,1 %
Plant’s electricity consumption	2950 MWh	3809 MWh	-22,6 %
Electricity total expenditure	408’322 €	477’585 €	-14,5 %
Loss of profit from recovered thermal energy	134’439 €	431’462 €	-68,8 %

Table 5.16: Comparison between Scenario 3 and 2018 plant’s performance

Useful thermal energy is doubled with respect to 2018 effective heat recovery: this constitutes an important bonus for the achievement of more White Certificates.
Cold energy production could increase by 47 %. WARGs could produce around 9400 MWh, that correspond to 85 % of total cold energy demand.

Nevertheless, the absorbers equivalent hours of operation decreases to slightly less than 4700 hours in a year, thus the CF is 54 %. This means that, by installing one additional WARG with nominal capacity equal to 1 MW_f, it would be necessary that both absorbers operate at partial load conditions for most of the year.

For example, if the mean hourly cold power demand is around 1500 kW, both WARGs can operate at 75 % of full load conditions; in this way, it would be possible to avoid that one of the two absorbers operates at less than 50 % of full load conditions, thus avoiding possible reduction in cold water production efficiency.

5.4 Trigeneration plant White Certificates

Fenice S.p.A. trigeneration plant nominal electric power is higher than 1 MW_e, therefore, as it was specified in **Paragraph 2.2** and **Paragraph 2.3,** it is necessary that PES is higher than 10% and First Law Efficiency must be higher than 75 %, in order to be considered as a High Efficiency Cogeneration (CAR) plant and to get White Certificates.

During 2018, First Law Efficiency was lower than 75 % (about 56 %) and the calculated PES was 4,52 %. This means that, in order to obtain White Certificates, it was necessary to introduce the Virtual Machine to give value to recovered thermal energy.

In 2018, the recognized White Certificates, as declared by Fenice S.p.A. company, were 1201; since White Certificates mean price relative to the organized market was 303,60 €/TOE [17], the revenues accounted for about 364'624 €.

In order to estimate the White Certificates potential profits for all optimized plant configurations, it is necessary to follow the procedure described in **Paragraph 2.2** and **Paragraph 2.3.**

Results of all calculations for the optimization Scenarios are reported in *Table 5.17*.

Since White Certificates mean price on the market during 2019 and 2020 was respectively equal to 260 €/TOE and 262,50 €/TOE [17], in *Table 5.18* there are shown also the White Certificates revenues obtained with the most updated TEE price.

	Scenario 1	**Scenario 2**	**Scenario 3**
$\boldsymbol{E\ (MWh)}$	27'906	27'906	27'906
$\boldsymbol{H_{CHP}\ (MWh)}$	11'896	15'480	17'077
$\boldsymbol{F\ (MWh)}$	64'504	64'504	64'504
$\boldsymbol{\eta_{global}}$	61,7 %	67,3 %	69,7 %
$\boldsymbol{CHP\ H_\eta}$	18,4 %	24,0 %	26,5 %
$\boldsymbol{CHP\ E_\eta}$	43,3 %	43,3 %	43,3 %
$\boldsymbol{Ref\ H_\eta}$	90 %	90 %	90 %
$\boldsymbol{Ref\ E_\eta}$	52,5 %	52,5 %	52,5 %
$\boldsymbol{Climatic\ correction\ factor}$	-0,104 %	-0,104 %	-0,104 %
$\boldsymbol{Electricity\ self-consumption}$	91,1 %	89,5 %	88,8 %
$\boldsymbol{PES}$	9,62 %	14,4 %	16,3 %
Virtual machine introduction			
$\boldsymbol{\eta_{CHP}}$	75 %	75 %	75 %
$\boldsymbol{\eta_{non-CHP,e}}$	43,3 %	43,3 %	43,3 %
$\boldsymbol{C_{eff}}$	1,363	1,363	1,363

E_{CHP} (MWh)	16’215	21’101	23’278
$E_{non-CHP}$ (MWh)	11’690	6’805	4’628
F_{CHP} (MWh)	37’482	48’774	53’806
$F_{non-CHP,e}$ (MWh)	27’022	15’730	10’698
$F_{non-CHP,h}$ (MWh)	0	0	0
$CHP\ H_{\eta}$	31,7 %	31,7 %	31,7 %
$CHP\ E_{\eta}$	43,3 %	43,3 %	43,3 %
$Electricity\ self-consumption$ %	100 %	100 %	100 %
PES	20,38 %	20,38 %	20,38 %
$\eta_{h,REF}$	90 %	90 %	90 %
$\eta_{e,REF}$	46 %	46 %	46 %
$RISP$ (MWh)	14’304	18’613	20’533
$Operating\ hours$	6480	6480	6480
$Mean\ Power\ CHP$	2,50	3,26	3,59
K	1,34	1,33	1,33
TEE	1’648	2’130	2’345
$TEE\ value$ $(€/TOE)$	303,60	303,60	303,60
$TEE\ updated\ value$ $(€/TOE)$	260,00	260,00	260,00
$TEE\ revenues$ (€)	500’333	646’668	711’942
$TEE\ updated\ revenues$ (€)	428’480	553’800	609’700
2018 $TEE\ revenues$ (€)	364’624	364’624	364’624

Table 5.17: White Certificates obtained by energy efficiency optimization

White Certificates revenues are much higher for all three optimization Scenarios, in particular, Scenario 3 shows an almost doubled income thanks to energy efficiency improvement.

It is necessary to perform a cash flow analysis to evaluate the benefits and costs of all three scenarios and to estimate the pay-back time of the different investment costs.

5.5 Cash flow analysis

In order to evaluate if these optimization Scenarios could represent a good investment solution, it is necessary to perform a cash flow analysis that considers all additional costs and the sources of revenues.

The additional costs of such optimization includes:

- HRU substitution and the installation of new diverter valve, connections, pipes and the dismantling of the already existing HRU
- New heat exchanger E-3502, with its mechanical installation and new electric connections and automatization.
- Installation of new WARGs with all the required connections and new pipelines.

The first two expenditures are in common for all optimization Scenarios, while the third one depends on the absorber nominal capacity that should be installed.

HRU substitution costs has been suggested by a professional thermotechnic engineer that operates in this energy engineering sector. His estimates for this type of intervention is a cost of around 200'000 €.

Therefore it is reasonable to assume that the cost of HRU substitution and new heat exchanger E-3502 installation could cost around 250'000 €.

In order to estimate the WARGs installation costs, a study from Prof. Alberto Poggio and Ing. Giulio Cerino for Iren Energia S.p.A. was consulted. The cost estimate for a new absorber with nominal capacity equal to 500 kW_f is a specific cost of around 250 €/kW_f. The projected cost for its installation and other supplies is about 25 % of WARG cost.

The sources of income for these new plant configurations are:

- The electricity saving consequently to a higher efficiency WARG cold water production
- The additional revenues obtained from White Certificates because of a greater valorization of recovered thermal energy from exhaust gases.

All costs and incomes are resumed in *Table 5.18*. It is important to consider that, in this case, all expenditures are CAPEX because they occur only once, namely when the optimization intervention is realized. On the contrary, revenues due to electricity savings and White Certificates occur every year. Yearly revenues are, therefore, the summation of those two quantities

Electricity savings reported in *Table 5.18* are obtained by performing the difference between

each optimization Scenario electricity balance (import-export on the grid) and 2018 real operating conditions electricity balance. These results are then rounded because they are estimates and cannot be considered as exact values.

All Scenarios cash flow analysis should also include the additional maintenance costs for the absorbers; nevertheless it is difficult to estimate accurately this expenditure and, moreover, it should also include the unknown maintenance money saving with respect to the original plant configuration, therefore these costs are neglected.

	Scenario 1	**Scenario 2**	**Scenario 3**
Additional absorbers	0 kW_f	500 kW_f	1000 kW_f
Absorber Cost	0 €	-125’000 €	-250’000 €
Absorber installation & other supplies	0 €	-31’250 €	-62’500 €
HRU & E-3502 substitution	-250’000 €	-250’000 €	-250’000 €
CAPEX Total Cost	**-250’000 €**	**-406’250 €**	**-562’500 €**
Electricity saving	-11’000 €	+45’000 €	+69’000 €
White Certificates additional revenue (2018)	+135’709 €	+282’044 €	+347’318 €
Yearly revenues	**+124’709 €**	**+327’044 €**	**+416’318 €**
Pay-Back Analysis			
Year 0	-250.000,00 €	-406.250,00 €	-562.500,00 €
Year 1	-125.291,00 €	-79.206,00 €	-146.182,00 €
Year 2	-582,00 €	247.838,00 €	270.136,00 €
Year 3	124.127,00 €	574.882,00 €	686.454,00 €
Year 4	248.836,00 €	901.926,00 €	1.102.772,00 €
Year 5	**373.545,00 €**	**1.228.970,00 €**	**1.519.090,00 €**

Table 5.18: Cash flow and Pay-back analysis

It is interesting to evaluate the pay-back and the pay-back time of each Scenario.

As expected, Scenario 1 is characterized by the lowest pay-back after 5 years of operation: estimated revenues are around 375’000 €. Indeed, the lower investment cost implies also lower incomes obtained by White Certificates economic valorization; moreover, it is the only Scenario that presents a negative electricity saving; this implies that more electricity must be imported from the national grid in order to supply it to electric chillers.

Nevertheless, this Scenario could benefit from money savings due to reduced absorbers

maintenance costs.

Scenario 2 revenues after 5 years are more than three times higher with respect to Scenario 1. The additional incomes by White Certificates monetary valorization and the affordable expenditures for only one absorber installation could lead to more than 1'000'000 € of revenues after 5 years.

Scenario 3 shows a +23,6 % of final profits with respect to Scenario 2, but at almost +40 % of initial additional costs for one absorber with nominal capacity equal to 1000 kW_f.

Both Scenario 2 and Scenario 3 become profitable after slightly more than 1 year of operation, as it can be noticed from *Figure 5.13*, while Scenario 1 becomes profitable after 2 years.

Break-even point of Scenario 2 and Scenario 3 occurs after almost 2 years of operation, and, after that, Scenario 3 could represent a higher source of income.

Nevertheless, it must be considered that Scenario 3 yearly maintenance costs could be higher with respect to Scenario 2, thus the final profit difference could be thinner.

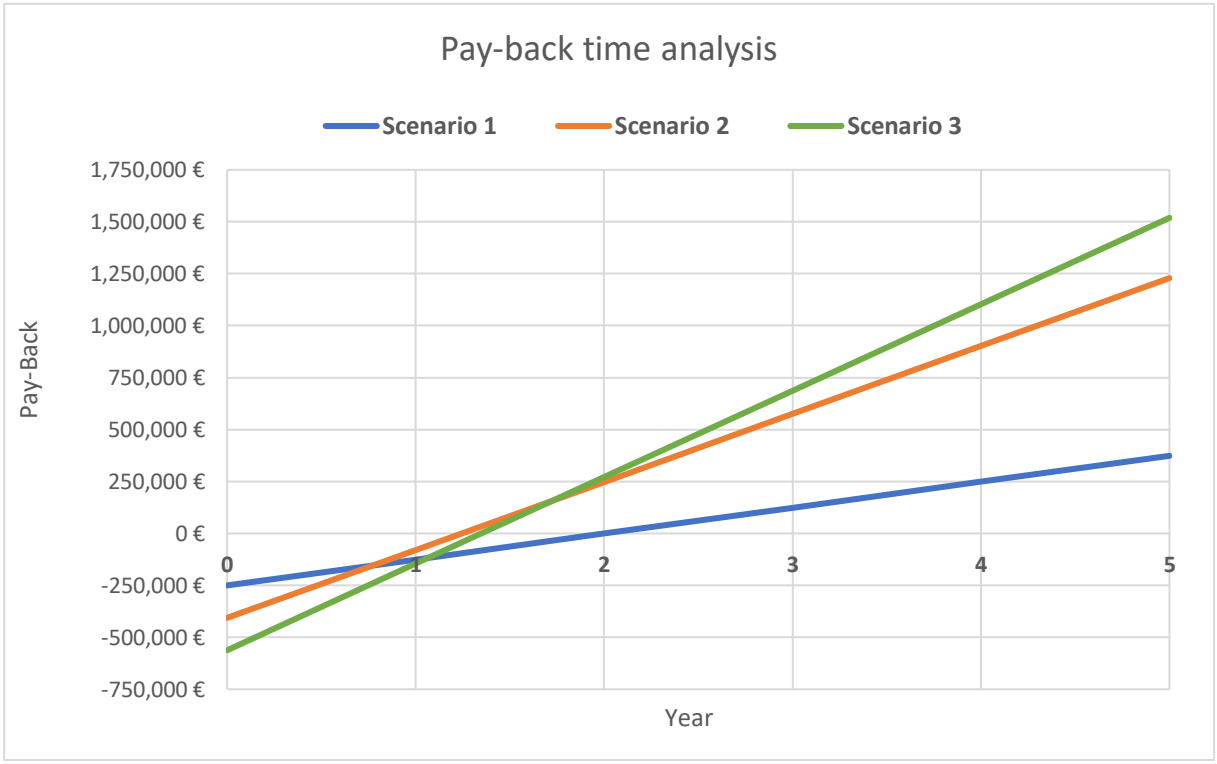

Figure 5.13: Optimization Scenarios pay-back analysis

5.5.1 Future cash flow analysis

It could be interesting to evaluate the cash flow analysis for future years. As an example, future PUN projections could be utilized in order to estimate the monetary value of electricity savings in the next years.

This analysis is focused on year 2024; futures PUN projections are extracted from the online website *eex.com* [19]. In order to estimate the costs of imported electricity from the national grid, data in *Table 5.6* have been used: a mean PUN value and a mean electricity unitary cost have been calculated. Their relative difference has been employed in order to estimate 2024 electricity unitary cost starting from PUN projections.

Mean 2018 PUN is equal to 61,29 €/MWh.

Mean 2018 imported electricity unitary cost is 173,22 €/MWh.

2024 latest future PUN projections estimate a value that is equal to 80,71 €/MWh (19/11/2021); thus, the imported electricity unitary cost can be assumed to be around 200 €/MWh.

In order to estimate the additional revenues obtained by White Certificates, a mean conservative value equal to 260 €/TOE has been used for this analysis; indeed White Certificates mean price on the market during 2019, 2020 and 2021 was between 260 and 270 €/TOE.

Results of this future estimates analysis are reported in *Table 5.20*.

	Scenario 1	**Scenario 2**	**Scenario 3**
Additional absorbers	0 kW_f	500 kW_f	1000 kW_f
Absorber Cost	0 €	-125’000 €	-250’000 €
Absorber installation & other supplies	0 €	-31’250 €	-62’500 €
HRU & E-3502 substitution	-250’000 €	-250’000 €	-250’000 €
CAPEX Total Cost	**-250’000 €**	**-406’250 €**	**-562’500 €**
Electricity saving	-62’000 €	+7’000 €	+35’000 €
White Certificates additional revenue (futures)	+63’856 €	+189’176 €	+245’076 €
Yearly revenues	**1.856,00 €**	**196.176,00 €**	**280.076,00 €**
Pay-Back Analysis			
Year 0	-250.000,00 €	-406.250,00 €	-562.500,00 €
Year 1	-248.144,00 €	-210.074,00 €	-282.424,00 €
Year 2	-246.288,00 €	-13.898,00 €	-2.348,00 €

Year 3	-244.432,00 €	182.278,00 €	277.728,00 €
Year 4	-242.576,00 €	378.454,00 €	557.804,00 €
Year 5	-240.720,00 €	574.630,00 €	837.880,00 €

Table 5.20: Future Cash flow and Pay-back analysis

Table 5.20 shows that Scenario 1 would be heavily unprofitable in the future because the reduced revenues by means of White Certificates could not compensate the increased costs for electricity and natural gas.

Scenario 2 and Scenario 3 become profitable after around 3 years of operation and their profits after 5 years are dramatically decreased with respect to revenues presented in *Table 5.18*.

In order to clearly visualize the reduction of profits in this future cash flow analysis, the y-axis in *Figure 5.14* has been set exactly as it is in the graph in *Figure 5.13*.

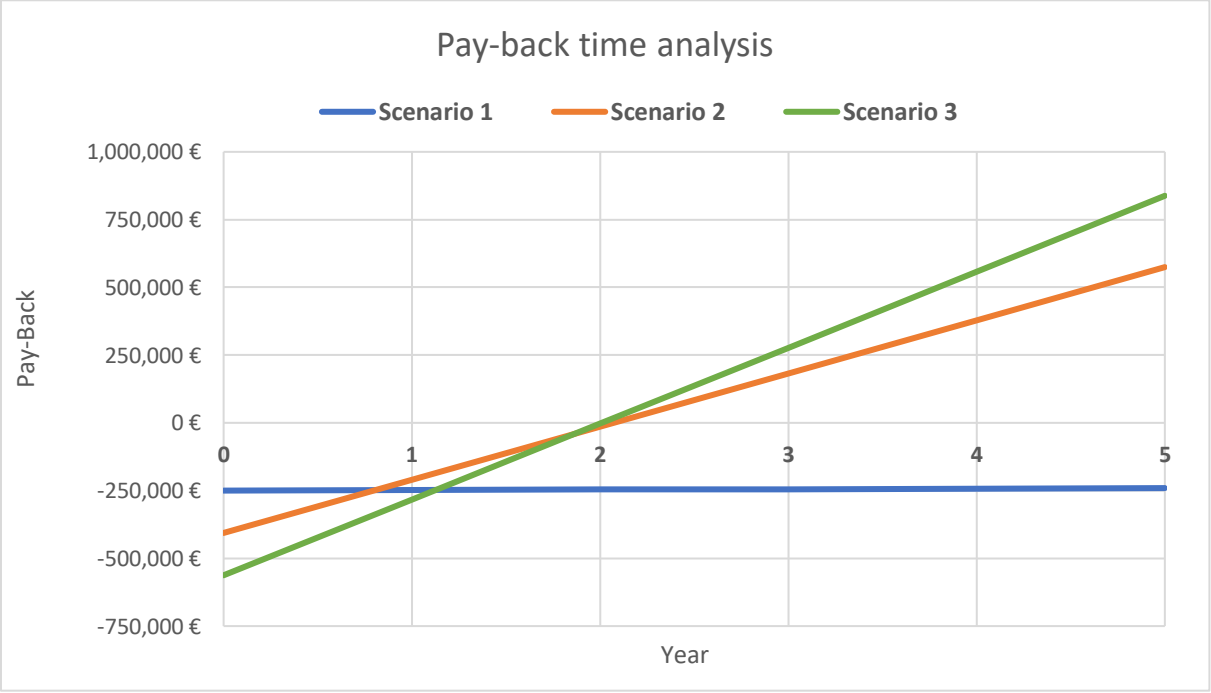

Figure 5.14: Optimization Scenarios future pay-back analysis

5.6 Considerations on CO_2 emissions

This economic analysis has been performed without considering the CO_2 emission costs ruled by the European ETS (Emission Trading System). The EU ETS is an emission trading scheme that aims at reducing the greenhouse gases emissions from industrial and aviation sectors.
ETS was introduced by the European legislation in the Directive 2003/87/CE.
It is based on a "cap and trade" system, thus a European emissions upper limit is established and each ton of CO_2 corresponds to one EU Allowance. These Allowances are sold at auction or allocated for free (particularly, to companies that may delocalize their production to countries with less stringent environmental legislation).
All companies that operate in sectors subject to EU ETS regulations must control their emissions and they have to compensate them with a correspondent amount of Allowances that can be traded on this market.
Total available Allowances decreases over time and this forces all companies to reduce their greenhouse gases emissions, but it also implies a price increase of traded Allowances.
EU ETS has been progressively modified from its introduction in 2005, and it has been divided in different trading periods, called "phases". Currently, we are in the 4th phase (2021-2030), that is subdivided in two allocations periods: 2021-2025 and 2025-2030.

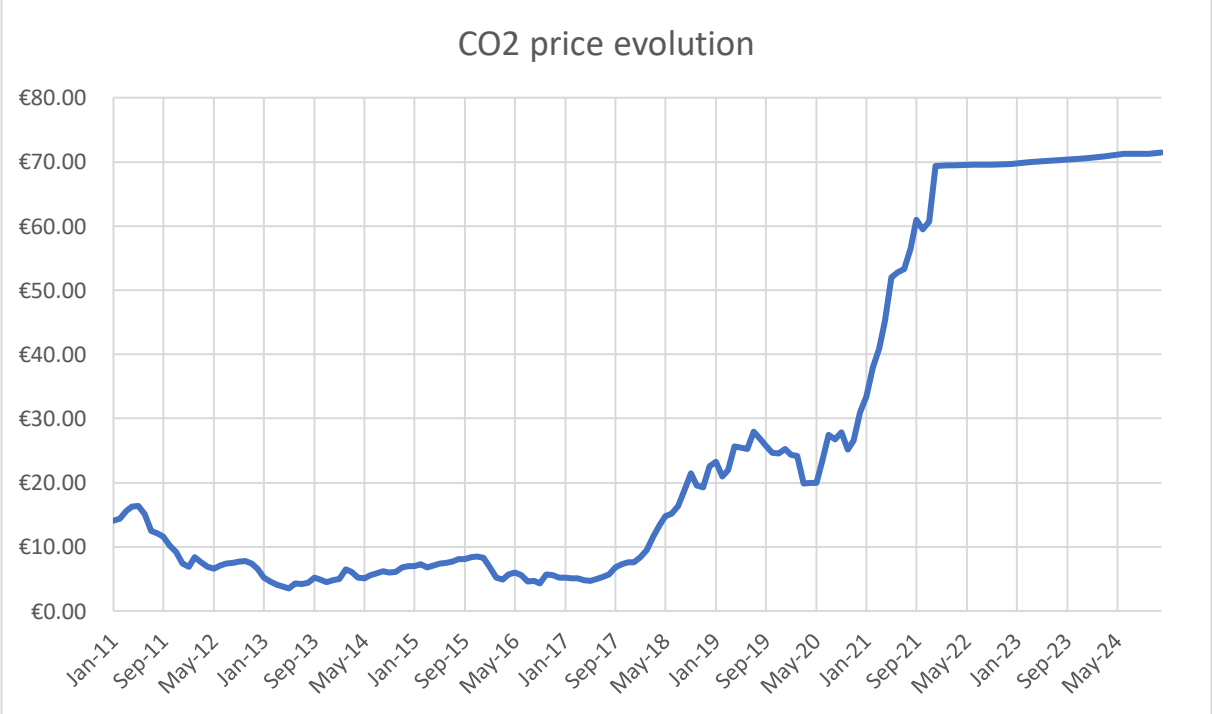

Figure 5.15: CO_2 price evolution in the last 10 years and future projections, monthly mean values [21], [22]

During 2018, CO_2 mean price was 15,88 €/ton, but it suddenly raised up to around 60 €/ton in November 2021.

EU Commission CO_2 price projection to 2030 suggest a value of 85 €/ton, but some analysts foresee a CO_2 unitary cost that may reach 100 €/ton.

Fenice S.p.A. trigeneration plant is not subject to EU ETS regulations, since, as it is described in the *Annex I* of *D.Lgs 47/2020*, only the energy plants with a thermal input higher than 20 MW_{th} must compensate their emissions with EU Allowances. Melfi trigeneration plant nominal thermal input is equal to 11,5 MW_{th}.

Nevertheless, it is interesting to evaluate the total cost that should incur for CO_2 emissions if this energy plant was included in the EU ETS regulations.

2018 Natural Gas consumption	6'369'470 Sm^3
2018 Natural Gas Input Power	64'504 MWh
	232'216 GJ
CO_2 Emission Factor [24]	55,83 kg/GJ
2018 CO_2 estimated emissions	12'965 tons
CO_2 price	70 €/ton
CO_2 total cost	907'550 €

Table 5.21: 2018 estimated CO_2 emissions and hypothetical cost

CO_2 price in *Table 5.21* is fixed to 70 €/ton; it is not equal to 2018 CO_2 price because this analysis aims at evaluating the emissions cost if the EU ETS legislation will be modified, for example, including all energy plants with halved total thermal input with respect to current Directive. This would imply that also Melfi trigeneration plant should compensate its emissions. 2024 projections estimate a CO_2 price close to 70 €/ton

It is not possible to determine how many free Allowances it would benefit, but from this cost analysis, it is clear that, even with the actual CO_2 price, the total emissions cost would be around 900'000 €.

A similar cost would be almost twice as the yearly additional revenues obtained by the optimized Scenario 3 in *Table 5.18* and even more than four times higher than future possible Scenario 3 yearly profits (*Table 5.20*), therefore it would heavily affect the energy plant yearly monetary balance.

6. Conclusions

The aim of this Master Thesis work is to analyze the performance of an existing trigeneration plant at the service of an industrial user and to evaluate possible optimization strategies to improve the energy efficiency of this plant.

This study highlighted the relevance of a good energy management system and of a detailed measurement of all physical quantities to evaluate the performance of each single plant's component and subsystem, in order to characterize their operation efficiency and to identify possible causes of performances reduction.

The 4th Chapter of this study was focused on the energy plant data analysis: results showed that, during the three analyzed years, the Rolls Royce internal combustion engine operated as efficiently as declared by the manufacturer.

Nevertheless the overall system efficiency was affected by the ineffectiveness of thermal recovery: in some particular low load conditions, especially because of double-effect absorbers malfunctioning or maintenance, the exhaust gases partially bypass the Heat Recovery Unit, thus causing an inadequate heating of the hot water circuit. In addition to that, a malfunctioning of the diverter valve logic prevented super-heated water to reach the desired temperature level, necessary to correctly supply double-effect absorbers.

This system issue affected the subsequent cold water production, indeed WARGs operated for most of the time at partial load conditions and with low COP. Moreover, the complexity of double-effect absorbers led to frequent maintenance and, therefore, to low equivalent hours of operation.

As a consequence of this cold energy production inefficiency, during all three analyzed years, it was necessary to continuously utilize the electric chillers, despite the absorbers nominal capacity could have been sufficient to cover the energy demand for most of the year.

Data analysis was also focused on the energy services that Fenice S.p.A. must provide to the industrial user. In particular, each energy service has been characterized by means of the energy signature method that allows to extrapolate the dependency of energy vectors on the external temperature. It enabled to understand the evolution of the various energy carriers demand throughout the years.

Starting from the cold energy demand trend, it was possible to identify possible energy efficiency measures to be implemented in order to improve the system performances and to mitigate the existing criticalities.

To improve the effectiveness of thermal recovery it has been proposed to substitute the current

Heat Recovery Unit with a hot water thermal recovery section, in order to simplify the energy plant configuration and to optimize cold water production.

Indeed, this HRU substitution implies the necessity to dismantle double-effect absorbers and to install new single-effect WARGs.

Three different scenarios have been proposed with regard to the new absorbers nominal cold power. Each of these scenarios have been analyzed in terms of ideal cold energy production, electricity savings and thermal recovery effectiveness with respect to the original plant configuration.

Moreover, a cash flow analysis have been performed to estimate the costs incurred because of new components installation and benefits derived from improved energy efficiency and, therefore, from the possibility to achieve more White Certificates

Results showed that Scenario 2 and Scenario 3 could represent the best options to revamp this trigeneration plant. Although Scenario 2 could bring similar profits and lower initial costs with respect to Scenario 3, this latter plant configuration can be preferred. The possibility to rely on a doubled nominal capacity absorber could allow to satisfy the cold energy demand even in case of future industrial user expansion with a subsequent increased demand.

By considering the futures of electricity and natural gas price, the monetary balance of all optimization scenarios is greatly reduced, therefore they must be considered in order to evaluate the trigeneration plant economic sustainability in the next years.

In the end, it was necessary to make a final consideration about CO_2 emission, its price evolution, and future costs projections. Currently, Fenice trigeneration plant is not subject to EU ETS regulations but the possibility of facing stricter environmental standards in terms of greenhouse gases emission could have negative implications on this plant’s economic balance and, thus, this may constitute a source of uncertainty for future years.

Bibliography

[1] IEA Reports, Tracking Industry 2020. Available online at: https://www.iea.org/reports/tracking-industry-2020

[2] United Nations, Paris Agreement 2015. Available online at: https://unfccc.int/sites/default/files/english_paris_agreement.pdf

[3] REN21, "Renewables 2020 Global Status Report"

[4] Amaze S.r.l., http://www.amaz-e.com/en/co-trigenerazione.html

[5] "Relazione annuale sulla cogenerazione in Italia", Ministero dello Sviluppo Economico, April 2020.

[6] "Linee guida per l'applicazione del Decreto del Ministero dello Sviluppo Economico 5 settembre 2011 – Cogenerazione ad Alto Rendimento (CAR)", Ministero dello Sviluppo Economico, Gennaio 2012.

[7] M. Gambini, M. Vellini, 2014, "High Efficiency Cogeneration: Electricity from cogeneration in CHP Plants", ScienceDirect. Available online at: https://www.sciencedirect.com/science/article/pii/S1876610215027666

[8] Regolamento Delegato (UE) 2015/2402 della commissione – del 12 ottobre 2015.

[9] Gestore dei Mercati Energetici, Mercati Ambientali, Titoli di Efficienza Energetica. Available online at: http://www.mercatoelettrico.org/It/Esiti/TEE/TEE.aspx

[10] J. Villarroel-Schneider, A. Malmquist, J.A. Araoz, J. Martí-Herrero, A. Martin, July 2019, "Performance Analysis of a Small-Scale Biogas-Based Trigeneration Plant: An Absorption Refrigeration System Integrated to an Externally Fired Microturbine", Energies, Available online at: https://www.mdpi.com

[11] T. Esaki, N. Kobayashi, H. Uchiyama, Y. Matsukuma, January 2019, "Characteristics of Absorption Equilibrium with HFC-134a and an Ionic Liquid Pair", ResearchGate. Available online at: https://www.researchgate.net/publication/332049496_Characteristics_of_Absorption_Equilibrium_with_HFC-134a_and_an_Ionic_Liquid_Pair

[12] A. Poggio, slides of "Impianti di cogenerazione" lectures

[13] T. Avanessian, M. Ameri, April 2014, "Energy, exergy, and economic analysis of single and double effect LiBr–H2O absorption chillers", ScienceDirect. Available online at: https://www.sciencedirect.com/science/article/abs/pii/S0378778814000516

[14] G. Ruscica, M. Badami, A. Portoraro, M. Mura B. Di Pietra, "Supporto allo sviluppo di modelli per la simulazione di impianti di micro cogenerazione per applicazione

residenziale e terziaria: principali indicatori energetici definiti dalla normativa vigente e prestazioni a regime parziale delle principali tecnologie disponibili in commercio", 2009, Ricerca Sistema Elettrico

[15] Decreto Legislativo 3 aprile 2006, n.152, Norme in materia ambientale. All. I alla parte Quinta, Parte III, punto 3, "Motori fissi a combustion interna"

[16] Allegato 1, Relazione Tecnica di Progetto impianto di trigenerazione di Melfi (PZ), June 2008.

[17] Gestore dei Mercati Energetici, Archivio Newsletter. Available online at: https://www.mercatoelettrico.org/it/Tools/ArchivioNewsletter.aspx

[18] Decreto Legge 23 Ottobre 2018, n.119.

[19] Eex.com. Available online at: https://www.eex.com/en/market-data/power/futures

[20] Powernext.com. Available online at: https://www.powernext.com/futures-market-data

[21] SendeCO_2, Prezzi CO_2. Available online at: https://www.sendeco2.com/it/prezzi-co2

[22] Eex.com. Available online at: https://www.eex.com/en/market-data/environmental-markets/derivatives-market

[23] Decreto Legislativo 47/2020, 9 giugno 2020; Allegato I.

[24] INEMAR, Fonti Inventari Emissioni. Available online at: https://www.inemar.eu/xwiki/bin/view/FontiEmissioni/RicercaFE?submitType=Ricerca&macid=1&setid=1&attid=5&comid=46&indid=-2&inqid=6&priid=-2&num_ris=50

Ringraziamenti

A conclusione di questo lavoro di Tesi, desidero ringraziare tutte le persone che mi hanno accompagnato in questo percorso di Laurea.
Ringrazio il mio Relatore, Prof. Alberto Poggio, il mio Correlatore Ing. Giulio Cerino Abdin e la Dott.ssa Chiara Monzani per la loro disponibilità, per il loro supporto e per avermi fornito indicazioni e spunti preziosi per la realizzazione di questa Tesi.
Questo lavoro è stato svolto in collaborazione con Fenice S.p.A.; ringrazio il manager Ernesto Rubicondo per avermi dato questa opportunità, il Project Manager Giuliano Gallu e, soprattutto, Pasquale Galiero dell'Unità Operativa di Melfi, per aver sempre risposto con tempestività alle numerose mail che gli ho inviato per chiedere tutti i dati necessari per lo svolgimento di questo studio, e per aver sempre chiarito con precisione ogni mio dubbio.
Ringrazio tutta la mia famiglia, mia mamma, mio papà, mio fratello che mi hanno sempre sostenuto e incoraggiato in questi cinque anni di Università.
Un grazie speciale ad Eleonora che mi è sempre stata accanto, anche nei momenti più difficili e stressanti, e che ha sopportato i miei sbalzi d'umore e le mie ansie durante le sessioni d'esame.
Ringrazio i miei amici, quelli di Borgaro e quelli conosciuti in questi anni di Politecnico, per i bei momenti di spensieratezza passati insieme, fisicamente e "da remoto", anche in questi due anni di pandemia.